Dissertation Submitted to
Graduate School of Science of Osaka University
for the Degree of Doctor of Philosophy

Hadronic Flux Tube in Dual Superconducting Vacuum of QCD

Yoshiaki Koma

~ 2001 ~

Research Center for Nuclear Physics (RCNP), Osaka University
Mihogaoka 10-1, Ibaraki, Osaka 567-0047, Japan

Acknowledgment

I would like to sincerely express my gratitude to Professor H. Toki for his continuous encouragement and helpful suggestions. I am very grateful to Dr. H. Suganuma (Tokyo Inst. Tech.) for fruitful, stimulating discussions on the interesting subject of nonperturbative QCD. I am really thankful to be able to work with them in my graduate study.

I am deeply indebted to Professor T. Suzuki (Kanazawa Univ.) for providing me several opportunities to visit Kanazawa University and for helpful discussions. I am also very grateful from my heart to Professor E. -M. Ilgenfritz for his valuable suggestions, continuous discussions, and encouragement. It is my great pleasure to thank Professor M. I. Polikarpov (ITEP, Moscow) for useful discussions. I would like to thank again them for their fruitful collaboration and for giving me lectures on the introduction of lattice QCD and demonstration.

I wish to thank Professor D. Ebert, Professor A. Hosaka (Numazu Coll. Tech.), Professor K. I. Kondo (Chiba Univ.), and Professor V. Dmitrašinović for helpful discussions and valuable advices for my study.

I would like to acknowledge Dr. A. Tanaka and Dr. H. Monden, Dr. S. Sasaki, and Dr. H. Ichie for their suggestive discussions and cheerful encouragement. I am also grateful to Dr. T. Watabe, Dr. K. Suzuki, Dr. T. Sakai, Dr. K. Itakura, Dr. Y. Nemoto, Dr. H. Matsufuru, Dr. S. Umisedo, Dr. K. Amemiya, Dr. K. Otsuki, Dr. M. Fukushima, Dr. F. Araki, Dr. N. Nakajima for their kind hospitality and useful discussions on physics. I would like to thank also S. Sugimoto, T. Takahashi, S. Yasui, I. Nakamura, N. Hamamoto for their warm friendship. I would like to thank all the members of Research Center for Nuclear Physics in Osaka University for their kind helps. Finally, I would like to express special thanks to Miho Takayama for precious discussions, collaboration, and kind help during my graduate course.

All lattice simulations in this thesis have been performed on the NEC SX4 at the Cybermedia Center, Osaka University .

Abstract

We study the hadronic flux tubes in Quantum Chromodynamics (QCD) in terms of the dual superconducting scenario of the nonperturbative vacuum in the 't Hooft Abelian gauge and the resulting dual Ginzburg-Landau (DGL) theory as an infrared effective theory of QCD. The essential prescription to derive the DGL theory from QCD is Abelian gauge fixing and Abelian projection. This scheme reduces the SU(N) gauge theory into an $[\mathrm{U}(1)]^{N-1}$ Abelian gauge theory with additional $N-1$ types of color-magnetic monopole currents corresponding to the homotopy group $\pi_2(\mathrm{SU}(N)/\mathrm{U}(1)^{N-1}) = \boldsymbol{Z}_{\infty}^{N-1}$. Performing the duality transformation, we introduce the dual gauge field which couples to the monopole current. When we sum over the monopole-current world lines in four-dimensional space time, assuming monopole condensation, we finally get a dual version of the Ginzburg-Landau theory.

First, in order to find the region of applicability of the DGL theory as an infrared effective theory of QCD, we study the quantitative relation between them at the quantum level by using their lattice formulation. For definiteness we refer to the SU(2) lattice gauge theory at $\beta_{\mathrm{SU(2)}} = 2.5115$, where we know an example of the color-electric field and monopole supercurrent profile of the flux tube, and to the corresponding U(1) DGL theory (dual Abelian Higgs (DAH) model). Paying attention to the monopole degrees of freedom as appearing in both theories, we combine the extended Swendsen method and the approximate analytical evaluation of the U(1) DGL theory in order to match the monopole actions. By Monte Carlo simulations with this set of couplings we measure the flux-tube profile and the string tension. We can partially reproduces the results of the SU(2) simulations. Remaining problems can be related to the vortex-loop vacuum structure appearing near the chosen parameters.

Second, we reformulate the $[\mathrm{U}(1)]^2$ DGL theory to make the Weyl symmetry manifest, which enables one to treat this in a quite similar way as in the U(1) DGL theory. We apply this to the systematic study of hadron structures, meson, baryon, and glueball states in terms of the open flux tube, Y-shaped flux tube, and the closed flux tube (flux-tube ring), respectively. The baryonic state is one of the most interesting and important application of the $[\mathrm{U}(1)]^2$ DGL theory, since this state can be treated only after taking into account the $[\mathrm{U}(1)]^2$ dual gauge symmetry originating from SU(3) gauge symmetry. In the glueball study, contrary to other hadrons containing valence quarks (meson, baryon) where the motion of quarks helps to stabilize the states, here we need to consider for the first time how such flux-tube ring can be stabilized by the flux-tube motion itself. For this purpose we apply the result of the string representation of the DGL theory, and describe the flux-tube ring as an relativistic closed string with an effective string tension. This description enables us to write down the Hamiltonian of the flux-tube ring. Analyzing the Schrödinger equation, we discuss the mass spectrum and the wave function of the glueball. The lowest glueball state is found to have a mass $M_G \sim 1.6$ GeV and a size $R_G \sim 0.5$ fm.

Contents

1 Introduction **1**

1.1 Approach to the nonperturbative QCD 1

1.2 Dual superconducting scenario 3

1.3 String picture of hadrons 4

1.4 Open problems to be dealt with in this thesis 8

2 Dual Abelian Higgs model derived from SU(2) gluodynamics **11**

2.1 SU(2) gluodynamics 11

2.1.1 Preliminaries 11

2.1.2 Singular gauge transformation 13

2.2 Abelian gauge fixing 13

2.2.1 Diagonalization of gauge dependent variable 13

2.2.2 Appearance of magnetic Dirac string 15

2.3 Abelian projection 17

2.3.1 Abelian gauge transformation of the gauge field 17

2.3.2 Abelian field strength tensor 18

2.3.3 Breaking of the Abelian Bianchi identity and monopole current 21

2.4 Dual Abelian Higgs model 22

2.4.1 Path-integral duality transformation 22

2.4.2 Ensemble of monopole currents 25

2.5 Summary and outlook 26

3 Classical properties of the DAH model **27**

3.1 Dual Higgs mechanism 27

3.2 Flux-tube solution 29

3.2.1 Flux quantization condition 29

3.2.2 Decomposition of the dual gauge field 30

3.2.3 Cylindrically symmetric system 31
3.3 Properties of the classical DAH vacuum 36
3.3.1 Bogomol'nyi limit 36
3.3.2 Interaction of flux tubes 37
3.4 Summary and outlook 37

4 Quantum properties of the DAH model 39
4.1 DAH model on the dual lattice 39
4.2 Classical flux-tube solution on the dual lattice 40
4.3 Monte Carlo simulation of the DAH model 45
4.3.1 Structure of the DAH vacuum 46
4.4 't Hooft loop operator in the DAH model 50
4.5 Summary and outlook 53

5 SU(2) gluodynamics and the DAH model on lattice 55
5.1 A few words about SU(2) lattice gauge theory 56
5.1.1 SU(2) Wilson action 56
5.1.2 Maximally Abelian (MA) gauge on lattice 57
5.1.3 Extraction of monopole currents 58
5.2 Monopole representation of the DAH model 60
5.2.1 Integrating the dual gauge field $B_\mu(s)$ and the monopole phase $\eta(s)$. 61
5.2.2 Integrating the monopole field modulus $\phi(s)$ 62
5.3 Extended Swendsen method 65
5.4 Input parameters of the DAH model 66
5.5 Monte Carlo simulation of the DAH model 68
5.5.1 Measuring the flux-tube profile in the DAH model 68
5.5.2 Measuring the string tension 70
5.6 Summary and outlook 73

6 Dual Ginzburg-Landau theory derived from SU(3) gluodynamics 75
6.1 SU(3) gluodynamics in the Abelian projection 75
6.2 Dual Ginzburg-Landau theory 80
6.3 Summary and outlook 82

7 Manifestly Weyl symmetric formulation of the DGL theory 85
7.1 Various representations of the dual gauge field 85
7.1.1 Cartan 3-8 representation 86

7.1.2 Color-electric representation . . . 87
7.1.3 Color-magnetic representation . . . 88
7.2 Hadronic flux-tube solutions . . . 89
7.2.1 Mesonic flux tube (q-$\bar{q}$ system) . . . 90
7.2.2 Baryonic flux tube (q-q-q system) . . . 91
7.3 Properties of the classical DGL vacuum . . . 92
7.3.1 Bogomol'nyi limit . . . 93
7.3.2 Interaction of flux tubes . . . 95
7.4 Summary and outlook . . . 96

8 Glueball as the flux-tube ring solution in the DGL theory 111
8.1 Flux-tube ring as the closed effective string . . . 112
8.2 Flux-tube ring solution . . . 114
8.3 Closed effective string as the glueball state . . . 116
8.4 Summary and discussions . . . 118

9 Summary and concluding remarks 123

A Monte Carlo method for the DAH model 127
A.1 Update of the dual gauge field . . . 127
A.2 Update of the monopole field . . . 130

List of Figures

1.1 QCD running coupling constant $\alpha_s(Q^2)$ 2
1.2 Color-electric field in the flux tube (3D) 6
1.3 Monopole supercurrent in the flux tube (3D) 6
1.4 Profile of the flux tube in the SU(2) lattice gauge theory in the MA gauge at $\beta_{\mathrm{SU(2)}} = 2.5115$ 7
1.5 String picture of hadrons corresponding to meson, baryon, and glueball . . . 9

2.1 Direction of the color-magnetic Dirac string in the Abelian gauge 17
2.2 Cancellation of the color-magnetic Dirac string in the Abelian field strength . 20

3.1 Quark and antiquark system with cylindrical symmetry 32
3.2 Profiles of ingredients of the flux tube 34
3.3 Structure of the color-electric field in the flux tube 35
3.4 Schematic figure of the linking between the induced electric field and the monopole supercurrent 35
3.5 Structure of the flux tube in the DAH model 38

4.1 Color-electric Dirac string dual to singular plaquettes 43
4.2 Profiles of the color-electric field, the monopole supercurrent, and the modulus of the monopole field in the mesonic flux tube (dual lattice formulation) . . . 44
4.3 Quark-antiquark potential of the mesonic flux tube in the DAH model (dual lattice formulation) 45
4.4 Phase diagram of the DAH model in the London limit 47
4.5 Plaquette energy density, modified hopping term, and vortex density as functions of mass parameter $\hat{m}_B = \hat{m}_\chi$ and coupling β_{DAH} 49
4.6 Profiles of the flux tube in the quantized DAH model (example) 52

5.1 Schematic understanding of the relation between original lattice and dual lattice in terms of differential form on lattice 59

5.2 Monopole currents projected into $\boldsymbol{R}^3$ in the SU(2) lattice gauge theory in the MA gauge with 16^4 at $\beta_{\mathrm{SU(2)}} = 2.5115$ 67
5.3 Profiles of the flux tube in the quantized DAH model corresponding to $\beta_{\mathrm{SU(2)}} = 2.5115$ 69
5.4 Profile of the color-electric field in the quantized DAH model as a function of radius, corresponding to $\beta_{\mathrm{SU(2)}} = 2.5115$ 70
5.5 Values of $\langle dS_{\mathrm{DAH}}/d\xi \rangle_{|\xi}$ as a function of ξ for various sizes of the 't Hooft loops 72
5.6 Quark-antiquark potential in the quantized DAH model corresponding to $\beta_{\mathrm{SU(2)}} = 2.5115$ 72

6.1 Distribution of the color-electric charge $\vec{Q}_j^{\mathrm{E}} = e\vec{w}_j$ and the color-magnetic charge $\vec{Q}_i^{\mathrm{M}} = g\vec{\epsilon}_i$ 79

7.1 Mesonic flux tube: Profiles of the color-electric field in the Cartan representation 97
7.2 Mesonic flux tube: Profiles of the monopole supercurrent in the Cartan representation 98
7.3 Mesonic flux tube: Profiles of the color-electric field in the color-electric representation 99
7.4 Mesonic flux tube: Profiles of the monopole supercurrent in the color-electric representation 100
7.5 Mesonic flux tube: Profiles of the color-electric field in the color-magnetic representation 101
7.6 Mesonic flux tube: Profiles of the monopole supercurrent in the color-magnetic representation 102
7.7 Mesonic flux tube: Profiles of the modulus of the monopole field 103
7.8 Quark-antiquark potential of the mesonic flux tube in the DGL theory 104
7.9 Baryonic flux tube: Profiles of the color-electric field in the Cartan representation 105
7.10 Baryonic flux tube: Profiles of the color-electric field in the color-electric representation 106
7.11 Baryonic flux tube: Profiles of the color-electric field in the color-magnetic representation 107
7.12 Baryonic flux tube: Profiles of the modulus of the monopole field 108
7.13 Three-quark potential of the baryonic flux tube in the DGL theory 109

8.1 Flux-tube ring 112
8.2 Coordinates for the flux-tube ring 115
8.3 Structure of the color-electric Dirac string of the possible flux-tube excitations without valence quarks in the DGL theory 115

8.4 Profiles of the color-electric field in the flux-tube ring in the DGL theory . . . 120
8.5 Profiles of the modulus of the monopole field in the flux-tube ring in the DGL theory . . . 121
8.6 Effective string tension of the flux-tube ring as a function of radius . . . 122
8.7 Estimation of the glueball mass . . . 122

Chapter 1

Introduction

1.1 Approach to the nonperturbative QCD

The analysis of Quantum Chromodynamics (QCD) at large distances is a very important subject in understanding not only the nontrivial vacuum structure, and its manifestations such as confinement and chiral symmetry breaking [1], but also the hadron mass spectrum observed in experiments [2] in terms of its ingredients, quarks and gluons. The QCD Lagrangian density has the SU(3) gauge symmetry, which is written by using the quark field q_f and the gluon field $\mathcal{A}_\mu$ as

$$\mathcal{L}_{\rm QCD} = -\frac{1}{2}{\rm tr}(G_{\mu\nu}G^{\mu\nu}) + \sum_{f=1}^{N_f} \bar{q}_f(i\gamma^\mu D_\mu - m_f)q_f, \tag{1.1.1}$$

where $G_{\mu\nu} = \partial_\mu \mathcal{A}_\nu - \partial_\nu \mathcal{A}_\mu + ie\,[\mathcal{A}_\mu, \mathcal{A}_\nu]$ is the SU(3) field strength tensor, and $D_\mu = \partial_\mu + ie\mathcal{A}_\mu$ the covariant derivative. The quark masses are m_f, and e is the SU(3) gauge coupling. N_f is the number of flavors. Due to the non-Abelian nature of the SU(3) group, the gluon fields carry color charge too, and interact with themselves. This feature is completely different from Abelian gauge theory like Quantum Electrodynamics (QED), where there is no self-interaction term of the Abelian gauge (photon) field. In QCD, the one-loop contribution from gluon self-energy and vertex at large momentum scale Q^2 leads to the running coupling constant

$$\alpha_s(Q^2) \equiv \frac{e(Q^2)}{4\pi} = \frac{12\pi}{(33-2N_f)\ln(Q^2/\Lambda^2_{\rm QCD})}, \tag{1.1.2}$$

where $\Lambda_{\rm QCD}$ is an important quantity, which provides a typical scale of the strong interaction. For large momentum transfers $Q \to \infty$, one finds that the coupling behaves as $\alpha_s(Q^2) \to 0$, which is called Asymptotic Freedom [3, 4]. On the other hand, for $Q \to \Lambda_{\rm QCD}$, the coupling becomes large and diverges to infinity, $\alpha_s(Q^2) \to \infty$. Clearly, in this region, perturbative expansions in α_s and therefore the expression (1.1.2), too, are not meaningful anymore. Such

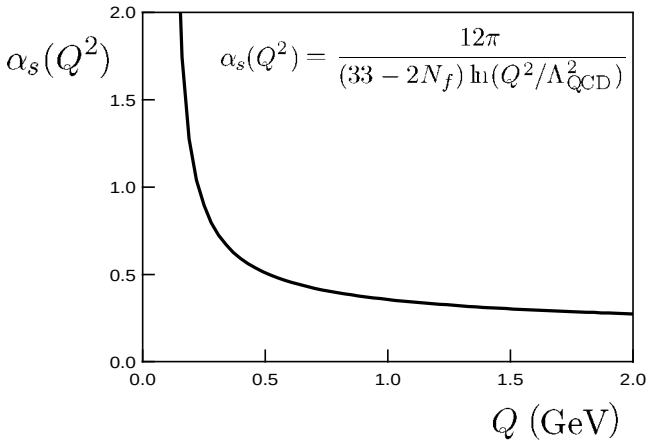

Figure 1.1: The QCD running coupling constant $\alpha_s(Q^2)$, where $\Lambda_{\rm QCD} = 0.1$ GeV.

behavior is opposite to that of the QED running coupling constant. Checking expression (1.1.2) with empirical data at a high scale $\alpha_s(Q^2 = M^2_{Z^0}) \sim 0.12$ [2] gives $\Lambda_{\rm QCD} \approx 0.10$ GeV for $N_f = 5$ (Top quark mass is known as $m_t \approx 170$ GeV, which is heavier than M_{Z^0}. On the other hand bottom quark mass is $m_b \approx 4$ GeV.). The typical behavior of $\alpha_s(Q^2)$ is shown in Fig. 1.1. Higher order corrections up to 4-loop give $\Lambda_{\rm QCD} \approx 0.22$ GeV [5].

In order to study the low energy region of QCD, we need to develop other techniques beyond the scope of perturbation theory. The lattice QCD formalism is one promising approach for this subject. The lattice discretization of space-time coordinates leads, infinite four-dimensional volume, to a finite-dimensional path-integral representation of the partition function. Then the sampling of vacuum fields can be performed directly by means of the Monte Carlo method. In fact, from the measurement of the expectation value of the Wilson loop, an useful operator to measure the excess of free energy of a bound state of the q-$\bar{q}$ system, an area-type exponential decay is found, which leads to a linear quark confinement potential [6]. The effect of dynamical quarks can be taken into account at a much higher cost. Therefore, up to recently, the light hadron mass spectrum has been simulated in quenched approximation and found to be in reasonable coincidence with the empirical data up to a well-understood systematic error [7]. In this sense, we can already say that the lattice QCD simulation is a very useful method to provide us detailed information assuring that QCD is the reliable fundamental theory of hadrons. The mechanisms how and why the QCD reproduces this face of nature is still under debate. Therefore, besides numerical lattice QCD simulation, it is quite important to investigate the corresponding infrared effective theory which is constructed from QCD by extracting the relevant degrees of freedom describing the infrared energy region. If the resulting framework has a simple form which can be dealt with

analytically, this is of big practical importance. Then this effective theory can be studied complementary with lattice QCD simulations. We hope to understand better the working principles behind the lattice results.

1.2 Dual superconducting scenario

In this context, we take up that the so-called "dual" superconducting scenario [8, 9], described by the dual Ginzburg-Landau (DGL) theory [10, 11], as a promising theoretical idea. The word "dual" represents a world where the role of electricity and magnetism is interchanged. This idea is applied to ordinary superconductivity where electrical charges (Cooper pairs) are condensed and magnetic field is confined. The essential prescription to derive the DGL theory from QCD is Abelian gauge fixing (selecting the "off-diagonal" gauge degrees of freedom) and Abelian projection (dropping off-diagonal gauge degrees of freedom) [12]. This is justified by the infrared Abelian dominance for the nonperturbative quantities, which was conjectured in Refs. [13]. This scheme reduces the SU(3) gauge theory into the $[\mathrm{U}(1)]^2$ Abelian gauge theory with additional two types of color-magnetic monopole currents, which can be understood by recalling the homotopy group $\pi_2(\mathrm{SU}(3)/\mathrm{U}(1)^2) = \pi_2(S_2 \times S_2) = \boldsymbol{Z}_\infty^2$. After summing over the monopole-current world lines in four-dimensional space time [14–16], assuming monopole condensation, we finally get a Ginzburg-Landau type Lagrangian density with the $[\mathrm{U}(1)]^2$ dual gauge symmetry:

$$\mathcal{L}_{\mathrm{DGL}} = -\frac{1}{4}\left(\partial_\mu \vec{B}_\nu - \partial_\nu \vec{B}_\mu + e\vec{\Sigma}^{\mathrm{E}}_{\mu\nu}\right)^2 + \sum_{i=1}^{3}\left[\left|\left(\partial_\mu + ig\vec{\epsilon}_i\cdot\vec{B}_\mu\right)\chi_i\right|^2 - \lambda\left(|\chi_i|^2 - v^2\right)^2\right], \quad (1.2.1)$$

where $\vec{B}_\mu$ and χ_i denote a two-component dual gauge field (axial vector) and a three-component monopole field (complex scalar)*, respectively. There are three coupling parameters, the dual gauge coupling g and the strength of monopole self-interaction λ, and the monopole condensate v. The dual gauge field appears during the step of path-integral duality transformation of the partition function. The quark field are included in the definition of $\vec{\Sigma}^{\mathrm{E}}_{\mu\nu}$, which describes the color-electric Dirac string singularity. In the dual form, we need such string in order to define the color-electric charge, which is similar but dual to the definition of the magnetic charge of the Dirac monopole [1]. It is important to note that recent studies of lattice QCD Monte-Carlo simulation in the maximally Abelian (MA) gauge [17–19] show numerical evidence of assumptions used to derive the DGL theory, infrared Abelian dominance [20–22] and monopole condensation [23–27], and their relation to nonperturbative phenomena like confinement [28, 29] and chiral symmetry breaking [30, 31]. In this sense, the DGL theory is qualitatively supported by numerical lattice QCD.

*The components of which have to fulfill some constraint.

According to the fact that QCD is based on SU(3) gauge theory, in the DGL theory, there appear three different types of the Abelian color charges both in the electric sector and the magnetic sector. The color-electric charges are defined as $e\vec{w}_j$ $(j = 1, 2, 3)$ and the color-magnetic charge $g\vec{\epsilon}_i$ $(i = 1, 2, 3)$, where $\vec{w}_j$ and $\vec{\epsilon}_i$ denote the weight vector and the root vector of the SU(3) algebra, respectively. These color charges satisfy the Dirac quantization condition, $e\vec{w}_j \cdot g\vec{\epsilon}_i = 2\pi m_{ij}$, where m_{ij} is an integer. These charges possess the global Weyl symmetry, which is permutation invariance among color labels of these charges. Hence, the Weyl invariance guarantees the color-singlet criterion of the theory. Recently, we have developed the DGL theory to make this Weyl symmetry manifest by the redefinition of the dual gauge field $B_{i\mu} \equiv g\vec{\epsilon}_i \cdot \vec{B}_\mu$ [32], and found that the DGL Lagrangian (1.2.1) can be written in the form, $\mathcal{L}_{\rm DGL} = \sum_{i=1}^{3} \mathcal{L}^{(i)}_{\rm DGL}$, where

$$\mathcal{L}^{(i)}_{\rm DGL} = -\frac{1}{4g'^2}\left(\partial_\mu B_{i\nu} - \partial_\nu B_{i\mu} + 2\pi \sum_{j=1}^{3} m_{ij}\Sigma^{\rm E}_{j\mu\nu}\right)^2 + |(\partial_\mu + iB_{i\mu})\,\chi_i|^2 - \lambda\left(|\chi_i|^2 - v^2\right)^2 . \tag{1.2.2}$$

Here the dual gauge coupling is redefined as $g' \equiv \sqrt{\frac{3}{2}}g$, and we have used the relation $\vec{\Sigma}^{\rm E}_{\mu\nu} = \sum_{j=1}^{3} \vec{w}_j \Sigma^{\rm E}_{j\,\mu\nu}$. The three dual gauge fields in (1.2.2) fulfill the constraint $\sum_{i=1}^{3} B_{i\mu} = 0$ due to $\sum_{i=1}^{3} \vec{\epsilon}_i = 0$. Clearly, this form is manifestly invariant under the permutation of labels i or j, since they are summed over. The resulting form apparently has a $[{\rm U}(1)]^3$ dual gauge symmetry. Thanks to this extension of the dual gauge symmetry, each piece of the DGL Lagrangian $\mathcal{L}^{(i)}_{\rm DGL}$ can be treated as a the U(1) dual Abelian Higgs (DAH) model corresponding to the infrared effective model of SU(2) gluodynamics in the Abelian projection. In this sense, an analysis of the U(1) DAH model is also useful to learn the essence of the dual superconductivity described by the DGL theory. More details of a derivation of the DAH model from the SU(2) gluodynamics will be discussed in chapter 2. The DGL theory is discussed in chapter 6, where we will obtain the DGL Lagrangian (1.2.1). The manifestly Weyl symmetric description like the expression (1.2.2) will be presented in chapter 7, where the application of the flux-tube solution to the understanding of hadron structure is discussed.

1.3 String picture of hadrons

In the dual superconducting vacuum as described by the DGL theory, the color-electric flux emanating from the color-electric charge is squeezed into an almost one-dimensional object like a string, due to the dual Meissner effect caused by monopole condensation. We call this hadronic color-electric flux tube, or simply the flux tube. An example of flux-tube profile is shown in Fig. 1.2. The color-electric flux emitted from the quark is absorbed by the antiquark,

forming the tube structure in between. This is due to the existence of induced color-electric field originating from monopole supercurrents through the dual Faraday law. As shown in Fig. 1.3, these supercurrents are circulating around the flux tube. Figs. 1.2 and 1.3 show the classical flux-tube solution, discussed first in chapter 3. Quarks together with gluons are then confined into the inside of a fuzzy rod (of large color-electric field strength), or Mercedes star-shaped objects, or rings, which correspond to the various hadronic objects like meson, baryon, glueball, respectively. The flux tube has a constant energy per unit length, the string tension, which characterizes the slope of the linear potential between the color charges. This is dual analogue to the formation of Abrikosov-Nielsen-Olesen (ANO) vortex in an ordinary superconductor [33, 34]. Here, magnetic monopoles play the same role as that of the electric Cooper pairs of BCS theory. Two typical scales of dual superconductivity are provided by the mass of the dual gauge field $m_B = \sqrt{3}gv$ and the mass of the monopole field $m_\chi = 2\sqrt{\lambda}v$. These masses characterize the thickness of the transition region between the normal phase (the interior of the flux tube) and the dual superconducting phase (the surrounding vacuum). They play a crucial role to determine the profile of the flux tube and the string tension of the flux tube. There is a vacuum property classified by the ratio of two masses $\kappa = m_\chi/m_B$, called the Ginzburg-Landau parameter; we have a type-I ($\kappa < 1$) or a type-II ($\kappa > 1$) vacuum. The border between the type-I and the type-II vacua given by $\kappa = 1$ is called the Bogomol'nyi limit, where one can find several results analytically [35, 36]. Details of the flux-tube solution are discussed in chapter 3 within the U(1) DAH model, and in chapter 7 within the $[\mathrm{U}(1)]^2$ DGL theory.

It should be noted that this flux-tube picture of hadrons is not in contradiction to the properties known from empirical data, such as the Regge trajectories and duality of scattering amplitude [37, 38]. The Regge slopes of hadrons provides the value of the string tension, $\sigma \simeq 1$ GeV/fm, which characterizes the strength of the confinement. In the extreme type-II limit ($\kappa \gg 1$), one can explicitly derive the string representation of the DGL theory [39–42], which can be regarded as the theory of the QCD string theory essentially described by the Nambu-Goto action and a rigidity term [43, 44]. It is expected that such effective hadronic string theory does not to contain the conformal anomaly [45], due to the presence of the Polchinski-Strominger term [46]. This means that one may be able to establish a quantum string theory within the four-dimensional space time [41]. In terms of the string description of hadrons, the linear rising inter-quark potential obtained by the area-law decay of the Wilson loop seems trivial. Before going over to the string representation, the hadronic flux tube can be regarded as a rather complicated collective excitation in the QCD vacuum. In a simplified form, the so-called flux-tube model can be applied even for the study of scattering properties of hadrons [47].

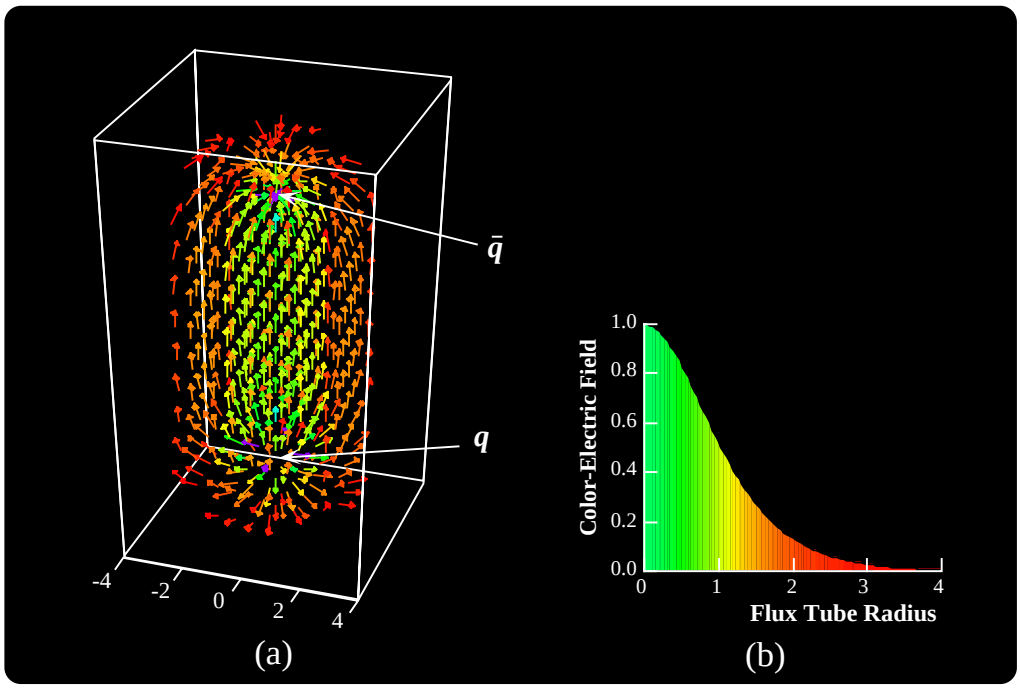

Figure 1.2: (a) The profile of color-electric field and (b) its strength in the flux tube.

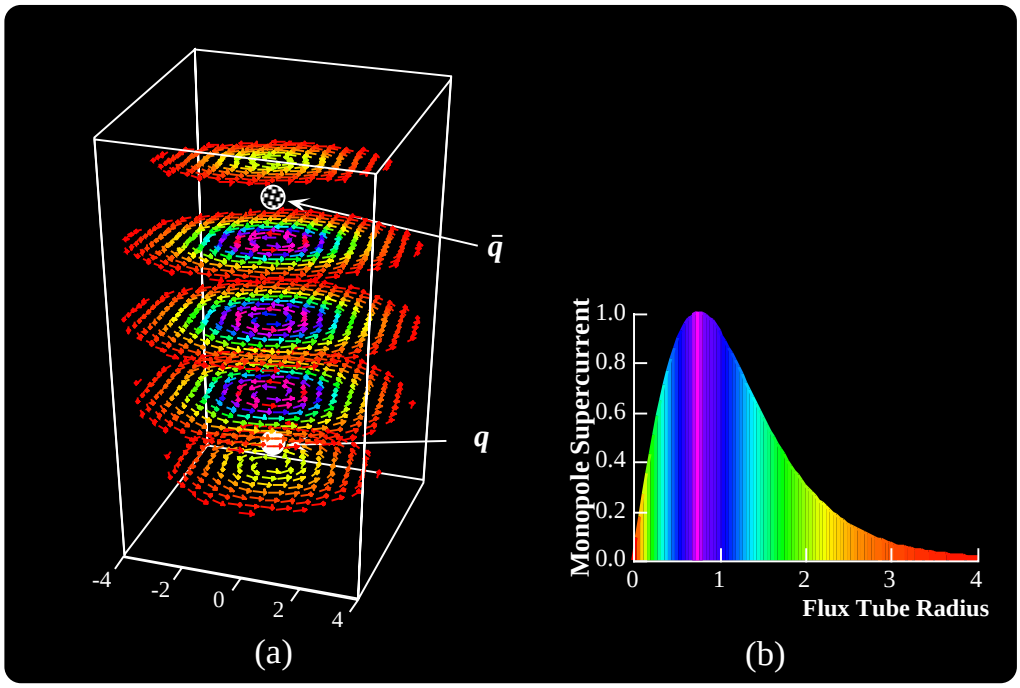

Figure 1.3: (a) The profile of monopole supercurrent and (b) its strength in the flux tube.

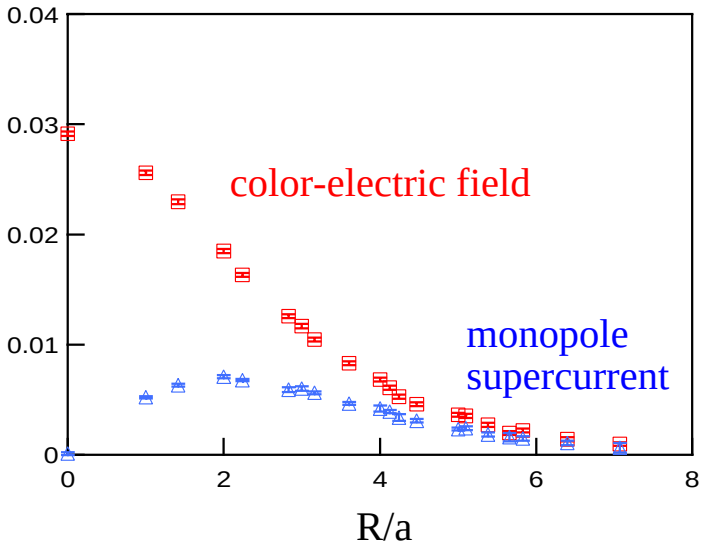

Figure 1.4: The profile of the flux tube in the SU(2) lattice gauge theory in the MA gauge at $\beta_{\mathrm{SU(2)}} = 2.5115$ (The lattice spacing represents $a = 0.086$ fm, determined from the string tension $\sqrt{\sigma} = 440$ MeV).

A few years ago, an interesting quantitative example of flux tube was identified in the Monte Carlo simulation of SU(2) lattice gauge theory, studied in the MA projection [48]. The authors have studied the profile of the color-electric flux between heavy quarks measuring the correlators of both the color-electric field $\boldsymbol{E}$ and the monopole supercurrents $\boldsymbol{k}$, with Abelian Wilson loops. So far, this type of measurement, performed on a 32^4 lattice at $\beta_{\mathrm{SU(2)}} = 2.5115$, has not been repeated to check the results for the scaling. Such correlators, divided by the expectation values of the Wilson loops themselves, describe the expectation values of color-electric field and monopole supercurrents induced by the presence of a static color-electric charges*. For the Abelian Wilson loop in the z-t plane, the z component $E_z(R)$ of $\boldsymbol{E}$ and the azimuthal component $k_\theta(R)$ of $\boldsymbol{k}$ were found to be non-vanishing as shown in Fig. 1.4. The distance from the center of the flux tube is $R = \sqrt{x^2 + y^2}$, and the azimuthal angle θ is defined as usual $\tan\theta = y/x$. Note that these quantities would vanish in vacuum. In presence of the color-electric current circulating around the Abelian Wilson loop, $\boldsymbol{E}$ and $\boldsymbol{k}$ are created and related through the dual Ampére law.

*Why this measurement provides the expectation values of operators in the vacuum with external source will be explained for a similar case in the section 4.4. The form $\langle O\rangle_{\mathrm{external}\ q-\bar{q}} = \langle WO\rangle_0/\langle W\rangle_0$, where W denotes the Wilson loop operator and O an another operator, physically corresponds to the dual object (4.4.5), the 't Hooft loop operator H [49].

1.4 Open problems to be dealt with in this thesis

Now, we would like to specify our view point on this subject. As explained in the previous sections, in order to get deeper theoretical insights into the hadronic properties in terms of quarks and gluons perturbing the vacuum, it is useful to pay attention to the dual superconducting picture of the QCD vacuum. In this framework the vacuum (monopole condensate) is present already at the tree level. Then this picture enables one to connect the string-like properties of hadrons with QCD.

On this level,

- the analysis of flux-tube (effective string) statics and dynamics described by the DGL theory should be done for the purpose of systematic understanding of the observed hadron properties.

We consider that for this purpose it is useful to apply the manifestly Weyl symmetric form of the DGL theory, as already explained in Eq. (1.2.2), which is based on the idea that the hadron should be a color-singlet state. Therefore, using this framework,

- we shall study the hadron structures corresponding to the meson, the baryon [50], and the glueball states [51] in terms of the flux-tube solution in the DGL theory.

In particular, the baryonic state is the most important application of the manifestly Weyl symmetric form of the DGL theory, since it contains all three types of the color-electric charges. As a new application of the flux-tube solution of the DGL theory to hadron structure, we present the study of the glueball state as a flux-tube ring. This idea is based on the extension of the open flux tube used in usual mesonic and baryonic states, with valence quarks at the ends, to the concept of a closed flux tube. The glueball, which is considered as a bound state of gluons without any valence quarks, can be regarded as a toroidal flux tube. We summarize the string picture of the hadronic states in Fig. 1.5. The mesonic and baryonic states are studied in chapter 7 on a classical level, and the glueball states will be discussed, for an attempt to quantize the flux-tube ring, in chapter 8.

Before doing such analysis,

- it is also important to find the region of applicability of the DGL theory.

First, this effective theory (1.2.1) cannot describe all properties of QCD (1.1.1). More important, being an effective theory, its couplings must be related to QCD. In other words, for quantitative descriptions of infrared QCD in the framework of the DGL theory we would like to know how to determine its coupling parameters *directly* from QCD.

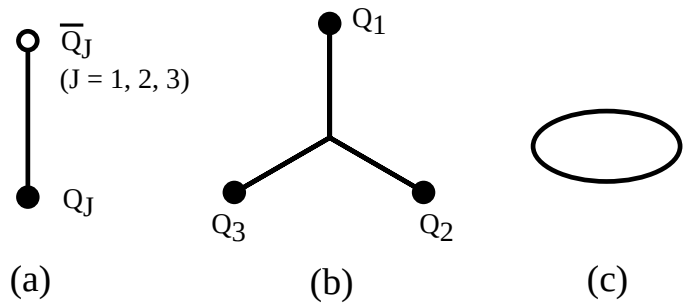

Figure 1.5: The string picture of hadrons corresponding to (a) meson, (b) baryon, and (c) glueball states.

As a first step in this direction, on a phenomenological level, recently an estimation of the parameters of the DAH model corresponding to the Abelian-projected SU(2) gauge theory has been performed in [52], where the template profile of the color-electric flux tube between heavy quark and antiquark shown in Fig. 1.4 has been analyzed. The profiles of the color-electric field and the monopole supercurrent has been fitted by the *classical flux-tube solution* of the DAH model. The result suggests that the masses of the dual gauge field and the monopole field are almost the same, approximately 1 GeV, such that the so-called Bogomol'nyi limit seems to be realized in the dual superconductor vacuum. The authors also mention that the string tension of the flux tube can be reproduced, as a classical energy per length, in the DAH model with the obtained parameter set within 94% of the original SU(2) string tension. This result support the hope that the DAH model as a classical field theory is rich enough to describe the infrared properties of SU(2) gluodynamics not only qualitatively but also quantitatively. However, the DAH model, related by duality to gluodynamics, is supposed to be an effective theory on the quantum level. Then the result of Ref. [52] is just a fit. A final statement on the status of the DAH model and on the parameter which correspond to gluodynamics can be made only when the profile of the flux tube known from gluodynamics is reproduced within the quantized DAH model. Notice that no prediction is made by Abelian-projected SU(2) gluodynamics for the profile of the monopole field. If this is successfully done, other vacuum properties can be studied: type of vacuum, renormalized dual photon mass, monopole mass, mass gap (glueball mass), field strength correlators, etc...

In this thesis,

- we restrict our task to the study of the quantitative relation between the SU(2) gluodynamics and the DAH model at the quantum level [53].

The aim of this study is first to know under which circumstances how much of the classical description of the flux tube in the Ginzburg-Landau type model can be reproduced by the

quantum version of it taken as an infrared effective model of non-Abelian gauge theory. Second, and not less important, we have to establish microscopically the link between SU(2) gluodynamics and the DAH model in a way which tells us the couplings of the latter. Of course, our final goal is to solve this problem for the SU(3) case.

For definiteness we refer to exactly the case of pure SU(2) gauge theory at $\beta_{\mathrm{SU(2)}} = 2.5115$, *i.e.*, the lattice vacuum we are interested in is exactly that where the flux-tube template comes from. Non-Abelian flux-tube data for other $\beta_{\mathrm{SU(2)}}$ are not yet available. Then, our strategy is the following: We focus attention to the *monopole* degrees of freedom, which are common ingredients of both the SU(2) gauge theory (in the Abelian projection, after performing the MA gauge fixing) and the DAH model. In the DAH model, the monopoles are figuring as the monopole field. They can be made explicit, however, in the so-called monopole representation of the DAH model. This offers the possibility to match the monopole action, known from the monopole content of the Abelian-projected SU(2) configurations, with the monopole action to be obtained from the monopole representation of the DAH model [54]. The first part comes from Monte Carlo simulation of SU(2) lattice gauge theory, Abelian projection, and then adopting the extended Swendsen method [55, 24] The second part is obtained analytically, such that one can infer the DAH model parameters. Finally, DAH simulations can be performed which should give the flux-tube profile and the string tension, both at the *quantum level*, to compare them with the SU(2) results. Studying the approach to the continuum limit would be worth of further studies. However, the matching should be done at a scale where the monopole dynamics is sufficiently simple. The details of this study, the Monte Carlo simulation of the SU(2) lattice gauge theory, the monopole representation of the DAH model, the extended Swendsen method, and the simulation of the DAH model will be presented in chapter 5. General features of the Monte Carlo simulation of the DAH model is discussed before in chapter 4, where some useful notation and technical details of the lattice DAH model are provided.

Chapter 2

Dual Abelian Higgs model derived from SU(2) gluodynamics

In this chapter we are going to derive the dual Abelian Higgs (DAH) model from the SU(2) gluodynamics. First, we adopt the Abelian gauge fixing, which shows the existence of Abelian magnetic monopoles in the SU(2) gauge theory. Second, by performing the Abelian projection method [12], we extract these monopoles as collective modes, which is based on the hypothesis of Abelian dominance in the nonperturbative vacuum [13]. At this stage, the SU(2) gluodynamics is reduced into an Abelian gauge theory including the Abelian magnetic monopoles as additional degrees of freedom, which form closed world-lines in four-dimensional space-time. Finally, we assume that the vacuum is characterized by the complicated clustering of these monopole world-lines. The partition function of grand canonical ensemble of such "monopole currents" system can be reformulated in terms of a "monopole field." In order to sum up these monopole trajectories including interactions, it is useful to introduce the dual gauge field which directly couples to monopole currents by a duality transformation. One finds that the resulting model is nothing else but the DAH model, describing the vacuum as the dual superconductor.

2.1 SU(2) gluodynamics

2.1.1 Preliminaries

We start from the SU(2) gluodynamics described by the action

$$S_{\mathrm{SU}(2)} = \int d^4x \mathcal{L}_{\mathrm{SU}(2)}, \tag{2.1.1}$$

where $\mathcal{L}_{\mathrm{SU(2)}}$ is the Lagrangian density in the Euclidean metric, given by

$$\mathcal{L}_{SU(2)} = \frac{1}{2}\mathrm{tr}G_{\mu\nu}G_{\mu\nu} + i\mathcal{A}^a_\mu J^a_\mu \tag{2.1.2}$$

where $\mathcal{A}_\mu$ denotes the SU(2) non-Abelian gauge field

$$\mathcal{A}_\mu = \mathcal{A}^a_\mu T^a, \qquad T^a \equiv \frac{\tau^a}{2}. \tag{2.1.3}$$

Here, T^a $(a = 1, 2, 3)$ are generators of the SU(2) Lie algebra satisfying the commutation relation $[T^a, T^b] = i\sum_{c=1}^{3}\varepsilon^{abc}T^c$. τ^a $(a = 1, 2, 3)$ are standard Pauli matrices

$$\tau^1 \equiv \begin{pmatrix} 0 & 1 \\ 1 & 0 \end{pmatrix}, \quad \tau^2 \equiv \begin{pmatrix} 0 & -i \\ i & 0 \end{pmatrix}, \quad \tau^3 \equiv \begin{pmatrix} 1 & 0 \\ 0 & -1 \end{pmatrix}, \tag{2.1.4}$$

which satisfy a normalization

$$\mathrm{tr}(\tau^a\tau^b) = 2\delta^{ab} \quad \text{or} \quad \mathrm{tr}(T^aT^b) = \frac{1}{2}\delta^{ab}. \tag{2.1.5}$$

The SU(2) quark current is introduced as the external source $J^a_\mu = e\bar{q}\gamma_\mu T^a q$, which couples to the SU(2) gauge field $\mathcal{A}^a_\mu$.

Now we can define the covariant derivative $\hat{D}_\mu$ based on the gauge principle as

$$\hat{D}_\mu = \hat{\partial}_\mu + ie\mathcal{A}_\mu, \tag{2.1.6}$$

then, the field strength tensor $G_{\mu\nu}$ written as

$$G_{\mu\nu} = \frac{1}{ie}\left\{\left[\hat{D}_\mu, \hat{D}_\nu\right] - \left[\hat{\partial}_\mu, \hat{\partial}_\nu\right]\right\} \tag{2.1.7}$$

$$= \partial_\mu\mathcal{A}_\nu - \partial_\nu\mathcal{A}_\mu + ie\left[\mathcal{A}_\mu, \mathcal{A}_\nu\right]. \tag{2.1.8}$$

Note that the hat "$\hat{}$" means that it operates on wave functions of the right. The commutator of derivative $\left[\hat{\partial}_\mu, \hat{\partial}_\nu\right]$ plays an important role to keep the SU(2) field strength tensor regular.

The action is invariant under the SU(2) gauge transformation (gauge principle), defined by using the element of SU(2) group $U(x) \in \mathrm{SU(2)}$ as

$$\mathcal{A}_\mu(x) \rightarrow \mathcal{A}'_\mu = U(x)\left(\mathcal{A}_\mu(x) + \frac{1}{ie}\partial_\mu\right)U^\dagger(x), \tag{2.1.9}$$

$$\hat{D}_\mu \rightarrow \hat{D}'_\mu = U\hat{D}_\mu U^\dagger = \hat{\partial}_\mu + ie\mathcal{A}'_\mu, \tag{2.1.10}$$

$$G_{\mu\nu}(x) \rightarrow G'_{\mu\nu}(x) = U(x)G_{\mu\nu}(x)U^\dagger(x). \tag{2.1.11}$$

Here $U(x)$ satisfies

$$UU^\dagger = 1 \quad \rightarrow \quad 0 = \partial_\mu(UU^\dagger) = (\partial_\mu U)U^\dagger + U\partial_\mu U^\dagger, \tag{2.1.12}$$

$$\det U = 1. \tag{2.1.13}$$

2.1.2 Singular gauge transformation

By using the covariant derivative (2.1.7), the field strength after the SU(2) gauge transformation $G'_{\mu\nu}(x)$ is explicitly computed as

$$\begin{aligned} G'_{\mu\nu} &= \frac{1}{ie} U \left\{ \left[\hat{D}_\mu, \hat{D}_\nu \right] - \left[\hat{\partial}_\mu, \hat{\partial}_\nu \right] \right\} U^\dagger \\ &= \frac{1}{ie} \left\{ U \left[\hat{D}_\mu, \hat{D}_\nu \right] U^\dagger - U \left[\hat{\partial}_\mu, \hat{\partial}_\nu \right] U^\dagger \right\} \\ &= \frac{1}{ie} \left\{ \left[U\hat{D}_\mu U^\dagger, U\hat{D}_\nu U^\dagger \right] - U \left[\hat{\partial}_\mu, \hat{\partial}_\nu \right] U^\dagger \right\} \\ &= \partial_\mu \mathcal{A}'_\nu - \partial_\nu \mathcal{A}'_\mu + ie \left[\mathcal{A}'_\mu, \mathcal{A}'_\nu \right] - \frac{1}{ie} U \left[\partial_\mu, \partial_\nu \right] U^\dagger, \end{aligned} \tag{2.1.14}$$

where we have used

$$\left[\hat{\partial}_\mu, \mathcal{A}'_\nu \right] = \hat{\partial}_\mu \mathcal{A}'_\nu - \mathcal{A}'_\nu \hat{\partial}_\mu = \partial_\mu \mathcal{A}'_\nu + \mathcal{A}'_\nu \hat{\partial}_\mu - \mathcal{A}'_\nu \hat{\partial}_\mu = \partial_\mu \mathcal{A}'_\nu. \tag{2.1.15}$$

It is important to note that if the gauge fixing function $U(x) \in \mathrm{SU}(2)$ is singular, that is $[\partial_\mu, \partial_\nu]U(x) \neq 0$, the last term in (2.1.14) remains. The Abelian gauge fixing is classified into this type.

2.2 Abelian gauge fixing

2.2.1 Diagonalization of gauge dependent variable

We consider some gauge dependent variable $X(x) \in \mathrm{su}(2)^*$

$$X(x) = X^a(x) T^a = \frac{1}{2} \begin{pmatrix} X^3(x) & X^1(x) - iX^2(x) \\ X^1(x) + iX^2(x) & -X^3(x) \end{pmatrix}. \tag{2.2.1}$$

Abelian gauge fixing is defined by the diagonalization of this kind of matrix by using the gauge fixing function $\Omega(x) \in \mathrm{SU}(2)$ as

$$X(x) \to X_d(x) = \Omega(x) X(x) \Omega(x)^\dagger = \begin{pmatrix} \lambda_+(x) & 0 \\ 0 & \lambda_-(x) \end{pmatrix}, \tag{2.2.2}$$

$$\lambda_\pm(x) \equiv \pm \frac{1}{2} \sqrt{X_1^2(x) + X_2^2(x) + X_3^2(x)}. \tag{2.2.3}$$

Here $\lambda_\pm(x)$ represent eigenvalues of $X(x)$. One finds that these eigenvalues degenerate as $\lambda_+(x) = \lambda_-(x)$ when the conditions

$$X_1(x) = X_2(x) = X_3(x) = 0 \tag{2.2.4}$$

*When we represent elements of Lie algebra, we use small characters.

are satisfied. Since each condition describes a three-dimensional surface, the locus where all of them are satisfied will be a world-line in four-dimensional space-time.

Now, the degeneracy point is our main interest. In order to understand the structure of the neighborhood of the degeneracy point, we parametrize the world-line by the proper time τ, and perform the Taylor expansion around a certain point $\boldsymbol{x}_0$ at fixed time t_0. Then we have

$$\begin{aligned} X(x) &= \underbrace{X^a(t_0,\boldsymbol{x}_0)}_{=0} T^a + \partial_i X^a(t_0,\boldsymbol{x}_0)(\boldsymbol{x}-\boldsymbol{x}_0)^i T^a + \underbrace{O((\boldsymbol{x}-\boldsymbol{x}_0)^2)}_{neglected} \\ &= C_i^a(\boldsymbol{x}-\boldsymbol{x}_0)^i T^a, \qquad (C_i^a \equiv \partial_i X^a(\boldsymbol{x}_0)) \,. \end{aligned} \tag{2.2.5}$$

If $\det C \neq 0$, this means that there exists an inverse mapping; So we can define a linear transformation to new coordinates

$$w^a \equiv C_i^a(\boldsymbol{x}-\boldsymbol{x_0})^i. \tag{2.2.6}$$

In terms of these new coordinates w^a, we find the hedgehog configuration near the degeneracy point $\boldsymbol{x}_0$, given by

$$X(w^a) = T^a w^a. \tag{2.2.7}$$

This is the simplest non-trivial solution corresponding to the homotopy group $\pi_2(\mathrm{SU}(2)/\mathrm{U}(1))$ $= \pi_2(S_2) = \boldsymbol{Z}_\infty$. The eigenvalue and the degeneracy point are represented by $\pm\frac{1}{2}\sqrt{w_1^2+w_2^2+w_3^2}$ and $w_1 = w_2 = w_3 = 0$, respectively.

Let us parametrize the new coordinate w_a by polar coordinates as

$$\boldsymbol{w} \equiv (w_1,w_2,w_3) \equiv (r\sin\theta\cos\phi \ , \ r\sin\theta\sin\phi \ , \ r\cos\theta), \tag{2.2.8}$$

then the gauge dependent variable $X(w)$ becomes

$$X(w) = \frac{1}{2}\begin{pmatrix} w_3 & w_1 - iw_2 \\ w_1 + iw_2 & -w_3 \end{pmatrix} = \frac{r}{2}\begin{pmatrix} \cos\theta & e^{-i\phi}\sin\theta \\ e^{i\phi}\sin\theta & -\cos\theta \end{pmatrix}. \tag{2.2.9}$$

Thus, one finds the gauge fixing function $\Omega(w) \in \mathrm{SU}(2)$ in the form

$$\Omega(w) = \begin{pmatrix} e^{i\phi}\cos\frac{\theta}{2} & \sin\frac{\theta}{2} \\ -\sin\frac{\theta}{2} & e^{-i\phi}\cos\frac{\theta}{2} \end{pmatrix} \quad (\equiv \Omega_1(w)). \tag{2.2.10}$$

This gauge fixing matrix $\Omega(w)$ diagonalizes $X(w)$ as

$$X_d = \Omega(w)X(w)\Omega^\dagger(w) = \frac{r}{2}\begin{pmatrix} 1 & 0 \\ 0 & -1 \end{pmatrix} = r\,T^3, \tag{2.2.11}$$

where the gauge dependent variable X has only a T^3 component. In this sense, the gauge degree of freedom in the SU(2) non-Abelian gauge theory is fixed by $\Omega(x)$ up to a remaining

the Abelian gauge symmetry. After this gauge fixing, as is clear from the expression (2.2.11), there remains only the maximal Abelian subgroup of SU(2), that is U(1).

It is worth noting that we have many choices of the Abelian gauge fixing function owing to the residual Abelian gauge symmetry. In fact, instead of $\Omega_1(w)$, it is possible to choose the form

$$\Omega(w) = \begin{pmatrix} \cos\frac{\theta}{2} & e^{-i\phi}\sin\frac{\theta}{2} \\ -e^{i\phi}\sin\frac{\theta}{2} & \cos\frac{\theta}{2} \end{pmatrix} \quad (\equiv \Omega_2(w)). \tag{2.2.12}$$

Here, $\Omega_1(w)$ and $\Omega_2(w)$ are related by the residual Abelian gauge symmetry as

$$\Omega_2 = \begin{pmatrix} e^{-i\phi} & 0 \\ 0 & e^{i\phi} \end{pmatrix} \Omega_1 = e^{-2i\phi T^3}\Omega_1. \tag{2.2.13}$$

By using this matrix $\Omega_2(w)$, one also leads to the equation (2.2.11).

2.2.2 Appearance of magnetic Dirac string

By the Abelian gauge fixing function $\Omega(x)$, the gauge field $\mathcal{A}_\mu(x)$ is transformed as

$$\mathcal{A}_\mu(x) \to \mathcal{A}^\Omega_\mu(x) = \Omega(x)\left(\mathcal{A}_\mu(x) + \frac{1}{ie}\partial_\mu\right)\Omega^\dagger(x). \tag{2.2.14}$$

Now, if the original gauge field $\mathcal{A}_\mu$ is regular, the first term of (2.2.14) is still regular. However, the second term provides a singularity. To confirm the appearance of singularity, let us compute the flux originating from the second term of (2.2.14). The flux is given by the path integral along a closed loop C ; r , $\theta = \text{const.}$, $\phi \in [0, 2\pi)$ as *

$$\begin{aligned} \Phi &\equiv \oint_{\mathrm{C}} dx^\mu \left[\frac{1}{ie}\Omega(x)\partial_\mu\Omega^\dagger(x)\right] \\ &= \oint_{\mathrm{C}} dw^a \left[\frac{1}{ie}\Omega(w)\frac{\partial}{\partial w^a}\Omega^\dagger(w)\right] \\ &= \frac{1}{ie}\int_0^{2\pi} d\phi\, \Omega(w)\,\frac{\partial}{\partial\phi}\,\Omega^\dagger(w), \end{aligned} \tag{2.2.15}$$

where we have used the form of $\partial/\partial w^a$ in the polar coordinate,

$$\frac{\partial}{\partial w^a} = \frac{\partial}{\partial r}\boldsymbol{e}_r + \frac{1}{r}\frac{\partial}{\partial\theta}\boldsymbol{e}_\theta + \frac{1}{r\sin\theta}\frac{\partial}{\partial\phi}\boldsymbol{e}_\phi. \tag{2.2.16}$$

*This is related to the surface integral of the field strength $\partial_\mu\mathcal{A}^\Omega_\nu - \partial_\nu\mathcal{A}^\Omega_\mu$ through the Stokes theorem. Here, we do not take into account other terms in the field strength tensor: $[\mathcal{A}^\Omega_\mu, \mathcal{A}^\Omega_\nu]$ and $\Omega[\partial_\mu, \partial_\nu]\Omega^\dagger$ [See, Eq. (2.1.14)], which play important roles when we discuss the Abelian projection.

Inserting $\Omega = \Omega_1$, the flux is explicitly calculated as

$$\begin{aligned}\Phi &\equiv \frac{1}{ie}\int_0^{2\pi} d\phi\, \Omega_1(w)\,\frac{\partial}{\partial\phi}\,\Omega_1^\dagger(w) \\ &= \frac{1}{ie}\int_0^{2\pi} d\phi \begin{pmatrix} e^{i\phi}\cos\frac{\theta}{2} & \sin\frac{\theta}{2} \\ -\sin\frac{\theta}{2} & e^{-i\phi}\cos\frac{\theta}{2} \end{pmatrix} \frac{\partial}{\partial\phi} \begin{pmatrix} e^{-i\phi}\cos\frac{\theta}{2} & -\sin\frac{\theta}{2} \\ \sin\frac{\theta}{2} & e^{i\phi}\cos\frac{\theta}{2} \end{pmatrix} \\ &= -\frac{4\pi}{e}\cos^2\frac{\theta}{2}T^3 \equiv \Phi_1(\theta). \end{aligned} \tag{2.2.17}$$

We find that this gives non-zero contribution even in the case that the closed path C is shrunk to one point, that is $\theta = 0$,

$$\Phi_1(\theta = 0) = -\frac{4\pi}{e}T^3. \tag{2.2.18}$$

On the other hand, for $\theta = \pi$, this flux vanishes. That is to say, along the axis at $\theta = 0$ there exists the flux expressed by the delta-function type, which implies the existence of the "Dirac string." Rewriting (2.2.17) as

$$\begin{aligned}\Phi_1(\theta) &= -\frac{4\pi}{e}\frac{(1+\cos\theta)}{2}T^3 \\ &= -\frac{4\pi}{e}T^3 + \frac{4\pi}{e}T^3\left(\frac{1-\cos\theta}{2}\right)T^3, \end{aligned} \tag{2.2.19}$$

one can recognize that the first term and the second term correspond to the flux which are originating from the "magnetic monopole" with the magnetic charge $4\pi/e = g$ and the "magnetic Dirac string," respectively. Here an interesting relation, $eg = 4\pi$, appears, which is the so-called Dirac quantization condition for the magnetic monopoles. This quantization condition guarantees the unobservability of the magnetic Dirac string whenever the Abelian gauge symmetry is not broken.

It is interesting to compare with $\Omega = \Omega_2$. In this case the flux is calculated similarly as

$$\Phi_2(\theta) = \frac{4\pi}{e}T^3 - \frac{4\pi}{e}\left(\frac{1+\cos\theta}{2}\right)T^3. \tag{2.2.20}$$

Here, the role of the first term and the second term are the same as the previous discussion. However, it should be noted that in this case the flux has non-vanishing value along the axis at $\theta = \pi$, which means that the direction of the magnetic Dirac string is different from previous case. In this sense, one can say that the position of the Dirac string can be varied by the residual Abelian gauge transformation. The direction of the Dirac string is defined by the sign of the charge e or g. If we define as $e > 0$ ($e < 0$), the flux of the Dirac string is absorbed (emitted) by the magnetic monopole (anti-monopole) [See, Fig. 2.1]

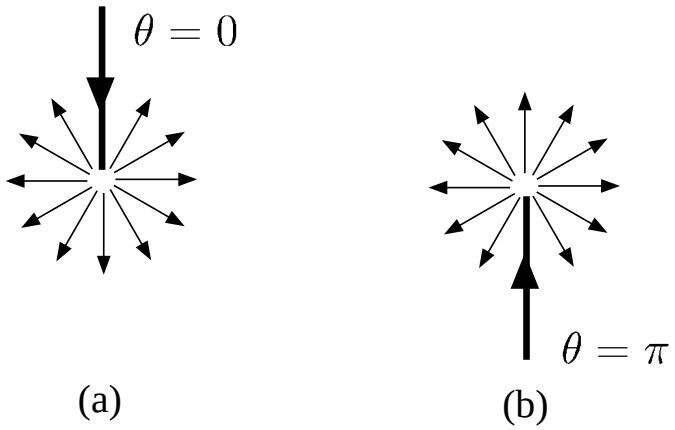

Figure 2.1: The direction of the color-magnetic Dirac string for the Abelian gauge fixing function (a) $\Omega_1(w)$ and (b) $\Omega_2(w)$.

2.3 Abelian projection

In the previous section, we have shown that the SU(2) gauge theory contains monopole-like singularities in the Abelian gauge. Our next task is to "extract" these singularities as monopoles. To do this, it is essential to adopt the Abelian projection method, which reduces the non-Abelian gauge theory into an Abelian gauge theory. The resulting Abelian gauge theory contains Abelian magnetic monopoles as additional degrees of freedom.

2.3.1 Abelian gauge transformation of the gauge field

In order to extract the Abelian gauge field from the theory after the Abelian gauge fixing, we perform the Abelian gauge transformation. Let $\mathcal{A}_\mu^\Omega$ be the gauge field after the Abelian gauge fixing as given in Eq. (2.2.14). Using the Cartan decomposition as

$$C_\mu^\Omega \equiv \frac{1}{\sqrt{2}}\left(\mathcal{A}_\mu^{\Omega 1} + i\mathcal{A}_\mu^{\Omega 2}\right), \quad E \equiv \frac{1}{\sqrt{2}}\left(T^1 + iT^2\right), \tag{2.3.1}$$

we write the gauge field $\mathcal{A}_\mu^\Omega$ as

$$\mathcal{A}_\mu^\Omega = \mathcal{A}_\mu^{\Omega a} T^a = \mathcal{A}_\mu^{\Omega 3} T^3 + C_\mu^\Omega E^\dagger + C_\mu^{\Omega *} E, \tag{2.3.2}$$

where the diagonal part and the off-diagonal part are exposed. Let us perform the Abelian gauge transformation by making use of $d(x) \in \mathrm{U}(1)_3$,

$$d(x) \equiv e^{ie\theta(x)T^3} = \begin{pmatrix} e^{ie\frac{\theta}{2}} & 0 \\ 0 & e^{-ie\frac{\theta}{2}} \end{pmatrix}. \tag{2.3.3}$$

Then, one finds the following transformation:

$$\begin{aligned} \mathcal{A}_\mu^\Omega \to \mathcal{A}_\mu^{\Omega d} &= d\left(\mathcal{A}_\mu^\Omega + \frac{1}{ie}\partial_\mu\right) d^\dagger \\ &= (\mathcal{A}_\mu^{\Omega 3} - \partial_\mu\theta)T^3 + e^{-ie\theta}C_\mu^\Omega E^\dagger + e^{ie\theta}C_\mu^{\Omega *}E. \end{aligned} \tag{2.3.4}$$

This suggests that the off-diagonal gluon parts C_μ^Ω and $C_\mu^{\Omega *}$ become charged matter fields and lose the property of a gauge field. Only the diagonal gluon $A_\mu^{\Omega 3}$ still behaves as an Abelian gauge field. Here, we have used the relation

$$[T^3, E] = E, \quad [T^3, E^\dagger] = -E^\dagger, \tag{2.3.5}$$

$$e^A B e^{-A} = B + [A, B] + \frac{1}{2!}[A, [A, B]] + \cdots. \tag{2.3.6}$$

Now, we have found which is the Abelian gauge field in terms of the residual Abelian gauge symmetry. Following the Abelian dominance hypothesis as a low-energy property of the non-Abelian gauge theory in a suitable Abelian gauge, we extract only the Abelian gauge field by dropping* the charged matter fields C_μ^Ω and $C_\mu^{\Omega *}$. This is the step of Abelian projection. Only the diagonal component of the gauge field defined by

$$\mathcal{A}_\mu^\Omega = \mathcal{A}_\mu^{\Omega 3}T^3 = \mathrm{tr}(\tau^3\mathcal{A}_\mu^\Omega)T^3 = \mathrm{tr}\left\{\tau^3\Omega\left(\mathcal{A}_\mu + \frac{1}{ie}\partial_\mu\right)\Omega^\dagger\right\}T^3 \tag{2.3.7}$$

is taken into account. The field strength tensor of the SU(2) gauge theory is then written as

$$\begin{aligned} G_{\mu\nu}^\Omega &= \partial_\mu\mathcal{A}_\nu^\Omega - \partial_\nu\mathcal{A}_\mu^\Omega + ie\underbrace{[\mathcal{A}_\mu^\Omega, \mathcal{A}_\nu^\Omega]}_{neglected} - \frac{1}{ie}\Omega[\partial_\mu, \partial_\nu]\Omega^\dagger \\ &= \partial_\mu\mathcal{A}_\nu^\Omega - \partial_\nu\mathcal{A}_\mu^\Omega - \frac{1}{ie}\Omega[\partial_\mu, \partial_\nu]\Omega^\dagger. \end{aligned} \tag{2.3.8}$$

It should be noted that we drop the off-diagonal gluon part after the Abelian gauge fixing, never before one. Since the Abelian gauge fixing is, of course, among the non-Abelian gauge transformations, the diagonal and off-diagonal components of the gauge field can mix each other. In other words, the gauge field which is finally aligned with the T^3 direction is originally spanned by all of the SU(2) generators T^1, T^2, and T^3.

2.3.2 Abelian field strength tensor

The Abelian component of the field strength tensor can be extracted multiplying by $\tau^3 = 2T^3$ and taking the trace. Then, after the Abelian projection the field strength tensor $F_{\mu\nu}$ is given

*In principle, these charged matter fields should be integrated out [56].

by

$$F_{\mu\nu} = \mathrm{tr}\left[\tau^3 G^{\Omega}_{\mu\nu}\right] = \mathrm{tr}\left[\tau^3\left(\partial_\mu \mathcal{A}^{\Omega}_{\nu} - \partial_\nu \mathcal{A}^{\Omega}_{\mu} - \frac{1}{ie}\Omega[\partial_\mu, \partial_\nu]\Omega^\dagger\right)\right]$$
$$= \partial_\mu A_\nu - \partial_\nu A_\mu - \frac{1}{ie}\mathrm{tr}\left[\tau^3 \Omega[\partial_\mu, \partial_\nu]\Omega^\dagger\right], \tag{2.3.9}$$

where we have defined the "Abelian gauge field" as

$$A_\mu \equiv \mathrm{tr}(\tau^3 \mathcal{A}^{\Omega}_{\mu}) = \mathrm{tr}\left\{\tau^3 \Omega\left(\mathcal{A}_\mu + \frac{1}{ie}\partial_\mu\right)\Omega^\dagger\right\}. \tag{2.3.10}$$

Here, if the field strength tensor $F_{\mu\nu}$ is regular, as evidence of this, the following Bianchi identity is satisfied:

$$\partial^*_\mu F^{\mu\nu} = 0, \qquad {}^*F^{\mu\nu} \equiv \frac{1}{2}\varepsilon^{\mu\nu\alpha\beta}F_{\alpha\beta}. \tag{2.3.11}$$

However, the last term in Eq. (2.3.9) breaks the Bianchi identity, which means that a magnetic current $k_\mu \neq 0$ appears. In what follows, we see this mechanism more precisely.

We introduce "auxiliary Higgs-like fields" $\hat{\phi}^a$ $(a = 1, 2, 3)$, defined by using the Abelian gauge fixing function Ω:

$$\hat{\phi}^a \tau^a \equiv \Omega^\dagger \tau^3 \Omega. \tag{2.3.12}$$

One finds that $\hat{\phi}^a$ have the following properties:

$$\sum_{a=1}^{3} \hat{\phi}^{a\,2} = 1, \tag{2.3.13}$$

$$\partial_\mu(\hat{\phi}^a \tau^a) = -[L_\mu, \hat{\phi}^a \tau^a], \tag{2.3.14}$$

$$L_\mu \equiv \Omega^\dagger \partial_\mu \Omega. \tag{2.3.15}$$

In general, the explicit form of ϕ^a depends on the choice of Abelian gauge fixing function $\Omega(w)$. For instance, for $\Omega_1(w)$ or $\Omega_2(w)$ this ϕ^a takes the form

$$\phi^a = (\sin\theta\cos\varphi,\ \sin\theta\sin\varphi,\ \cos\theta), \tag{2.3.16}$$

which parametrizes the simplest hedgehog configuration of monopole. In this case, the relation (2.3.13) is trivial. Here, L_μ itself leads to the relation

$$\partial_\mu L_\nu - \partial_\nu L_\mu + [L_\mu, L_\nu] = \Omega^\dagger[\partial_\mu, \partial_\nu]\Omega \neq 0, \tag{2.3.17}$$

which corresponds to the breaking of the Maurer-Cartan formula $(dL + L \wedge L = 0)$.

By virtue of the relations (2.3.13), (2.3.14), (2.3.15) and (2.3.17), the Abelian gauge field A_μ can be written as

$$A_\mu = \hat{\phi}^a \mathcal{A}^a_\mu - \frac{1}{ie}\mathrm{tr}[\hat{\phi}^a \tau^a L_\mu]. \tag{2.3.18}$$

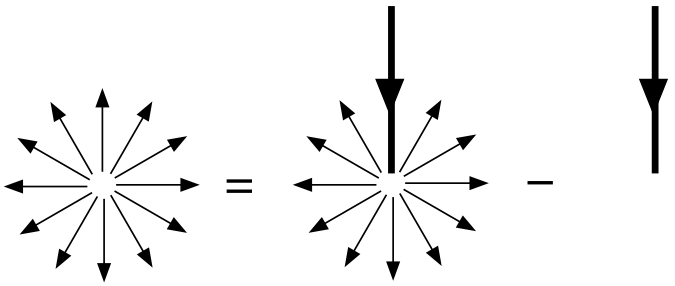

$$F_{\mu\nu} \quad = \quad \partial_\mu A_\nu - \partial_\nu A_\mu \quad - \quad \frac{1}{ie}\mathrm{tr}\left[\tau^3 \Omega[\partial_\mu, \partial_\nu]\Omega^\dagger\right]$$

Figure 2.2: The cancellation of the color-magnetic Dirac string in the Abelian field strength obtained by the Abelian projection method.

Then, we also have the relation

$$\partial_\mu A_\nu - \partial_\nu A_\mu = \partial_\mu(\hat{\phi}^a \mathcal{A}^a_\nu) - \partial_\nu(\hat{\phi}^a \mathcal{A}^a_\mu) - \frac{1}{e}\epsilon^{abc}\hat{\phi}^a \partial_\mu \hat{\phi}^b \partial_\nu \hat{\phi}^c + \frac{1}{ie}\mathrm{tr}\left[\tau^3 \Omega[\partial_\mu, \partial_\nu]\Omega^\dagger\right], \quad (2.3.19)$$

which leads to the Abelian field strength tensor

$$F_{\mu\nu} = \partial_\mu(\hat{\phi}^a \mathcal{A}^a_\nu) - \partial_\nu(\hat{\phi}^a \mathcal{A}^a_\mu) - \frac{1}{e}\epsilon^{abc}\hat{\phi}^a \partial_\mu \hat{\phi}^b \partial_\nu \hat{\phi}^c. \quad (2.3.20)$$

The last term resembles the 't Hooft-Polyakov tensor used in the discussion of the 't Hooft-Polyakov monopole in the Georgi-Glashow model [57, 58]. We find that the non-commutable term of the derivative in (2.3.19) is "exactly" canceled by the same term in (2.3.9) [See, Fig. 2.2]. This corresponds to the cancellation of the magnetic Dirac string. One finds that the Abelian field strength tensor $F_{\mu\nu}$ can be defined without the magnetic Dirac string. Due to this fact, we can safely define the magnetic charge of the monopole.

Here, by inserting the explicit form of $\Omega(w)$, one can easily confirm that the non-commutable term of the derivative is nothing but the magnetic Dirac string. In fact, if we use $\Omega(w) = \Omega_1(w)$, we get

$$\frac{1}{ie}\mathrm{tr}\left[\tau^3 \Omega_1[\partial_\mu, \partial_\nu]\Omega_1^\dagger\right] = -\frac{4\pi}{e}\epsilon_{\mu\nu}\theta(z)\delta(x)\delta(y)\hat{\phi}^3 = -\frac{4\pi}{e}\epsilon_{\mu\nu}\theta(z)\delta(x)\delta(y). \quad (2.3.21)$$

For another form of Abelian gauge fixing function Ω_2, we have

$$\frac{1}{ie}\mathrm{tr}\left[\tau^3 \Omega_2[\partial_\mu, \partial_\nu]\Omega_2^\dagger\right] = -\frac{4\pi}{e}\epsilon_{\mu\nu}\theta(-z)\delta(x)\delta(y)\hat{\phi}^3 = +\frac{4\pi}{e}\epsilon_{\mu\nu}\theta(-z)\delta(x)\delta(y), \quad (2.3.22)$$

where $\epsilon_{\mu\nu}$ denotes $\epsilon_{12} = -\epsilon_{21} = 1$, $\epsilon_{11} = \epsilon_{22} = 0$. The relation $\phi^3 = \cos\theta$ in (2.3.16) is used. Note that the direction of the Dirac string coincides with the singular flux discussed in the subsection 2.2.2.

2.3.3 Breaking of the Abelian Bianchi identity and monopole current

Due to the presence of the last term in (2.3.20), we have the equation

$$\begin{aligned} \partial_\mu {}^*F^{\mu\nu} &= \partial_\mu \frac{1}{2}\epsilon^{\mu\nu\rho\sigma}F_{\rho\sigma} \\ &= -\frac{1}{2e}\epsilon^{\mu\nu\rho\sigma}\epsilon^{abc}\partial_\mu(\hat{\phi}^a\partial_\rho\hat{\phi}^b\partial_\sigma\hat{\phi}^c) \quad \equiv k^\nu \neq 0, \end{aligned} \tag{2.3.23}$$

where the current of the Abelian magnetic monopole k^μ appears. Of course, the Abelian Bianchi identity is now broken. More explicitly, one can calculate the the magnetic charge of the monopole g by considering the spatial integral of k^0 as

$$k^0 = -\frac{1}{2e}\epsilon^{\mu 0\rho\sigma}\epsilon^{abc}\partial_\mu(\hat{\phi}^a\partial_\rho\hat{\phi}^b\partial_\sigma\hat{\phi}^c) = \frac{1}{2e}\epsilon^{ijk}\epsilon^{abc}\partial_i(\hat{\phi}^a\partial_j\hat{\phi}^b\partial_k\hat{\phi}^c). \tag{2.3.24}$$

Thus, the magnetic charge g is calculated as

$$\begin{aligned} g &= \int_{V^{(\mathrm{phys})}} d^3x k^0 \\ &= \frac{1}{2e}\int_{V^{(\mathrm{phys})}} d^3x \partial_i \left(\epsilon^{ijk}\epsilon^{abc}\hat{\phi}^a\partial_j\hat{\phi}^b\partial_k\hat{\phi}^c\right) \\ &= \frac{1}{2e}\oint_{\partial V^{(\mathrm{phys})}(=S_2^{(\mathrm{phys})})} dS_i\epsilon^{ijk}\epsilon^{abc}\hat{\phi}^a\partial_j\hat{\phi}^b\partial_k\hat{\phi}^c \\ &= \frac{1}{2e}\oint_{\partial V^{(\mathrm{int})}(=S_2^{(\mathrm{int})})} \epsilon^{abc}\hat{\phi}^a d\hat{\phi}^b\wedge d\hat{\phi}^c, \end{aligned} \tag{2.3.25}$$

where $dS_1 = dx_2\wedge dx_3$, $dS_2 = dx_3\wedge dx_1$, and $dS_3 = dx_1\wedge dx_2$. By making use of the parametrization of ϕ^a in (2.3.16), we finally get

$$g = \frac{1}{2e}\int_0^\pi d\theta\int_0^{2\pi} d\varphi\, 2\sin\theta = \frac{1}{2e}\cdot 8\pi = \frac{4\pi}{e}. \tag{2.3.26}$$

This is the magnetic charge of the monopole for the simplest hedgehog configuration. In general, the parametrization of (2.3.16) can be more complicated due to another choice of the Abelian gauge fixing function Ω [See, Eq. (2.3.12)]. In such case, we have the generalized relation

$$n = \frac{1}{8\pi}\oint_{\partial V^{(\mathrm{int})}(=S_2)} \epsilon^{abc}\hat{\phi}^a d\hat{\phi}^b\wedge d\hat{\phi}^c, \tag{2.3.27}$$

where n is an integer characterizing the homotopy class of the mapping $S_2^{(\mathrm{phys})}\to S_2^{(\mathrm{int})}$: $\pi_2(\mathrm{SU}(2)/\mathrm{U}(1)) = \pi_2(S_2) = \boldsymbol{Z}_\infty$. This integer is nothing but the covering (winding) number counting how often the mapping from one one sphere is wrapped around the other sphere. Thus, we have the generalized Dirac quantization condition for the magnetic monopoles

$$eg = 4\pi n. \tag{2.3.28}$$

To summarize, the Abelian projection after some Abelian gauge fixing reduce the non-Abelian gauge theory into an Abelian gauge theory including magnetic monopoles.

2.4 Dual Abelian Higgs model

In this section we construct the dual Abelian Higgs (DAH) model based on the Abelian field strength tensor obtained by the Abelian projection method. In the previous section, we have obtained monopole currents as a result of the Abelian projection [12] assuming Abelian dominance [13]. Now, we imagine that the complicated cluster of monopole currents in four-dimensional space-time leads to a nontrivial vacuum, where color confinement takes place*. This situation can be regarded as monopoles condensation analogous to the Cooper pair condensation in the ordinary superconductor. Indeed, this dual superconducting picture of the vacuum is numerically supported by the recent studies of lattice gauge theory in the maximally Abelian gauge [17–31].

2.4.1 Path-integral duality transformation

We know that the Abelian field strength tensor derived from SU(2) gluodynamics in the Abelian projection has the form (2.3.9),

$$F_{\mu\nu} = (\partial \wedge A)_{\mu\nu} + g\Sigma^{\rm M}_{\mu\nu}, \tag{2.4.1}$$

where $(\partial \wedge A)_{\mu\nu} \equiv \partial_\mu A_\nu - \partial_\nu A_\mu$, which satisfies the Bianchi identity $\partial_\mu {}^*(\partial \wedge A)_{\mu\nu} = 0$. We have defined $\Sigma^{\rm M}_{\mu\nu}$ as

$$\begin{aligned} g\Sigma^{\rm M}_{\mu\nu} &\equiv -\frac{1}{ie}{\rm tr}\left[\tau^3 \Omega[\partial_\mu, \partial_\nu]\Omega^\dagger\right] \\ &= g\int_{\Sigma^{\rm M}} \varepsilon_{\mu\nu\alpha\beta} d\sigma^{\rm M}_{\alpha\beta}(\bar{x}(\xi))\delta(x - \bar{x}(\xi)). \end{aligned} \tag{2.4.2}$$

The last expression means that the string singularity is represented as a nonlocal term. Note that when the Dirac string is a straight line, this nonlocal term is explicitly written by using a constant four-vector n_μ, describing the direction of the string, as

$$\begin{aligned} g\Sigma^{\rm M}_{\mu\nu} &= \int d^4y \langle x|\frac{1}{n\cdot\partial}|y\rangle \varepsilon_{\mu\nu\alpha\beta} n_\alpha k_\beta(y) \\ &\equiv \frac{1}{n\cdot\partial}\varepsilon_{\mu\nu\alpha\beta} n_\alpha k_\beta, \end{aligned} \tag{2.4.3}$$

where $\langle x|\frac{1}{n\cdot\partial}|y\rangle$ is the kernel which satisfies the equation

$$(n\cdot\partial)_x \langle x|\frac{1}{n\cdot\partial}|y\rangle = \delta^{(4)}(x-y). \tag{2.4.4}$$

This solution is found to be

$$\langle x|\frac{1}{n\cdot\partial}|y\rangle = \left[p\theta((x-y)\cdot n) - (1-p)\theta((y-x)\cdot n)\right]\delta^{(3)}(\vec{x}_\perp - \vec{y}_\perp). \tag{2.4.5}$$

*An example of a cluster of monopole currents is shown in Fig. 5.2, where the lattice formalism is adopted.

Here p is an arbitrary real number and $\delta^{(3)}(x)$ is the δ-function defined on a three dimensional hyper-surface which has the normal vector n_μ, so that $\vec{x}_\perp$ and $\vec{y}_\perp$ are three-vectors (generically not spatial) which are perpendicular to n_μ. Factorizing the magnetic charge from the current as $k_\mu = \frac{4\pi}{e}\hat{k}_\mu = g\hat{k}_\mu$, we have the relation

$$\Sigma^{\mathrm{M}}_{\mu\nu} = \frac{1}{n\cdot\partial}\varepsilon_{\mu\nu\alpha\beta}n_\alpha\hat{k}_\beta. \tag{2.4.6}$$

In any case, the term $g\Sigma^{\mathrm{M}}_{\mu\nu}$ breaks the Bianchi identity as

$$g\partial_\mu {}^*\Sigma^{\mathrm{M}}_{\mu\nu} = \frac{g}{2}\varepsilon_{\mu\nu\lambda\rho}\partial_\mu\Sigma^{\mathrm{M}}_{\lambda\rho} = k_\nu, \tag{2.4.7}$$

where the star " * " denotes the dual quantity.

Now, we come back to the action of SU(2) gluodynamics after the Abelian projection, which has the form

$$S_{\mathrm{AP-SU(2)}}[A_\mu, j_\mu, \Sigma^{\mathrm{M}}_{\mu\nu}] = \int d^4x \left\{ \frac{1}{4}\left((\partial\wedge A)_{\mu\nu} + g\Sigma^{\mathrm{M}}_{\mu\nu}\right)^2 + iA_\mu j_\mu \right\}, \tag{2.4.8}$$

where $j_\mu = \frac{e}{2}\bar{q}\gamma_\mu q$ is the Abelian electric current, which is treated as an external source. The factor 1/2, the weight of the SU(2) algebra, comes from the projection $\mathrm{tr}(T^3T^3) = 1/2$. Due to this fact, again we would like to mention that the Dirac quantization condition for the fundamental charge is given by $\frac{e}{2}g = 2\pi$. Thus, the resulting partition function is written as

$$\mathcal{Z} = \int \mathcal{D}A_\mu \mathcal{D}j_\mu \mathcal{D}\Sigma^{\mathrm{M}}_{\mu\nu} \exp\left\{ -S_{\mathrm{AP-SU(2)}}[A_\mu, j_\mu, \Sigma^{\mathrm{M}}_{\mu\nu}] \right\}. \tag{2.4.9}$$

Here, we adopt the first-order formalism to achieve the duality transformation of the effective action [59]. During this step, the monopole currents naturally appears in the action as dynamical variables which couple to the "dual gauge field." In contrast to Zwanziger's formulation [60], this approach enables us to directly connect the Abelian-projected theory with its dual form [61].

First, we introduce an auxiliary antisymmetric tensor $B_{\mu\nu}$ through the identity

$$\exp\left\{ -\frac{1}{4}\int d^4x (\partial\wedge A)^2_{\mu\nu} \right\} = \int \mathcal{D}B_{\mu\nu} \exp\left\{ -\frac{1}{4}\int d^4x \left(B^2_{\mu\nu} + 2i^* B_{\mu\nu}(\partial\wedge A)_{\mu\nu} \right) \right\}. \tag{2.4.10}$$

Inserting this into the partition function, we get

$$\begin{aligned}
\mathcal{Z} &= \int \mathcal{D}A_\mu \mathcal{D}j_\mu \mathcal{D}\Sigma^{\mathrm{M}}_{\mu\nu} \mathcal{D}B_{\mu\nu} \\
&\quad \times \exp\left[-\int d^4x \left\{ \frac{1}{4}\left(B^2_{\mu\nu} + 2i^* B_{\mu\nu}(\partial\wedge A)_{\mu\nu} + 2g\Sigma^{\mathrm{M}}_{\mu\nu}(\partial\wedge A)_{\mu\nu} + (g\Sigma^{\mathrm{M}}_{\mu\nu})^2 \right) + iA_\mu j_\mu \right\} \right] \\
&= \int \mathcal{D}A_\mu \mathcal{D}j_\mu \mathcal{D}\Sigma^{\mathrm{M}}_{\mu\nu} \mathcal{D}B_{\mu\nu} \\
&\quad \times \exp\left[-\int d^4x \left\{ \frac{1}{4}B^2_{\mu\nu} + \frac{1}{4}(g\Sigma^{\mathrm{M}}_{\mu\nu})^2 - i\left(\partial_\mu {}^* B_{\mu\nu} - ig\partial_\mu \Sigma^{\mathrm{M}}_{\mu\nu} - j_\nu \right) A_\nu \right\} \right].
\end{aligned} \tag{2.4.11}$$

We can integrate over the Abelian gauge field A_μ, which leads to a delta-function in the measure

$$\delta\left(\partial_\mu {}^*B_{\mu\nu} - ig\partial_\mu \Sigma^{\rm M}_{\mu\nu} - j_\mu\right). \tag{2.4.12}$$

This resolution then has the form

$$B_{\mu\nu} = (\partial \wedge B)_{\mu\nu} + ig^*\Sigma^{\rm M}_{\mu\nu} + \frac{e}{2}\Sigma^{\rm E}_{\mu\nu}, \tag{2.4.13}$$

where the dual gauge field " B_μ " is naturally introduced. Here, we have introduced the "electric" Dirac string $\Sigma^{\rm E}_{\mu\nu}$, which satisfies the equation

$$\frac{e}{2}\partial_\mu {}^*\Sigma^{\rm E}_{\mu\nu} = j_\nu. \tag{2.4.14}$$

This $\Sigma^{\rm E}_{\mu\nu}$ can be represented in a analogous form to Eq. (2.4.2) as

$$\Sigma^{\rm E}_{\mu\nu} \equiv \int_{\Sigma^{\rm E}} \varepsilon_{\mu\nu\alpha\beta} d\sigma^{\rm E}_{\alpha\beta}(\bar{x}(\eta))\delta(x - \bar{x}(\eta)). \tag{2.4.15}$$

For the straight electric Dirac string, we have the more explicit expression

$$\Sigma^{\rm E}_{\mu\nu} = \frac{1}{n\cdot\partial}\varepsilon_{\mu\nu\alpha\beta} n_\alpha \hat{j}_\beta, \tag{2.4.16}$$

where we have denoted $\frac{e}{2}\hat{j}_\mu = j_\mu$. Similar to the definition of the magnetic charge in the above discussion, the Eq. (2.4.14) can be considered as the breaking of the "dual" Bianchi identity, which is indeed necessary to define the "electric" charge in the dual world. We get the following expression after the integration of $B_{\mu\nu}$,

$$\begin{aligned}
\mathcal{Z} &= \int \mathcal{D}\Sigma^{\rm E}_{\mu\nu}\mathcal{D}\Sigma^{\rm M}_{\mu\nu}\mathcal{D}B_\mu \exp\left[-\int d^4x \left\{\frac{1}{4}\left((\partial\wedge B)_{\mu\nu} + \frac{e}{2}\Sigma^{\rm E}_{\mu\nu}\right)^2 - ik_\mu B_\mu + i\pi^*\Sigma^{\rm M}_{\mu\nu}\Sigma^{\rm E}_{\mu\nu}\right\}\right] \\
&= \left\langle \int \mathcal{D}\Sigma^{\rm E}_{\mu\nu}\mathcal{D}B_\mu \exp\left[-\int d^4x \left\{\frac{1}{4}\left((\partial\wedge B)_{\mu\nu} + \frac{e}{2}\Sigma^{\rm E}_{\mu\nu}\right)^2 - ik_\mu B_\mu\right\}\right]\right\rangle_{k_\mu},
\end{aligned} \tag{2.4.17}$$

where we have used the equation (2.4.7), and accordingly, the dual gauge field B_μ couples to monopole currents k_μ. One finds that the square term of $\Sigma^{\rm M}_{\mu\nu}$ is exactly cancelled. The integration over $\Sigma^{\rm M}_{\mu\nu}$ is written as a certain average of the monopole currents denoted as $\langle\cdots\rangle_{k_\mu}$. It is interesting to note that the last term in the first line ${}^*\Sigma^{\rm M}_{\mu\nu}\Sigma^{\rm E}_{\mu\nu}$ represent the "linking" between the electric sector and the magnetic sector, which counts the number how many times the electric Dirac string are linked by the magnetic Dirac string. This term is explicitly written by using (2.4.2) and (2.4.15) as

$$\int d^4x i\pi^*\Sigma^{\rm M}_{\mu\nu}\Sigma^{\rm E}_{\mu\nu} = 2\pi i\varepsilon_{\mu\nu\alpha\beta}\int_{\Sigma^{\rm M}} d\sigma^{\rm M}_{\mu\nu}(\bar{x}(\xi))\int_{\Sigma^{\rm E}} d\sigma^{\rm E}_{\alpha\beta}(\bar{x}(\eta))\delta(\bar{x}(\xi) - \bar{x}(\eta)) = 2\pi i L, \tag{2.4.18}$$

where L is the linking number (integer). Then, this term does not influence $\mathcal{Z}$ as long as the Dirac quantization condition is satisfied.

2.4.2 Ensemble of monopole currents

Now, we assume that the monopole currents are distributed in a complicated way forming long range loops in four-dimensional space-time, which we call a clustering of monopole currents. Since one monopole current itself forms a closed loop, it can be parametrized as

$$k_\mu(x) = g\sum_{n=1}^{N}\oint_{\partial\Sigma^{\mathrm{M}}} dx_\mu^{(n)}(s)\delta(x-x^{(n)}(s)), \tag{2.4.19}$$

where $x^{(n)}(s)$ parametrizes the world line of n-th monopole trajectory in four-dimensional space-time. Then, the complicated clustering of monopole currents would be described by the "grand canonical ensemble" of these closed monopole loops, which leads to the expression

$$\begin{aligned}\left\langle \exp\left[i\int d^4x k_\mu B_\mu\right]\right\rangle_{k_\mu} &= \sum_{N=0}^{\infty}\frac{1}{N!}\prod_{l=1}^{N}\left[\int_0^\infty \frac{ds_l}{s_l}\exp(-s_l M^2)\oint \mathcal{D}x^{(l')}(s_l')\right] \\ &\quad\times\exp\left[\sum_{l=1}^{N}\int_0^{s_l} ds_l'\left(-\frac{1}{4}\dot{x}^{(l')\,2}(s_l')+ig\dot{x}_\mu^{(l')}(s_l')B_\mu(x^{(l')}(s_l'))\right)\right. \\ &\quad\left.-\lambda\sum_{l,k=1}^{N}\int_0^{s_l} ds_l'\int_0^{s_k} ds_k''\delta[x^{(l')}(s_l')-x^{(k'')}(s_k'')]\right],\end{aligned} \tag{2.4.20}$$

where $x_\mu^{(l')}(s_l')$ parametrizes one closed loop of monopole current. As shown in Refs. [16, 59], this partition function can be rewritten as the partition function of the well-known dual Abelian Higgs model, which describes the dynamics of the dual gauge field B_μ coupled to a complex scalar monopole field χ

$$\begin{aligned}\mathcal{Z} &= \int \mathcal{D}\Sigma_{\mu\nu}^{\mathrm{E}}\mathcal{D}B_\mu\mathcal{D}\chi\mathcal{D}\chi^* \\ &\quad\times\exp\left[-\int d^4x\left\{\frac{1}{4}\left((\partial\wedge B)_{\mu\nu}+\frac{e}{2}\Sigma_{\mu\nu}^{\mathrm{E}}\right)^2+|(\partial_\mu+igB_\mu)\chi|^2+\lambda(|\chi|^2-v^2)^2\right\}\right],\end{aligned} \tag{2.4.21}$$

where M^2 is represented as $M^2=-2\lambda v^2$. If $\lambda<0$, which means $M^2>0$, the monopole loop density is suppressed by the factor $\exp(-s_lM^2)$. On the other hand, if $\lambda>0$ (*i.e.* $M^2<0$), infinitely long monopole loops can appear. The delta function in Eq. (2.4.20) representing the short-range (repulsive) interaction between monopole currents plays an important role to keep the monopole loop density finite, which leads to the self-interaction term of the monopole field ($\lambda\chi^4$). This situation is described as monopole condensation. In a view point from the lattice formulation [15], M^2 can be regarded as the free energy of the system written in the form $M^2=\alpha-\ln(2D-1)$, where α is the monopole self-energy and D the dimension of the system, then $\ln(2D-1)$ represents the entropy of the system (The factor $2D-1$ comes from that the monopole-current system can be regarded as a self-avoiding random walk system.).

Hence, one understands that the sign of λ is related to the valance of energy-entropy of the monopole-current system. In this case, $\lambda < 0$ ($\lambda > 0$) corresponds to the energy (entropy) dominant system.

2.5 Summary and outlook

In this chapter, we have obtained the dual Abelian Higgs (DAH) model as an infrared effective model of the SU(2) gluodynamics based on mainly 't Hooft's Abelian projection and the path-integral duality transformation. The resulting DAH action has the form

$$S_{\rm DAH}[B, \Sigma^{\rm E}, \chi, \chi^*] = \int d^4x \left\{ \frac{1}{4} \left((\partial \wedge B)_{\mu\nu} + \frac{e}{2} \Sigma^{\rm E}_{\mu\nu} \right)^2 + |(\partial_\mu + igB_\mu)\chi|^2 + \lambda(|\chi|^2 - v^2)^2 \right\}. \tag{2.5.1}$$

In the following chapter, we mainly study this DAH model, its classical properties by investigating the DAH action (chapter 3) and the effects of the corresponding quantum theory by studying the partition function of the DAH model (chapter 4). The quantum effects are studied by means of the Monte Carlo simulation on the "dual lattice." The parameter fixing of the DAH model will be attempted from SU(2) gluodynamics (chapter 5). The extension to SU(3) gluodynamics is straightforward, which will be addressed in chapter 6.

Chapter 3

Classical properties of the DAH model

In this chapter, we study the classical properties of the DAH model. The DAH model describes the vacuum as a dual superconductor as a result of monopole condensation analogously to the Cooper pair condensation in the case of ordinary superconductivity. Since the dual gauge field, which connects the color-electric sector and the color-magnetic sector, becomes massive through the dual Higgs mechanism, the color-electric field cannot penetrate into the whole vacuum due to the finite propagation range of the dual gauge field. In this sense, the color-electric field is excluded from the vacuum, or we can say, confined by the vacuum. This is called the dual Meissner effect. Since the color-electric source appears as the "color-electric Dirac string" in this vacuum, the color-electric field can survive only around this string forming an one-dimensional object, which we call color-electric flux tube, or simply the "flux tube." The DAH model possesses such flux tubes as topologically stable solution.

3.1 Dual Higgs mechanism

In this section, we explain the dual Higgs mechanism in the DAH model. We start from the Lagrangian density of the DAH model obtained in the previous chapter, which has the form*

$$\mathcal{L}_{\rm DAH} = \frac{1}{4}{}^*F_{\mu\nu}^2(B,\Sigma^{\rm E}) + |(\partial_\mu + i\hat{g}B_\mu)\chi|^2 + \hat{\lambda}(|\chi|^2 - \hat{v}^2)^2, \tag{3.1.1}$$

where B_μ and χ are the dual gauge field and the complex scalar monopole field, respectively. The dual gauge coupling is given by $\hat{g}$, and $\hat{\lambda}$ characterizes the strength of monopole self

*In order to avoid confusion, the symbol "$\hat{}$" is reserved for the parameters of the DAH model. Later, we consider the DGL theory corresponding to the SU(3) gluodynamics in the Abelian projection. In that case, we do not use this notation.

interaction. The monopole condensate $\hat{v}$ determines the mass scale of the DAH model. The dual field strength tensor ${}^*F_{\mu\nu}$ has the form

$$ {}^*F_{\mu\nu}(B,\Sigma^{\rm E}) = \partial_\mu B_\nu - \partial_\nu B_\mu + \frac{e}{2}\Sigma^{\rm E}_{\mu\nu}. \tag{3.1.2} $$

Here, the nonlocal term $\Sigma^{\rm E}_{\mu\nu}$ represents the color-electric Dirac string, which is related to the external quark current $j_\mu = \frac{e}{2}\bar{q}\gamma_\mu q$ through the broken dual Bianchi identity $\frac{e}{2}\partial_\mu {}^*\Sigma^{\rm E}_{\mu\nu} = j_\nu$. The factor $1/2$ is the weight of the SU(2) algebra. Accordingly, $e/2$ becomes the Abelian color-electric charge in SU(2) gluodynamics in the Abelian projection. Here, the term $(\partial \wedge B)_{\mu\nu} = \partial_\mu B_\nu - \partial_\nu B_\mu$ in the dual field strength tensor contains another color-electric Dirac string attached to the color-electric charge of a quark (since the dual Bianchi identity $\partial_\mu {}^*(\partial\wedge B)_{\mu\nu} = 0$ is satisfied), which is exactly cancelled by the color-electric Dirac string in the nonlocal term. In other words, the color-electric charge of the quark is defined by the cancellation of the color-electric Dirac string in the dual field strength tensor [62].

It should be noted that the color-electric Dirac string is "dual" to the original magnetic Dirac string which is attached to a magnetic monopole in the Abelian gauge theory. One may remember that the direction of a magnetic Dirac string can be varied by a singular Abelian gauge transformation, and hence, the magnetic Dirac string is unphysical in the sense that one cannot detect it. In our case, however, the symmetry which is responsible for the direction of the color-electric Dirac string is the *dual gauge symmetry*, achieved by a set of transformation :

$$ \begin{aligned} &\chi \to \chi e^{if}, \quad \chi^* \to \chi^* e^{-if}, \quad B_\mu \to B_\mu - \frac{1}{\hat{g}}\partial_\mu f, \\ &-\frac{1}{\hat{g}}[\partial_\mu,\partial_\nu]f + \frac{e}{2}\Sigma^{\rm E}_{\mu\nu} \to \frac{e}{2}\Sigma^{\rm E}_{\mu\nu}{}' \end{aligned} \tag{3.1.3} $$

where the dual gauge fixing function can be singular ($[\partial_\mu,\partial_\nu]f \neq 0$). The last relation in (3.1.3) determines the new direction of the color-electric Dirac string. This dual gauge symmetry is broken by monopole condensation $\langle 0|\chi|0\rangle = \hat{v}$. This is the so-called dual Higgs mechanism, which is realized by inserting $\chi = \left(\hat{v} + \phi/\sqrt{2}\right)e^{i\eta}$ (where $\phi,\eta \in \Re$) into the DAH Lagrangian as

$$ \begin{aligned} \mathcal{L}_{\rm DAH} &= \frac{1}{4}{}^*F^2_{\mu\nu}(B',\Sigma^{\rm E}) + \frac{1}{2}m_B^2 B_\mu'^2 + \frac{1}{2}\left[(\partial_\mu\phi)^2 + m_\chi^2\phi^2\right] \\ &\quad + \hat{g}^2 B_\mu'^2\left(\sqrt{2}\hat{v}\phi + \frac{\phi^2}{2}\right) + \hat{\lambda}\left(\sqrt{2}\hat{v}\phi^3 + \frac{\phi^4}{4}\right), \end{aligned} \tag{3.1.4} $$

where the phase of the monopole field η is absorbed into the dual gauge field as $B'_\mu = B_\mu + \partial_\mu\eta/\hat{g}$, and accordingly, the dual gauge field and the monopole field acquire the masses $m_B \equiv \sqrt{2}\hat{g}\hat{v}$ and $m_\chi \equiv 2\sqrt{\hat{\lambda}}\hat{v}$, respectively. In that case, only the region where the field $\chi \approx 0$

resembles the normal phase as opposed to the dual superconductor vacuum, which means that the color-electric field can survive only in the region $\chi \approx 0$. Then, the color-electric Dirac string has a physical meaning, since the "normal region" follows the color-electric Dirac string so as to minimize the energy of the system forming the color-electric flux tube. It means that the shape and the size of this normal region are determined by the direction of the color-electric Dirac string and length, respectively. The width of the flux tube is characterized by the inverse masses m_B^{-1} and m_χ^{-1}, which correspond to the penetration depth of the color-electric field and the coherence length of the monopole field, respectively. One important vacuum property, the type of dual superconductivity, is governed by the ratio of these two lengths, the so-called Ginzburg-Landau (GL) parameter

$$\hat{\kappa} \equiv \frac{m_B^{-1}}{m_\chi^{-1}} = \frac{\sqrt{2\hat{\lambda}}}{\hat{g}}. \tag{3.1.5}$$

Here, $\hat{\kappa} = 1$ is the critical case, the so-called Bogomol'nyi limit, and the vacuum is classified into two types divided by this limit: $\hat{\kappa} < 1$ belongs to the type-I vacuum and $\hat{\kappa} > 1$ is the type-II vacuum. The profile functions connecting the normal phase in the center of the flux tube with the dual superconducting phase outside are classically determined by the field equations

$$\partial_\mu {}^*F_{\mu\nu} = -i\hat{g}\left(\chi^*\partial_\nu\chi - \chi\partial_\nu\chi^*\right) + 2\hat{g}^2 B_\nu \chi^*\chi \equiv k_\nu, \tag{3.1.6}$$

$$\left(\partial_\mu + i\hat{g}B_\mu\right)^2 \chi = 2\hat{\lambda}\chi(\chi^*\chi - \hat{v}^2), \tag{3.1.7}$$

where k_μ is the *monopole supercurrent* which circulates in a certain transition region, separating confined normal phase inside from the dual superconducting phase. Solving these field equations, the boundary conditions of fields are determined by the position of the color-electric Dirac string.

3.2 Flux-tube solution

In this section we study the topologically stable solution, the flux-tube solution related to a separated quark and antiquark system by solving the classical field equations in the DAH model. The flux quantization condition and the boundary condition for solving the field equations are clarified first.

3.2.1 Flux quantization condition

In order to obtain the topologically stable solution, it is important to provide the proper boundary condition which satisfies the "flux quantization condition" [34]. The flux is given

by the surface integral of the dual field strength tensor as

$$\Phi \equiv \iint {}^*F_{\mu\nu} d\sigma^{\mu\nu} = \oint B_\mu dx^\mu + \frac{e}{2} \iint \Sigma^{\rm E}_{\mu\nu} d\sigma^{\mu\nu}, \tag{3.2.1}$$

where $\sigma^{\mu\nu}$ is a two-dimensional surface element in four-dimensional space-time. By using the polar decomposition of the monopole field as $\chi = \phi e^{i\eta}$ ($\phi, \eta \in \Re$) in the field equation (3.1.6), we get

$$B_\mu = \frac{k_\mu}{2\hat{g}^2\phi^2} - \frac{1}{\hat{g}}\partial_\mu \eta. \tag{3.2.2}$$

We substitute this expression into (3.2.1) and integrate along a large closed loop where the monopole supercurrent k_μ is vanishing. Thus we get

$$\Phi = \frac{e}{2} \iint \Sigma^{\rm E}_{\mu\nu} d\sigma^{\mu\nu} - \frac{1}{\hat{g}} \oint \partial_\mu \eta dx^\mu. \tag{3.2.3}$$

This expression suggests that there are two possibilities to obtain a flux-tube configuration. One is originated from the singularity in $\Sigma^{\rm E}_{\mu\nu}$ and the other is from the singularity in $\partial_\mu \eta$. Clearly, the former case corresponds to the flux-tube with finite length, which has the color-electric source and sink at both ends. Since the nonlocal term $\Sigma^{\rm E}_{\mu\nu}$ can be expressed by the delta-function type singularity, this surface integral is already quantized. The quantized flux just corresponds to the color-electric charge attached to both ends of the Dirac string, which can be understand as the Gauss law. On the other hand, the latter case, since the only requirement on the phase $\eta(x)$ is that $\chi(x)$ should be a single valued, the line integral does not necessarily vanish. It means that $\eta(x)$ can be varied by $2\pi n$ (n-integer), which leads the flux $2\pi n/\hat{g}$. Integer n is regarded as the winding number of the flux tube corresponding to the topological charge. However, it is important to note that the phase $\eta(x)$ does not contain the information of quarks. It means that the singular line originating from the phase $[\partial_\mu, \partial_\nu]\eta(x) \neq 0$ does not have ends, or we can say that it is closed. Hence, the singularity from the phase η cannot lead to the open flux tube corresponding to a q-$\bar{q}$ system. For the hadrons with no valence quarks, such as the glueball state represented by a closed flux tube, the flux-tube ring [51], we need to take into account the singularity from the phase η, which will be addressed in the chapter8. In what follows, we assume that there is no singularity in $\partial_\mu \eta$ to concentrate on the open flux tube. In such case, the phase can be simply absorbed into the dual gauge field B_μ by the replacement $B_\mu + \partial_\mu \eta/\hat{g} \to B_\mu$.

3.2.2 Decomposition of the dual gauge field

In order to expose the behavior of the dual gauge field, it is useful to decompose the dual gauge field into two parts, the regular (no Dirac string) part and the singular (Dirac string)

part [62],

$$B_\mu \equiv B_\mu^{\rm reg} + B_\mu^{\rm sing}. \tag{3.2.4}$$

The singular dual gauge field $B_\mu^{\rm sing}$ is determined so as to cancel the color-electric Dirac string in the non-local term as

$$\partial_\mu B_\nu^{\rm sing} - \partial_\nu B_\mu^{\rm sing} + \frac{e}{2}\Sigma_{\mu\nu}^{\rm E} \equiv \frac{e}{2}C_{\mu\nu}, \tag{3.2.5}$$

where the r.h.s. has the form*

$$C_{\mu\nu}(x) = \frac{1}{4\pi^2}\int d^4y \frac{1}{|x-y|^2} {}^*(\partial \wedge j(y))_{\mu\nu}. \tag{3.2.6}$$

One finds that the role of $C_{\mu\nu}$ resembles the 't Hooft-Polyakov tensor used when we computed the magnetic charge in the previous chapter [57, 58], since this term appears after the cancellation of the Dirac string. Note that if there is no quark source, we do not need to have $B_\mu^{\rm sing}$. Now, the dual field strength tensor is rewritten as

$${}^*F_{\mu\nu} = (\partial \wedge B^{\rm reg})_{\mu\nu} + \frac{e}{2}C_{\mu\nu}. \tag{3.2.7}$$

In the static q-$\bar{q}$ system, where the color-electric source is given by

$$j_\mu(x) = \frac{e}{2}\delta_{\mu 0}\left[\delta\left(\boldsymbol{x}-\boldsymbol{x}_1\right) - \delta\left(\boldsymbol{x}-\boldsymbol{x}_2\right)\right], \tag{3.2.8}$$

the $C_{\mu\nu}$ turns out to be the color-electric field which is originating from the color-electric charge like the electric field induced by an electric charge. Let us denote the color-electric field as $E_k^{\rm Coulomb} = \epsilon_{ijk}C_{ij}$, then we obtain

$$\boldsymbol{E}^{\rm Coulomb}(\boldsymbol{x}) = \frac{e}{8\pi}\left(\frac{\boldsymbol{x}-\boldsymbol{x}_1}{|\boldsymbol{x}-\boldsymbol{x}_1|^3} - \frac{\boldsymbol{x}-\boldsymbol{x}_2}{|\boldsymbol{x}-\boldsymbol{x}_2|^3}\right). \tag{3.2.9}$$

We note that the cross term of the regular dual field tensor ${}^*F_{\mu\nu}^{\rm reg} \equiv (\partial \wedge B^{\rm reg})_{\mu\nu}$ and $C_{\mu\nu}$ can be integrated out, and the square of $C_{\mu\nu}$ and its integration gives the "Coulomb energy" including the self-energy of the color-electric charge.

3.2.3 Cylindrically symmetric system

Let us now consider a system with cylindrical geometry, where all field variables can be described in cylindrical coordinates (r, φ, z) as shown in Fig. 3.1. Here, we set $\boldsymbol{x}_1 = (0, 0, -a/2)$,

*The differential form is useful to derive the Eq. (3.2.6). Let us denote the dual field strength tensor $*F = dB + \frac{e}{2}\Sigma$, where $*$ denotes the Hodge dual, and d expresses the exterior derivative, which defines the mapping from k-form to $(k+1)$-form, satisfying $d^2 = 0$. The breaking of the dual Bianchi identity is expressed as $d\Sigma = *j$. We write as $B^{\rm sing} = \frac{e}{2}N$, where $N = -\Delta^{-1}\delta\Sigma$. Here, Δ^{-1} can be regarded as the Coulomb propagator, given by the inverse of $\Delta = (d+\delta)^2 = d\delta + \delta d$: $\Delta\Delta^{-1} = \Delta^{-1}\Delta = 1$ (δ is the codifferential, which defines the mapping from k-form to $(k-1)$-form, satisfying $\delta^2 = 0$). By using $[d, \Delta^{-1}] = 0$, we have a relation $dN = -\Sigma + \Delta^{-1}\delta * j$, which leads to the final expression $*F = dB^{\rm reg} + \frac{e}{2}C$, where $C = \Delta^{-1}\delta * j$.

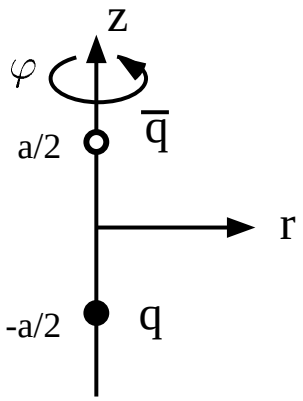

Figure 3.1: The q-$\bar{q}$ system with the cylindrical symmetry.

and $\boldsymbol{x}_2 = (0, 0, a/2)$. Then, the q-$\bar{q}$ distance is given by a. In this system, we get an explicit form of the singular dual gauge field $B_\mu^{\rm sing}$ from the relation (3.2.5) as

$$\boldsymbol{B}^{\rm sing} = -\frac{e}{8\pi r}\left(\frac{z+a/2}{\sqrt{r^2+(z+a/2)^2}} - \frac{z-a/2}{\sqrt{r^2+(z-a/2)^2}}\right)\boldsymbol{e}_\varphi, \tag{3.2.10}$$

where φ is the azimuthal angle around the z-axis and r denotes the radial coordinate.

We first investigate the ideal system for the limit $a \to \infty$:

$$\lim_{a\to\infty} \boldsymbol{B}^{\rm sing} = -\frac{e}{4\pi r}\boldsymbol{e}_\varphi = -\frac{1}{\hat{g}r}\boldsymbol{e}_\varphi, \tag{3.2.11}$$

where we have used the Dirac quantization condition $e\hat{g} = 4\pi$. Then, the fields depend only on the radial coordinate,

$$\phi = \phi(r), \quad \boldsymbol{B}^{\rm reg} = B^{\rm reg}(r)\boldsymbol{e}_\varphi \equiv \frac{\tilde{B}^{\rm reg}(r)}{r}\boldsymbol{e}_\varphi, \tag{3.2.12}$$

and the field equations (3.1.6) and (3.1.7) are written as

$$\frac{d^2\tilde{B}^{\rm reg}}{dr^2} - \frac{1}{r}\frac{d\tilde{B}^{\rm reg}}{dr} - 2\hat{g}\left(\hat{g}\tilde{B}^{\rm reg} - 1\right)\phi^2 = 0, \tag{3.2.13}$$

$$\frac{d^2\phi}{dr^2} + \frac{1}{r}\frac{d\phi}{dr} - \left(\frac{\hat{g}\tilde{B}^{\rm reg}-1}{r}\right)^2\phi_i - 2\hat{\lambda}\phi(\phi^2 - \hat{v}^2) = 0, \tag{3.2.14}$$

where the monopole supercurrent is given by $\boldsymbol{k} = k(r)\boldsymbol{e}_\varphi$, where

$$k(r) = -2\hat{g}\left(\frac{\hat{g}\tilde{B}^{\rm reg}-1}{r}\right)\phi^2. \tag{3.2.15}$$

The string tension can be defined as the energy of the flux tube per unit length

$$\sigma = 2\pi\int_0^\infty r dr\left[\frac{1}{2}\left(\frac{1}{r}\frac{d\tilde{B}^{\rm reg}}{dr}\right)^2 + \left(\frac{d\phi}{dr}\right)^2 + \left(\frac{\hat{g}\tilde{B}^{\rm reg}-1}{r}\right)^2\phi^2 + \hat{\lambda}(\phi^2-\hat{v}^2)^2\right]. \tag{3.2.16}$$

Since the flux-tube solution should have a finite string tension (energy), one finds the explicit form of boundary conditions:

$$\begin{aligned} \tilde{B}^{\rm reg} &= 0, \quad \phi = 0 \quad \text{as} \quad r \to 0, \\ \tilde{B}^{\rm reg} &= \frac{1}{\hat{g}}, \quad \phi = \hat{v} \quad \text{as} \quad r \to \infty, \end{aligned} \tag{3.2.17}$$

which, of course, satisfies the flux quantization condition.

The existence of the flux-tube solution can be shown analytically in the extreme type-II limit: $m_\chi \gg m_B$, the so-called London limit. In this vacuum, one can treat the field equations (3.2.13) and (3.2.14) analytically within the mean field approximation $\phi \simeq \hat{v}$ with the cutoff $m_B = m_B\ \theta(r - m_\chi^{-1})$. Note that the mean field approximation itself is valid at large r ($\gg m_\chi^{-1}$) and breaks for small r at the core region of the flux-tube. Thus, we only consider the outside region of the cutoff $r > m_\chi^{-1}$. The use of the mean field approximation leads to the dual London equation from Eq. (3.2.13),

$$\frac{d^2\tilde{B}^{\rm reg}}{dr^2} - \frac{1}{r}\frac{d\tilde{B}^{\rm reg}}{dr} - 2\hat{g}(\hat{g}\tilde{B}^{\rm reg} - 1)\hat{v}^2 = 0. \tag{3.2.18}$$

The field equation for the ϕ field is decoupled here, since it is automatically satisfied, which does not depend on the behavior of the dual gauge field $\tilde{B}^{\rm reg}$. The replacements $r \equiv m_B^{-1}\hat{r}$ and $\tilde{B}^{\rm reg}(\hat{r}) \equiv n/\hat{g} - \hat{r}K(\hat{r})$ give

$$\frac{d^2K}{d\hat{r}^2} + \frac{1}{\hat{r}}\frac{dK}{d\hat{r}} - \left(1 + \frac{1}{\hat{r}^2}\right)K = 0. \tag{3.2.19}$$

We know that the solution is given by the first-order modified Bessel function $K_1(\hat{r})$, which asymptotically behaves as $K_1(\hat{r}) \simeq \sqrt{\frac{\pi}{2\hat{r}}}e^{-\hat{r}}$. Thus one obtains the profiles of the dual gauge field and the color-electric field,

$$\tilde{B}^{\rm reg}(\hat{r}) \simeq \frac{n}{\hat{g}} - \hat{r}\sqrt{\frac{\pi}{2\hat{r}}}e^{-\hat{r}}, \qquad E_z(\hat{r}) \sim \sqrt{\frac{\pi}{2\hat{r}}}e^{-\hat{r}}. \tag{3.2.20}$$

The color-electric field is excluded from the vacuum and hence confined inside a cylindrical region $\hat{r} < 1$ ($r < m_B^{-1}$), which means that m_B defines the thickness of the flux-tube configuration.

In order to get the flux-tube solution in an arbitrary type of vacua, we need to solve the coupled field equations directly. Due to the non-linearity of monopole self-interaction, however, it is hard to solve the field equations analytically, which means that some numerical techniques are required. In Fig. 3.2, we show the numerical solution of the flux-tube profile for the case $m_B = m_\chi$. This is a solution obtained by the finite difference method. Clearly, one finds that the color-electric field is confined in a finite region around the center (the Dirac string). One also finds that the boundary conditions (3.2.17) are fulfilled.

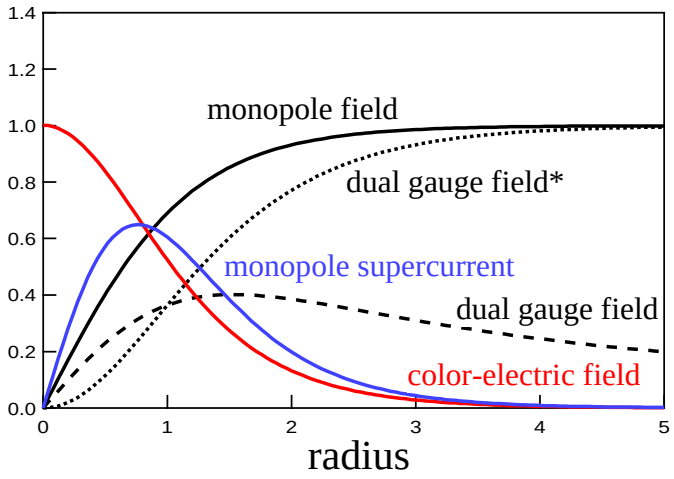

Figure 3.2: The profiles of ingredients of the flux tube, the color-electric field $E(\hat{r})$, the dual gauge field $B^{\rm reg}(\hat{r})$ (" $*$ " represents $\tilde{B}^{\rm reg}(\hat{r})$), the monopole field $\phi(\hat{r})$, and the monopole supercurrent $k(\hat{r})$, for the Bogomol'nyi limit ($m_B = m_\chi$), where $\hat{r} \equiv m_B^{-1} r$.

For the case that the quark-antiquark a is finite, as shown in Fig. 3.1, we need to solve the following field equations:

$$\frac{\partial^2 \tilde{B}^{\rm reg}}{\partial r^2} - \frac{1}{r}\frac{\partial \tilde{B}^{\rm reg}}{\partial r} + \frac{\partial^2 \tilde{B}^{\rm reg}}{\partial z^2} - 2\hat{g}\left(\hat{g}\tilde{B}^{\rm reg} - \frac{1}{2}\left(\frac{z+a/2}{\sqrt{r^2+(z+a/2)^2}} - \frac{z-a/2}{\sqrt{r^2+(z-a/2)^2}}\right)\right)\phi^2 = 0, \tag{3.2.21}$$

$$\frac{\partial^2 \phi}{\partial r^2} + \frac{1}{r}\frac{\partial \phi}{\partial r} + \frac{\partial^2 \phi}{\partial z^2} - \left(\frac{\hat{g}\tilde{B}^{\rm reg} - \frac{1}{2}\left(\frac{z+a/2}{\sqrt{r^2+(z+a/2)^2}} - \frac{z-a/2}{\sqrt{r^2+(z-a/2)^2}}\right)}{r}\right)^2 \phi - 2\hat{\lambda}\phi(\phi^2 - \hat{v}^2) = 0. \tag{3.2.22}$$

where the fields have the z dependence as $\tilde{B}^{\rm reg} = \tilde{B}^{\rm reg}(r,z)$ and $\phi = \phi(r,z)$. The boundary condition of the dual gauge field for infinitely distant region $r, z \to \infty$, is modified as

$$\tilde{B}^{\rm reg} \to \frac{1}{2\hat{g}}\left(\frac{z+a/2}{\sqrt{r^2+(z+a/2)^2}} - \frac{z-a/2}{\sqrt{r^2+(z-a/2)^2}}\right). \tag{3.2.23}$$

The resulting profile of the color-electric field, which is defined from the dual field strength tensor (3.2.7) as

$$\begin{aligned} \boldsymbol{E} &= \boldsymbol{\nabla} \times \boldsymbol{B}^{\rm reg} + \frac{e}{2}\boldsymbol{C} \\ &= \boldsymbol{E}^{\rm reg} + \boldsymbol{E}^{\rm Coulomb}, \end{aligned} \tag{3.2.24}$$

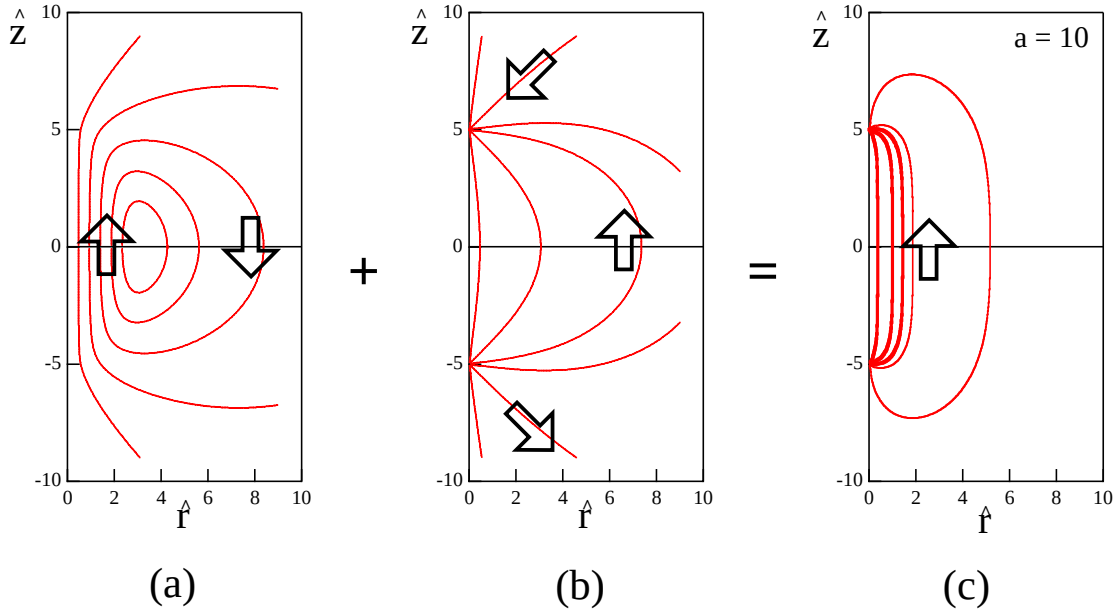

Figure 3.3: The profile of the color-electric field in the Bogomol'nyi limit on r-z plane. The sum of (a) the regular part $\boldsymbol{E}^{\rm reg}$ and (b) the Coulomb part $\boldsymbol{E}^{\rm Coulomb}$ creates (c) the flux tube structure.

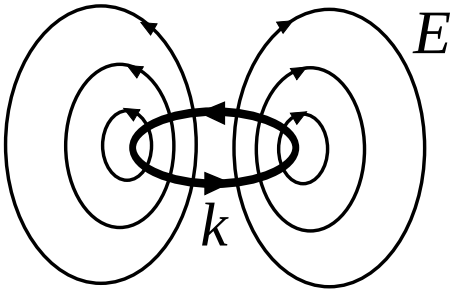

Figure 3.4: The schematic figure of the linking between the induced electric field and the monopole supercurrent.

is shown in Fig. 3.3. It is interesting to note that "induced" color-electric field in $\boldsymbol{E}^{\rm reg}$ prevents the usual Coulombic color-electric field in $\boldsymbol{E}^{\rm Coulomb}$ from penetrating into the dual-superconducting vacuum. By compensation, the color-electric field is forced to form a flux-tube structure. This situation is also understood in terms of a dual Faraday law, since we can consider the induced color-electric field is originating from the appearance of color-magnetic monopole supercurrent $k_\mu \neq 0$, circulating in a certain transition region between the normal phase and the dual superconducting phase. They are always "linked" to each other as shown in Fig. 3.4.

3.3 Properties of the classical DAH vacuum

In this section, we discuss more closely the vacuum properties of the DAH model within the classical level by paying attention to a special case, corresponding to the border between the type-I and the type-II vacuum. This is the so-called Bogomol'nyi limit. This limit is an interesting case which allows to derive several analytical results [35, 36].

3.3.1 Bogomol'nyi limit

Let us continue to study the cylindrically symmetric system. In this system, the string tension (3.2.16) is exactly rewritten as,

$$\begin{aligned}\sigma &= 2\pi\hat{v}^2 + 2\pi\int_0^\infty rdr\left[\frac{1}{2}\left(\frac{1}{r}\frac{d\tilde{B}^{\rm reg}}{dr} \pm \hat{g}(\phi^2-\hat{v}^2)\right)^2\right. \\ &\left. + \left(\frac{d\phi}{dr} \pm \left(\hat{g}\tilde{B}^{\rm reg}-1\right)\frac{\phi}{r}\right)^2 + \frac{1}{2}\left(2\hat{\lambda}-\hat{g}^2\right)(\phi^2-\hat{v}^2)^2\right]. \end{aligned} \tag{3.3.1}$$

Here, it is obvious that if the couplings satisfy the relation

$$\hat{g}^2 = 2\hat{\lambda}, \tag{3.3.2}$$

the self-interaction term of the monopole field disappears, and only terms which have a quadratic form remain in the r integral. Then, we find that this string tension is reduced to

$$\sigma = 2\pi\hat{v}^2, \tag{3.3.3}$$

when the two "first-order" differential equations (corresponding to the quadratic terms in the string tension (3.3.1)) are fulfilled:

$$\frac{d\phi}{dr} \pm \left(\hat{g}\tilde{B}^{\rm reg}-1\right)\frac{\phi}{r} = 0, \tag{3.3.4}$$

$$\frac{1}{r}\frac{d\tilde{B}^{\rm reg}}{dr} \pm \hat{g}(\phi^2-\hat{v}^2) = 0. \tag{3.3.5}$$

The profiles of the color-electric field and the monopole field can be obtained for the minimum energy configuration by solving these first-order differential equations, taking into account the boundary condition as discussed above [35, 36]. Note that these field equations of course are reproduced from the second-order differential equations (3.2.13) and (3.2.14) when the relation (3.3.2) is imposed.

Let us consider the meaning of (3.3.2). We have two characteristic mass scales: the mass of the dual gauge field $m_B = \sqrt{2}\hat{g}\hat{v}$ and the monopole field $m_\chi = 2\sqrt{\hat{\lambda}}\hat{v}$. Thus, the Bogomol'nyi limit in the DAH model is a particular symmetry between the dual gauge field and the

monopole field, since the relation (3.3.2) is nothing else but $m_B = m_\chi$, corresponding to the GL-parameter $\hat{\kappa} = 1$ [See, Eq. (3.1.5)]. The Bogomol'nyi limit will turn out as a critical limit, important to separate the vacuum into two types, type-I and type-II.

3.3.2 Interaction of flux tubes

One interesting property of the vacuum is probed by the interaction of flux tubes. This depends of whether the superconducting vacuum is type-I or type-II. Here, we consider the interaction between two parallel flux tubes. In general, flux tubes would interact with each other. However, in the Bogomol'nyi limit, apparently, there is no interaction between them. This can be understood through an investigation of the generalized string tension for an exotic state where the color-electric charges at the ends are $n \times e/2$ and $n \times -e/2$, where n is an integer. In this system, we easily get the generalized string tension,

$$\sigma_n = 2\pi n \hat{v}^2, \tag{3.3.6}$$

just proportional to n. This means that, for instance, the energy of two separated flux tubes, with winding $n = 1$ each, and one flux tube with winding number $n = 2$ are the same, independent of the separation distance of two flux tubes. This implies that the interaction energy vanishes. It is considered that this comes from the balance of propagation range of the dual gauge field and the monopole field since $m_B = m_\chi$. In the type-I or in the type-II vacuum, away from the Bogomol'nyi limit, the interaction range of these fields are not in balance, and the flux-tube interaction manifestly appears. The string tension is not proportional to the winding number n any more. From the expression on the string tension (3.3.1), we can understand the following property: While two parallel flux tubes in the type-I vacuum experience attraction, the flux tubes repel each other in the type-II vacuum. Numerical investigations of the interaction between two or more parallel flux tubes are given in Refs. [64, 65].

3.4 Summary and outlook

In this chapter, we have studied the classical properties of the DAH model. The structure of the topologically stable solution related to the q-$\bar{q}$ system, the flux-tube solution, is discussed. What we have learned about the flux tube is summarized in Fig. 3.5. Our next interest is directed to the "quantum" properties of the the DAH model, which is described by the partition function of the DAH model. This will be given in next chapter. In order to study this, we will introduce the dual lattice formulation, which enables us to study the quantum effect described by the DAH partition function by means of the Monte Carlo simulation. Using

the dual lattice formulation, it is also possible to solve the classical field equations numerically more elegant way. Then the study of quantum properties of the flux-tube solution becomes also possible.

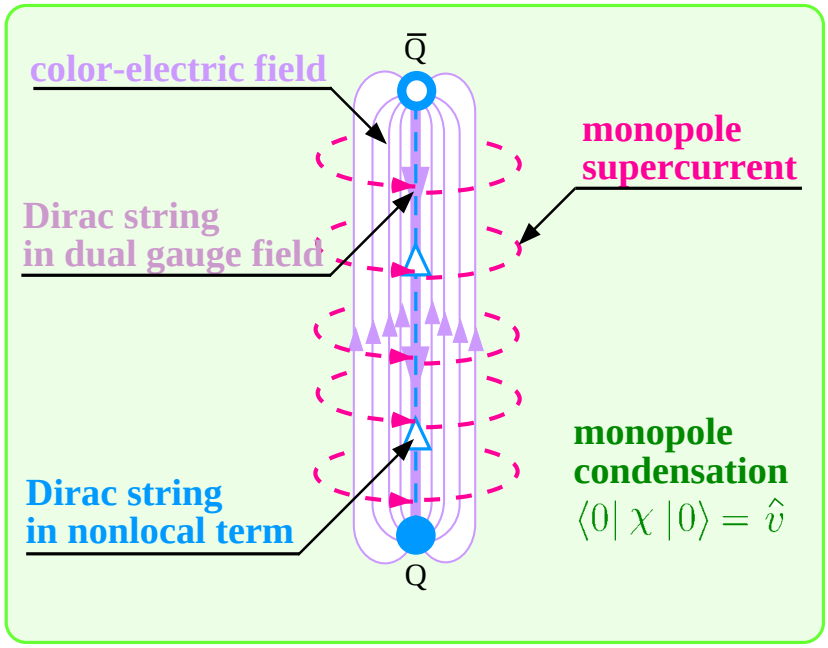

Figure 3.5: The structure of the flux tube in the DAH model [cf. Figs. 1.2 and 1.3].

Chapter 4

Quantum properties of the DAH model

The main topic of this chapter is the study of the properties of the quantized DAH model using the dual lattice formulation. The use of the dual lattice enables us to investigate not only the classical profiles of the flux tube in a more elegant way compared with the previous chapter, but also the quantum properties of the DAH model by means of the Monte Carlo simulation on the dual lattice. Then, it would be interesting to study, for instance, how the classical profile of the flux tube is modified in the quantum vacuum. In this chapter, therefore, we first formulate the DAH model on the dual lattice, and explain how we can get the classical flux-tube solution. Next, based on this formulation, we perform the Monte Carlo simulation and study the quantum effect. To evaluate this, we especially study some order parameters in the DAH model. This information is important to explore the phase diagram, which is an important step to determine the vacuum structure of the DAH model at the quantum level corresponding to chromodynamics.

4.1 DAH model on the dual lattice

In this section, we formulate the DAH model on the dual lattice. The DAH model describes the Abelian dual gauge field $B_\mu(x)$, a complex scalar monopole field $\chi(x)$, and the external color-electric Dirac string $\Sigma^{\rm E}_{\mu\nu}(x)$. First, we define these fields on the dual lattice. Let the dual gauge field be defined on *dual links* as $B_\mu(s)$, the monopole field on *dual sites* as $\chi(s)$, and the dual field strength tensor and the color-electric Dirac string term on *dual plaquettes* as ${}^*F_{\mu\nu}(s)$ and $\Sigma^{\rm E}_{\mu\nu}(s)$, where $s \equiv (x, y, z, t)$ is a set of four-discretized coordinates. The color-electric source and sink are attached to the ends of the color-electric Dirac string. Next, we

go over to dimensionless fields by the transformation :

$$B_\mu(s) \to \frac{\hat{B}_\mu(s)}{a\hat{g}}, \quad \chi(s) \to \hat{v}\hat{\chi}(s), \quad \Sigma^{\rm E}_{\mu\nu}(s) \to \frac{\hat{\Sigma}^{\rm E}_{\mu\nu}(s)}{a^2}, \tag{4.1.1}$$

where a is dual lattice spacing, which has the dimension of length and can be reinserted when needed. Accordingly, the scale is absorbed into the definition of masses, of the dual gauge field $m_B \equiv \sqrt{2}\hat{g}\hat{v}$, and of the monopole field $m_\chi \equiv 2\sqrt{\tilde{\lambda}}\hat{v}$. Then, the action of the DAH model on the dual lattice is given by

$$S = \sum_s \left[\frac{\beta_{\rm DAH}}{2} \sum_{\mu<\nu} {}^*\hat{F}^2_{\mu\nu}(s) + \tilde{\gamma} \sum_\mu \left| \hat{\chi}(s) - e^{i\hat{B}_\mu(s)}\hat{\chi}(s+\hat{\mu}) \right|^2 + \tilde{\lambda}\left(|\hat{\chi}(s)|^2 - 1 \right)^2 \right], \tag{4.1.2}$$

where the couplings are defined as

$$\beta_{\rm DAH} \equiv 1/\hat{g}^2, \quad \tilde{\gamma} \equiv \frac{\beta_{\rm DAH}\hat{m}_B^2}{2}, \quad \tilde{\lambda} \equiv \frac{\beta_{\rm DAH}\hat{m}_B^2\hat{m}_\chi^2}{8}. \tag{4.1.3}$$

The dimensionless masses are defined by $\hat{m}_B \equiv m_B \cdot a$ and $\hat{m}_\chi \equiv m_\chi \cdot a$. The integral $\int d^4x$ is replaced by $\sum_s a^4$. The dimensionless dual field strength tensor with the external source is given by

$${}^*\hat{F}_{\mu\nu}(s) = \hat{B}_\mu(s) + \hat{B}_\nu(s+\hat{\mu}) - \hat{B}_\mu(s+\hat{\nu}) - \hat{B}_\nu(s) + 2\pi\hat{\Sigma}^{\rm E}_{\mu\nu}(s), \tag{4.1.4}$$

where the relation between the color-electric charge and the color-magnetic charge, the Dirac quantization condition, $eg = 4\pi$ is used to get the factor 2π in front of $\hat{\Sigma}^{\rm E}_{\mu\nu}(s)$. The color-electric flux quantization is now realized by taking

$$\hat{\Sigma}^{\rm E}_{\mu\nu}(s) = \pm 1, \tag{4.1.5}$$

on just a single plaquette in the $\mu\nu$ plane. The sign depends on the direction of the flux. In the dual lattice formulation, the kinetic term of the monopole field is written as

$$(\partial_\mu + i\hat{g}B_\mu)\chi \quad \to \quad \frac{\hat{v}}{a}\left(U_\mu(s)\hat{\chi}(s+\hat{\mu}) - \hat{\chi}(s) \right), \tag{4.1.6}$$

where $U_\mu(s)$ is a (compact) dual link variable,

$$U_\mu(s) = \exp\left(ia\hat{g}B_\mu(s)\right) = \exp\left(i\hat{B}_\mu(s)\right). \tag{4.1.7}$$

4.2 Classical flux-tube solution on the dual lattice

In this section, we adopt the above dual lattice formulation for the purpose of solving the field equations in the static three-dimensional system, and try to obtain the profile of the color-electric flux tube on the dual lattice.

In the static three-dimensional system, we only need space-like links μ or $\nu = 1, 2, 3$ and s is three-dimensional lattice point. Hereafter, we use i, j, and k to specify spatial links. Note that a four-dimensional Monte Carlo simulation of the DAH model is possible if we add the time-like link contribution, which will be considered in the next section. The field equation on the dual lattice is obtained when we formulate the cooling procedure, which aims to minimize the action (4.1.2). We require that the first derivative of the action with respect to the dual gauge field and the monopole field becomes zero. For the dual gauge field $\hat{B}_{i=1,2,3}(s)$, this condition leads to

$$\frac{\partial S}{\partial \hat{B}_i(s)} = \beta_{\rm DAH}\left({}^*\hat{F}_{ij}(s) + {}^*\hat{F}_{ji}(s-\hat{j}) + {}^*\hat{F}_{ik}(s) + {}^*\hat{F}_{ki}(s-\hat{k}) + \hat{m}_B^2 b_i^{(2)}(s)\right) \equiv \beta_{\rm DAH} X_i(s), \tag{4.2.1}$$

which corresponds to Eq. (3.1.6) in the continuum limit. Here we have defined

$$\begin{aligned} b_i^{(1)}(s) &\equiv \hat{\chi}_R(s)\left(\hat{\chi}_R(s+\hat{i})\cos\hat{B}_i(s) - \hat{\chi}_I(s+\hat{i})\sin\hat{B}_i(s)\right) \\ &\quad + \hat{\chi}_I(s)\left(\hat{\chi}_R(s+\hat{i})\sin\hat{B}_i(s) + \hat{\chi}_I(s+\hat{i})\cos\hat{B}_i(s)\right), \qquad (4.2.2) \\ b_i^{(2)}(s) &\equiv \hat{\chi}_R(s)\left(\hat{\chi}_R(s+\hat{i})\sin\hat{B}_i(s) + \hat{\chi}_I(s+\hat{i})\cos\hat{B}_i(s)\right) \\ &\quad - \hat{\chi}_I(s)\left(\hat{\chi}_R(s+\hat{i})\cos\hat{B}_i(s) - \hat{\chi}_I(s+\hat{i})\sin\hat{B}_i(s)\right). \qquad (4.2.3) \end{aligned}$$

The labels $i, j, k = 1, 2, 3$ should be taken cyclically. We realize that the four terms of the dual field strength tensor ${}^*\hat{F}_{ij}(s) \sim {}^*\hat{F}_{ki}(s-\hat{k})$ in (4.2.1) are nothing else but the sum of plaquettes attached to the link at s pointing into i-direction. The subscript of the monopole field R, I denote its real and its imaginary part. respectively. The candidate value of the dual gauge potential, which locally satisfies the dual lattice field equations $X_i(s) = 0$, is obtained by a relaxation step taking into account the second derivative of the action, *a la* Newton and Raphson as

$$\begin{aligned} \hat{B}_i(s) \to \hat{B}_i'(s) &= \hat{B}_i(s) - \left(\frac{\partial^2 S}{\partial \hat{B}_i^2(s)}\right)^{-1} \frac{\partial S}{\partial \hat{B}_i(s)} \\ &= \hat{B}_i(s) - \frac{X_i(s)}{4 + \hat{m}_B^2 b_i^{(1)}(s)}. \end{aligned} \tag{4.2.4}$$

For the monopole field, similarly, the local solution is given by the update a formula

$$\begin{aligned} \hat{\chi}_R(s) \to \hat{\chi}_R'(s) = \hat{\chi}_R(s) - \frac{X_R(s)}{6 + \frac{1}{2}\hat{m}_\chi^2\left(\hat{\chi}_R^2(s) + \hat{\chi}_I^2(s) - 1\right)} \\ + \frac{\hat{m}_\chi^2 \hat{\chi}_R(s)\left(\hat{\chi}_R(s) X_R(s) + \hat{\chi}_I(s) X_I(s)\right)}{\left\{6 + \frac{1}{2}\hat{m}_\chi^2\left(\hat{\chi}_R^2(s) + \hat{\chi}_I^2(s) - 1\right)\right\}\left\{6 + \frac{1}{2}\hat{m}_\chi^2\left(\hat{\chi}_R^2(s) + \hat{\chi}_I^2(s) - 1\right) + \hat{m}_\chi^2\left(\hat{\chi}_R^2(s) + \hat{\chi}_I^2(s)\right)\right\}}, \end{aligned} \tag{4.2.5}$$

$$\hat{\chi}_I(s) \to \hat{\chi}'_I(s) = \hat{\chi}_I(s) - \frac{X_I(s)}{6 + \frac{1}{2}\hat{m}_\chi^2 \left(\hat{\chi}_R^2(s) + \hat{\chi}_I^2(s) - 1\right)} + \frac{\hat{m}_\chi^2 \hat{\chi}_I(s) \left(\hat{\chi}_R(s) X_R(s) + \hat{\chi}_I(s) X_I(s)\right)}{\left\{6 + \frac{1}{2}\hat{m}_\chi^2 \left(\hat{\chi}_R^2(s) + \hat{\chi}_I^2(s) - 1\right)\right\}\left\{6 + \frac{1}{2}\hat{m}_\chi^2 \left(\hat{\chi}_R^2(s) + \hat{\chi}_I^2(s) - 1\right) + \hat{m}_\chi^2 \left(\hat{\chi}_R^2(s) + \hat{\chi}_I^2(s)\right)\right\}}, \tag{4.2.6}$$

where

$$\begin{aligned} X_R(s) &= 6\hat{\chi}_R(s) - \sum_{i=1}^{3}\Big\{\Big(\hat{\chi}_R(s+\hat{i})\cos\hat{B}_i(s) - \hat{\chi}_I(s+\hat{i})\sin\hat{B}_i(s)\Big) \\ &\quad + \Big(\hat{\chi}_R(s-\hat{i})\cos\hat{B}_i(s-\hat{i}) + \hat{\chi}_I(s-\hat{i})\sin\hat{B}_i(s-\hat{i})\Big)\Big\} \\ &\quad + \frac{1}{2}\hat{m}_\chi^2 \hat{\chi}_R(s)\left(\hat{\chi}_R^2(s) + \hat{\chi}_I^2(s) - 1\right), \end{aligned} \tag{4.2.7}$$

$$\begin{aligned} X_I(s) &= 6\hat{\chi}_I(s) - \sum_{i=1}^{3}\Big\{\Big(\hat{\chi}_R(s+\hat{i})\sin\hat{B}_i(s) + \hat{\chi}_I(s+\hat{i})\cos\hat{B}_i(s)\Big) \\ &\quad + \Big(\hat{\chi}_R(s-\hat{i})(-\sin\hat{B}_i(s-\hat{i})) + \hat{\chi}_I(s-\hat{i})\cos\hat{B}_i(s-\hat{i})\Big)\Big\} \\ &\quad + \frac{1}{2}\hat{m}_\chi^2 \hat{\chi}_I(s)\left(\hat{\chi}_R^2(s) + \hat{\chi}_I^2(s) - 1\right). \end{aligned} \tag{4.2.8}$$

The dual lattice field equation for the monopole field are $X_R(s) = X_I(s) = 0$, which corresponds to Eq. (3.1.7) in the continuum limit.

One finds that the form of the classical profile does not depend on the coupling $\beta_{\rm DAH}$, since this is factored out from the field equation. Hence, one can set any $\beta_{\rm DAH}$ to study the behavior of profile. At the same time, this implies that it is not necessary to specify the lattice spacing a. Once the masses m_B and m_χ are provided in physical units, the lattice spacing a is known to characterize thickness and length of the flux tube. It is noted that when we discuss the classical string tension of the flux tube, $\beta_{\rm DAH}$ should be taken into account. In such case, a also becomes important, since the dimensionful physical quantities are recovered by using this a.

We find that the boundary condition of the dual lattice field equations becomes very easy to handle, since all we have to do is to place a set of plaquettes $\hat{\Sigma}^{\rm E}_{\mu\nu}(s) \neq 0$ which is pierced by the color-electric Dirac string in the three dimensional space. For instance, if we assume that a straight color-electric Dirac string is placed on the z-axis, which means that the quark and the anti-quark are placed on the z-axis, the only non-vanishing plaquette is $\hat{\Sigma}^{\rm E}_{12}(s)$, where $s = (0, 0, z)$ and z belongs to the region between a quark and an anti-quark. A schematic figure is shown in Fig. 4.1(a), where the non-vanishing plaquettes are shaded. They form

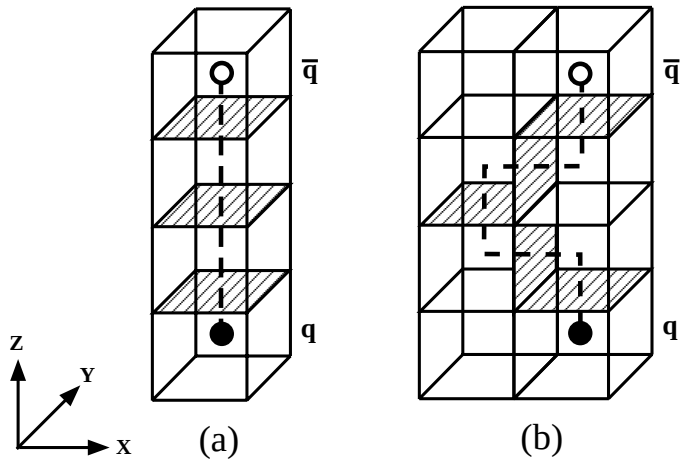

Figure 4.1: The color-electric Dirac string dual to singular plaquettes (shaded) ending in external charges.

a connected stack of plaquettes dual to the color-electric Dirac string connecting q and $\bar{q}$. Here, $\hat{\Sigma}^{\rm E}_{\mu\nu}(s) = +1$ (-1) means that the color-electric Dirac string is regarded piercing the $\mu\nu$-plane at s to $\mu \wedge \nu$ $(-\mu \wedge \nu)$ direction.

In Fig. 4.2 we show the profiles of the color-electric field, the color-magnetic current which circulates around the flux tube, and the modulus of the monopole field. Here a 32^3 dual lattice is used, and the mass parameters are taken as $\beta_{\rm DAH} = 1$, $\hat{m}_B = \hat{m}_\chi = 0.5$. The quark and the antiquark position are taken as $s \equiv (x, y, z) = (0, 0, -8)$ and $(0, 0, 8)$, respectively. The color-electric field is given by the space-space components of the dual field strength tensor (4.1.4), ${}^*\hat{F}_{ij}$ $(i, j = 1, 2, 3)$. The color-magnetic current is minus of the last term of $X_{i=1,2,3}(s)$ in (4.2.1), $k_\mu(s) = -\hat{m}_B^2 b_i^2(s)$, which corresponds to $k_\mu(x)$ in (3.1.6) in the continuum limit. The length of the arrows in these figures shows the relative strength of fields. In the figure showing the color-electric field, one can observe the Coulombic behaviors of the field at (near) the position of the quark (source) and the antiquark (sink). Here, in order to obtain the vector variables defined on sites from the color-electric fields on plaquettes and the color-magnetic currents on links, the appropriate averages like $\hat{F}^{\rm fig}_{ij}(s) \equiv (\hat{F}_{ij}(s) + \hat{F}_{ij}(s + \hat{k}))/2$, where $(i, j, k : cyclic)$, etc. are associated with centers of cubes. This is also where the quark and the antiquark are located. Note that the parameter set used here is optimal for a 32^3 dual lattice and intended to compare with Ref. [52], where the relation of the flux-tube profile between the classical solution of the DAH model and that of the Abelian projected SU(2) lattice gauge theory [48] is discussed.

The relation $\hat{m}_B = \hat{m}_\chi$ implies that the vacuum is at the Bogomol'nyi limit, just between the type-I and the type-II vacuum. The inter-quark potential is shown in Fig. 4.3. One

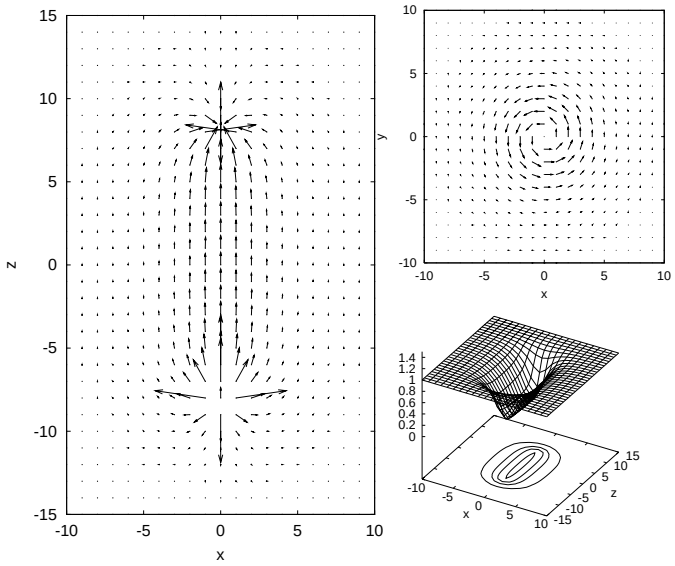

Figure 4.2: The profiles of the color-electric field in the x-z plane at $y = 0$ (left), the monopole supercurrent in the x-y plane at $z = 0$ (right-upper), and the modulus of the monopole field in the x-z plane at $y = 0$ (right-lower) of the mesonic flux tube in the DAH model. The quark and the antiquark are placed at $(x, y, z) = (0, 0, -8)$ and $(0, 0, 8)$, respectively.

finds that the slope of the linear part of the potential, which is the string tension, obeys the analytic result on the Bogomol'nyi limit, as $\sigma^L = 2\pi\hat{v}^2 \cdot a^2 = \beta_{\rm DAH}\pi\hat{m}_B^2 \sim 0.78$ [35, 36]. Here, the superscript " ^{L} " denotes the dimensionless string tension. Note that the force always contains a Coulomb self-energy, which is included in a constant term in the potential $V(R/a)$. If we choose a finer dual lattice, smaller a, the self energy becomes large, and accordingly, the constant takes a larger value. In such case, we could observe the fine structure of the short-distance behavior of the potential.

It is worth emphasizing that the dual lattice formulation presented here is also applicable to the "bending" flux tube [See, Fig. 4.1(b)]. If we assume that the bending is restricted in x-z plane, that means that a x-component of the color-electric Dirac string appears, *i.e.* some terms $\hat{\Sigma}^{\rm E}_{23}(s)$ have non-vanishing value, ± 1. In this case, the sign of this plaquette is similarly treated as discussed above. In this sense, the dual lattice formulation is quite useful to obtain various shapes of the flux-tube solutions in the DAH model numerically. In the chapter 7, we investigate the DGL theory with the similar technique, which corresponds to the SU(3) gluodynamics in the Abelian projection. In the DGL theory, there appears a flux-tube structure which includes three valence quarks corresponding to the baryonic state. In order to study such a flux configuration, we need the skill to deal with the bending flux tube.

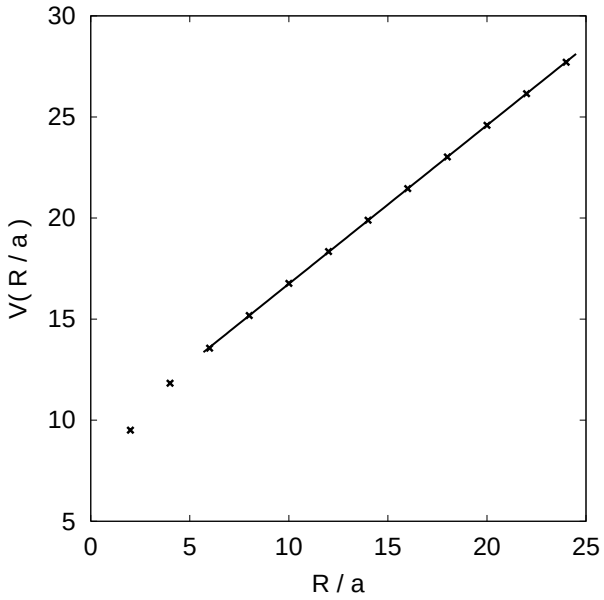

Figure 4.3: The quark-antiquark potential the mesonic flux tube in the DAH model, where R/a denotes the q-$\bar{q}$ distance. The parameter set is taken as $\beta_{\rm DAH} = 1$, $\hat{m}_B = \hat{m}_\chi = 0.5$.

4.3 Monte Carlo simulation of the DAH model

In this section, in order to study the general properties of the DAH model including quantum fluctuation, we perform the Monte Carlo simulations on the dual lattice. Now, we take into account all directions of dual links $\mu = 1, 2, 3, 4$ and a four-dimensional lattice. Some details on the Monte Carlo simulation of the DAH model are summarized in the Appendix A. Here we only mention the general idea. We have two fields, the dual gauge field and the monopole field, which are updated in alternating order. The sweep is vectorized. Detailed balance requires to do the update in an even-odd checkerboard fashion.

First, we explain the treatment of the dual gauge field part. The kinetic part of the action for the dual gauge field has a Gaussian form. Therefore, we can prepare a candidate dual gauge field by mapping flat random numbers to Gaussian ones by using the Box-Muller transformation. This would be all of the so-called heat-bath algorithm, if the dual gauge field would be a the free field. However, the dual gauge field interacts with the monopole field, by the kinetic term of the latter. It means that the additional term in the action containing the dual gauge field should be taken into account. To repair the above heat-bath method, a Metropolis acceptance check must follow. This combined procedure is also applied to generate monopole fields which sample the weight of the action. For this case the kinetic term of the monopole field is Gaussian. So it is also possible to adopt the heat-bath algorithm. The self-

interaction term of the monopole field can be taken into account by a Metropolis acceptance check.

By supplying the dual gauge field $B_\mu(s)$ and the monopole fields $\chi(s)$, $\chi^*(s)$ sampled according to the weight $\exp(-S_{\rm DAH}[B_\mu, \chi, \chi^*])$, we can simulate the DAH model. In other words, on an ensemble of fields provided by this weight, we can compute the expectation value of an operator $\mathcal{O}[B_\mu, \chi, \chi^*]$,

$$\begin{aligned} \langle \mathcal{O}[B_\mu, \chi, \chi^*] \rangle &= \frac{1}{\mathcal{Z}} \int \mathcal{D}B_\mu \mathcal{D}\chi \mathcal{D}\chi^* \mathcal{O}[B_\mu, \chi, \chi^*] \exp(-S_{\rm DAH}[B_\mu, \chi, \chi^*]) \\ &\approx \frac{1}{N} \sum_{i=1}^{N} \mathcal{O}[\{B_\mu, \chi, \chi^*\}_i], \end{aligned} \tag{4.3.1}$$

as a simple arithmetic average, relying on "important sampling." The label i denotes the i-th vacuum configuration in a Monte Carlo sequence. $\mathcal{Z}$ is the partition function

$$\mathcal{Z} = \int \mathcal{D}B_\mu \mathcal{D}\chi \mathcal{D}\chi^* \exp(-S_{\rm DAH}[B_\mu, \chi, \chi^*]). \tag{4.3.2}$$

To summarize, by iterating these update, we will finally get the thermalized configuration of the dual gauge field and the monopole field (with an external source). It means that we can prepare an vacuum including all the quantum fluctuation of fields, which enable us to calculate the expectation value of some operators. Since the DAH model contains three parameters, the dual gauge coupling $\beta_{\rm DAH} = 1/g^2$, the mass of the dual gauge field $\hat{m}_B$ and the monopole field $\hat{m}_\chi$, the properties of the vacuum represented by the simulation ensemble $\{B_\mu, \chi, \chi^*\}$ depend on the choice of these parameters.

4.3.1 Structure of the DAH vacuum

As a preparation for the study of flux tubes, we investigate the structure of the DAH vacuum without external charges at the quantum level, the so-called phase diagram, in terms of the DAH parameters, $\beta_{\rm DAH}$, $\hat{m}_B$, $\hat{m}_\chi$. To begin, it is useful to remember first the London limit case ($m_\chi \to \infty$). In this limit, it is known that the DAH vacuum possesses two types of phases, the Coulomb and the Higgs phase[66], as shown schematically in Fig. 4.4, where $\beta_{\rm DAH} = 1/g^2$, $\tilde{\gamma} = \beta_{\rm DAH}\hat{m}_B^2/2$. As a driving mechanism for the appearance of two phases, topological excitations, so-called "vortex excitations" originating from the multi-valuedness of the phase of the monopole field, are held responsible [66, 67]. The vortex excitation is a closed color-electric Dirac string forming a more or less complex network. In fact, in this limit, the DAH model can be analytically rewritten in terms of its string representation by virtue of that the modulus of the monopole field can be fixed as $|\hat{\chi}| = 1$ [68]*. In terms of

*Precisely speaking, Refs. [66–68] are studies of the Abelian Higgs (AH) model. However, since the DAH model differs only in the interpretation of the AH model, we can make use of these studies.

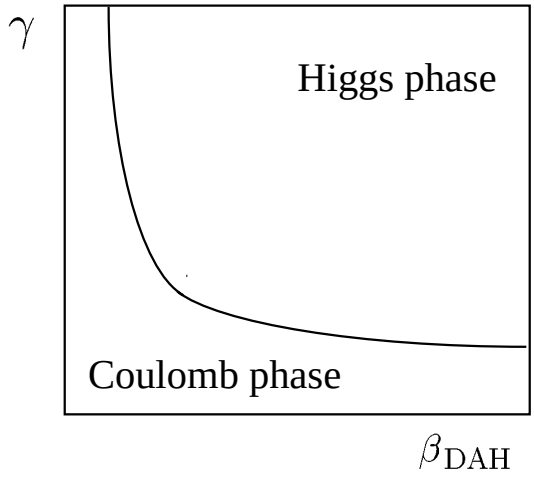

Figure 4.4: The phase diagram of the DAH model in the London limit $m_\chi \to \infty$.

the string representation of the DAH model, the existence of vortex excitations is manifest. Regarding the density of vortex excitation as an important order parameter, it is shown that we can classify two phases of the DAH model [67].

In the field theory, turning attention to topological excitations is often helpful in understanding the phases of the system. For instance, in compact U(1) gauge theory, there appear magnetic monopoles originating from the periodicity of the lattice gauge action. They play an important role in the confining phase transition through magnetic monopole condensation [69–71]. At the same time, the Monte Carlo method is very useful to simulate the system, since analytical understanding is sometimes restricted to ideal cases. In the DAH model for general parameter case, the phase structure determined in the London limit case would be modified. Moreover, we do not have an exact expression of the string representation of the DAH model for general parameter case. In this sense, and for our purpose we need to resort to a Monte Carlo exploration of the phase structure.

In this section, we would like to specially pay attention to the Bogomol'nyi limit case ($\hat{m}_B = \hat{m}_\chi$). Note that some studies of the DAH model show that the Bogomol'nyi limit is nearby the realistic at the classical level [52]. Then, it would be interesting to investigate the vacuum structure of at the quantum level by virtue of the Monte Carlo method.

In order to scan the phases of the DAH vacuum, in the following, we evaluate expectation values of several observables in a grid of points in the parameter plane. Besides the vortex density some of them are expected too, as candidates of order parameters. If some drastic changes of the value of the expectation values are observed, it can be a signal of a phase transition.

(1) Plaquette energy density:

$$\frac{\beta_{\rm DAH}}{2}\langle {}^*\hat{F}^2_{\mu\nu}\rangle \equiv \frac{\frac{\beta_{\rm DAH}}{2}\sum_{s,\mu<\nu} {}^*F^2_{\mu\nu}(s)}{N_p}, \tag{4.3.3}$$

where N_p is total numbers of dual plaquettes.

(2) Modified hopping term:

$$\frac{{\rm Re}\langle\chi^* U_\mu \chi\rangle}{\langle\chi^2\rangle} \equiv \frac{{\rm Re}\sum_{s,\mu}(\hat{\chi}^*(s)U_\mu(s)\hat{\chi}(s+\hat{\mu}))/N_l}{\sum_s |\hat{\chi}(s)|^2/N_s}, \tag{4.3.4}$$

where N_l, and N_s denote total numbers of dual links, and dual sites.

(3) Vortex density:

$$\langle |N^{\rm E}_{\mu\nu}|\rangle \equiv \frac{\sum_{s,\mu<\nu}|N^{\rm E}_{\mu\nu}(s)|}{N_p}, \tag{4.3.5}$$

where $N^{\rm E}_{\mu\nu}(s) \in \boldsymbol{Z}$ is the modulo 2π of the vortex current $J_{\mu\nu}(s)$. The vortex current is constructed from the phase of the monopole field $\eta(s)$, where $\hat{\chi}(s) = \phi(s)\exp(i\eta(s))$. First, we subtract the multiple of 2π from the derivative of the phase as

$$\partial_\mu \tilde{\eta}(s) = \partial_\mu \eta(s) - 2\pi n^{\rm E}_\mu(s), \tag{4.3.6}$$

where $n^{\rm E}_\mu(s) \in \boldsymbol{Z}$ is the modulo 2π of $\hat{B}_\mu(s) + \partial_\mu\eta(s)$. Then, the vortex current is given by

$$J_{\mu\nu}(s) = [\partial_\mu, \partial_\nu]\tilde{\eta}(s). \tag{4.3.7}$$

Note that if the modified phase $\tilde{\eta}(s)$ is regular, the vortex current vanishes. We add more explanation about the vortex density. The vortex density is the fraction of plaquettes which are pierced by the color-electric Dirac string which is generated as excitations in the vacuum configuration. Since the origin of appearance of such Dirac strings is the singular phase in the monopole field, it forms closed sheet (world sheet of closed color-electric Dirac string) on the dual lattice. From this value, we can learn that the quantum vacuum is how far from the classical vacuum. If there exists a non-vanishing vortex density, the profile of the flux tube inserted as the external source would be modified. Moreover, if such vortex excitations dominate in the vacuum, the structure of the flux tube would be "destroyed." We imagine that when the vacuum fluctuation becomes large, the vortex density takes the large value. Then, the vortex density is expected as a good order parameter to characterize the Coulomb phase of the DAH vacuum.

We show the numerical results of the expectation values of observables in Fig. 4.5. These observables are measured in the vacuum without external color-electric sources, $\hat{\Sigma}^{\rm E}_{\mu\nu}(s) = 0$,

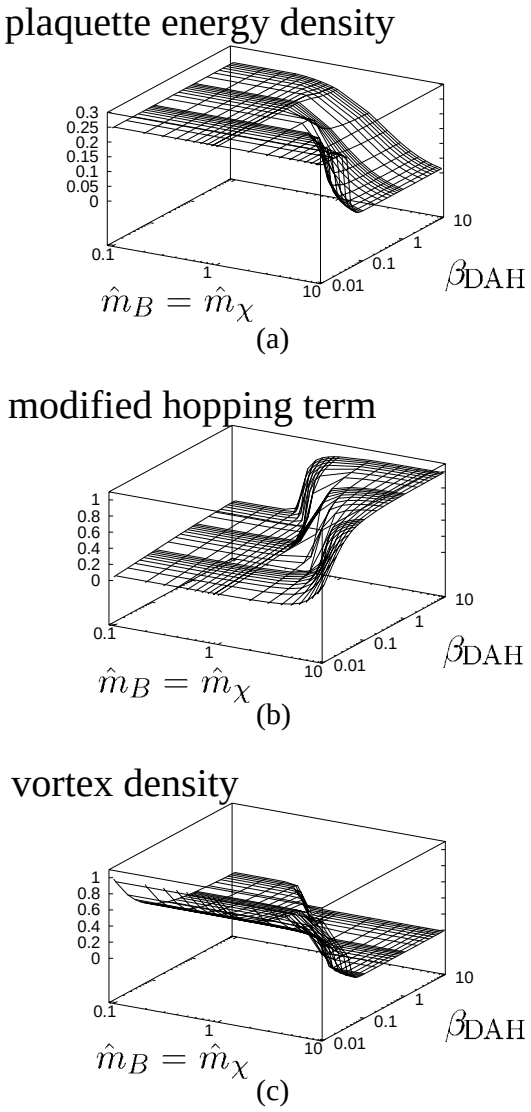

Figure 4.5: Observables: (a) plaquette energy density, (b) modified hopping term, (c) vortex density, as functions of mass $\hat{m}_B = \hat{m}_\chi$ and $\beta_{\rm DAH}$.

and periodic boundary conditions are adopted for all directions. The lattice size was 10^4. For one set of parameter $\beta_{\rm DAH}$, $\hat{m}_B = \hat{m}_\chi$, we take 300 configurations with 5 skipped configuration in between; 200 measurements are skipped for the thermalization. Note that the error is sufficiently small, hence, it is not shown.

From the behaviors of observables, one finds that for a large $\beta_{\rm DAH}$ and a large mass region, the plaquette energy density goes to zero, and the modified hopping term is almost given by one. At the same time, the vortex density is almost zero. On the other hands, for a small $\beta_{\rm DAH}$ and a small mass region, the plaquette energy density is constant around the value 0.25,

the modified hopping term is approaching by zero, and the vortex density has non-vanishing value there, which indicate the Higgs phase. A plateau around the value 0.4 is observed, which is a signal of vortex condensation. Hence, from this result, we find that the vacuum is essentially separated into two types, the Higgs phase and the Coulomb phase, similar to the London limit as shown in Fig. 4.4. Note that the modified hopping term can be regarded as an order parameter. Thus, we expect that the DAH model possesses at least two phases at the quantum level, independent of the mass ratio $\hat{\kappa}$. In any case, we could extract the information on the vacuum structure for a reduced parameter set for the Bogomol'nyi limit $\hat{\kappa} = 1$ case. In the following, we often refer to this phase structure as a "map" of quantum vacuum.

4.4 't Hooft loop operator in the DAH model

In this section, we introduce the 't Hooft loop operator [49] as four-dimensional extension of the color-electric Dirac string, which is inserted as the external source. The 't Hooft loop operator essentially can be regarded as the dual version of the Wilson loop. This operator is then used to study the response of the DAH vacuum to external color-electric charges. For instance, the investigation of the profiles of the flux tube, the evaluation of the string tension, are important applications of the 't Hooft loop operator.

The 't Hooft loop operator H in the continuum theory is defined by the difference of the action with and without the external source as

$$H \equiv \exp\left[-\frac{\beta_{\rm DAH}}{4}\int d^4x \left((\partial \wedge B)_{\mu\nu} + 2\pi\Sigma^{\rm E}_{\mu\nu}\right)^2 + \frac{\beta_{\rm DAH}}{4}\int d^4x (\partial \wedge B)^2_{\mu\nu}\right]. \tag{4.4.1}$$

Here $\Sigma^{\rm E}_{\mu\nu}$ denotes the external source as already discussed, which describes the position of the color-electric Dirac string. The expectation value of the 't Hooft operator in the DAH model is then defined by*

$$\begin{aligned}
\langle H\rangle_{\Sigma^{\rm E}=0} &\equiv \frac{\int \mathcal{D}B\ H\ e^{-\frac{\beta_{\rm DAH}}{4}\int d^4x(\partial\wedge B)^2_{\mu\nu}}}{\int \mathcal{D}B e^{-\frac{\beta_{\rm DAH}}{4}\int d^4x(\partial\wedge B)^2_{\mu\nu}}} &(4.4.2)\\
&= \frac{\int \mathcal{D}B e^{-\frac{\beta_{\rm DAH}}{4}\int d^4x\left((\partial\wedge B)_{\mu\nu}+2\pi\Sigma^{\rm E}_{\mu\nu}\right)^2}}{\int \mathcal{D}B e^{-\frac{\beta_{\rm DAH}}{4}\int d^4x(\partial\wedge B)^2_{\mu\nu}}} &(4.4.3)\\
&= \frac{\int \mathcal{D}B e^{-S_{\rm DAH}[B,\Sigma^{\rm E}]}}{\int \mathcal{D}B e^{-S_{\rm DAH}[B]}}. &(4.4.4)
\end{aligned}$$

By making use of the 't Hooft operator, we can define the expectation value of another

*Here, we shall omit to write the monopole field part. One should regard such contribution is, of course, included.

operator $\mathcal{O}$,

$$\langle\mathcal{O}\rangle_{\Sigma^{\rm E}\neq 0}=\frac{\int\mathcal{D}Be^{-S_{\rm DAH}[B,\Sigma^{\rm E}]}\mathcal{O}}{\int\mathcal{D}Be^{-S_{\rm DAH}[B,\Sigma^{\rm E}]}}=\frac{\frac{\int\mathcal{D}Be^{-S_{\rm DAH}[B,\Sigma^{\rm E}]}\mathcal{O}}{\int\mathcal{D}Be^{-S_{\rm DAH}[B]}}}{\frac{\int\mathcal{D}Be^{-S_{\rm DAH}[B,\Sigma^{\rm E}]}}{\int\mathcal{D}Be^{-S_{\rm DAH}[B]}}}=\frac{\frac{\int\mathcal{D}Be^{-S_{\rm DAH}[B]}H\mathcal{O}}{\int\mathcal{D}Be^{-S_{\rm DAH}[B]}}}{\frac{\int\mathcal{D}BHe^{-S_{\rm DAH}[B]}}{\int\mathcal{D}Be^{-S_{\rm DAH}[B]}}}=\frac{\langle H\mathcal{O}\rangle_{\Sigma^{\rm E}=0}}{\langle H\rangle_{\Sigma^{\rm E}=0}}. \tag{4.4.5}$$

Here $\langle ...\rangle_{\Sigma^{\rm E}\neq 0}$ denotes an average in the vacuum with an external source (source-in vacuum), and $\langle ...\rangle_{\Sigma^{\rm E}=0}$ without external source (pure vacuum). This relation suggests that the expectation value of an operator $\mathcal{O}$ in the source-in vacuum is the same as the ratio of the expectation value of $\mathcal{O}$ multiplied by 't Hooft loop operator in the pure vacuum and the expectation value of 't Hooft loop operator itself in the pure vacuum. In this sense, the measurement of an operator in the source-in vacuum can be regarded as a correlation function between an operator and the 't Hooft loop operator. The operator $\mathcal{O}$, which can be regarded as a local probe, is now specified to measure the distribution of the color-electric field, the magnetic current, the modulus of the monopole field etc.

In the dual lattice formulation, the 't Hooft loop operator is defined by

$$H\equiv\exp\left[-\frac{\beta_{\rm DAH}}{2}\sum_{s,\mu<\nu}\Big((\partial\wedge\hat{B})_{\mu\nu}(s)+2\pi\hat{\Sigma}^{\rm E}_{\mu\nu}(s)\Big)^2+\frac{\beta_{\rm DAH}}{2}\sum_{s,\mu<\nu}(\partial\wedge\hat{B})_{\mu\nu}(s)^2\right], \tag{4.4.6}$$

where the definition (4.4.5) is also applicable in the lattice formulation.

Finally, we would like to measure the profiles of the flux tube by inserting the 't Hooft loop. We prepare the vacuum including the 't Hooft loop from the beginning. This corresponds to the direct measurement of the l.h.s. of Eq. (4.4.5). The probe is the field strength ${}^*\hat{F}_{\mu\nu}(s)=(\partial\wedge B)_{\mu\nu}(s)+2\pi\Sigma^{\rm E}_{\mu\nu}(s)$ defined in (4.1.4), the Higgs modulus $\sqrt{|\hat{\chi}(s)|^2}$, and the magnetic supercurrent $k_i(s)=-\hat{m}_B^2 b_i^{(2)}(s)$. Here, $b_i^{(2)}(s)$ is defined in (4.2.3). For an input parameter, we use here $\beta_{\rm DAH}=0.4$, $\hat{m}_B=\hat{m}_\chi=2.0$. This point just belongs to the phase transition region as discussed in the previous section. The vortex density is about 14%, which means that a non-trivial noisy contribution from the vortex excitation enters.

In Fig. 4.6, we show the profiles of the flux tube for the middle plane of the q-$\bar{q}$ system, where the lattice size is 16^4 and open boundary conditions are adopted for the spatial direction of the lattice. When we insert the 't Hooft loop, the periodicity is broken due to the appearance of magnetic supercurrent which circulates around the Dirac string in each time slice. Thus, in principle, we cannot use a small lattice to measure the profiles. However, the use of open boundary condition enables us to circumvent this problem, which means that we can use a relatively small lattice. We have taken 1000 configurations to perform for the average, with 5 sweeps in between, after a thermalization of 30 sweeps. The 't Hooft loop size is 8×16, placed on z-t plane. The measurements are performed at the middle of z axis.

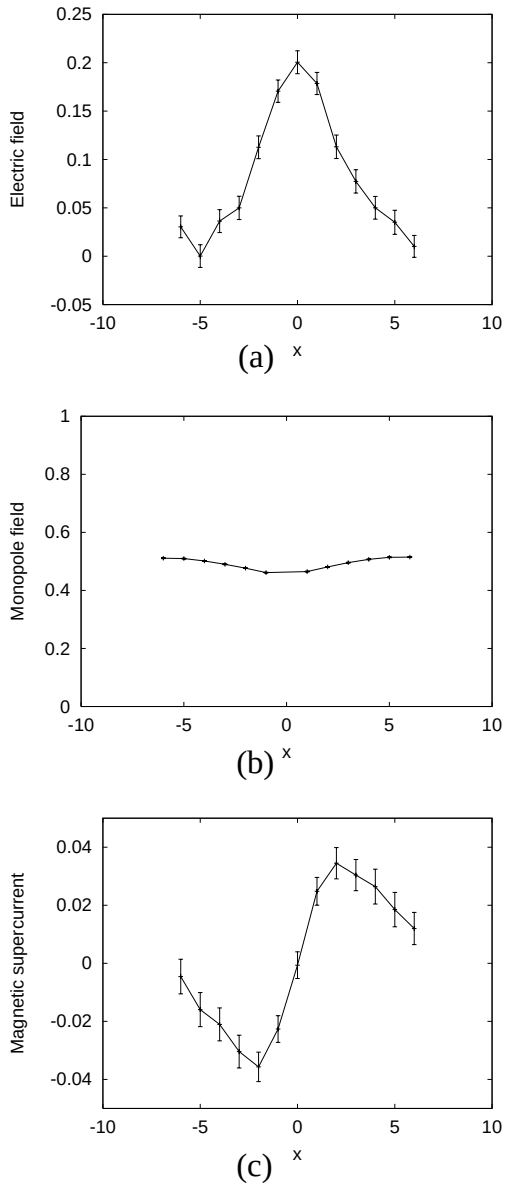

Figure 4.6: The profiles of the flux tube, (a) color-electric field, (b) modulus of the monopole field, (c) color-magnetic monopole supercurrent, as a function of x, at $y = 0$ and $z = 0$.

In order to get three-dimensional variables, we first take the average along the time direction. Then, all data are similarly treated as in the section 4.2. The profiles are shown as a function of x, where $s = (x, 0, 0)$. One finds that the color-electric field is localized around the center (the place of the 't Hooft loop). In this sense, the color-electric field is still confined forming a tube structure. At the same time, the magnetic supercurrent circulates around the center. However, it is important to note that the behavior of the modulus of the monopole field is

completely different from the classical one. Near the center, only small deviation from the constant value is found. Moreover, this constant is not given by one (smaller than one).

To summarize this section, we mention our experiences of scanning the profiles of the flux tube for several points. In the Higgs phase, described by large masses and large β_{DAH}, where the vortex density essentially vanishes, we could obtain the flux-tube profile which is quite similar to the classical one. On the other hand, in the Coulomb phase, described by small masses and small β_{DAH}, where we have large non-vanishing vortex density, it becomes quite difficult to extract the dual superconducting signal from the profile. We never got a good profile for the magnetic supercurrent. In other words, in the Coulomb phase, the 't Hooft loop as the external source is not sufficient to see the flux-tube profile. In our experience, at 30 % vortex density the flux-tube structure is no more recognized. In this sense, the vortex density is a quite important quantity to determine not only the phase diagram, but also the profiles of the flux tube in the quantum vacuum.

4.5 Summary and outlook

In this chapter, we have studied the quantized DAH model using the dual lattice formulation. We have found that this formulation is quite useful not only to obtain the classical flux-tube solution in a numerically more elegant way, but also to evaluate the quantum effect described by the partition function of the DAH model. As a remarkable fact, whether we can observe the profile of the flux tube is very sensitive to the density of vortex loops. For the large vortex density, the classical structure of profile, obtained by solving the field equations, is destroyed.

In the next chapter, we study the quantitative relation between the DAH model and the SU(2) gluodynamics. In other words, we try to fix the DAH couplings from SU(2) gluodynamics. Then, the information of the vacuum structure of the DAH model at the quantum level would be useful to understand the meaning of the resulting couplings of the DAH model.

Chapter 5

SU(2) gluodynamics and the DAH model on lattice

We have shown a derivation of the DAH model from the SU(2) gluodynamics in the chapter 2. During this step, however, the relation of couplings in both models remained unclear, since we did not know how to determine the value of the self-coupling of the monopole field and monopole condensate. In other words, compensating for the unknown information about the nonperturbative non-Abelian vacuum by freely adjustable couplings, we could construct the DAH model as an infrared effective model of SU(2) gluodynamics.

In this chapter, we would like to try to fix the DAH couplings by making use of the Monte Carlo simulation on the lattice, especially, by matching SU(2) original lattice and U(1) Higgs dual lattice, and study how quantitatively well the DAH model can serve as infrared effective model replacing SU(2) gluodynamics at the quantum level. Our strategy is the following: We pay attention to monopoles, since both the SU(2) gluodynamics and the DAH model have these degrees of freedom in common, as shown in the chapter 2. On the SU(2) lattice, we can extract such monopole currents by Abelian projection after the maximally Abelian (MA) gauge fixing. These currents can be used to extract a monopole action which - on the other hand - can be derived from the DAH model [54]. This extraction from an ensemble of monopole currents is done by means of the inverse Monte Carlo method, the extended Swendsen method [24, 55]. This procedure leads finally to the couplings of the DAH model. By using the obtained parameters, we can simulate the DAH model on the dual lattice, and compare the simulation results with the original SU(2) one. In particular, we pay attention to the profile of the color-electric flux tube and the string tension that have been obtained at $\beta_{\mathrm{SU(2)}} = 2.5115$.

5.1 A few words about SU(2) lattice gauge theory

In this section, we start from the SU(2) lattice gauge theory, and explain how to extract the monopole currents in the MA gauge.

5.1.1 SU(2) Wilson action

In the lattice formulation, the space-time coordinates are discretized with the lattice spacing a. The standard lattice action in the SU(2) gauge theory is given by

$$S_{\mathrm{SU}(2)}[U] = \beta_{\mathrm{SU}(2)} \sum_{s,\mu<\nu} \left\{ 1 - \frac{1}{2} \mathrm{Re\ tr}[U_{\mu\nu}(s)] \right\}, \tag{5.1.1}$$

where $U_{\mu\nu}(s) \in \mathrm{SU}(2)$ are plaquette variables

$$U_{\mu\nu}(s) = U_\mu(s) U_\nu(s+\hat{\mu}) U_\mu^\dagger(s+\hat{\nu}) U_\nu^\dagger(s) \tag{5.1.2}$$

and $U_\mu(s) \in \mathrm{SU}(2)$ denote link variables

$$U_\mu(s) = e^{iae\mathcal{A}_\mu(s)} = e^{iae\mathcal{A}_\mu^a(s)T^a}, \tag{5.1.3}$$

where e and $T^a = \tau^a/2$ denote the gauge coupling and the generator of the SU(2) gauge group. The coupling is defined by*

$$\beta_{\mathrm{SU}(2)} = \frac{4}{e^2}. \tag{5.1.4}$$

This lattice action is used to generate a configuration of the vacuum as a set of link variables $\{U_\mu(s)\}$, where the heat-bath algorithm can be adopted without additional Metropolis steps. In the continuum limit $a \to 0$, this SU(2) lattice action reproduces the well-known form of the action of the SU(2) gauge theory,

$$\lim_{a\to 0} S_{\mathrm{SU}(2)}[U] \to \frac{1}{2} \int d^4x \mathrm{tr} G_{\mu\nu} G_{\mu\nu}, \tag{5.1.5}$$

where

$$G_{\mu\nu} = \partial_\mu \mathcal{A}_\nu - \partial_\nu \mathcal{A}_\mu + ie[\mathcal{A}_\mu, \mathcal{A}_\nu]. \tag{5.1.6}$$

This lattice action is used to simulate the physical expectation value of an observable (operator) $\mathcal{O}[U_\mu]$, based on the path integral representation of the partition function, as

$$\begin{aligned} \langle \mathcal{O}[U_\mu] \rangle &= \frac{\int dU \mathcal{O}[U_\mu] \exp\left(-S[U_\mu]\right)}{\int dU \exp\left(-S[U_\mu]\right)} \\ &\approx \frac{1}{N} \sum_{i=1}^{N} \mathcal{O}[\{U_\mu\}_i], \end{aligned} \tag{5.1.7}$$

*Note that $\beta_{\mathrm{SU(N)}} = 2N/e^2$.

where a configuration of link variables denoted $\{U_\mu\}_i$ are generated by the Monte Carlo method. The configurations of link variables are generated by a vectorized heat bath procedure in the local SU(2) group, in the checkerboard realization. They are sampling the weight $\exp(-S_{\mathrm{SU}(2)}[U_\mu])$, such that all configuration can be considered equally important. Then, the expectation value of the operator is obtained as the average of the value of the operator for many configurations. In the SU(2) case, reflecting the non-Abelian property, the Heat-bath reconstruction of the SU(2) link variables is only somewhat more involved than the Abelian case. For our purpose, we were not interested in calculating averages, but to transform the configurations into a particular gauge, suppress the non-diagonal gluons, and to produce an ensemble of importance-weighted monopole currents.

5.1.2 Maximally Abelian (MA) gauge on lattice

The maximally Abelian (MA) gauge fixing is achieved by the gauge transformation

$$U_\mu(s) \to U_\mu^{\mathrm{MA}}(s) = V(s)U_\mu(s)V^\dagger(s+\hat{\mu}), \tag{5.1.8}$$

so as to maximize the variable

$$R \equiv \sum_{s,\mu} \mathrm{tr}\left\{\tau_3 U_\mu(s)\tau_3 U_\mu^\dagger(s)\right\} = 2\sum_{s,\mu}\left[1 - 2\left(\left\{U_\mu^1(s)\right\}^2 + \left\{U_\mu^2(s)\right\}^2\right)\right] \tag{5.1.9}$$

where $V(s)$ and $V^\dagger(s+\hat{\mu})$ correspond to the MA gauge fixing functions located on the sites s and $s+\hat{\mu}$, respectively. Then, the operator

$$X(s) = \sum_\mu \left[U_\mu(s)\tau_3 U_\mu^\dagger(s) + U_\mu^\dagger(s-\hat{\mu})\tau_3 U_\mu(s-\hat{\mu})\right] \tag{5.1.10}$$

is diagonalized. To see this, let us consider the infinitesimal gauge transformation, $V(s) = 1 + i\alpha^a(s)\tau_a$. Here, R is transformed as $R \to R' = R + \delta R$. Then, we have

$$\begin{aligned}
\delta R &= i\sum_{s,\mu}\alpha^a(s)\mathrm{tr}\left[\tau_a\left[U_\mu(s)\tau_3 U_\mu^\dagger(s),\tau_3\right]\right] \\
&\quad + i\sum_{s,\mu}\alpha^a(s+\hat{\mu})\mathrm{tr}\left[\tau_a\left[U_\mu^\dagger(s)\tau_3 U_\mu(s),\tau_3\right]\right] + O(\alpha^2) \\
&= i\sum_{s,\mu}\alpha^a(s)\mathrm{tr}\left[\tau_a\left[X(s),\tau_3\right]\right].
\end{aligned} \tag{5.1.11}$$

Here, if R is already maximized, then δR should vanish. This means that $X(s)$ is diagonalized, since the relation $[X(s),\tau_3] = 0$ is satisfied for all sites. In this gauge, the absolute value of off-diagonal components $U_\mu^1(s)$ and $U_\mu^2(s)$ are rendered as small as possible.

5.1.3 Extraction of monopole currents

We briefly review the procedure of extraction of Abelian monopole currents from SU(2) lattice gauge field configurations. After the MA gauge fixing, by using the Cartan decomposition, the SU(2) link variables can be factorized into the diagonal (Abelian) link variable $u_\mu(s) \in \mathrm{U}(1)_3$ and the off-diagonal (charged matter field) parts $c_\mu(s)$, $c^*_\mu(s) \in \mathrm{SU}(2)/\mathrm{U}(1)_3$ as

$$U^{\mathrm{MA}}_\mu(s) = \begin{pmatrix} \sqrt{1-|c_\mu(s)|^2} & -c^*_\mu(s) \\ c^*_\mu(s) & \sqrt{1-|c_\mu(s)|^2} \end{pmatrix} \begin{pmatrix} u_\mu(s) & 0 \\ 0 & u^*_\mu(s) \end{pmatrix}, \tag{5.1.12}$$

where $u_\mu(s)$ is explicitly written as

$$u_\mu(s) = e^{i\theta_\mu(s)} \quad (-\pi < \theta_\mu(s) < \pi). \tag{5.1.13}$$

The corresponding Abelian field strength (plaquette) is then has the form

$$\theta_{\mu\nu}(s) \equiv \theta_\mu(s) + \theta_\nu(s+\hat{\mu}) - \theta_\mu(s+\hat{\nu}) - \theta_\nu(s) \qquad (-4\pi < \theta_{\mu\nu}(s) < 4\pi). \tag{5.1.14}$$

The U(1) link variables are extracted by the Abelian projection, dropping the off-diagonal gluon contributions in Eq. (5.1.12). They are, in general, multiple valued functions reflecting the compactness of the residual U(1) gauge group. It means that U(1) link variables contain some topological defects, the monopoles. Let us divide the Abelian plaquettes into two parts as

$$\theta_{\mu\nu}(s) \equiv \bar{\theta}_{\mu\nu}(s) + 2\pi n_{\mu\nu}(s) \qquad (-\pi < \bar{\theta}_{\mu\nu}(s) < \pi), \tag{5.1.15}$$

where $n_{\mu\nu}(s) \in \boldsymbol{Z}$ is the modulo 2π of $\theta_{\mu\nu}(s)$. Here, the defect becomes manifest through the breaking of the Bianchi identity

$$\partial_\mu {}^*\theta_{\mu\nu}(s) = \frac{1}{2}\varepsilon_{\mu\nu\rho\sigma}\partial_\nu n_{\rho\sigma}(s+\hat{\mu}) \equiv k_\nu(s) \neq 0 \tag{5.1.16}$$

where $k_\mu(s)$ describes the monopole current as defined by DeGrand and Toussaint in compact QED [70]. The first term of r.h.s. in (5.1.15) satisfies the Bianchi identity $\partial_\mu {}^*\bar{\theta}_{\mu\nu}(s) = 0$. Note that the magnetic current carries integer values, the so-called topological charge. In this case, the limit of monopole currents are $|k_\mu(s)| \leq 2$. The monopole currents are conserved as

$$\partial'_\mu k_\mu(s) = 0, \tag{5.1.17}$$

where ∂'_μ is the backward derivative, which guarantees the conservation of monopole current at each site of the dual lattice. Therefore, monopole currents form closed loops on the dual lattice in four-dimensional space-time.

Finally, we would like to mention the relation of original lattice (where quarks and gluons are defined) and dual lattice. The latter is already adopted to formulate the DAH model

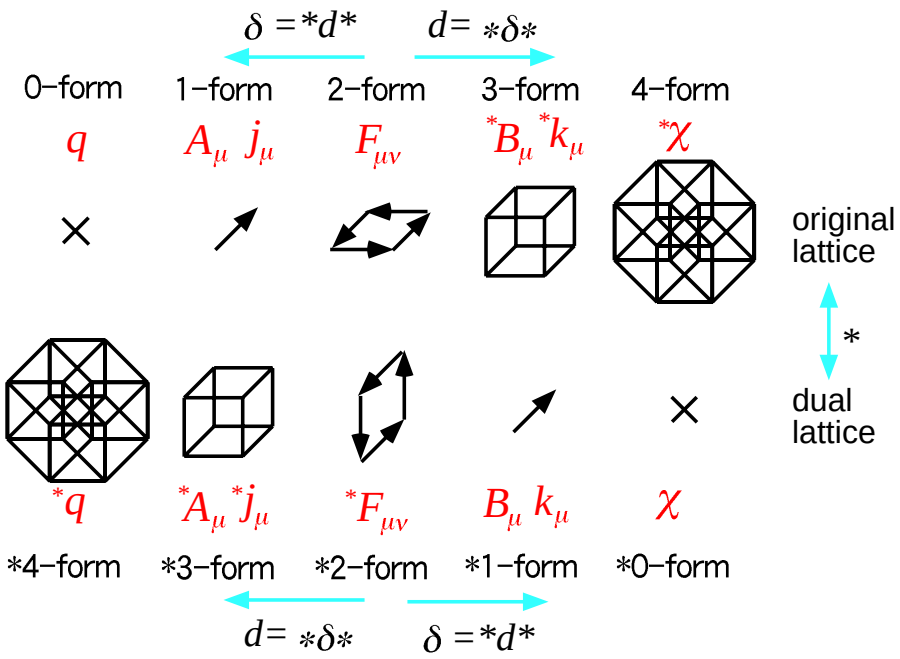

Figure 5.1: The schematic understanding of the relation between original lattice and dual lattice in terms of differential form on lattice.

on lattice in chapter 4. To understand this relation the differential form on lattice is quite useful. In four dimensional space-time, original sites, original links, and original plaquettes can be interpreted as dual hypercubes, dual cubes, and dual plaquettes on dual lattice by the duality transformation. This is achieved by the Hodge dual " $*$ " as shown in Fig. 5.1. The monopole currents $k_\mu(s)$ correspond to 3-form variables defined by three-dimensional cubes on the original lattice. Then we obtain $*1$-form variables in the dual description, which can be defined on dual links. The direction of monopole currents are perpendicular to the three-dimensional cubes on the original lattice. Notice that this is the place where the dual gauge field is also defined. In the original lattice, the exterior derivative " d " express the mapping from k-form to $(k+1)$-form, whereas the mapping from $*k$-form to $*(k+1)$-form on the dual lattice due to the relation $d = *\delta *$. Here, " δ " denotes codifferential corresponding to the mapping from k-form to $(k-1)$-form, satisfying a relation $\delta = *d*$. Then this also has the meaning of mapping from $*k$-form to $*(k-1)$-form. The breaking of the Abelian Bianchi identity is understood as $\delta * F = k$.

5.2 Monopole representation of the DAH model

In this section we derive the monopole representation of the DAH model with no external sources* We start from the lattice partition function given by

$$\mathcal{Z}_{\rm DAH} = \int_{-\infty}^{\infty} \mathcal{D}B \int_{-\infty}^{\infty} \mathcal{D}\chi \int_{-\infty}^{\infty} \mathcal{D}\chi^* \exp\left\{-S_{\rm DAH}[B,\chi,\chi^*]\right\} , \tag{5.2.1}$$

where the form of the lattice action $S_{\rm DAH}$ is defined in (4.1.2). Once the kinetic term of the monopole field is written as

$$\tilde{\gamma}\sum_{\mu}|\chi(s)-U_\mu(s)\chi(s+\hat{\mu})|^2 = -\tilde{\gamma}\sum_{\mu}(\chi^*(s)U_\mu(s)\chi(s+\hat{\mu})+h.c.)+8\tilde{\gamma}|\chi(s)|^2, \tag{5.2.2}$$

the lattice DAH action (4.1.2) has the form

$$\begin{aligned} S_{\rm DAH}[B,\chi,\chi^*] &= \sum_s\Bigg[\frac{\beta_{\rm DAH}}{2}\sum_{\mu<\nu}{}^*F_{\mu\nu}^2(s) - \tilde{\gamma}\sum_{\mu}(\chi^*(s)U_\mu(s)\chi(s+\hat{\mu})+h.c.) \\ &\quad +8\tilde{\gamma}|\chi(s)|^2+\tilde{\lambda}\left(|\chi(s)|^2-1\right)^2\Bigg]. \end{aligned} \tag{5.2.3}$$

Inserting the polar decomposition of the monopole field into modulus and phase

$$\chi(s) = \phi(s)\exp(i\eta(s)) \tag{5.2.4}$$

into the action (5.2.3), we get

$$\begin{aligned} S_{\rm DAH}[B,\phi,\eta] &= \sum_s\Bigg[\frac{\beta_{\rm DAH}}{2}\sum_{\mu<\nu}{}^*F_{\mu\nu}^2(s) - 2\tilde{\gamma}\sum_{\mu}\phi(s)\phi(s+\hat{\mu})\cos(d\eta_\mu(s)+B_\mu(s)) \\ &\quad +8\tilde{\gamma}\phi^2(s)+\tilde{\lambda}(\phi^2(s)-1)^2\Bigg], \end{aligned} \tag{5.2.5}$$

where $d\eta_\mu(s) \equiv \eta(s+\hat{\mu})-\eta(s)$.

Let us now adopt the Villain approximation,

$$\exp\left(a\cos b\right) = \sum_{l\in\boldsymbol{Z}}\exp\left\{a-\frac{a}{2}\left(b+2\pi l\right)^2\right\} , \tag{5.2.6}$$

where the sum over l goes over all integers which representing the periodicity of the cosine. Then the partition function is given by

$$\mathcal{Z}_{\rm DAH} = \int_{-\infty}^{\infty}\mathcal{D}B\int_{-\pi}^{\pi}\mathcal{D}\eta\int_{0}^{\infty}\mathcal{D}\phi^2\sum_{l\in\boldsymbol{Z}}\exp\left\{-S_{\rm DAH}[B,\phi,\eta;l]\right\} , \tag{5.2.7}$$

where the action has the form

$$\begin{aligned} S_{\rm DAH}[B,\phi,\eta;l] &= \sum_s\Bigg[\frac{\beta_{\rm DAH}}{2}\sum_{\mu<\nu}{}^*F_{\mu\nu}^2(s) + \tilde{\gamma}\sum_{\mu}(\phi(s)-\phi(s+\hat{\mu}))^2 \\ &\quad +\tilde{\gamma}\sum_{\mu}\phi(s)\phi(s+\hat{\mu})(d\eta_\mu(s)+B_\mu(s)+2\pi l)^2+\tilde{\lambda}(\phi^2(s)-1)^2\Bigg] \end{aligned} \tag{5.2.8}$$

*In this chapter, we shall omit the explicit hat "ˆ" of fields which denote lattice variables.

5.2.1 Integrating the dual gauge field $B_\mu(s)$ and the monopole phase $\eta(s)$

In order to integrate out the dual gauge field $B_\mu(s)$ and the phase $\eta(s)$, we insert the identity

$$\begin{aligned} const. &= \left\{\prod_{s,\mu}\frac{1}{\sqrt{4\tilde{\gamma}\phi(s)\phi(s+\hat{\mu})}}\right\}\int_{-\infty}^{\infty}\mathcal{D}H\exp\left\{-\sum_{s,\mu}\frac{1}{4\tilde{\gamma}\phi(s)\phi(s+\hat{\mu})}[H_\mu(s)\right. \\ &\left.-2i\tilde{\gamma}\phi(s)\phi(s+\hat{\mu})(d\eta_\mu(s)+B_\mu(s)+2\pi l)]^2\right\} \end{aligned} \tag{5.2.9}$$

into the partition function. Then, the action (5.2.8) becomes

$$\begin{aligned} S_{\rm DAH}[B,\phi,\eta,H;l] &= \sum_s\left[\frac{\beta_{\rm DAH}}{2}\sum_{\mu<\nu}{}^*F_{\mu\nu}^2(s)+\tilde{\gamma}\sum_\mu(\phi(s)-\phi(s+\hat{\mu}))^2+\sum_\mu\frac{H_\mu^2(s)}{4\tilde{\gamma}\phi(s)\phi(s+\hat{\mu})}\right. \\ &\left.-i\sum_\mu H_\mu(s)\left(d\eta_\mu(s)+B_\mu(s)+2\pi l\right)+\tilde{\lambda}(\phi^2(s)-1)^2\right]. \end{aligned} \tag{5.2.10}$$

By using the Poisson resummation formula

$$\int_{-\infty}^{\infty}\mathcal{D}H\sum_{l\in\boldsymbol{Z}}e^{2\pi i(H,l)}f(H)=\sum_{k\in\boldsymbol{Z}}f(k), \tag{5.2.11}$$

we get for the partition function

$$\mathcal{Z}_{\rm DAH}=\int_{-\infty}^{\infty}\mathcal{D}B\int_{-\pi}^{\pi}\mathcal{D}\eta\int_0^{\infty}\mathcal{D}\phi^{-2}\sum_{k\in\boldsymbol{Z}}\exp\left\{-S_{\rm DAH}[B,\phi,\eta;k]\right\}, \tag{5.2.12}$$

where

$$\begin{aligned} S_{\rm DAH}[B,\phi,\eta;k] &= \sum_s\left[\frac{\beta_{\rm DAH}}{2}\sum_{\mu<\nu}{}^*F_{\mu\nu}^2(s)+\tilde{\gamma}\sum_\mu(\phi(s)-\phi(s+\hat{\mu}))^2+\sum_\mu\frac{k_\mu^2(s)}{4\tilde{\gamma}\phi(s)\phi(s+\hat{\mu})}\right. \\ &\left.-i\sum_\mu k_\mu(s)\left(d\eta_\mu(s)+B_\mu(s)\right)+\tilde{\lambda}(\phi^2(s)-1)^2\right]. \end{aligned} \tag{5.2.13}$$

Note that the measure of the monopole field modulus has changed as follows

$$\mathcal{D}\phi^2\times\prod_{\mu=-4}^{4}\phi^{-\frac{1}{2}}=2\phi\mathcal{D}\phi\times\phi^{-4}=2\phi^{-3}\mathcal{D}\phi=\mathcal{D}\phi^{-2}. \tag{5.2.14}$$

Here, the action related to the phase $\eta(s)$ is extracted as

$$-i\sum_{s,\mu}k_\mu(s)d\eta_\mu(s)=-i(k,d\eta)=-i(\delta k,\eta), \tag{5.2.15}$$

where we have used the abbreviated notation of a differential form on lattice. Then the phases $\eta(s)$ can be integrated out to give a δ-constraint

$$\int_{-\pi}^{\pi}\mathcal{D}\eta\exp\left\{i(\delta k,\eta)\right\}=\delta(\delta k). \tag{5.2.16}$$

The current $k_\mu(s)$ is regarded as the monopole current, and this delta function expresses its conservation. Moreover, adopting the Landau gauge $\delta B = 0$, the kinetic term of the dual gauge field can be written in shorthand as

$$\sum_{s,\mu<\nu} {}^*F^2_{\mu\nu}(s) = (dB, dB) = (B, \delta dB) = (B, (\delta d + d\delta)B) = (B, \Delta B)\,. \tag{5.2.17}$$

Then the action originating from the dual gauge field $B_\mu(s)$ in (5.2.13) is

$$\begin{aligned} & \frac{\beta_{\rm DAH}}{2} \sum_{s,\mu<\nu} {}^*F^2_{\mu\nu}(s) - i \sum_{s,\mu} k_\mu(s) B_\mu(s) \\ = \;& \frac{\beta_{\rm DAH}}{2}(B, \Delta B) - i(k, B) \\ = \;& \frac{\beta_{\rm DAH}}{2}(B - \frac{i}{\beta_{\rm DAH}}\Delta^{-1}k)\Delta(B - \frac{i}{\beta_{\rm DAH}}\Delta^{-1}k) + \frac{1}{2\beta_{\rm DAH}}(k, \Delta^{-1}k)\,, \end{aligned} \tag{5.2.18}$$

where Δ^{-1} represents the Coulomb propagator on lattice. Then, we can integrate out the dual gauge field $B_\mu(s)$ as a Gaussian integral for $B' \equiv B - i\Delta^{-1}k/\beta_{\rm DAH}$. The result is

$$\mathcal{Z}_{\rm DAH} = \sum_{k \in \boldsymbol{Z}, \delta k = 0} \exp\{-S^{\rm mon}_G[k]\} \int_0^\infty \mathcal{D}\phi^{-2} \exp\{-S^{\rm mon}_H[\phi; k]\}\,, \tag{5.2.19}$$

where

$$S^{\rm mon}_G[k] \equiv \frac{1}{2\beta_{\rm DAH}}(k, \Delta^{-1}k), \tag{5.2.20}$$

$$S^{\rm mon}_H[\phi; k] \equiv \tilde{\gamma} \sum_{s,\mu} (\phi(s) - \phi(s+\hat{\mu}))^2 + \sum_{s,\mu} \frac{k^2_\mu(s)}{4\tilde{\gamma}\phi(s)\phi(s+\hat{\mu})} + \tilde{\lambda} \sum_s (\phi^2(s) - 1)^2 \tag{5.2.21}$$

5.2.2 Integrating the monopole field modulus $\phi(s)$

We evaluate now the $\phi(s)$ integral. Let us rescale the variable as $\phi(s) \to \phi(s)/\sqrt{\tilde{\gamma}}$, then the action (5.2.21) becomes

$$S^{\rm mon}_H[\phi; k] = \sum_{s,\mu} (\phi(s) - \phi(s+\hat{\mu}))^2 + \sum_{s,\mu} \frac{k^2_\mu(s)}{4\phi(s)\phi(s+\hat{\mu})} + \lambda_0 \sum_s (\phi^2(s) - \tilde{\gamma})^2, \tag{5.2.22}$$

where

$$\lambda_0 \equiv \frac{\tilde{\lambda}}{\tilde{\gamma}^2}, \quad v_0^{-1} \equiv \tilde{\gamma}. \tag{5.2.23}$$

By introducing $y(s)$ defined by $y(s) \equiv \phi^{-2}(s)$, we have

$$\int_0^\infty \mathcal{D}\phi^{-2} \exp\{-S^{\rm mon}_H[\phi; k]\} \;=\; \int_0^\infty \mathcal{D}y \exp\{-S^{\rm mon}_H[y; k]\} \tag{5.2.24}$$

where

$$S_H^{\rm mon}[y;k] = \sum_{s,\mu}\left(\frac{1}{\sqrt{y(s)}}-\frac{1}{\sqrt{y(s+\hat{\mu})}}\right)^2 + \frac{1}{4}\sum_{s,\mu}\sqrt{y(s)y(s+\hat{\mu})}k_\mu^2(s) + \lambda_0\sum_s\left(\frac{1}{y(s)}-v_0^{-1}\right)^2. \quad (5.2.25)$$

Let us put $y(s) = v_0 + \tilde{y}(s)$, and change the integral region $\int_0^\infty \mathcal{D}\tilde{y} \to \int_{-\infty}^\infty \mathcal{D}\tilde{y}$. The approximation up to $\tilde{y}^2(s)$ leads to

$$\begin{aligned}
&\int_{-\infty}^{\infty}\mathcal{D}\tilde{y}\exp\left\{-S_H^{\rm mon}[\tilde{y};k]\right\} \\
&= \exp\left\{-\frac{v_0}{4}\|k\|^2\right\}\int_{-\infty}^{\infty}\mathcal{D}\tilde{y}\exp\Bigg\{-\frac{1}{4v_0^3}\|\tilde{y}(s)-\tilde{y}(s+\hat{\mu})\|^2 \\
&-\frac{1}{8}\sum_s\sum_{\mu=-4}^{4}k_\mu^2(s)\tilde{y}(s) - \frac{1}{16v_0}\sum_s\sum_{\mu=1}^{4}k_\mu^2(s)\tilde{y}(s)\tilde{y}(s+\hat{\mu}) \\
&+\frac{1}{32v_0}\sum_s\sum_{\mu=-4}^{4}k_\mu^2(s)\tilde{y}^2(s) - \frac{\lambda_0}{v_0^4}\sum_s\tilde{y}^2(s) + O(\tilde{y}^3(s))\Bigg\}. \quad (5.2.26)
\end{aligned}$$

Now we are in the position to evaluate the Gaussian integral over $\tilde{y}(s)$. Using the convenient definitions of variables

$$p(s) = \sum_{\mu=-4}^{4}k_\mu^2(s), \quad (5.2.27)$$

$$A(s) = \frac{\lambda_0}{v_0^4}+\frac{2}{v_0^3}-\frac{1}{32v_0}p(s), \quad (5.2.28)$$

$$B_\mu(s) = -\frac{1}{2v_0^3}+\frac{1}{16v_0}k_\mu^2(s), \quad (5.2.29)$$

$$C(s,t) = A(s)\delta_{s,t}+D(s,t), \quad (5.2.30)$$

$$D(s,t) = \frac{1}{2}\sum_{\mu=1}^{4}(B_\mu(s)\delta_{s+\hat{\mu},t}+B_\mu(t)\delta_{t+\hat{\mu},s}), \quad (5.2.31)$$

$$\xi(s) = \frac{1}{16}A^{-1}(s)p(s), \quad (5.2.32)$$

we obtain the monopole action in the form

$$S_H^{\rm mon}[k] = \frac{v_0}{4}\|k\|^2 - \frac{1}{2^8}\sum_s A^{-1}(s)p^2(s) + \frac{1}{2}{\rm Tr}\ln C(s,t) + \sum_s\sum_{\mu=1}^{4}\xi(s)D(s,t)\xi(t) - \sum_{s,t}\sum_{u,w}\xi(s)D(s,u)C^{-1}(u,w)D(w,t)\xi(t). \quad (5.2.33)$$

Here we assume that λ_0 is large. Thus, we neglect the fourth and fifth term in (5.2.33), since the fourth term yields the non-local interaction of order $1/\lambda_0^2$ and the fifth term is of order $1/\lambda_0^3$.

Inserting (5.2.28) into (5.2.33), the second term is evaluated as

$$-\frac{1}{2^8}\sum_{s,t}\delta_{s,t}A^{-1}(s)p^2(s) \;=\; \left[-\frac{v_0^4}{2^8\lambda_0}\right]\sum_s p^2(s)+O(1/\lambda_0^2). \tag{5.2.34}$$

The trace term is evaluated as

$$\begin{aligned}\frac{1}{2}\mathrm{Tr}\ln C(s,t) &= \frac{1}{2}\mathrm{Tr}\ln A(s)\delta_{s,t}+\frac{1}{2}\mathrm{Tr}\ln\|\delta_{s,t}+A^{-1}(s)D(s,t)\|\\ &= \frac{1}{2}\sum_s\ln A(s)-\frac{1}{4}\sum_{s,t}\frac{D(s,t)D(t,s)}{A(s)A(t)}\\ &= const+\left[-\frac{v_0^3}{2^5\lambda_0}\right]\|k\|^2+O(1/\lambda_0^2).\end{aligned} \tag{5.2.35}$$

Hence, up to $O(1/\lambda_0)$ the action is

$$S_H^{\mathrm{mon}}[k] \;=\; \left(\frac{v_0}{4}-\frac{v_0^3}{2^5\lambda_0}\right)\|k\|^2-\frac{v_0^4}{2^8\lambda_0}\sum_s\left(\sum_{\mu=-4}^{4}k_\mu^2(s)\right)^2. \tag{5.2.36}$$

Finally, we obtain the monopole representation of the DAH model, which is expressed exclusively in terms of monopole currents, as

$$\mathcal{Z}_{\mathrm{DAH}}=\sum_{k\in\boldsymbol{Z}}\exp\left\{-S_{\mathrm{DAH}}[k]\right\}, \tag{5.2.37}$$

where

$$S_{\mathrm{DAH}}[k]=\frac{1}{2\beta_{\mathrm{DAH}}}(k,\Delta^{-1}k)+\left(\frac{v_0}{4}-\frac{v_0^3}{2^5\lambda_0}\right)\|k\|^2-\frac{v_0^4}{2^8\lambda_0}\sum_s\left(\sum_{\mu=-4}^{4}k_\mu^2(s)\right)^2. \tag{5.2.38}$$

This form of action is adopted in a fit, using monopole current configurations extracted from SU(2) lattice gluodynamics in the Abelian projection from the MA gauge. For this purpose Swendsen's inverse Monte Carlo method, extended from spin to current models by Shiba and Suzuki [24, 55], is used. Once the couplings,

$$g_1\equiv\frac{1}{2\beta_{\mathrm{DAH}}}, \tag{5.2.39}$$

$$g_2\equiv\frac{v_0}{4}-\frac{v_0^3}{2^5\lambda_0}, \tag{5.2.40}$$

$$g_3\equiv\frac{v_0^4}{2^8\lambda_0}, \tag{5.2.41}$$

are determined by this procedure, we can translate this information into our standard (field) representation of the DAH model (4.1.2) by the definition (5.2.23). Note that couplings g_1, g_2, and g_3 describe the strength of the Coulomb, the 2-point, and the 4-point interaction of the monopole current, respectively.

5.3 Extended Swendsen method

We briefly explain the iterative method used to determine the monopole action corresponding to Abelian-projected SU(2) lattice gluodynamics [24, 55]. We start from the action written as a sum of various terms,

$$S[k] = \sum_i g_i S_i[k], \tag{5.3.1}$$

where $\{S_i[k]\}$ is a set of independent operators depending on the monopole current, $\{g_i\}$ are the corresponding coupling constants, which can be recovered by the following method from an ensemble of configurations $\{k\}$.

We start from a general observation. Let us consider the expectation value of a certain operator $\mathcal{O}[k]$,

$$\langle \mathcal{O}[k] \rangle = \frac{\left(\prod_{s,\mu} \sum_{k_\mu(s)=-\infty}^{\infty}\right)\left(\prod_s \delta_{\partial'_\mu k_\mu(s),0}\right) \mathcal{O}[k] \exp\{-\sum_i g_i S_i[k]\}}{\left(\prod_{s,\mu} \sum_{k_\mu(s)=-\infty}^{\infty}\right)\left(\prod_s \delta_{\partial'_\mu k_\mu(s),0}\right) \exp\{-\sum_i g_i S_i[k]\}}, \tag{5.3.2}$$

where ∂'_μ denotes a backward derivative and the Kronecker delta enforces monopole current conservation. Here, we define $\hat{S}_i[k]$ as a part of $S_i[k]$ which depends on the monopole current running around a particular plaquette $(s', \hat{\mu}', \hat{\nu}')$: $\hat{k}_{\mu'}(s')$, $\hat{k}_{\nu'}(s'+\hat{\mu}')$, $\hat{k}_{\mu'}(s'+\hat{\nu}')$, and $\hat{k}_{\nu'}(s')$. Then, one finds that the partial (local) average of the operator $\mathcal{O}$ defined by

$$\overline{\mathcal{O}}[k, \{g_i\}] = \frac{\sum_{M=m_1}^{m_2} \mathcal{O}[\bar{k}] \exp\left\{-\sum_i g_i \hat{S}_i[\bar{k}]\right\}}{\sum_{M=m_1}^{m_2} \exp\left\{-\sum_i g_i \hat{S}_i[\bar{k}]\right\}} \tag{5.3.3}$$

has the property

$$\langle \mathcal{O}[k] \rangle = \langle \overline{\mathcal{O}}[k] \rangle, \tag{5.3.4}$$

i.e. it can be substituted instead of $\mathcal{O}[k]$ in the average. Here, the $\bar{k}$ run over

$$\bar{k}_\mu(s) = k_\mu(s) + M\left(\delta_{s,s'}\delta_{\mu,\mu'} + \delta_{s,s'+\hat{\mu}'}\delta_{\mu,\nu'} - \delta_{s,s'+\hat{\nu}'}\delta_{\mu,\mu'} - \delta_{s,s'}\delta_{\mu,\nu'}\right), \tag{5.3.5}$$

where the limits m_1 and m_2 guarantee that no $\bar{k}$ exceeds the maximum value of monopole charge. In the DGT monopole case, this is $|\bar{k}| \leq 2$.

Let us define an operator $\widetilde{\mathcal{O}}[k] \equiv \overline{\mathcal{O}}[k, \{\tilde{g}_i\}]$ using a guessed set of couplings $\{\tilde{g}_i\}$ in (5.3.3). Then we can compare its average with the ensemble average of $\mathcal{O}[k]$. For a correct guess, $\tilde{g}_i = g_i$ for all i, one must find

$$\langle \mathcal{O}[k] \rangle = \langle \widetilde{\mathcal{O}}[k] \rangle. \tag{5.3.6}$$

We apply this for the operators $\{S_i[k]\}$. As long as $\tilde{g}_i \neq g_i$ for an index i, we expand the difference $\langle S_i - \widetilde{S}_i \rangle$ up to the first order of $(g_i - \tilde{g}_i)$ and get an algebraic equation:

$$\langle S_i - \widetilde{S}_i \rangle = \sum_j \langle \widetilde{S}_i \widetilde{S}_j - \widetilde{S_i S_j} \rangle (g_j - \tilde{g}_j). \tag{5.3.7}$$

We solve this equation iteratively for g_i until the set of coupling constants is found, which corresponds to the ensemble averages in the sense of Eq. (5.3.2). Note that in our case, operators are given by

$$S_1[k] = (k, \Delta^{-1} k) = \sum_{s,t} \sum_{\mu=1}^{4} k_\mu(s) \Delta^{-1}(s-t) k_\mu(t), \tag{5.3.8}$$

$$S_2[k] = \|k\|^2 = \sum_s \sum_{\mu=1}^{4} k_\mu^2(s), \tag{5.3.9}$$

$$S_3[k] = \sum_s \left(\sum_{\mu=-4}^{4} k_\mu^2(s) \right)^2. \tag{5.3.10}$$

5.4 Input parameters of the DAH model

We already have the monopole action derived from the DAH model as given in (5.2.38). Now, we can determine the couplings (5.2.39), (5.2.40), and (5.2.41) by using the extended Swendsen method. Note that this is the place where the original non-Abelian dynamics enters our specification of a proper infrared effective description.

We have generated several samples, each of 40 configurations of the SU(2) lattice gauge field, representing the vacuum at $\beta_{\mathrm{SU}(2)} = 2.5115$ equivalent to a scale $a_{\mathrm{SU}(2)} = 0.086$ fm [48]. The lattice spacing $a_{\mathrm{SU}(2)}$ has been inferred from a comparison with the full non-Abelian string tension assumed to be equal to $\sigma_{\mathrm{SU}(2)} = (0.440\ \mathrm{GeV})^2$. These configurations have been put into MA gauge by a standard over-relaxation gauge fixing procedure. After the Abelian projection, we have localized the trajectories of *elementary* U(1) monopoles according to the method of DeGrand and Toussaint [70]. No blocking to type I or type II Abelian monopoles has been done, in order to have the same lattice spacing. Hence, the lattice spacing of the DAH model a_{DAH} is the same as $a_{\mathrm{SU}(2)}$. In Fig. 5.2, we show one configuration of monopole world line clusters on the 16^4 lattice (projected to a 16^3 lattice by contracting the Euclidean time direction).

Then, by fitting the samples of monopole current configurations by means of the extended Swendsen method, we have found the couplings g_i $(i = 1, 2, 3)$ for $\beta_{\mathrm{SU}(2)} = 2.5115$ as

$$g_1 = 12.47 \pm 0.20,$$
$$g_2 = 0.4834 \pm 0.031,$$

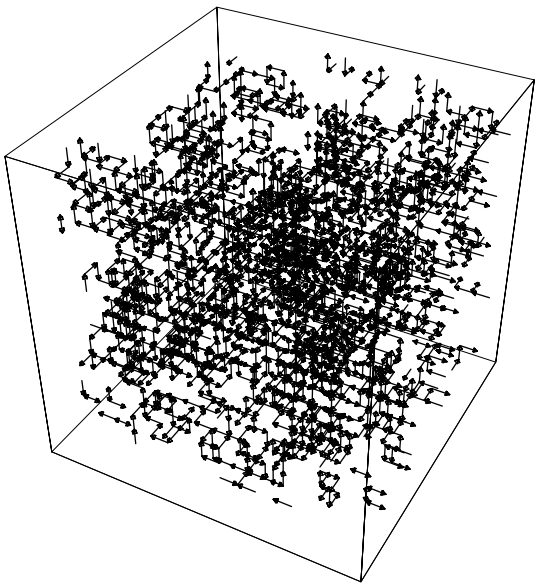

Figure 5.2: The monopole currents projected into $\boldsymbol{R}^3$ in the SU(2) lattice gauge theory in the MA gauge with 16^4 ($\beta_{\mathrm{SU(2)}} = 2.5115$). There appears a global network of monopole world lines.

$$g_3 = 0.01563 \pm 0.00305. \tag{5.4.1}$$

The lattice size dependence of parameters is checked by using another lattice size, for instance 10^4 lattice. However, no strong size dependence is observed.

Solving the coupled algebraic equations (5.2.39), (5.2.40) and (5.2.41), we obtain β_{DAH}, v_0 and λ_0:

$$\begin{aligned} &\beta_{\mathrm{DAH}} = 0.04007, \\ &\lambda_0 = 5.488 = \tilde{\lambda}/\tilde{\gamma}^2, \\ &v_0 = 2.165 = \tilde{\gamma}^{-1}. \end{aligned} \tag{5.4.2}$$

Then, from (5.2.23), we find the coupling parameters of the original DAH model, $\tilde{\gamma}$ and $\tilde{\lambda}$. The corresponding bare mass parameters are given from the relation (4.1.3) by

$$\begin{aligned} \hat{m}_B &= \sqrt{\frac{2\tilde{\gamma}}{\beta_{\mathrm{DAH}}}} = \sqrt{\frac{2}{\beta_{\mathrm{DAH}} v_0}} = 4.801, \\ \hat{m}_\chi &= 2\sqrt{\frac{\tilde{\lambda}}{\tilde{\gamma}}} = 2\sqrt{\frac{\lambda_0}{v_0}} = 3.184. \end{aligned} \tag{5.4.3}$$

We emphasize that these masses have no resemblance to the renormalized masses. From the analysis of the phase diagram of the DAH model, we find that this parameter set belongs to

just the phase transition region between the Coulomb phase and the Higgs phase. The set of parameter $\beta_{\rm DAH}$, $\tilde{\gamma}$, and $\tilde{\lambda}$ has been used to simulate the DAH model (4.1.2).

In the following two sections, we shall concentrate on how well the DAH model (4.1.2) is able to reproduce the original SU(2) results, *i.e.*, the profile of the color-electric flux tube, which has been reported by Bali *et al.* [48], and the string tension. This will require two different sets of lattice simulations, with color-electric Dirac strings inserted into the vacuum and the measurement of 't Hooft loops in the vacuum.

5.5 Monte Carlo simulation of the DAH model

In this section, we study the profile of the color-electric flux tube and the string tension for the obtained parameter set in the previous section.

5.5.1 Measuring the flux-tube profile in the DAH model

First, we study the profiles of the color-electric flux tube. The numerical techniques how to measure the profiles are the same as explained in the chapter 4. The 't Hooft loop is inserted from the beginning whenever the configuration of the dual gauge field and the monopole field are generated in the DAH vacuum. Open boundary conditions are adopted for the spatial directions of the dual lattice. The lattice size used is 24^4 and the 't Hooft loop is placed at z-t plane with the size 12×24. We concentrate on the middle of the z axis for measurements.

In Fig. 5.3, we show the results, where we have taken 48500 configurations for the average at every 10 sweeps after a thermalization of 200 sweeps. Three-dimensional variables are obtained after averaging the time slices. As discussed in the chapter 4, clearly, these profiles are different from the classical ones, which is due to the presence of non-vanishing vortex density, where the vortex density is about 50 % [See, Fig. 4.5].

We would like to compare these results with the original SU(2) ones which is shown in Fig. 1.4. As explained, the lattice spacing of the DAH model $a_{\rm DAH}$ is the same $a_{\rm SU(2)} = 0.086$ fm. One may find that the behavior of the color-electric field seems to roughly coincide with each other. However, since we could not get good profile for the magnetic supercurrent (only tiny signal of circulation of current around the center is observed), we should consider that this is accidental. Now, contrary to the original SU(2) gluodynamics, we have the monopole field. One finds that the behavior of this field is completely different from the classical one. No deviation of the modulus of monopole field around the center is found. It takes a constant value around 0.6 (< 1) everywhere.

In Fig. 5.4, we show the profile of the color-electric from another point of view, where we have assumed cylindrical symmetry around the center, taking the average appropriately.

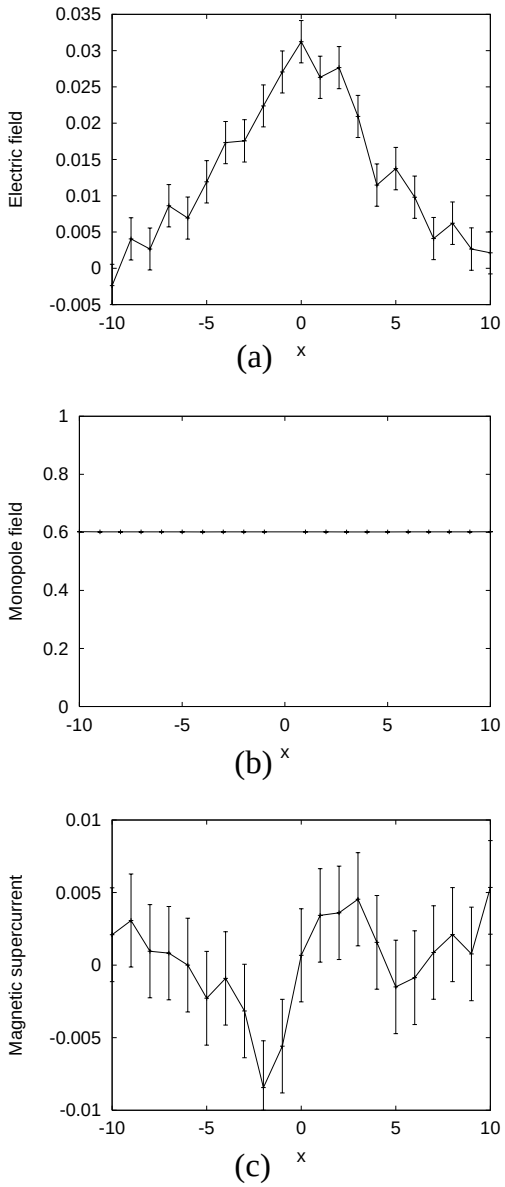

Figure 5.3: The profiles of the flux tube, (a) color-electric field, (b) modulus of the monopole field, (c) color-magnetic monopole supercurrent, as a function of x, at $y = 0$ and $z = 0$, corresponding to $\beta_{\mathrm{SU}(2)} = 2.5115$.

Since now we are using a finite size of the 't Hooft loop, this contains information of ends of the color-electric Dirac string, that is, the Coulomb field. As discussed in the chapter 3 [See, Fig. 3.3], we can decompose the contents of the color-electric field of the flux tube into two parts, the induced field and the Coulombic field, respectively. An important point is that if there is no induced color-electric field, we only have Coulombic field, which penetrates into

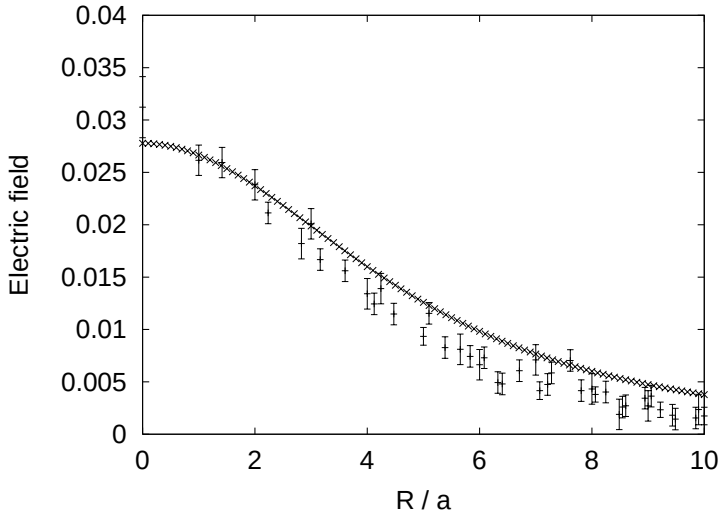

Figure 5.4: The profile of the color-electric field as a function of radius corresponding to $\beta_{\mathrm{SU(2)}} = 2.5115$, where the lattice spacing is $a_{\mathrm{DAH}} = 0.086$ fm. The solid line represents a contribution from the Coulombic color-electric field.

the whole vacuum. In this sense, the profile of the color-electric field of the flux tube should have a different curve expected from the Coulombic behavior. Here, the solid line shown in Fig. 5.4 corresponds to the Coulombic color-electric field, which can be calculated from the explicit form of $C_{\mu\nu}$ in Eq. (3.2.9). One finds that lattice data show the deviation from the Coulomb behavior. In this sense, the color-electric field, which is originating from the q-$\bar{q}$ system, is confined forming a tube structure.

5.5.2 Measuring the string tension

In the previous subsection we have described our study of the properties of the flux tube in the quantum DAH model. However, we have found that it is difficult to extract the corresponding classical parameters of the DAH model, since the form of the profiles are clearly different from the classical one due to the existence of non-vanishing vortex density. Then, it is important to measure another more direct quantity to compare with the original SU(2) result. Therefore, in this subsection, we measure the string tension of the flux tube in terms of the expectation value of the 't Hooft loop operator [49].

In order to know the free energy of this state with external sources, *i.e.* in excess to the vacuum, we need to know the partition function corresponding to the simulations of the last section and then to calculate the ratio with the partition function without external sources. Exactly, this ratio is defined by the expectation value of the 't Hooft loop operator. Within the dual theory it serves as a substitute for the Wilson loop (in the case of the non-Abelian

or Abelian projected theory), the starting point from which the quark-antiquark force can be calculated.

It is well known that a Monte Carlo simulation does not provide the partition function together with the vacuum expectation values, in our case of the dual field strength or the monopole current. The 't Hooft loop operator as ratio of partition functions can, however, be obtained by a series of simulations with Gibbs measures interpolating between $\Sigma^{\mathrm{E}}_{\mu\nu}(s) = 0$ and $\Sigma^{\mathrm{E}}_{\mu\nu}(s) = 1$ on the subset of plaquettes which are dual to the area of the 't Hooft loop. We introduced a parameter $\xi \in [0,1]$ continuously modifying $\Sigma^{\mathrm{E}}_{\mu\nu}(s) \to \xi\Sigma^{\mathrm{E}}_{\mu\nu}(s)$ in (4.1.4).

With this generalization, the partition function $\mathcal{Z}_{\mathrm{DAH}}[\Sigma^{\mathrm{E}}]$ becomes a function of ξ via

$$\mathcal{Z}_{\mathrm{DAH}}[\xi\Sigma^{\mathrm{E}}] = \int_{-\infty}^{\infty} \mathcal{D}B \int_{-\infty}^{\infty} \mathcal{D}\chi \int_{-\infty}^{\infty} \mathcal{D}\chi^* \exp\left\{-S_{\mathrm{DAH}}[B, \xi\Sigma^{\mathrm{E}}, \chi, \chi^*]\right\}, \tag{5.5.1}$$

with the action $S_{\mathrm{DAH}}[B, \xi\Sigma^{\mathrm{E}}, \chi, \chi^*]$ from eq. (4.1.2) now containing, instead of ${}^*F_{\mu\nu}(s)$,

$${}^*F_{\mu\nu}[B, \xi\Sigma^{\mathrm{E}}](s) = B_\mu(s) + B_\nu(s+\hat{\mu}) - B_\mu(s+\hat{\nu}) - B_\nu(s) + 2\pi\xi\Sigma^{\mathrm{E}}_{\mu\nu}(s). \tag{5.5.2}$$

Then the logarithmic derivative of the partition function with respect to ξ is simply

$$\begin{aligned}
\frac{\partial}{\partial\xi} \ln \mathcal{Z}_{\mathrm{DAH}}[\xi\Sigma^{\mathrm{E}}] &= \frac{1}{\mathcal{Z}_{\mathrm{DAH}}[\xi\Sigma^{\mathrm{E}}]} \frac{\partial \mathcal{Z}_{\mathrm{DAH}}[\xi\Sigma^{\mathrm{E}}]}{\partial\xi} \\
&= -2\pi\beta_{\mathrm{DAH}} \left\langle \sum_s \sum_{\mu<\nu} {}^*F_{\mu\nu}[B, \xi\Sigma^{\mathrm{E}}](s)\Sigma^{\mathrm{E}}_{\mu\nu}(s) \right\rangle_{|\xi} \\
&= -\left\langle \frac{dS_{\mathrm{DAH}}}{d\xi} \right\rangle_{|\xi},
\end{aligned} \tag{5.5.3}$$

where $\langle ... \rangle_{|\xi}$ indicates that the average is taken with respect to the interpolating Gibbs measure modified by $\xi \in [0,1]$.

Here, we find that the excess of free energy $\Delta F(R,T)$ can be computed from (5.5.3), by integration over the ξ parameter, as

$$\Delta F(R,T) = 2\pi\beta_{\mathrm{DAH}} \int_0^1 d\xi \left\langle \sum_{s,\mu<\nu} {}^*F_{\mu\nu}[B, \xi\Sigma^{\mathrm{E}}](s)\Sigma^{\mathrm{E}}_{\mu\nu}(s) \right\rangle_{|\xi}, \tag{5.5.4}$$

where this value is related with the expectation value of the 't Hooft loop operator as

$$\langle H \rangle = \frac{\mathcal{Z}_{\mathrm{DAH}}[\Sigma^{\mathrm{E}}]}{\mathcal{Z}_{\mathrm{DAH}}[0]} = \exp\left(-\Delta F(R,T)\right) \sim \exp\left(-\|A\|\sigma a^2\right), \tag{5.5.5}$$

where $\|A\| \equiv R \times T$ denotes the number of plaquettes contributing to the sum in (5.5.3). Here, "$\sim$" expresses the expectation that if the 't Hooft loop satisfies the area law decay, with $\|A\|a^2$ just the area A of the minimal surface, we can extract the string tension σ. More precisely, the excess is expected to contain other terms besides of the area term, depending

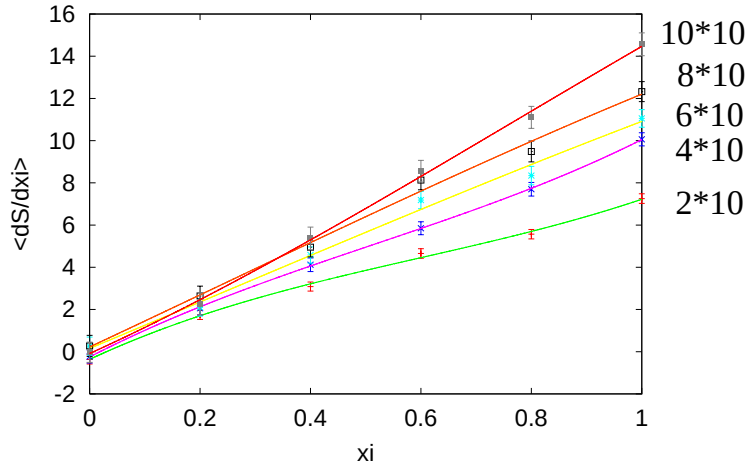

Figure 5.5: The value of $\langle dS_{\rm DAH}/d\xi\rangle_{|\xi}$ as a function of ξ for various sizes of the 't Hooft loops 2×10, 4×10, 6×10, 8×10, and 10×10.

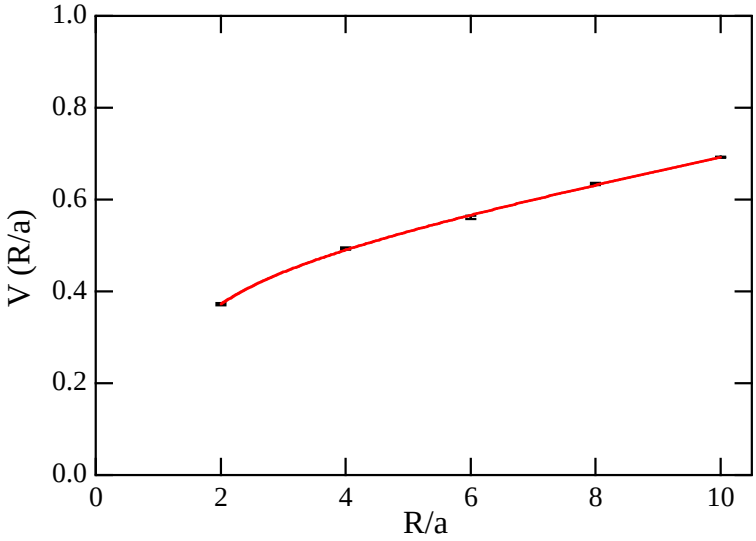

Figure 5.6: The inter-quark potential as a function of q-$\bar{q}$ distance, where the lattice spacing is $a_{\rm DAH} = 0.086$ fm.

only on the size of area $\|A\|$. In any case, once the excess of free energy is calculated for various sizes of the 't Hooft loops, at the set of couplings of the DAH model as determined earlier, we can extract the inter-quark potential.

In Fig. 5.5, we show the value of $\langle dS_{\rm DAH}/d\xi\rangle_{|\xi}$ as a function of ξ for various sizes of the 't Hooft loops 2×10, 4×10, 6×10, 8×10, and 10×10. The solid line is a polynomial fit of the data for each size of the 't Hooft loops. Then the excess of free energy is calculated by integrating over ξ. Dividing this by the constant temporal length T of loops, we finally get

the inter-quark potential as shown in Fig. 5.6. Clearly, this curve contains a linearly rising part. Fitting this slope by using the ansatz

$$V(x) = A + \frac{C}{x} + \sigma^L x, \tag{5.5.6}$$

we find the value

$$A = 0.44 \pm 0.02, \tag{5.5.7}$$

$$C = -0.25 \pm 0.03, \tag{5.5.8}$$

$$\sigma^L = 0.027 \pm 0.002. \tag{5.5.9}$$

The dimensionful string tension $\sigma = \sigma^L / a_{\rm DAH}^2$ is then calculated by restoring the lattice spacing $a_{\rm DAH} = a_{\rm SU(2)} = 0.086$ fm, as

$$\sqrt{\sigma} = 0.38 \pm 0.02 \text{ GeV}. \tag{5.5.10}$$

Note that this value reproduces $0.38/0.44 = 86\%$ of the SU(2) string tension $\sqrt{\sigma_{\rm SU(2)}}$. This result is very exciting for us, since this suggests that the most infrared property of the SU(2) gluodynamics can be reproduced by the DAH model quantitatively well at the quantum level.

5.6 Summary and outlook

Finally, we would like to summarize this chapter. We have studied the quantitative relation between the Abelian-projected SU(2) gluodynamics and the dual Abelian Higgs (DAH) model on the lattice, extending the comparison to the quantum level. The input bare parameters of the DAH model are obtained by making use of the extended Swendsen method, where monopole currents from SU(2) lattice gauge theory in the maximally Abelian (MA) gauge are fitted by a monopole action. The latter is then put into relation to the monopole representation of the DAH model. The profile of the color-electric flux tube and the string tension (from dual 't Hooft loops) are reproduced within the DAH model by means of Monte Carlo simulations. We have specially paid attention to the case $\beta_{\rm SU(2)} = 2.5115$. Our result of the string tension shows that SU(2) lattice gauge theory in the MA gauge is quantitatively well reproduced by quantized DAH model.

Our next task is to take the continuum limit of this study both the SU(2) gauge theory and the DAH model. However, we consider that the matching should be performed at a large scale where the monopole-current dynamics is sufficiently simple. Then, we can argue the renormalized mass parameters of the DAH model. For this purpose, we need also to reanalyze the flux-tube profile in SU(2) gluodynamics for another $\beta_{\rm SU(2)}$. If we could succeed this procedure, the extension to the SU(3) gluodynamics is interesting.

Chapter 6

Dual Ginzburg-Landau theory derived from SU(3) gluodynamics

In this chapter, we construct the dual Ginzburg-Landau (DGL) theory as an infrared effective theory for SU(3) gluodynamics [10, 11]. The maximal Abelian subgroup is extended to U(1)×U(1) reflecting the SU(3) gauge symmetry. In contrast with the DAH model derived from the SU(2) gluodynamics, the DGL theory has three types of color-electric charge and color-magnetic charge, which are carried by the quark fields and the monopole fields, respectively. The interaction between them is achieved by two independent dual gauge fields. This feature provides an interesting property of the flux-tube solution, which enables us to discuss not only the mesonic state given by the quark-antiquark system, but also the baryonic state as a combination of three quarks.

6.1 SU(3) gluodynamics in the Abelian projection

In this section, we consider the Abelian-projected SU(3) gluodynamics. The SU(3) gluodynamics is given by the Lagrangian density

$$\mathcal{L}_{\mathrm{SU(3)}} = \frac{1}{2}\mathrm{tr}G_{\mu\nu}G_{\mu\nu} + i\mathcal{A}^a_\mu J^a_\mu \tag{6.1.1}$$

where $\mathcal{A}_\mu$ denotes the SU(3) non-Abelian gauge field $\mathcal{A}_\mu = \mathcal{A}^a_\mu T^a$. The SU(3) generators $T^a = \lambda^a/2$ $(a = 1, \cdots, 8)$ satisfy the commutation relations $[T^a, T^b] = i\sum_{c=1}^{8} f^{abc}T^c$, where f^{abc} are the so-called structure constants of the SU(3) Lie algebra, where λ^a $(a = 1, \cdots, 8)$ are the Gell-Mann matrices. The field strength tensor $G_{\mu\nu}$ is written as

$$G_{\mu\nu} = \frac{1}{ie}\left\{\left[\hat{D}_\mu, \hat{D}_\nu\right] - \left[\hat{\partial}_\mu, \hat{\partial}_\nu\right]\right\}, \tag{6.1.2}$$

where $\hat{\partial}_\mu$ denotes the covariant derivative

$$\hat{D}_\mu = \hat{\partial}_\mu + ie\mathcal{A}_\mu. \tag{6.1.3}$$

The SU(3) quark current is introduced as an external source $J^a_\mu = e\bar{q}\gamma_\mu T^a q$, which couples to the SU(3) gauge field $\mathcal{A}^a_\mu$.

Here, we also perform the Abelian gauge fixing, which diagonalizes a certain gauge dependent variable $X(x) \in \mathrm{su}(3)$ as

$$X(x) \to \Omega(x)X(x)\Omega(x)^\dagger = \begin{pmatrix} \zeta_1(x) & & 0 \\ & \zeta_2(x) & \\ 0 & & \zeta_3(x) \end{pmatrix} \equiv X_d(x), \tag{6.1.4}$$

where resulting maximally Abelian subgroup is U(1)×U(1) group due to a suitable Abelian gauge fixing function $\Omega(x) \in \mathrm{SU}(3)$. The non-Abelian gauge field $\mathcal{A}_\mu \in \mathrm{su}(3)$ is simultaneously transformed as

$$\mathcal{A}_\mu \to \mathcal{A}^\Omega_\mu = \Omega(x)\left(\mathcal{A}_\mu + \frac{1}{ie}\partial_\mu\right)\Omega^\dagger(x). \tag{6.1.5}$$

Accordingly, the field strength tensor is transformed as

$$G_{\mu\nu} \to G^\Omega_{\mu\nu} = \partial_\mu\mathcal{A}^\Omega_\nu - \partial_\nu\mathcal{A}^\Omega_\mu + ie\left[\mathcal{A}^\Omega_\nu, \mathcal{A}^\Omega_\mu\right] - \frac{1}{ie}\Omega[\partial_\mu, \partial_\nu]\Omega^\dagger. \tag{6.1.6}$$

When degeneracy points exist in the eigenvalues $\zeta_i(x)$ $(i = 1, 2, 3)$, singularities arise from the second term of (6.1.5) as monopoles. In this case, there are three cases for the appearance of monopoles: $\zeta_1(x) = \zeta_2(x)$, $\zeta_2(x) = \zeta_3(x)$, and $\zeta_3(x) = \zeta_1(x)$. Since two of these conditions are essential, independent monopoles are occurring in two types. This number is related to the residual Abelian gauge symmetry U(1)×U(1). Here, the order of three eigenvalues is not essential. We can exchange these eigenvalues among each other in terms of the residual symmetry, the so-called global Weyl symmetry. Such monopoles can be extracted by the Abelian projection method similarly to the SU(2) case in chapter 2, which correspond to the homotopy group $\pi_2(\mathrm{SU}(3)/\mathrm{U}(1)^2) = \pi_2(S_2 \times S_2) = \boldsymbol{Z}^2_\infty$. Before the Abelian projection, we decompose the gauge field into the diagonal gluon part and the off-diagonal gluon part by the Cartan decomposition, which reads for the gauge field

$$\mathcal{A}^\Omega_\mu = \vec{\mathcal{A}}^\Omega_\mu \cdot \vec{H} + \sum_{i=1}^{3}(\mathcal{C}^{\Omega i}_\mu E^\dagger_i + \mathcal{C}^{\Omega i*}_\mu E_i), \tag{6.1.7}$$

where we have defined as

$$\vec{H} \equiv (T_3, T_8), \quad \vec{\mathcal{A}}_\mu \equiv (\mathcal{A}^{\Omega 3}_\mu, \mathcal{A}^{\Omega 8}_\mu), \tag{6.1.8}$$

and

$$\mathcal{C}^{\Omega 1}_\mu \equiv \frac{1}{\sqrt{2}}(\mathcal{A}^{\Omega 1}_\mu + i\mathcal{A}^{\Omega 2}_\mu), \quad \mathcal{C}^{\Omega 2}_\mu \equiv \frac{1}{\sqrt{2}}(\mathcal{A}^{\Omega 4}_\mu - i\mathcal{A}^{\Omega 5}_\mu), \quad \mathcal{C}^{\Omega 3}_\mu \equiv \frac{1}{\sqrt{2}}(\mathcal{A}^{\Omega 6}_\mu + i\mathcal{A}^{\Omega 7}_\mu). \tag{6.1.9}$$

We have also used the step operators $E_{\pm i}$

$$E_{\pm 1} \equiv \frac{1}{\sqrt{2}}(T_1 \pm iT_2), \quad E_{\pm 2} \equiv \frac{1}{\sqrt{2}}(T_4 \mp iT_5), \quad E_{\pm 3} \equiv \frac{1}{\sqrt{2}}(T_6 \pm iT_7), \tag{6.1.10}$$

where $E_i^\dagger = E_{-i}$. The redefined SU(3) generators $\vec{H}$ and $E_{\pm i}$ $(i = 1, 2, 3)$ satisfy the relation:

$$\left[\vec{H}, E_{\pm i}\right] = \pm\vec{\epsilon}_i E_{\pm i}, \quad [E_{\pm i}, E_{\pm j}] = \mp\frac{1}{\sqrt{2}}\sum_{k=1}^{3}\varepsilon_{ijk}E_{\mp k}, \quad [E_i, E_{-j}] = \delta_{ij}\vec{\epsilon}_i \cdot \vec{H}, \tag{6.1.11}$$

$$\mathrm{tr}[E_{-i}E_j] = \mathrm{tr}[E_i E_{-j}] = \frac{1}{2}\delta_{ij}, \quad \mathrm{tr}[E_i E_j] = \mathrm{tr}[E_{-i}E_{-j}] = 0, \tag{6.1.12}$$

where $\vec{\epsilon}_i$ $(i = 1, 2, 3)$ are the root vectors of the SU(3) algebra, given by

$$\vec{\epsilon}_1 = \left(-\frac{1}{2}\,, \frac{\sqrt{3}}{2} \right), \quad \vec{\epsilon}_2 = \left(-\frac{1}{2}\,, -\frac{\sqrt{3}}{2} \right), \quad \vec{\epsilon}_3 = (\ 1\ ,\ 0\ ). \tag{6.1.13}$$

Here, the residual Abelian gauge symmetry is $\mathrm{U}(1)_3 \times \mathrm{U}(1)_8$. In order to confirm the role of the gauge field in terms of the residual symmetry, let us consider the Abelian gauge transformation given by a function $d(x) \in \mathrm{U}(1)_3 \times \mathrm{U}(1)_8$,

$$d(x) \equiv d(x)^3 \times d(x)^8 = e^{ie\vec{\theta}(x)\cdot\vec{H}} \quad ; \quad \vec{\theta}(x) \equiv (\theta^3(x), \theta^8(x)). \tag{6.1.14}$$

The gauge field (6.1.7) is then transformed as

$$\begin{aligned} \mathcal{A}_\mu \to \mathcal{A}_\mu^{\Omega^d} &= d\left(\mathcal{A}_\mu^\Omega + \frac{1}{ie}\partial_\mu\right)d^\dagger \\ &= \left(\vec{\mathcal{A}}_\mu^\Omega - \partial_\mu\vec{\theta}\right)\cdot\vec{H} + \sum_{i=1}^{3}\left(e^{-ie\vec{\theta}\cdot\vec{\epsilon}_i}\mathcal{C}_\mu^{\Omega i}E_i^\dagger + e^{ie\vec{\theta}\cdot\vec{\epsilon}_i}\mathcal{C}_\mu^{\Omega i*}E_i\right). \end{aligned} \tag{6.1.15}$$

From this expression, we find that while the diagonal gluon part $\vec{\mathcal{A}}_\mu$ behaves as the Abelian gauge field, the off-diagonal gluon parts $\mathcal{C}_\mu^{\Omega i}$ and $\mathcal{C}_\mu^{\Omega i*}$ become charged matter fields in terms of the residual Abelian gauge symmetry.

We extract the Abelian component by the Abelian projection method, which is based on the Abelian dominance hypothesis for the low-energy properties of the gluodynamics. The Abelian field strength tensor is then given by

$$\begin{aligned} \vec{F}_{\mu\nu} &\equiv 2\mathrm{tr}\left[\vec{H}G_{\mu\nu}^\Omega\right] \\ &= \partial_\mu\vec{A}_\nu - \partial_\mu\vec{A}_\nu - \frac{2}{ie}\mathrm{tr}\left[\vec{H}\Omega[\partial_\mu, \partial_\nu]\Omega^\dagger\right], \end{aligned} \tag{6.1.16}$$

where the Abelian gauge field $\vec{A}_\mu$ is defined by

$$\vec{A}_\mu \equiv 2\mathrm{tr}[\vec{H}\mathcal{A}_\mu^\Omega] = 2\mathrm{tr}\left[\vec{H}\Omega\left(\mathcal{A}_\mu + \frac{1}{ie}\partial_\mu\right)\Omega^\dagger\right]. \tag{6.1.17}$$

Analogously to the SU(2) case, the last term of the Abelian field strength tensor describes the color-magnetic Dirac string between monopoles, which can be expressed by $g\vec{\Sigma}^{\rm M}_{\mu\nu}$:

$$-\frac{2}{ie}{\rm tr}\left[\vec{H}\Omega[\partial_\mu,\partial_\nu]\Omega^\dagger\right]=g\vec{\Sigma}^{\rm M}_{\mu\nu}, \tag{6.1.18}$$

where the Dirac quantization condition $eg=4\pi$ is taken into account. The direction of the Dirac string depends on the choice of the Abelian gauge fixing function $\Omega(x)\in{\rm su}(3)$. The Abelian Bianchi identity is now broken as

$$\partial_\mu{}^*\vec{F}_{\mu\nu}=g\partial_\mu{}^*\vec{\Sigma}^{\rm M}_{\mu\nu}=\vec{k}_\nu\neq 0, \tag{6.1.19}$$

where $\vec{k}_\mu$ is a two-component Abelian monopole current. The color-magnetic Dirac string $\vec{\Sigma}^{\rm M}_{\mu\nu}$ also can be written in the following form by using the root vectors of SU(3) algebra $\vec{\epsilon}_i$ as

$$\vec{\Sigma}^{\rm M}_{\mu\nu}=\sum_{i=1}^{3}\vec{\epsilon}_i\Sigma^{\rm M}_{i\mu\nu}=\sum_{i=1}^{3}\vec{\epsilon}_i\int_{\Sigma^{\rm M}_i}\varepsilon_{\mu\nu\alpha\beta}d\sigma^{\rm M}_{i\alpha\beta}(\bar{x}_i(\xi))\delta(x-\bar{x}_i(\xi)). \tag{6.1.20}$$

Note that this is a realization of the manifest global-Weyl symmetry, which is an important residual symmetry in the Abelian-projected SU(3) gluodynamics. The monopole current can be also written in a Weyl symmetric form as

$$\vec{k}_\nu=g\sum_{i=1}^{3}\vec{\epsilon}_i\partial_\mu{}^*\Sigma^{\rm M}_{i\mu\nu}=g\sum_{i=1}^{3}\vec{\epsilon}_i\hat{k}_{i\nu}, \tag{6.1.21}$$

where $\hat{k}_{i\nu}\equiv\partial_\mu{}^*\Sigma^{\rm M}_{i\mu\nu}$. In this sense, the color-magnetic charge of the monopole is defined by $\vec{Q}^{\rm M}_i\equiv g\vec{\epsilon}_i$ as shown in Fig. 6.1. The labels $i=1,2,3$ correspond to the color-magnetic charges, dual red ($^*R$), dual blue ($^*B$) and dual green ($^*G$). Here, the star " * " represents dual quantity. In such expression, however, one always should remember that all color-magnetic Dirac strings are not independent due to the relation $\sum_{i=1}^{3}\vec{\epsilon}_i=0$.

The resulting action of the SU(3) gluodynamics in the Abelian projection after the Abelian gauge fixing has the form

$$S_{\rm AP-SU(3)}[\vec{A}_\mu,\vec{j},\vec{\Sigma}^{\rm M}_{\mu\nu}]=\int d^4x\left\{\frac{1}{4}\left((\partial\wedge\vec{A})_{\mu\nu}+g\vec{\Sigma}^{\rm M}_{\mu\nu}\right)^2+i\vec{A}_\mu\cdot\vec{j}_\mu\right\} \tag{6.1.22}$$

where $\vec{j}_\mu$ is the Abelian color-electric current, which has the form $\vec{j}_\mu=e\bar{q}\vec{H}\gamma_\mu q$. Since the quark field is regarded as a fundamental representation of SU(3) group as

$$q=\begin{pmatrix}q_1\\q_2\\q_3\end{pmatrix}, \tag{6.1.23}$$

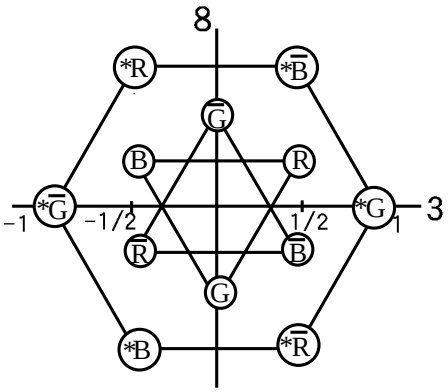

Figure 6.1: The distribution of the color-electric charge $\vec{Q}_j^{\rm E} = e\vec{w}_j$ and the color-magnetic charge $\vec{Q}_i^{\rm M} = g\vec{\epsilon}_i$, which is defined on the the weight vectors and the root vectors of the SU(3) algebra.

and the diagonal part of the SU(3) generators is expressed by

$$\vec{H} = (T_3, T_8) = \begin{pmatrix} \vec{w}_1 & 0 & 0 \\ 0 & \vec{w}_2 & 0 \\ 0 & 0 & \vec{w}_3 \end{pmatrix}, \tag{6.1.24}$$

where $\vec{w}_j$ $(j = 1, 2, 3)$ are the weight vectors of the SU(3) algebra

$$\vec{w}_1 = \left(\frac{1}{2}, \frac{1}{2\sqrt{3}}\right), \quad \vec{w}_2 = \left(-\frac{1}{2}, \frac{1}{2\sqrt{3}}\right), \quad \vec{w}_3 = \left(0, -\frac{1}{\sqrt{3}}\right), \tag{6.1.25}$$

we obtain a manifestly Weyl symmetric representation of the color-electric current,

$$\vec{j}_\mu = e\sum_{j=1}^{3} \vec{w}_j \; \bar{q}_j \gamma_\mu q_j. \tag{6.1.26}$$

Hence, $\vec{Q}_j^{\rm E} \equiv e\vec{w}_j$ $(j = 1, 2, 3)$ can be regarded as the Abelian color-electric charge as shown in Fig. 6.1. The labels $j = 1, 2, 3$ correspond to the three types of the color-electric charges red (R), blue (B), and green (G). Note that due to the relation $\sum_{j=1}^{3} \vec{w}_j = 0$, the color-electric charges are not all independent. It is useful to introduce the color-electric Dirac string $\vec{\Sigma}_{\mu\nu}^{\rm E}$, which leads to the dual version of the broken Abelian Bianchi identity $e\partial_\mu {}^*\Sigma_{\mu\nu}^{\rm E} = \vec{j}_\nu$. The color-electric current also can be represented in the Weyl symmetric form by using the weight vectors of the SU(3) algebra $\vec{w}_j$ like the color-magnetic current (6.1.21) as

$$\vec{j}_\nu = e\sum_{j=1}^{3} \vec{w}_j \partial_\mu {}^*\Sigma_{j\mu\nu}^{\rm E} = e\sum_{j=1}^{3} \vec{w}_j \hat{j}_{j\nu} \tag{6.1.27}$$

where $\hat{j}_{j\nu} \equiv \partial_\mu {}^*\Sigma_{j\mu\nu}^{\rm E}$. The position of the color-electric Dirac string is explicitly parametrized as

$$\vec{\Sigma}_{\mu\nu}^{\rm E} = \sum_{j=1}^{3} \vec{w}_j \int_{\Sigma_j^{\rm E}} \varepsilon_{\mu\nu\alpha\beta} d\sigma_{j\alpha\beta}^{\rm E}(\bar{x}_j(\eta))\delta(x - \bar{x}_j(\eta)). \tag{6.1.28}$$

6.2 Dual Ginzburg-Landau theory

In this section, based on the Abelian-projected SU(3) gluodynamics, we construct the DGL theory as an infrared effective theory. Let us perform the path-integral duality transformation for the partition function of the Abelian-projected SU(3) gluodynamics as in the SU(2) case [59]. Then, we obtain its dual expression as

$$\begin{aligned}\mathcal{Z} &= \int \mathcal{D}\vec{A}_\mu \mathcal{D}\vec{j}_\mu \mathcal{D}\vec{\Sigma}^{\rm M}_{\mu\nu} \exp\left\{-S_{\rm AP-SU(3)}[\vec{A}_\mu, \vec{j}_\mu, \vec{\Sigma}^{\rm M}_{\mu\nu}]\right\} \\ &= \int \mathcal{D}\vec{\Sigma}^{\rm E}_{\mu\nu} \mathcal{D}\vec{\Sigma}^{\rm M}_{\mu\nu} \mathcal{D}\vec{B}_\mu \\ &\quad \times \exp\left[-\int d^4x \left\{\frac{1}{4}\left((\partial \wedge \vec{B})_{\mu\nu} + e\vec{\Sigma}^{\rm E}_{\mu\nu}\right)^2 - i\vec{k}_\mu \cdot \vec{B}_\mu + i\frac{eg}{2} {}^*\vec{\Sigma}^{\rm M}_{\mu\nu} \cdot \vec{\Sigma}^{\rm E}_{\mu\nu}\right\}\right], \quad (6.2.1)\end{aligned}$$

where the two-component dual gauge field $\vec{B}_\mu$ is naturally introduced, which couples to the two-component monopole current $\vec{k}_\mu$. Analogously to the SU(2) case, one finds that the linking term appears in the partition function, which is explicitly can be written as

$$\begin{aligned}\int d^4x i\frac{eg}{2} {}^*\vec{\Sigma}^{\rm M}_{\mu\nu} \cdot \vec{\Sigma}^{\rm E}_{\mu\nu} &= i\frac{eg}{2} \sum_{i=1}^3 \vec{\epsilon}_i {}^*\Sigma^{\rm M}_{i\mu\nu} \cdot \sum_{j=1}^3 \vec{w}_j \Sigma^{\rm E}_{j\mu\nu} \\ &= ieg \sum_{i=1}^3 \sum_{j=1}^3 \frac{m_{ij}}{2} \varepsilon_{\mu\nu\alpha\beta} \int_{\Sigma^{\rm M}_i} d\sigma^{\rm E}_{i\mu\nu}(\bar{x}_i(\xi)) \int_{\Sigma^{\rm E}_j} d\sigma^{\rm E}_{j\alpha\beta}(\bar{x}_j(\eta)) \delta(\bar{x}_i(\xi) - \bar{x}_j(\eta)) \\ &= 2\pi \sum_{i=1}^3 \sum_{j=1}^3 m_{ij} L_{ij}, \quad (6.2.2)\end{aligned}$$

where L_{ij} denotes the linking number (integer) as already discussed in the SU(2) case. Here, we have used an interesting relation of the root vectors and the weight vectors of the SU(3) algebra, which is given by

$$\vec{\epsilon}_i \cdot \vec{w}_j = \frac{1}{2} \begin{pmatrix} 0 & 1 & -1 \\ -1 & 0 & 1 \\ 1 & -1 & 0 \end{pmatrix} = \frac{1}{2} \sum_{k=1}^3 \epsilon_{ijk} \equiv \frac{1}{2} m_{ij}, \quad (6.2.3)$$

where m_{ij} is an integer which takes 0 or ± 1. We have also used here the Dirac quantization condition $eg = 4\pi$ to get the factor 2π. More precisely, this condition is written by $e\vec{w}_j \cdot g\vec{\epsilon}_i = 2\pi m_{ji}$. Clearly, the Dirac quantization condition is important to guarantee the harmlessness of the linking term. It is interesting to note that the color-electric Dirac string and the color-magnetic Dirac string labeled by the same foot, that is, $i = j$, never couple since the linking term always vanishes.

We assume that the monopole currents are clustering in the vacuum as in the SU(2) case. Thus, we consider the grand canonical ensemble of monopole currents,

$$\vec{k}_\mu(x) = g \sum_{i=1}^3 \vec{\epsilon}_i \sum_{n=1}^N \oint_{\partial \Sigma^{\rm M}_i} dx^{(n)}_{i\mu}(s) \delta(x - x^{(n)}_i(s)). \quad (6.2.4)$$

Here, $x_i^{(n)}(s)$ parametrizes the world line of the n-th closed monopole trajectory carrying the color-magnetic charge $g\vec{\epsilon}_i$ in four-dimensional space-time. In order to sum over monopole currents, it is useful to pay attention to the Weyl symmetry of the monopole charges. Our strategy is the following: We first consider a three-component dual gauge field instead of the original two-component $\vec{B}_\mu$, given by

$$B_{i\mu} \equiv \vec{\epsilon}_i \cdot \vec{B}_\mu \quad (i = 1, 2, 3), \tag{6.2.5}$$

where we need to take into account the constraint $\sum_{i=1}^3 B_{i\mu} = 0$ due to the relation $\sum_{i=1}^3 \vec{\epsilon}_i = 0$. By this definition, the interaction between the dual gauge field and monopole currents becomes manifestly Weyl symmetric, which is given by three similar terms. It means that we can repeat the same summation technique as in the SU(2) case for each of three sets [cf. Eq. (2.4.20)]. Thus, we get three types of complex-scalar monopole fields χ_i $(i = 1, 2, 3)$. The resulting action apparently has $[\mathrm{U}(1)]^3$ dual gauge symmetry, which is realized by the set of transformations

$$\chi_i \to e^{i\varphi_i}\chi_i, \quad \chi_i^* \to e^{-i\varphi_i}\chi_i^*, \quad B_{i\mu} \to B_{i\mu} - \frac{1}{g}\partial_\mu\varphi_i \quad (i = 1, 2, 3). \tag{6.2.6}$$

We find that in order to keep the summation of the redefined dual gauge field invariant as $\sum_{i=1}^3 B_{i\mu} = 0$, the phases have to satisfy a constraint

$$\sum_{i=1}^3 \partial_\mu \varphi_i = 0. \tag{6.2.7}$$

That is to say, the sum of phases φ_i should be constant, which we take equal to zero. Thus, we finally get the partition function of the dual Ginzburg-Landau (DGL) theory

$$\begin{aligned} \mathcal{Z} \;=\; & \int \mathcal{D}\vec{\Sigma}^{\mathrm{E}}_{\mu\nu}\mathcal{D}\vec{B}_\mu \left(\prod_{i=1}^3 \mathcal{D}\chi_i \mathcal{D}\chi_i^*\right) \delta\Big(\sum_{i=1}^3 \arg\chi_i\Big) \\ & \times \exp\left[-\int d^4x \left\{ \frac{1}{4}\left((\partial \wedge \vec{B})_{\mu\nu} + e\vec{\Sigma}^{\mathrm{E}}_{\mu\nu}\right)^2 + \sum_{i=1}^3 \left[\left| (\partial_\mu + ig\vec{\epsilon}_i \cdot \vec{B}_\mu)\chi_i \right|^2 + \lambda\left(|\chi|^2 - v^2\right)^2 \right] \right\} \right], \end{aligned} \tag{6.2.8}$$

where the constraint for the phases of the monopole field $\sum_{i=1}^3 \arg\chi_i = 0$ is expressed by a δ-functional.

To summarize, the DGL Lagrangian is obtained as*

$$\mathcal{L}_{\mathrm{DGL}} \;=\; \frac{1}{4}{}^*\vec{F}^2_{\mu\nu}(\vec{B}, \vec{\Sigma}^{\mathrm{E}}) + \sum_{i=1}^3 \left[\left| \left(\partial_\mu + ig\vec{\epsilon}_i \cdot \vec{B}_\mu\right)\chi_i \right|^2 + \lambda\left(|\chi_i|^2 - v^2\right)^2 \right], \tag{6.2.9}$$

*In the DGL theory, we do not use "$\hat{}$" for the parameters in order to distinguish from the DAH model.

where the dual field strength tensor has the form

$$ {}^*\vec{F}_{\mu\nu}(\vec{B},\vec{\Sigma}^{\rm E}) = \partial_\mu \vec{B}_\nu - \partial_\nu \vec{B}_\mu + e\vec{\Sigma}^{\rm E}_{\mu\nu}. \tag{6.2.10} $$

In this Lagrangian, $\vec{B}_\mu$ and χ_i denote the two-component dual gauge field and the three-component complex scalar monopole field. The quark field is included in the color-electric Dirac string term $\vec{\Sigma}^{\rm E}_{\mu\nu}$. One finds that this Lagrangian has quite a similar form as the DAH model discussed in previous chapters. Then, a similar scenario is expected to occur. It means that the DGL vacuum is described as the dual superconductor, where the color-electric field is excluded from the vacuum due to the dual Meissner effect caused by monopole condensation.

The typical scales of the DGL theory are exhibited by taking into account the dual Higgs mechanism as the DAH model. By inserting $\chi_i = \left(v + \phi_i/\sqrt{2}\right) e^{i\eta_i}$ (where $\phi_i, \eta_i \in \Re$) into the DGL Lagrangian (6.2.9), we get

$$ \begin{aligned} \mathcal{L}_{\rm DGL} &= \frac{1}{4} {}^*\vec{F}^2_{\mu\nu}(\vec{B}', \vec{\Sigma}^{\rm E}_{\mu\nu}) + \frac{1}{2} m_B^2 \vec{B}'^2_\mu + \sum_{i=1}^{3} \frac{1}{2} \left[(\partial_\mu \phi_i)^2 + m_\chi^2 \phi_i^2 \right] \\ &\quad + \sum_{i=1}^{3} \left[g^2 (\vec{\epsilon}_i \cdot \vec{B}'_\mu)^2 \left(\sqrt{2} v \phi_i + \frac{\phi_i^2}{2} \right) + \lambda \left(\sqrt{2} v \phi_i^3 + \frac{\phi_i^4}{4} \right) \right], \end{aligned} \tag{6.2.11} $$

where the phase of the monopole field η_i is absorbed into the definition of the dual gauge field $\vec{B}'_\mu$, as $\vec{\epsilon}_i \cdot \vec{B}'_\mu = \vec{\epsilon}_i \cdot \vec{B}_\mu + \partial_\mu \eta_i / g$, and accordingly the dual gauge field and the monopole field acquire masses, $m_B = \sqrt{3} g v$, $m_\chi = 2\sqrt{\lambda} v$, respectively. Since these inverse masses correspond to the penetration depth of the color-electric field and the coherence length of the monopole field, respectively, the Ginzburg-Landau (GL) parameter is defined:

$$ \kappa \equiv \frac{m_B^{-1}}{m_\chi^{-1}} = \frac{\sqrt{2\lambda}}{g_{\rm m}} = \frac{2\sqrt{\lambda}}{\sqrt{3} g}. \tag{6.2.12} $$

As explained in the U(1) DAH model, $\kappa = 1$ is a case of special interest, the Bogomol'nyi limit [72, 32], which will be discussed in the following chapter. In general, the vacuum is separated into two types by the Bogomol'nyi limit: $\kappa < 1$ belongs to the type-I vacuum and $\kappa > 1$ is the type-II vacuum.

6.3 Summary and outlook

In this chapter, we have derived the dual Ginzburg-Landau (DGL) theory as an infrared effective theory of SU(3) gluodynamics (SU(3) QCD) based on the 't Hooft Abelian projection and the path-integral duality transformation. We have found that the resulting form has a quite structure as the U(1) DAH model derived from SU(2) gluodynamics, describing the dual superconductivity of the vacuum. However, the dual gauge symmetry is now extended

to $[\mathrm{U}(1)]^2$ reflecting the original SU(3) gauge symmetry, and there appear three types of color-electric charge and color-magnetic charge. This fact will turn out to be important when we discuss realistic hadrons observed in experiments in terms of the flux-tube solution.

Chapter 7

Manifestly Weyl symmetric formulation of the DGL theory

In the DGL theory, the color-electric charge of the quark is given by three components as R, B and G, which is spanned by the weight vector of SU(3) algebra. On the other hands, the color-magnetic charge of the monopole is defined by components as ${}^*R$, ${}^*B$ and ${}^*G$, which is spanned by the root vector of SU(3) algebra. Now, we are interested in the color-singlet state corresponding to the meson and the baryon, which should be invariant under the exchange of the color charges. Hence, it is important to pay attention to the Weyl symmetry in the DGL theory. However, since the dual gauge field $\vec{B}_\mu$ which connects the color-electric charge and the color-magnetic charge has only two components in the sense of the Cartan decomposition, and accordingly the independent color-electric flux has two components, we cannot observe the Weyl symmetric structure in the color-electric flux tube itself. This fact makes it difficult to see the Weyl invariant structure of hadronic states. In order to expose the Weyl symmetric structure of the flux tube in the DGL theory, it would be favorable to represent the dual gauge field also in a Weyl symmetric way.

In this chapter, therefore, we reformulate the DGL theory to make its global Weyl symmetry manifest, which we call the manifestly Weyl invariant formulation. Then, we would like to study the hadronic flux-tube solution corresponding to the mesonic and the baryonic states using this Weyl symmetric framework.

7.1 Various representations of the dual gauge field

In this section, we write the DGL Lagrangian in various representations of the dual gauge field, among which the Weyl symmetric representation of the dual gauge field is also discussed [50]. We first pay attention to the original Cartan representation of the dual gauge field with two

components. Next, we will discuss other two possible representations of the dual gauge field, the color-electric representation and the color-magnetic representation, which are achieved by spanning the dual gauge field with the weight vector and the root vector, respectively.

7.1.1 Cartan 3-8 representation

The two-component dual gauge field $\vec{B}_\mu$ can be written as

$$\vec{B}_\mu \equiv \frac{1}{g}\left(B^3_\mu, \frac{B^8_\mu}{\sqrt{3}}\right). \tag{7.1.1}$$

The factor $\sqrt{3}$ is to make 3- and 8- components symmetric. The dual field strength tensor becomes

$$\begin{aligned} {}^*\vec{F}_{\mu\nu} &= \frac{1}{g}\Bigg(\partial_\mu B^3_\nu - \partial_\nu B^3_\mu + 2\pi(\Sigma^{\rm E}_{1\,\mu\nu} - \Sigma^{\rm E}_{2\,\mu\nu}), \\ &\quad \frac{1}{\sqrt{3}}\left\{\partial_\mu B^8_\nu - \partial_\nu B^8_\mu + 2\pi(\Sigma^{\rm E}_{1\,\mu\nu} + \Sigma^{\rm E}_{2\,\mu\nu} - 2\Sigma^{\rm E}_{3\,\mu\nu})\right\}\Bigg) \\ &\equiv \frac{1}{g}\left({}^*F^3_{\mu\nu}, \frac{{}^*F^8_{\mu\nu}}{\sqrt{3}}\right), \end{aligned} \tag{7.1.2}$$

where we use the Weyl symmetric form the color-electric Dirac string $\vec{\Sigma}^{\rm E}_{\mu\nu} = \sum_{j=1}^3 \Sigma^{\rm E}_{j\,\mu\nu}$. The Dirac quantization condition $eg = 4\pi$ is also used here to get the factor 2π in front of $\Sigma^{\rm E}_{j\,\mu\nu}$. The DGL Lagrangian is written as

$$\begin{aligned} \mathcal{L}^{3-8}_{\rm DGL} &= \frac{1}{4g^2}({}^*F^3_{\mu\nu})^2 + \frac{1}{12g^2}({}^*F^8_{\mu\nu})^2 \\ &\quad + \left|\left(\partial_\mu + i\frac{1}{2}\left(-B^3_\mu + B^8_\mu\right)\right)\chi_1\right|^2 + \lambda\left(|\chi_1|^2 - v^2\right)^2 \\ &\quad + \left|\left(\partial_\mu + i\frac{1}{2}\left(-B^3_\mu - B^8_\mu\right)\right)\chi_2\right|^2 + \lambda\left(|\chi_2|^2 - v^2\right)^2 \\ &\quad + \left|\left(\partial_\mu + iB^3_\mu\right)\chi_3\right|^2 + \lambda\left(|\chi_3|^2 - v^2\right)^2. \end{aligned} \tag{7.1.3}$$

Note that the Lagrangian (7.1.3) is invariant under the $[{\rm U}(1)]^2$ dual gauge transformation,

$$\begin{aligned} &\chi_i \to \chi_i e^{if_i}, \quad \chi^*_i \to \chi^*_i e^{-if_i} \qquad (i = 1, 2, 3), \\ &(B^3_\mu,\ B^8_\mu) \to \left(B^3_\mu - \partial_\mu f_3,\ B^8_\mu - (\partial_\mu f_1 - \partial_\mu f_2)\right), \end{aligned} \tag{7.1.4}$$

where the phases f_i fulfill the constraint $\sum_{i=1}^3 f_i = 0$ [10, 11].

The field equations are given by

$$\begin{aligned} \frac{1}{g^2}\partial_\mu {}^*F^3_{\mu\nu} &= +\frac{i}{2}\left(\chi^*_1\partial_\nu\chi_1 - \chi_1\partial_\nu\chi^*_1\right) - \frac{1}{2}\left(-B^3_\nu + B^8_\nu\right)\chi^*_1\chi_1 \\ &\quad + \frac{i}{2}\left(\chi^*_2\partial_\nu\chi_2 - \chi_2\partial_\nu\chi^*_2\right) - \frac{1}{2}\left(-B^3_\nu - B^8_\nu\right)\chi^*_2\chi_2 \\ &\quad - i\left(\chi^*_3\partial_\nu\chi_3 - \chi_3\partial_\nu\chi^*_3\right) + 2B^3_\nu\chi^*_3\chi_3, \end{aligned} \tag{7.1.5}$$

$$\frac{1}{3g^2}\partial_\mu {}^*F^8_{\mu\nu} = -\frac{i}{2}\left(\chi_1^*\partial_\nu\chi_1 - \chi_1\partial_\nu\chi_1^*\right) + \frac{1}{2}\left(-B^3_\nu + B^8_\nu\right)\chi_1^*\chi_1 + \frac{i}{2}\left(\chi_2^*\partial_\nu\chi_2 - \chi_2\partial_\nu\chi_2^*\right) - \frac{1}{2}\left(-B^3_\nu - B^8_\nu\right)\chi_2^*\chi_2, \tag{7.1.6}$$

$$\left(\partial_\mu + \frac{i}{2}\left(-B^3_\mu + B^8_\mu\right)\right)^2\chi_1 = 2\lambda\chi_1\left(\chi_1^*\chi_1 - v^2\right), \tag{7.1.7}$$

$$\left(\partial_\mu + \frac{i}{2}\left(-B^3_\mu - B^8_\mu\right)\right)^2\chi_2 = 2\lambda\chi_2\left(\chi_2^*\chi_2 - v^2\right), \tag{7.1.8}$$

$$\left(\partial_\mu + iB^3_\mu\right)^2\chi_3 = 2\lambda\chi_3\left(\chi_3^*\chi_3 - v^2\right). \tag{7.1.9}$$

From these field equations, we find the boundary conditions : If ${}^*F^3_{\mu\nu}$ and ${}^*F^8_{\mu\nu}$ have a non-vanishing nonlocal term $\Sigma^{\rm E}_{j\,\mu\nu}$, the dual gauge field B^3_μ and B^8_μ also have the singular part. At the locus where the dual gauge field is singular, the monopole field is required to disappear. At large distance from the singularity, the monopole field χ_i approaches the vacuum expectation value v and the dual gauge field asymptotically vanishes, $B^3_\mu = B^8_\mu = 0$. These field equations are to be solved by using the dual lattice formulation, and one will find that these boundary conditions are realized.

7.1.2 Color-electric representation

The dual gauge field can be expressed by using the weight vector $\vec{w}_j$, where the label $j = 1, 2, 3$ corresponds to the color-electric charge, R, B and G. In this sense, we call this the color-electric representation of the dual gauge field, which is defined by

$$\vec{B}_\mu \equiv \sqrt{\frac{2}{g_{\rm e}^2}}\sum_{j=1}^{3}\vec{w}_j B^{\rm e}_{j\,\mu}, \tag{7.1.10}$$

where

$$g_{\rm e} \equiv \frac{3}{\sqrt{2}}g, \quad B^{\rm e}_{j\,\mu} \equiv \sqrt{2}g_{\rm e}\vec{w}_j\cdot\vec{B}_\mu. \tag{7.1.11}$$

Note that now the dual gauge field is written as a three-component field, however all of them are not independent since $\sum_{j=1}^{3} B^{\rm e}_{j\,\mu} = 0$. The dual field strength tensor has the form

$${}^*\vec{F}_{\mu\nu} = \sqrt{\frac{2}{g_{\rm e}^2}}\sum_{j=1}^{3}\vec{w}_j\left(\partial_\mu B^{\rm e}_{j\,\nu} - \partial_\nu B^{\rm e}_{j\,\mu} - 2\pi\Sigma^{\rm E}_{j\,\mu\nu}\right), \tag{7.1.12}$$

where $eg = 4\pi$ is used. Then, we get the Lagrangian

$$\mathcal{L}^{\rm electric}_{\rm DGL} = \frac{1}{4g_{\rm e}^2}\sum_{j=1}^{3}\left({}^*F^{\rm e}_{j\,\mu\nu}\right)^2 + \sum_{i=1}^{3}\left[\left|\left(\partial_\mu + i\frac{1}{3}\sum_{j=1}^{3}m_{ij}B^{\rm e}_{j\,\mu}\right)\chi_i\right|^2 + \lambda\left(|\chi_i|^2 - v^2\right)^2\right], \tag{7.1.13}$$

where

$$ {}^*F^{\rm e}_{j\,\mu\nu} \equiv \partial_\mu B^{\rm e}_{j\,\nu} - \partial_\nu B^{\rm e}_{j\,\mu} + 2\pi \left(2\Sigma^{\rm E}_{j\,\mu\nu} - \sum_{k=1}^{3} m_{jk}^2 \Sigma^{\rm E}_{k\,\mu\nu} \right). \tag{7.1.14} $$

Here, we have used the relations

$$ g\vec{\epsilon}_i \cdot \vec{B}_\mu = g\vec{\epsilon}_i \cdot \sqrt{\frac{2}{g_{\rm e}^2}} \sum_{j=1}^{3} \vec{w}_j B^{\rm e}_{j\,\mu} = \frac{1}{3} \sum_{j=1}^{3} m_{ij} B^{\rm e}_{j\,\mu}, \tag{7.1.15} $$

$$ \vec{\epsilon}_i = \vec{w}_j - \vec{w}_k \quad (i,j,k : cyclic). \tag{7.1.16} $$

Apparently, the Lagrangian (7.1.13) is invariant under the $[\mathrm{U}(1)]^3$ dual gauge transformation, which is defined by

$$ \begin{aligned} &\chi_i \to \chi_i e^{if_i}, \quad \chi_i^* \to \chi_i^* e^{-if_i}, \\ &B^{\rm e}_{j\,\mu} \to B^{\rm e}_{j\,\mu} + \sum_{i=1}^{3} m_{ji} \partial_\mu f_i, \end{aligned} \tag{7.1.17} $$

where $i, j = 1, 2, 3$. However, this does not mean an increase of the gauge degrees of freedom because of the constraint $\sum_{j=1}^{3} B^{\rm e}_{j\,\mu} = 0$.

The field equations for $j = 1, 2, 3$ and $i = 1, 2, 3$ are given by

$$ \frac{1}{g_{\rm e}^2} \partial^\nu {}^*F^{\rm e}_{j\,\mu\nu} = \sum_{i=1}^{3} m_{ij} \left[-\frac{i}{3} \left(\chi_i^* \partial_\mu \chi_i - \chi_i \partial_\mu \chi_i^* \right) + 2 \sum_{k=1}^{3} m_{ik} B^{\rm e}_{k\,\nu} \chi_i^* \chi_i \right], \tag{7.1.18} $$

$$ \left(\partial_\mu + i \frac{1}{3} \sum_{j=1}^{3} m_{ij} B^{\rm e}_{j\,\mu} \right)^2 \chi_i = -2\lambda \chi_i (\chi_i^* \chi_i - v^2). \tag{7.1.19} $$

We find that each field equation has U(1) structure, apart from the matrix structure in the labels i and j. The boundary condition is given by a similar discussion as in the Cartan representation of the dual gauge field. The main difference is that the dual gauge field represented here experiences the color-electric Dirac string singularity in a Weyl symmetric way. The dual lattice formulation will make this situation clear.

7.1.3 Color-magnetic representation

The dual gauge field can also be spanned by using the root vector $\vec{\epsilon}_i$, where the label $i = 1, 2, 3$ corresponds to the monopole charge, ${}^*R$, ${}^*B$ and ${}^*G$. In this sense, we call this the color-magnetic representation of the dual gauge field [32], defined by

$$ \vec{B}_\mu \equiv \sqrt{\frac{2}{3g_{\rm m}^2}} \sum_{i=1}^{3} \vec{\epsilon}_i B^{\rm m}_{i\,\mu}, \tag{7.1.20} $$

where

$$ g_{\rm m} \equiv \sqrt{\frac{3}{2}} g, \qquad B^{\rm m}_{i\,\mu} \equiv \sqrt{\frac{2}{3}} g_{\rm m} \vec{\epsilon}_i \cdot \vec{B}_\mu. \tag{7.1.21} $$

Note that $B^{\rm m}_{i\,\mu}$ are not all independent since $\sum_{i=1}^{3} B^{\rm m}_{i\,\mu} = 0$. One may remember that this representation was already used when we have summed over monopole currents. The dual field strength tensor is written as

$$ {}^*\vec{F}_{\mu\nu} = \sqrt{\frac{2}{3g_{\rm m}^2}} \sum_{i=1}^{3} \vec{\epsilon}_i \left(\partial_\mu B^{\rm m}_{i\,\nu} - \partial_\nu B^{\rm m}_{i\,\mu} + 2\pi \sum_{j=1}^{3} m_{ij} \Sigma^{\rm E}_{j\,\mu\nu} \right), \tag{7.1.22} $$

where we use $eg = 4\pi$. Hence, the Lagrangian in terms of the color-magnetic representation of the dual gauge field is given by

$$ \mathcal{L}^{\rm magnetic}_{\rm DGL} = \sum_{i=1}^{3} \left[\frac{1}{4g_{\rm m}^2} \left({}^*F^{\rm m}_{i\,\mu\nu} \right)^2 + \left| \left(\partial_\mu + iB^{\rm m}_{i\,\mu} \right) \chi_i \right|^2 + \lambda \left(|\chi_i|^2 - v^2 \right)^2 \right], \tag{7.1.23} $$

where

$$ {}^*F^{\rm m}_{i\,\mu\nu} \equiv \partial_\mu B^{\rm m}_{i\,\nu} - \partial_\nu B^{\rm m}_{i\,\mu} + 2\pi \sum_{j=1}^{3} m_{ij} \Sigma^{\rm E}_{j\,\mu\nu}. \tag{7.1.24} $$

Here, we have used the relations

$$ \vec{w}_i = -\frac{1}{3} \left(\vec{\epsilon}_j - \vec{\epsilon}_k \right) \quad (i, j, k : cyclic). \tag{7.1.25} $$

Since the Lagrangian (7.1.23) has a quite similar form as the U(1) DAH model, except for the labels i and j, one finds that the dual gauge symmetry becomes very easy to observe,

$$ \chi_i \to \chi_i e^{if_i}, \quad \chi_i^* \to \chi_i^* e^{-if_i}, \quad B^{\rm m}_{i\,\mu} \to B^{\rm m}_{i\,\mu} - \partial_\mu f_i \qquad (i = 1, 2, 3), \tag{7.1.26} $$

and accordingly the Lagrangian (7.1.23) has the extended dual gauge symmetry $[\mathrm{U}(1)]^3$ with a constraint $\sum_{i=1}^{3} B^{\rm m}_{i\,\mu} = 0$. This is the same as in the color-electric representation of the dual gauge field.

The field equations for $i = 1, 2, 3$ have the form

$$ \frac{1}{g_{\rm m}^2} \partial_\mu {}^*F^{\rm m}_{i\,\mu\nu} = -i \left(\chi_i^* \partial_\nu \chi_i - \chi_i \partial_\nu \chi_i^* \right) + 2B^{\rm m}_{i\,\nu} \chi_i^* \chi_i, \tag{7.1.27} $$

$$ \left(\partial_\mu + iB^{\rm m}_{i\,\mu} \right)^2 \chi_i = 2\lambda \chi_i (\chi_i^* \chi_i - v^2), \tag{7.1.28} $$

which is exactly the same as the field equation in the U(1) DAH model, replicated with respect to the index i. In this sense, the boundary conditions can be taken similarly as in the U(1) case. Therefore, the color-magnetic representation of the dual gauge field is particularly convenient as compared with other representations.

7.2 Hadronic flux-tube solutions

In order to solve the field equation with various representations of the dual gauge field, we adopt the dual lattice formulation as the DAH model, but extended to more degrees of

freedom. In this subsection, we first investigate the mesonic flux tube, and next the baryonic flux tube. We use the words "mesonic" or "baryonic" to distinguish the real color-singlet hadron from the classical state that we deal with in this paper. For instance, if we want to obtain real meson or baryon state, we need to consider the quantum state given by

$$\begin{aligned} |meson\rangle &= \frac{1}{\sqrt{3}}\left(|R\bar{R}\rangle + |B\bar{B}\rangle + |G\bar{G}\rangle\right), \\ |baryon\rangle &= \frac{1}{\sqrt{6}}\left(|RBG\rangle + |BGR\rangle + |GRB\rangle - |RGB\rangle - |GBR\rangle - |BRG\rangle\right), \end{aligned}$$

where $R\bar{R}$ denotes R-$\bar{R}$ flux tube, and so forth. In the classical solution, we can only treat a piece of these states. However, even then it is necessary to pay attention to the Weyl symmetry, since all states can be reduced to the same classical state for the meson and the baryon, respectively.

7.2.1 Mesonic flux tube (q-$\bar{q}$ system)

Since the three types of the color-electric charge are represented by non-vanishing plaquettes $\hat{\Sigma}^{\rm E}_{1\,\mu\nu}(s)$, $\hat{\Sigma}^{\rm E}_{2\,\mu\nu}(s)$ and $\hat{\Sigma}^{\rm E}_{3\,\mu\nu}(s)$, the mesonic state corresponding to $|R\bar{R}\rangle$, $|B\bar{B}\rangle$ and $|G\bar{G}\rangle$ are given by some stacks of connected plaquettes of each color. For example, when we consider the straight R-$\bar{R}$ flux-tube system, all we have to do is to put only one of the color-electric Dirac string plaquette locally $\hat{\Sigma}^{\rm E}_{1\,\mu\nu}(s) \neq 0$ like in Fig. 4.1(a), whereas $\hat{\Sigma}^{\rm E}_{2\,\mu\nu}(s) = \hat{\Sigma}^{\rm E}_{3\,\mu\nu}(s) = 0$ all over the three dimensional space. For the B-$\bar{B}$ flux-tube system, we set $\hat{\Sigma}^{\rm E}_{2\,\mu\nu}(s) \neq 0$ and $\hat{\Sigma}^{\rm E}_{3\,\mu\nu}(s) = \hat{\Sigma}^{\rm E}_{1\,\mu\nu}(s) = 0$, for the G-$\bar{G}$ flux-tube system, $\hat{\Sigma}^{\rm E}_{3\,\mu\nu}(s) \neq 0$ and $\hat{\Sigma}^{\rm E}_{1\,\mu\nu}(s) = \hat{\Sigma}^{\rm E}_{2\,\mu\nu}(s) = 0$.

In Figs. 7.1-7.6, we show the profiles of the color-electric field and corresponding monopole current of R-$\bar{R}$, B-$\bar{B}$, and G-$\bar{G}$ flux-tube system for various representation of the dual gauge field, the Cartan representation, the color-electric representation, and the color-magnetic representation, respectively. We find that the last two representations enable us to see the Weyl symmetric structure of the flux tube. The Dirac string structures in the dual gauge field with various representations is summarized schematically in Table. 1.

The profile of the monopole field is shown in Fig. 7.7. One finds that this does not depend on the choice of the representation of the dual gauge field, since the monopole field is defined on the SU(3) root vector. That is the reason why this distribution is similar to the color-electric field in the color-magnetic representation of the dual gauge field. The inter-quark potential is shown in Fig. 7.8, which, of course, does not depend on the representation. The parameter set used here is the same as in the U(1) case. We took $\beta_{\rm DGL} \equiv 1/g^2 = 1$, $\hat{m}_B = \hat{m}_\chi = 0.5$. This set is simply to see the behavior of the profiles and to compare the string tension of the potential with the analytical value in the Bogomol'nyi limit, $\sigma^L = 4\pi v^2 \cdot a^2 = 4\beta_{\rm DGL}\pi\hat{m}_B^2/3$

Table 7.1: The color-electric Dirac string structure in the dual gauge field in the q-$\bar{q}$ system for various representations (for Figs. 7.1-7.7) is schematically summarized. Here, $\uparrow$ and $\downarrow$ correspond to the one Dirac string singularity. If we circulate around these singularities in counter-clockwise way, they lead to the phase $+2\pi$ and -2π, respectively. Notice that $\Uparrow = 2\times\uparrow$ and $\Downarrow = 2\times\downarrow$.

	3-8 basis		electric basis			magnetic basis		
	B^3_μ	B^8_μ	$B^{\rm e}_{1\,\mu}$	$B^{\rm e}_{2\,\mu}$	$B^{\rm e}_{3\,\mu}$	$B^{\rm m}_{1\,\mu}$	$B^{\rm m}_{2\,\mu}$	$B^{\rm m}_{3\,\mu}$
R-$\bar{R}$	$\downarrow_c$	$\downarrow_c$	$\Downarrow_e$	$\uparrow_e$	$\uparrow_e$	0	$\uparrow_m$	$\downarrow_m$
B-$\bar{B}$	$\uparrow_c$	$\downarrow_c$	$\uparrow_e$	$\Downarrow_e$	$\uparrow_e$	$\downarrow_m$	0	$\uparrow_m$
G-$\bar{G}$	0	$\Uparrow_c$	$\uparrow_e$	$\uparrow_e$	$\Downarrow_e$	$\uparrow_m$	$\downarrow_m$	0

[72, 32], which will be discussed in the next section. One finds that the analytical string tension is reproduced by the numerical potential in Fig. 7.8. In order to get quantitatively realistic results, we need more information about the parameter set of the DGL theory from the SU(3) gluodynamics as done in the chapter 5.

It is worth noting that in the mesonic case, we can reduce the $[{\rm U}(1)]^2$ DGL theory to the U(1) DAH model. Let us see this in the R-$\bar{R}$ system with the Cartan representation of the dual gauge field, as an example. Other systems and other representations can be treated similarly. Here, we already know the profiles of the color-electric flux tube and the contribution of the dual gauge field and the monopole field as shown in Figs. 7.1 and 7.7. Thus, one can take $B^3_\mu = B^8_\mu \equiv B_\mu$ and $\chi_1 = v$, $\chi_2 \equiv \chi^*$, $\chi_3 \equiv \chi$. The DGL Lagrangian (7.1.3) is reduced to the form,

$$\begin{aligned}\mathcal{L}^{3\text{-}8}_{\rm DGL} &= \frac{1}{3g^2}\left(\partial_\mu B_\nu - \partial_\nu B_\mu + 2\pi\Sigma^{\rm E}_{1\,\mu\nu}\right)^2 \\ &\quad +2\left[\left|\left(\partial_\mu + iB_\mu\right)\chi\right|^2 + \lambda\left(|\chi|^2 - v^2\right)^2\right]. \end{aligned} \tag{7.2.1}$$

The redefinitions of the couplings and the fields

$$g \equiv \frac{2}{\sqrt{3}}\hat{g}, \quad \lambda \equiv 2\hat{\lambda}, \quad v \equiv \frac{1}{\sqrt{2}}\hat{v}, \quad B_\mu \to \hat{g}B_\mu, \quad \chi \to \frac{\chi}{\sqrt{2}}, \tag{7.2.2}$$

lead to the Lagrangian of the DAH model as is given in (3.1.1).

7.2.2 Baryonic flux tube (q-q-q system)

We solve the field equations in the presence of three types of the color-electric charges. Since these color-electric charges are defined in the weight vector diagram of SU(3) algebra, and the color-electric Dirac strings which are attached to these charges carry the same quantity,

respectively, these Dirac strings can join at a certain point to cancel each other ($\sum_{j=1}^{3} e\vec{w}_j = 0$), which we call a junction. Here, we consider the simple case that the three types of the color-electric charge are placed on the corners of a regular triangle. The non-vanishing plaquettes $\hat{\Sigma}^{\mathrm{E}}_{1\,\mu\nu}(s)$, $\hat{\Sigma}^{\mathrm{E}}_{2\,\mu\nu}(s)$ and $\hat{\Sigma}^{\mathrm{E}}_{3\,\mu\nu}(s)$ are properly included so as to minimize the length of the color-electric Dirac string, which corresponds to the energy minimization condition. Then, the position of the junction is given by the Fermat point [73]. As a result, we get a typical Y-shaped flux-tube object in the DGL theory, *i.e.* the baryonic flux tube.

In Figs. 7.9-7.11, we show the profiles of the color-electric field corresponding to the Cartan, the color-electric, and the color-magnetic representations of the dual gauge field. The Weyl symmetric structure can be observed in the last two representations. The monopole field does not depend on the representation, for the same reason as in the discussion of the mesonic flux tube, which is shown in Fig. 7.12. One finds that all of these profiles faithfully reflect the structure of the color-electric Dirac string. The potential is obtained analogously to the mesonic system, which is shown in Fig. 7.13. Here, parametrizing the potential of the linear part as

$$V(\boldsymbol{x}_1, \boldsymbol{x}_2, \boldsymbol{x}_3) \sim \sigma^L \sum_{i=1}^{3} |\boldsymbol{x}_i - \boldsymbol{x}_J|, \tag{7.2.3}$$

where $\boldsymbol{x}_i$ and $\boldsymbol{x}_J$ denote the position of the quarks and of the junction on the dual lattice, respectively, we can extract the string tension σ^L. One finds that this is almost reproduced by the analytical one, since $\sigma^L \sim 1.0 \sim 4\beta_{\mathrm{DGL}}\pi\hat{m}_B^2/3$. It is interesting to note that while each profile of the color-electric field in the color-electric representation has a form similar to the 8-flux in the Cartan representation, the color-electric field in the color-magnetic representation provides the 3-flux type structure. It is, of course, possible to study the energy and the field distribution corresponding to different shapes of the baryonic flux tube for a static configuration. This will be addressed in future investigations.

7.3 Properties of the classical DGL vacuum

Since the dual gauge symmetry is now extended to $[\mathrm{U}(1)]^2$ corresponding to SU(3) gluodynamics, some interesting feature are expected to appear for the vacuum properties compared with the U(1) DAH model. In this section, we discuss the vacuum properties of the DGL theory by using a similar technique as in the U(1) DAH model. To do this, it is useful to pay attention to the Bogomol'nyi limit, the border of type-I and type-II vacuum.

7.3.1 Bogomol'nyi limit

Let us consider the q-$\bar{q}$ system given by the DGL theory with the color-magnetic representation of the dual gauge field. We first divide the dual gauge field into two parts: the regular part and the singular part, where the role of each term are the same as in the U(1) DAH model. Then, we write

$$B^{\rm m}_{i\,\mu} \equiv B^{\rm m:reg}_{i\,\mu} + B^{\rm m:sing}_{i\,\mu} \quad (i=1,2,3), \tag{7.3.1}$$

where the singular part is determined so as to define the color-electric charge density $C_{j\,\mu\nu}$ as

$$(\partial \wedge B^{\rm m:sing}_i)_{\mu\nu} + 2\pi \sum_{j=1}^{3} m_{ij} \Sigma^{\rm E}_{j\,\mu\nu} = 2\pi \sum_{j=1}^{3} m_{ij} C_{j\,\mu\nu}. \tag{7.3.2}$$

Here, m_{ij} is an integer given by $m_{ij} = \sum_{k=1}^{3} \varepsilon_{ijk} = \{-1, 0, 1\}$ [See. Eq. (6.2.3)]. The meaning of $C_{j\,\mu\nu}$ is the same as in the U(1) DAH model, it has the information about the position of the ends of the color-electric Dirac string. Note that now there exist three types of color-electric charge. The dual field strength tensor is rewritten as

$$^*F_{i\,\mu\nu} \;=\; (\partial \wedge B^{\rm m:reg}_i)_{\mu\nu} + 2\pi \sum_{j=1}^{3} m_{ij} C_{j\,\mu\nu}. \tag{7.3.3}$$

Let us consider an ideal system; infinitely long string with cylindrical symmetry. In this case, the fields depend only on the radial coordinate r as

$$\phi_i = \phi_i(r), \quad \boldsymbol{B}^{\rm m:reg}_i = B^{\rm m:reg}_i(r)\boldsymbol{e}_\varphi \equiv \frac{\tilde{B}^{\rm m:reg}_i(r)}{r}\boldsymbol{e}_\varphi, \tag{7.3.4}$$

where $\phi_i(r)$ is the modulus of the monopole field $\chi_i = \phi_i \exp(i\eta_i)$, and φ denotes the azimuthal angle. Note that the phase of the monopole field is now assumed to be regular $[\partial_\mu, \partial_\nu]\eta_i$, which is absorbed into the regular part of the dual gauge field by the replacement $B^{\rm m:reg}_i + \partial_\mu \eta_i \to B^{\rm m:reg}_i$. The contribution from the Coulomb term $C_{j\,\mu\nu}$ is neglected. Then, the solution of (7.3.2) is easily found to be

$$\boldsymbol{B}^{\rm m:sing}_i = -\frac{m_{ij}}{r}\boldsymbol{e}_\varphi. \tag{7.3.5}$$

Then, the field equations are given by

$$\frac{d^2\phi_i}{dr^2} + \frac{1}{r}\frac{d\phi_i}{dr} - \left(\frac{\tilde{B}^{\rm m:reg}_i - m_{ij}}{r}\right)^2 \phi_i - 2\lambda\phi_i(\phi_i^2 - v^2) = 0, \tag{7.3.6}$$

$$\frac{d^2\tilde{B}^{\rm m:reg}_i}{dr^2} - \frac{1}{r}\frac{d\tilde{B}^{\rm m:reg}_i}{dr} - 2g^2_{\rm m}\left(\tilde{B}^{\rm m:reg}_i - m_{ij}\right)\phi_i^2 = 0, \tag{7.3.7}$$

The string tension can be computed as the energy of the flux-tube per unit length,

$$\sigma = 2\pi \sum_{i=1}^{3} \int_0^\infty r dr \left[\frac{1}{2g^2_{\rm m}}\left(\frac{1}{r}\frac{d\tilde{B}^{\rm m:reg}_i}{dr}\right)^2 + \left(\frac{d\phi_i}{dr}\right)^2 + \left(\frac{\tilde{B}^{\rm m:reg}_i - m_{ij}}{r}\right)^2 \phi_i^2 + \lambda(\phi_i^2 - v^2)^2\right], \tag{7.3.8}$$

To make energy of the system finite, we have to postulate the boundary conditions:

$$\begin{aligned}
&\tilde{B}_i^{\text{m:reg}} = 0, \quad \phi_i = \begin{cases} 0 & (i \neq j) \\ v & (i = j) \end{cases} \qquad \text{as} \quad r \to 0, \\
&\tilde{B}_i^{\text{m:reg}} = m_{ij}, \quad \phi_i = v \qquad\qquad\quad \text{as} \quad r \to \infty.
\end{aligned} \tag{7.3.9}$$

Since now we have quite similar forms of the field equations and the string tension as in the case of U(1) dual gauge symmetry, except only the labels of i and j which classify the kinds of the monopole and the quark corresponding to $[\mathrm{U}(1)]^3_{\mathrm{m}}$ dual gauge symmetry, we can use the same strategy to find the Bogomol'nyi limit as in the U(1) DAH model [cf. Eqs. (7.3.6), (7.3.7), and (3.2.16)]. Thus, we can write the string tension (7.3.8) exactly in the form,

$$\begin{aligned}
\sigma &= 2\pi \sum_{i=1}^{3} |m_{ij}| v^2 + 2\pi \sum_{i=1}^{3} \int_0^\infty r dr \left[\frac{1}{2g_{\mathrm{m}}^2} \left(\frac{1}{r} \frac{d\tilde{B}_i^{\text{m:reg}}}{dr} \pm g_{\mathrm{m}}^2 (\phi_i^2 - v^2) \right)^2 \right. \\
&\quad \left. + \left(\frac{d\phi_i}{dr} \pm \left(\tilde{B}_i^{\text{m:reg}} - m_{ij} \right) \frac{\phi_i}{r} \right)^2 + \frac{1}{2} \left(2\lambda - g_{\mathrm{m}}^2 \right) (\phi_i^2 - v^2)^2 \right].
\end{aligned} \tag{7.3.10}$$

From this expression we find the Bogomol'nyi limit,

$$g_{\mathrm{m}}^2 = 2\lambda, \quad \text{or} \quad 3g^2 = 4\lambda. \tag{7.3.11}$$

In this limit the string tension is reduced to

$$\sigma = 2\pi \sum_{i=1}^{3} |m_{ij}| v^2 = 4\pi v^2, \tag{7.3.12}$$

provided the profiles of the dual gauge field and the monopole field are determined by the first-order differential equations,

$$\frac{d\phi_i}{dr} \pm \left(\tilde{B}_i^{\text{m:reg}} - m_{ij} \right) \frac{\phi_i}{r} = 0, \tag{7.3.13}$$

$$\frac{1}{r} \frac{d\tilde{B}_i^{\text{m:reg}}}{dr} \pm g_{\mathrm{m}}^2 (\phi_i^2 - v^2) = 0. \tag{7.3.14}$$

These field equations, of course, reproduce the second-order differential equations (7.3.6) and (7.3.7) when the relation (7.3.11) is satisfied.

Here, to obtain the string tension of the form (7.3.10) and the saturated string tension (7.3.12), we have paid attention to the boundary conditions of the fields (7.3.9) by taking into account the relation (6.2.3). For instance, let us consider the R-$\bar{R}$ flux-tube, which is given by the label $j = 1$. In this system, the monopole field ϕ_1 which has the magnetic charge $g\vec{\epsilon}_1$ is decoupled from the system, since ϕ_1 does not feel any singularity of the flux-tube core, and accordingly, the regular dual gauge field $B_1^{\text{m:reg}}$ is also decoupled. The behavior of the other fields is interesting: ϕ_2 and ϕ_3 behave as the same monopole field, and $B_2^{\text{m:reg}}$ and

$B_3^{\mathrm{m:reg}}$ provides the $\mathrm{U}(1)_{i=2}$ flux tube and $\mathrm{U}(1)_{i=3}$ *anti* flux tube due to the sign of the m_{ij}, which takes 1 and -1, respectively. Here, both dual gauge fields are related to each other through the constraint $\sum_{i=1}^{3} B_i^{\mathrm{m:reg}} = 0$, and $\mathrm{U}(1)_{i=3}$ anti flux tube can be regarded as the $\mathrm{U}(1)_{i=2}$ flux tube, or vise versa. As a result, these flux tubes provide the same string tension $2\pi v^2$, and finally, we get two times of this string tension, $2 \times 2\pi v^2$. This is caused by the $[\mathrm{U}(1)]^2_{\mathrm{m}}$ dual gauge symmetry. We note that since this discussion is the Weyl symmetric, final expression for the string tension (7.3.12) does not depend on what kind of the color-electric charges $\vec{Q}_j^{\mathrm{E}}$ sits at the ends. The profiles of the color-electric field can be obtained by solving the first order equations (7.3.13) and (7.3.14) by taking into account the above discussion as is discussed in Refs. [35, 36].

The meaning of (7.3.11) is the following. We know that in the DGL theory has two characteristic scales expressed by combinations of three parameters, g, λ and v. One is the mass of the dual gauge field $m_B = \sqrt{2} g_{\mathrm{m}} v = \sqrt{3} g v$ and the other is the mass of the monopole field $m_\chi = 2\sqrt{\lambda} v$. These masses have been extracted from the DGL Lagrangian by taking into account the dual Higgs mechanism as shown in Eq. (6.2.11). Thus, the Bogomol'nyi limit in the DGL theory (7.3.11) is the supersymmetry between the dual gauge field and the monopole field $m_B = m_\chi$, or $\kappa = 1$ [See. Eq. (6.2.12)]. This is an extension which is already discussed in the U(1) DAH model.

7.3.2 Interaction of flux tubes

We would like to discuss the interaction of flux tubes. Now, we have three different types of mesonic flux tubes, such as given by R-$\bar{R}$, B-$\bar{B}$, and G-$\bar{G}$, depending on the color-electric charge attached to both ends of the tube. For the interaction between two parallel flux tubes of the "same type," such as the system R-$\bar{R}$ and R-$\bar{R}$, we can expect that U(1) DAH like properties appear, since we know that such case the DGL theory can be reduced the U(1) DAH model [See, subsection. 7.2.1]. It means that in the Bogomol'nyi limit there seems to be no interaction between them. Moreover, in the type-I or in the type-II vacuum, which is away from the Bogomol'nyi limit, the flux-tube interaction manifestly appears. In the type-I vacuum, an attractive force appears. On the other hand, in the type-II vacuum, flux tubes repel each other.

It is interesting to investigate what happens if two parallel flux tubes of "different types" are placed at a certain distance [74]. We find that now this system has a remarkable aspect owing to the Weyl symmetry. For instance, let us consider the interaction between R-$\bar{R}$ and B-$\bar{B}$. We find that the interaction between them is attractive, since if we suppose that these flux tubes are unified into one flux tube, it becomes $\bar{G}$-G (See the relation (6.2.3)). It means that the energy of the system after unification is reduced into a half of the initial one. The

same interaction property would be observed in the process, B-$\bar{B}$ + G-$\bar{G}$ $\rightarrow$ $\bar{R}$-R and G-$\bar{G}$ + R-$\bar{R}$ $\rightarrow$ $\bar{B}$-B. These investigations show that if we pay attention to the Weyl symmetry, we can easily obtain qualitative information about the flux-tube interaction.

7.4 Summary and outlook

In this chapter, we have reformulated the DGL theory to make the global Weyl symmetry among color charges manifest, and applied to the investigation of hadron structures corresponding to meson and baryon states in terms of the open and Y-shaped flux-tube solutions in the DGL theory. The baryonic state is one of the most interesting and important application of the DGL theory, since this state can be treated only after taking into account the $[\mathrm{U}(1)]^2$ dual gauge symmetry originating from SU(3) gauge symmetry. We have found that the manifestly Weyl symmetric approach, in particular, given by the color-magnetic representation of the dual gauge field is the most convenient one for this subject, since the resulting DGL theory can be dealt with in a quite similar way as in the U(1) DAH model.

In order to extract the quantitative information of hadronic states in terms of the flux tube, we should determine the couplings of the DGL theory from SU(3) gluodynamics (SU(3) QCD) as in the chapter 5, which is our next interest for further investigation.

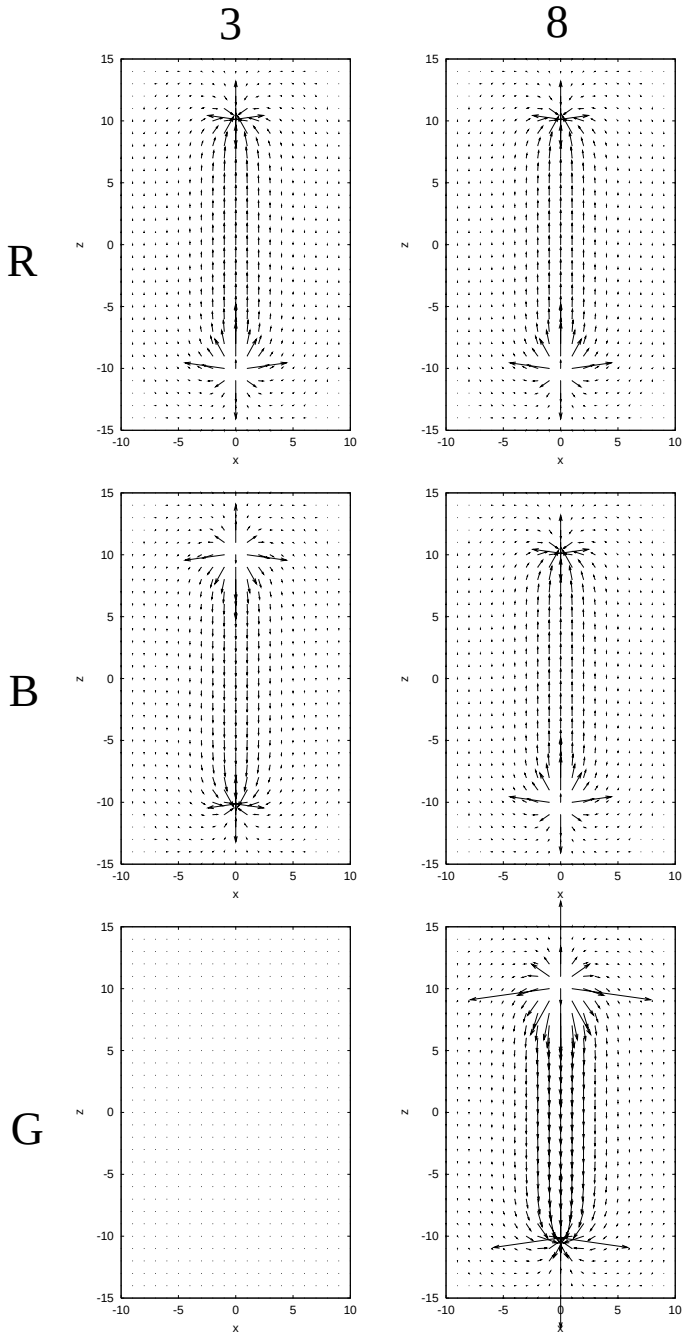

Figure 7.1: The profiles of the color-electric field in the Cartan representation for 3- (left) and 8- (right) components in the R-$\bar{R}$ (upper), the B-$\bar{B}$ (middle), and the G-$\bar{G}$ (lower) systems in the x-z plane at $y = 0$. The quark and the antiquark are placed at $(x, y, z) = (0, 0, -10)$ and $(0, 0, 10)$, respectively.

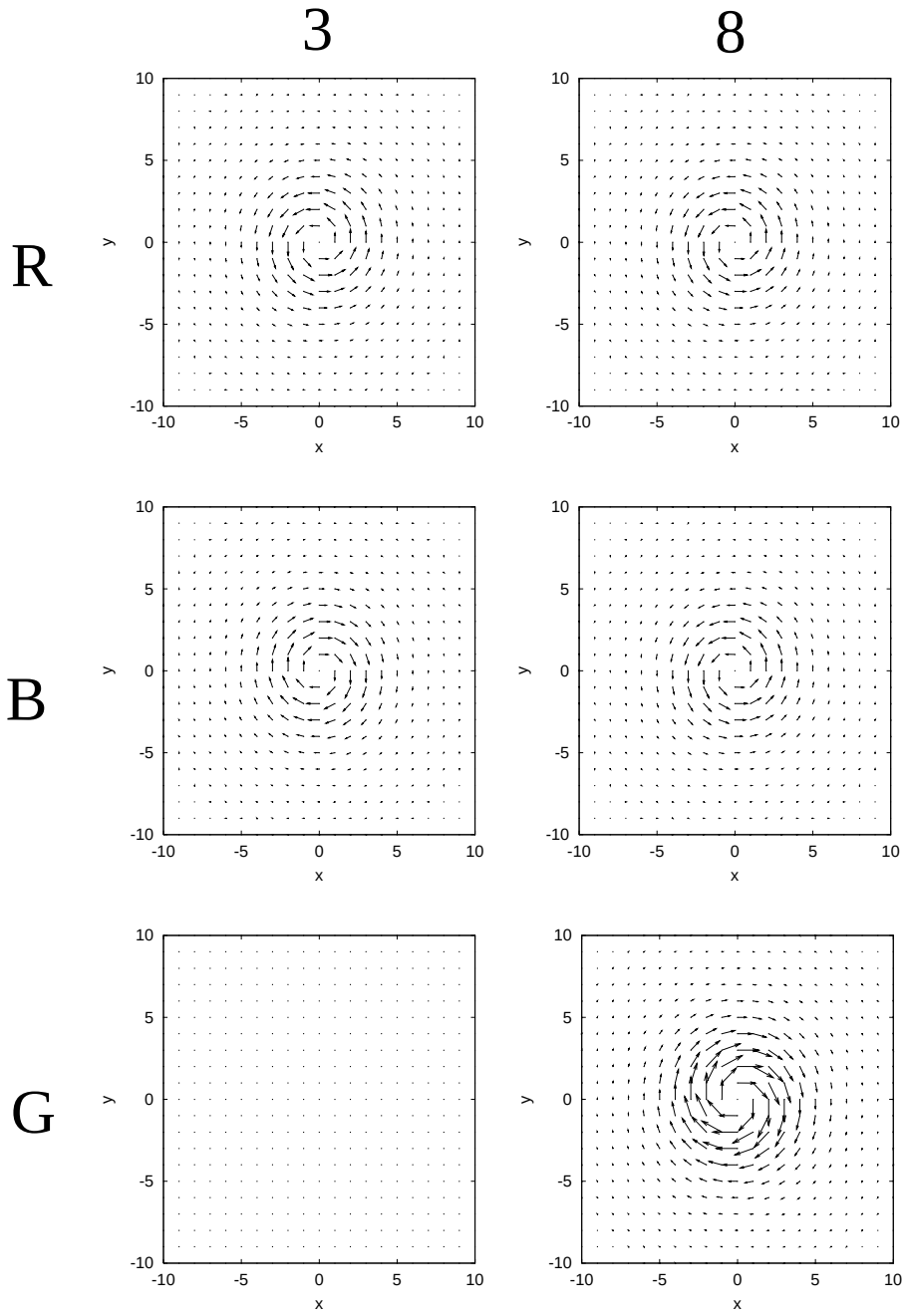

Figure 7.2: The profiles of the monopole supercurrent in the Cartan representation for 3- (left) and 8- (right) components in the R-$\bar{R}$ (upper), the B-$\bar{B}$ (middle), and the G-$\bar{G}$ (lower) systems in the x-y plane at $z = 0$. The quark and the antiquark are placed at $(x, y, z) = (0, 0, -10)$ and $(0, 0, 10)$, respectively.

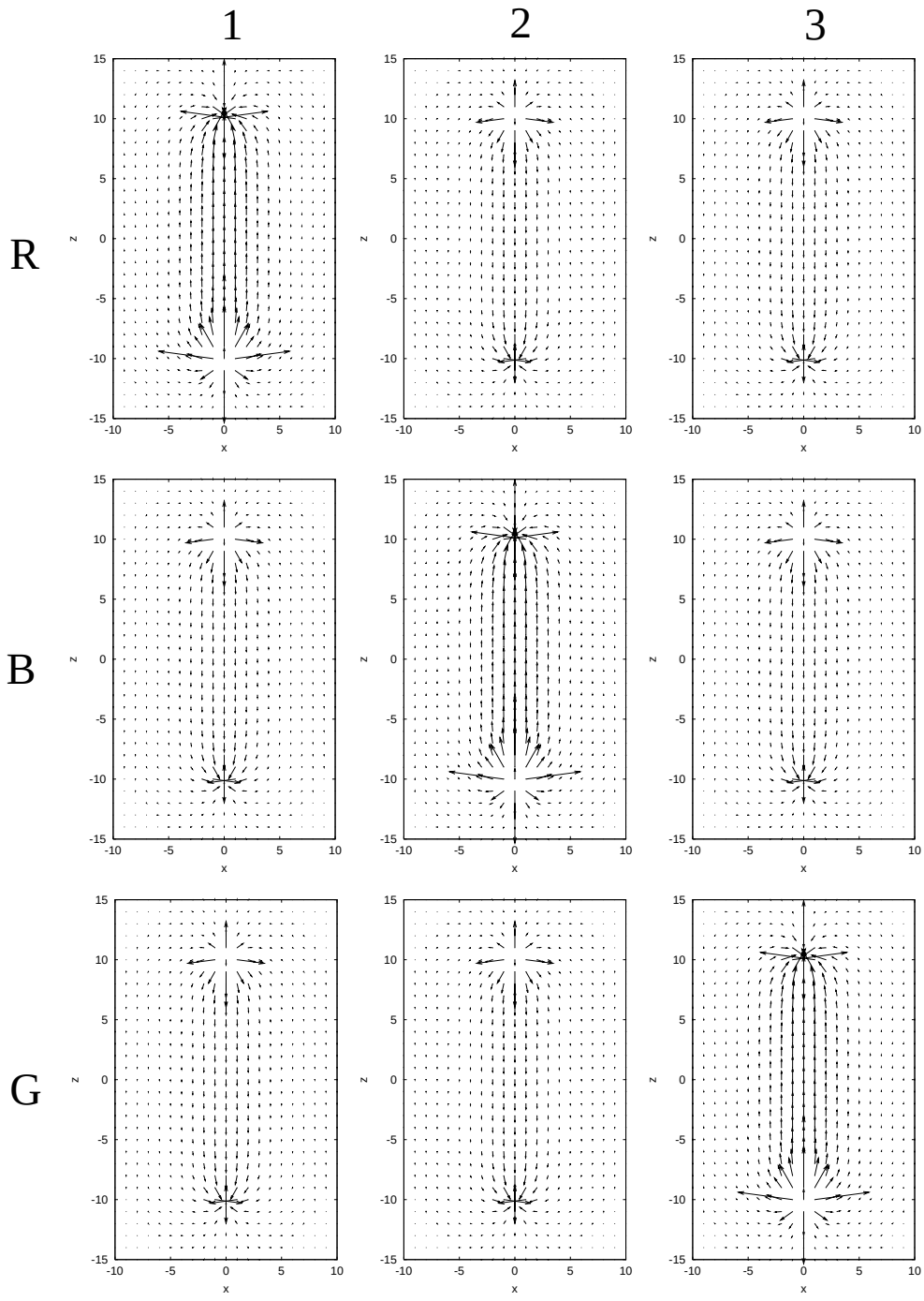

Figure 7.3: The profiles of the color-electric field in the color-electric representation, expressed on the weight vectors of the SU(3) algebra, $\vec{w}_1$ (left), $\vec{w}_2$ (center), and $\vec{w}_3$ (right) in the R-$\bar{R}$ (upper), the B-$\bar{B}$ (middle), and the G-$\bar{G}$ (lower) systems in the x-z plane at $y = 0$. The quark and the antiquark are placed at $(x, y, z) = (0, 0, -10)$ and $(0, 0, 10)$, respectively.

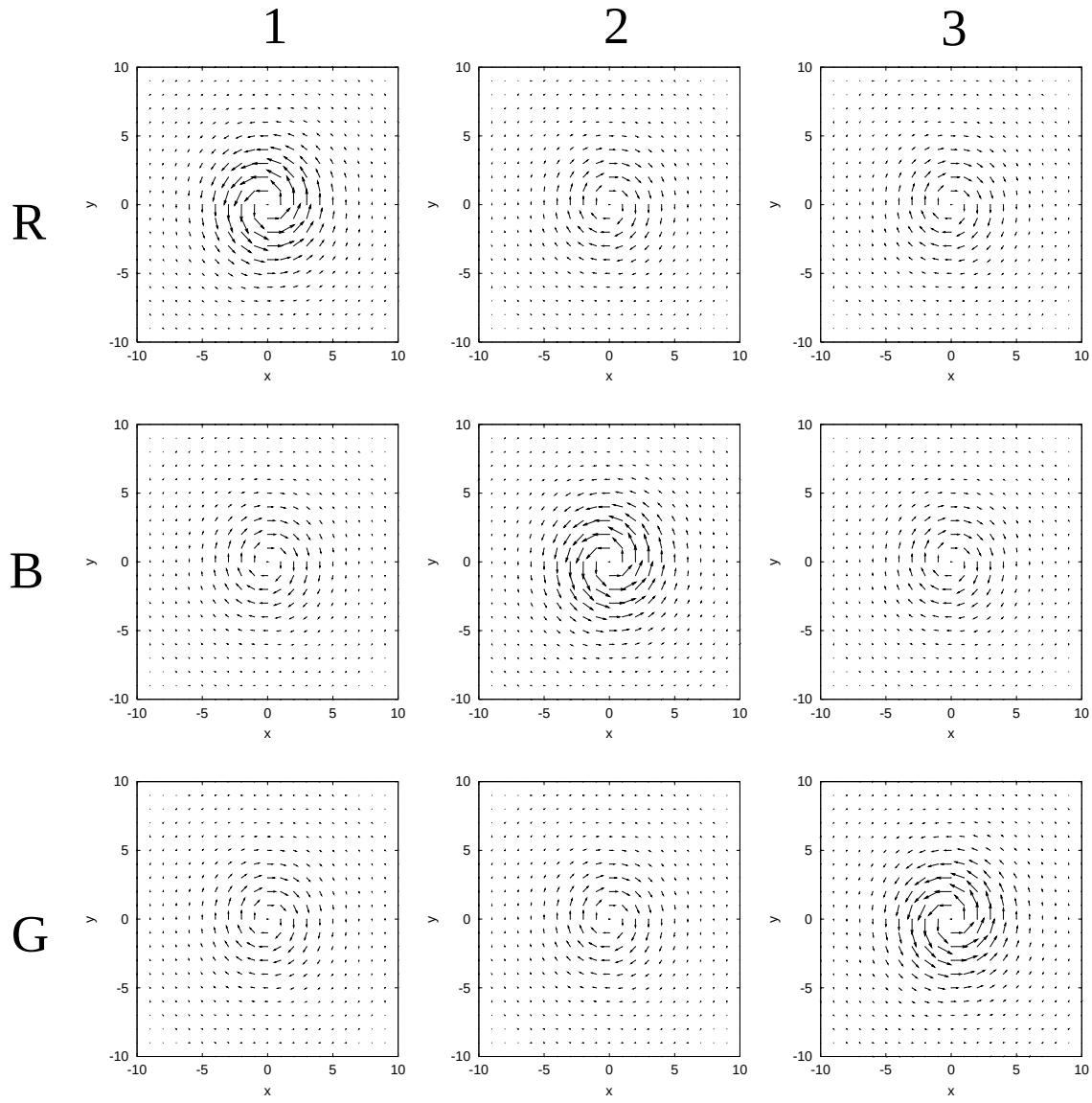

Figure 7.4: The profiles of the monopole supercurrent in the color-electric representation, expressed on the weight vectors of the SU(3) algebra, $\vec{w}_1$ (left), $\vec{w}_2$ (center), and $\vec{w}_3$ (right) in the R-$\bar{R}$ (upper), the B-$\bar{B}$ (middle), and the G-$\bar{G}$ (lower) systems in the x-y plane at $z = 0$. The quark and the antiquark are placed at $(x, y, z) = (0, 0, -10)$ and $(0, 0, 10)$, respectively.

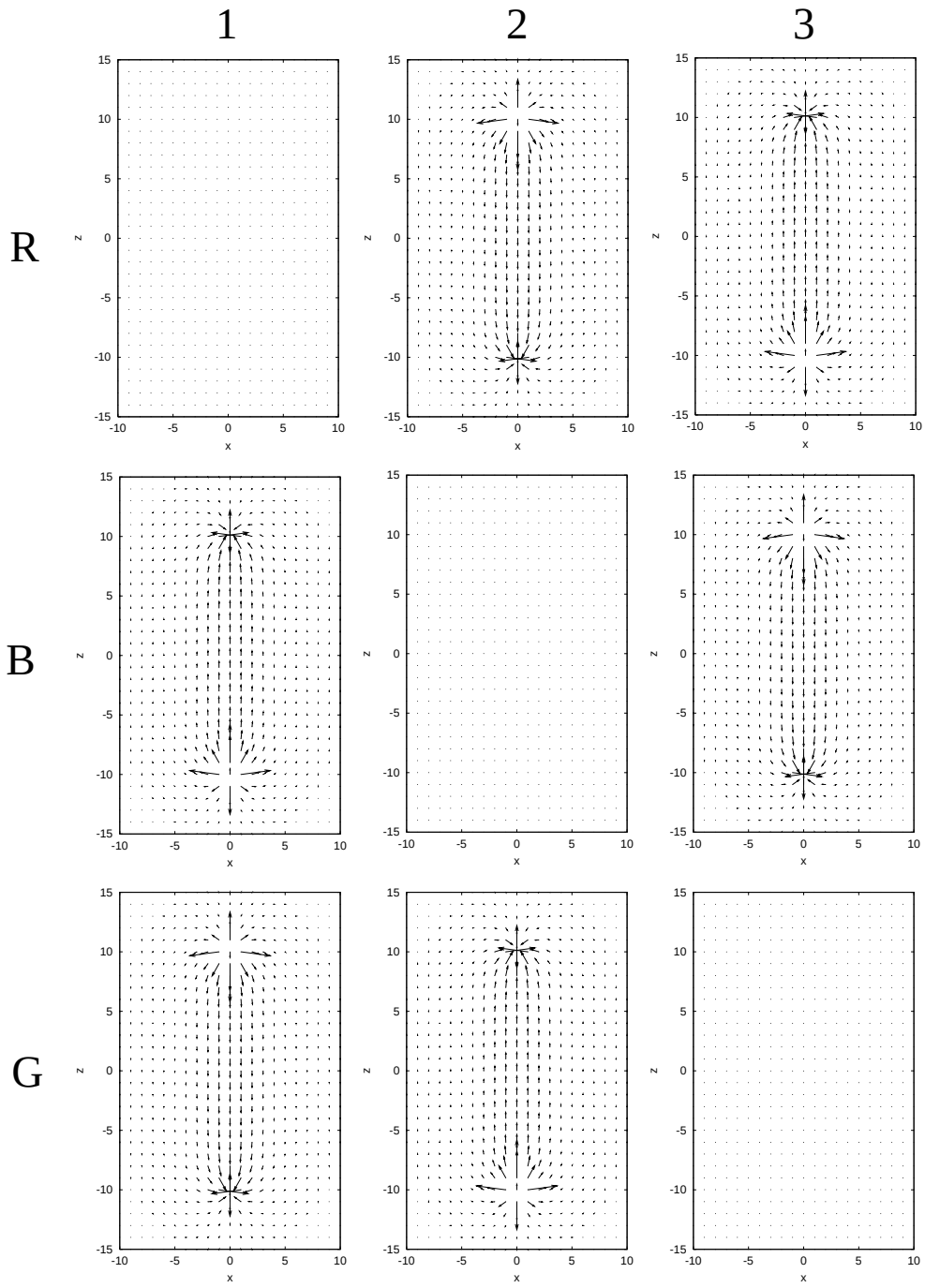

Figure 7.5: The profiles of the color-electric field in the color-magnetic representation, expressed on the root vectors of the SU(3) algebra, $\vec{\epsilon}_1$ (left), $\vec{\epsilon}_2$ (center), and $\vec{\epsilon}_3$ (right) in the R-$\bar{R}$ (upper), the B-$\bar{B}$ (middle), and the G-$\bar{G}$ (lower) systems in the x-z plane at $y = 0$. The quark and the antiquark are placed at $(x, y, z) = (0, 0, -10)$ and $(0, 0, 10)$, respectively.

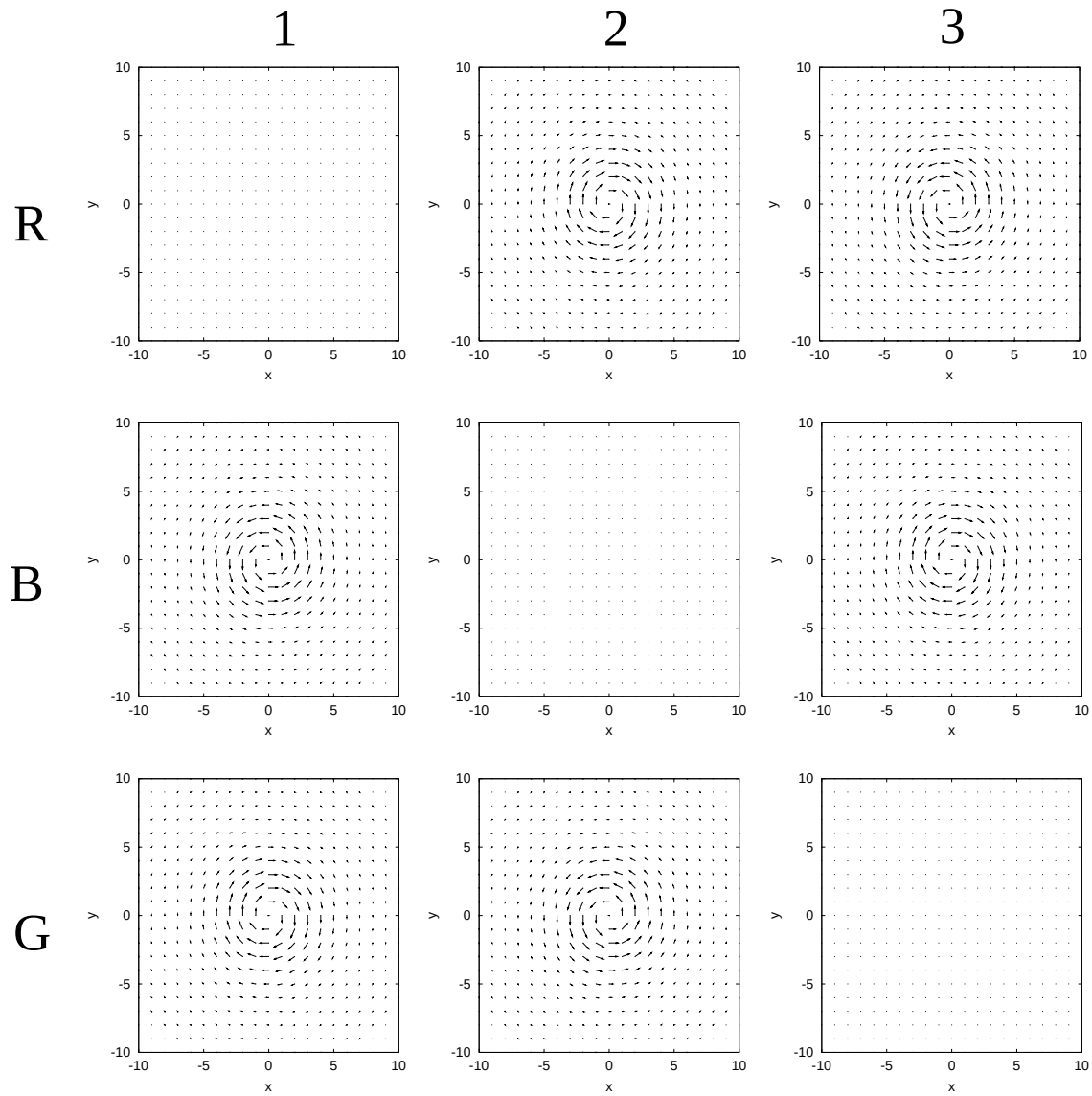

Figure 7.6: The profiles of the monopole supercurrent in the color-magnetic representation, expressed on the root vectors of the SU(3) algebra, $\vec{\epsilon}_1$ (left), $\vec{\epsilon}_2$ (center), and $\vec{\epsilon}_3$ (right) in the R-$\bar{R}$ (upper), the B-$\bar{B}$ (middle), and the G-$\bar{G}$ (lower) systems in the x-y plane at $z = 0$. The quark and the antiquark are placed at $(x, y, z) = (0, 0, -10)$ and $(0, 0, 10)$, respectively.

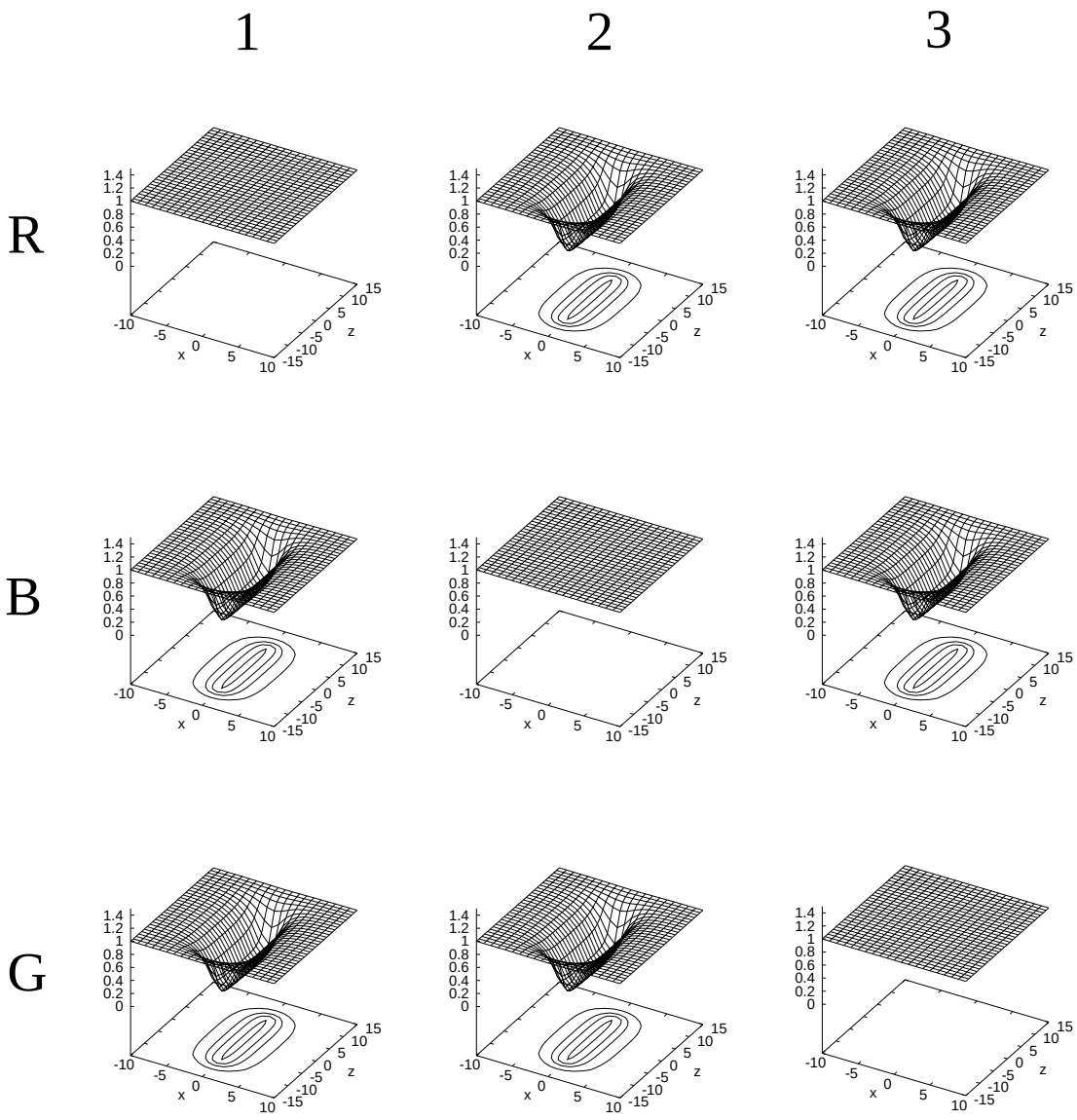

Figure 7.7: The profiles of the modulus of the monopole field of $|\chi_1|$ (left), $|\chi_2|$ (center), and $|\chi_3|$ (right) in the R-$\bar{R}$ (upper), the B-$\bar{B}$ (middle), and the G-$\bar{G}$ (lower) systems in the x-z plane at $y = 0$. The quark and the antiquark are placed at $(x, y, z) = (0, 0, -10)$ and $(0, 0, 10)$, respectively.

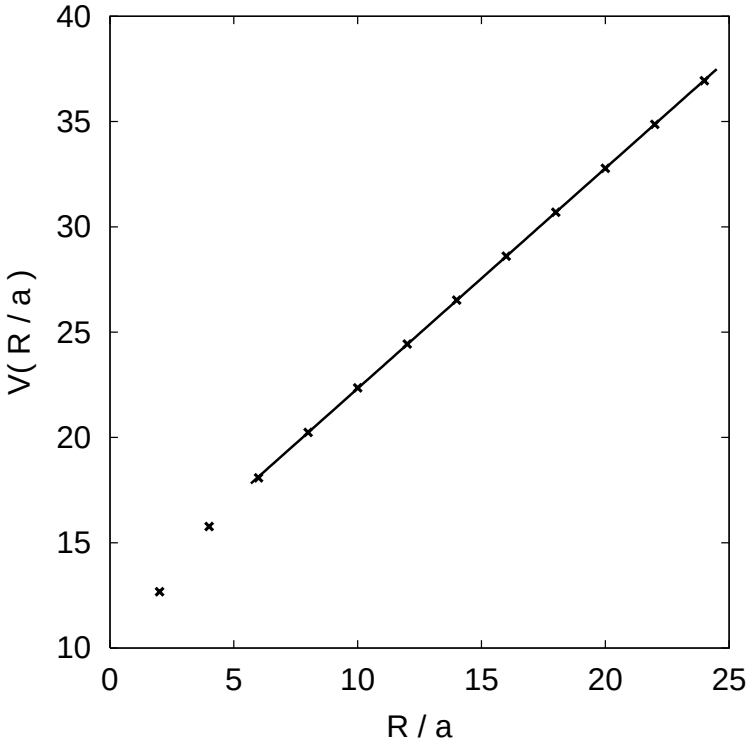

Figure 7.8: The quark-antiquark potential in the DGL theory, where R/a denotes the q-$\bar{q}$ distance. The parameter set is taken as $\beta_{\mathrm{DGL}} = 1$, $\hat{m}_B = \hat{m}_\chi = 0.5$.

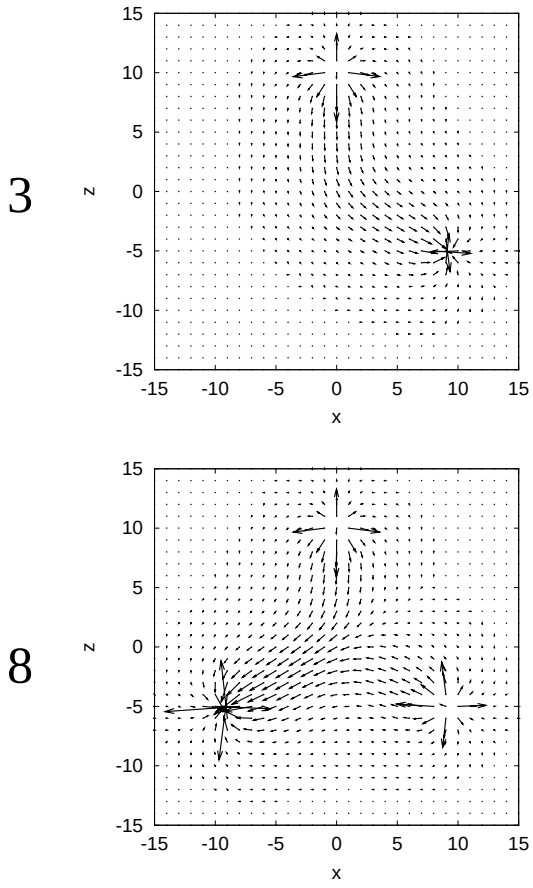

Figure 7.9: The profiles of the color-electric field in the Cartan representation for 3- (upper) and 8- (lower) components in the baryonic flux tube in the x-z plane at $y = 0$. The junction and the quarks are located at $(x, y, z) = (0, 0, 0)$, and $R(0, 0, 9)$, $B(9, 0, -5)$, $G(-9, 0, -5)$, respectively.

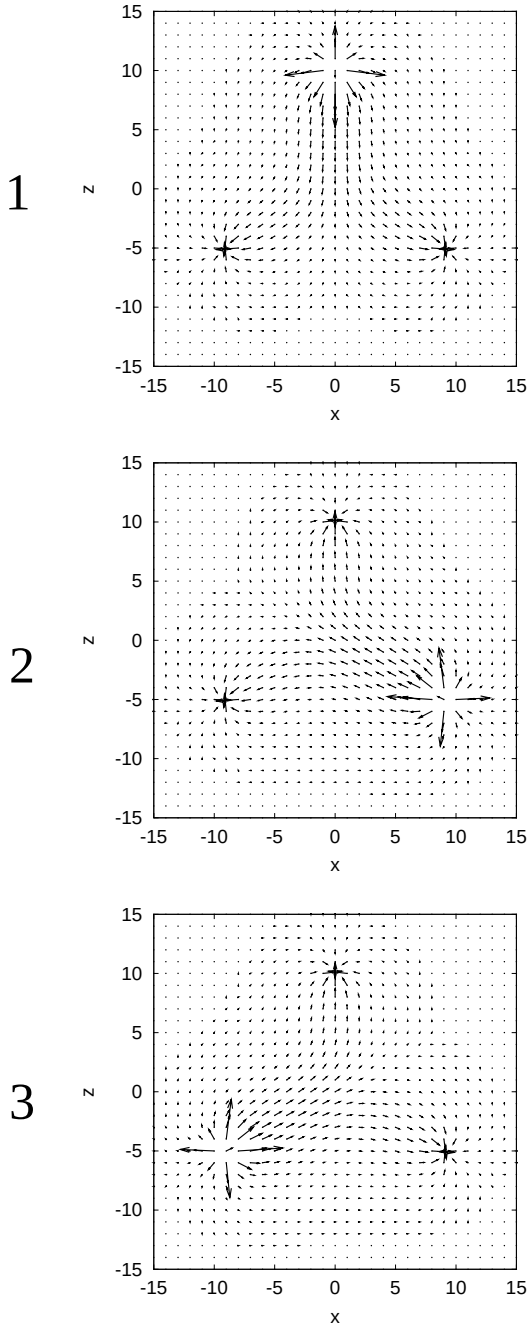

Figure 7.10: The profiles of the color-electric field in the color-electric representation, expressed on the weight vectors of the SU(3) algebra, $\vec{w}_1$ (upper), $\vec{w}_2$ (middle), and $\vec{w}_3$ (lower) in the baryonic flux tube in the x-z plane at $y = 0$. The junction and the quarks are located at $(x, y, z) = (0, 0, 0)$, and $R(0, 0, 9)$, $B(9, 0, -5)$, $G(-9, 0, -5)$, respectively.

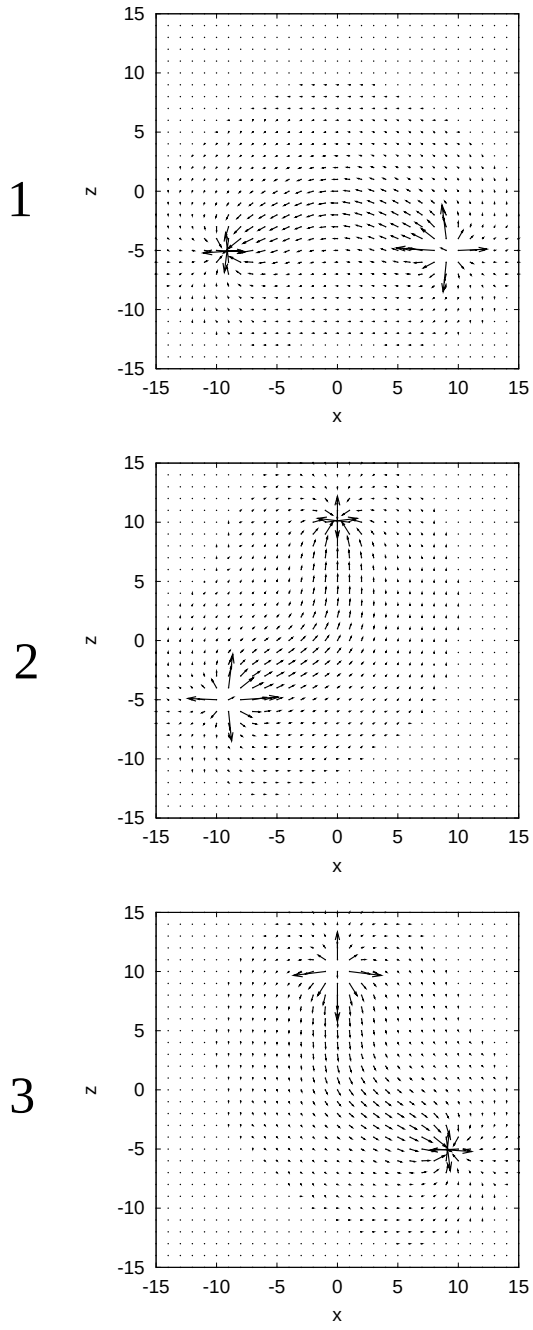

Figure 7.11: The profiles of the color-electric field in the color-magnetic representation, expressed on the root vectors of the SU(3) algebra, $\vec{\epsilon}_1$ (upper), $\vec{\epsilon}_2$ (middle), and $\vec{\epsilon}_3$ (lower) in the baryonic flux tube in the x-z plane at $y = 0$. The junction and the quarks are located at $(x, y, z) = (0, 0, 0)$, and $R(0, 0, 9)$, $B(9, 0, -5)$, $G(-9, 0, -5)$, respectively.

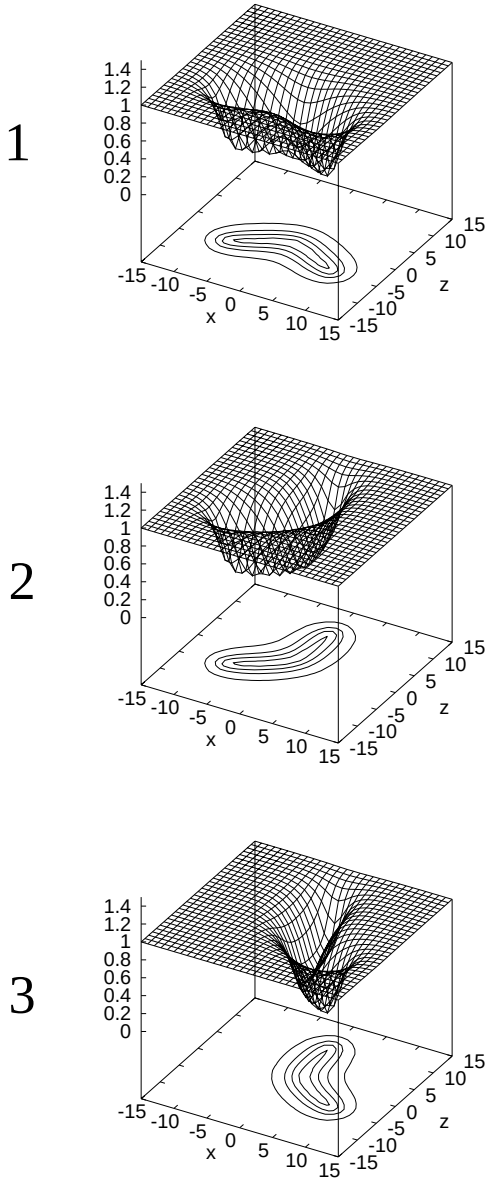

Figure 7.12: The profiles of the modulus of the monopole field of $|\chi_1|$ (upper), $|\chi_2|$ (middle), and $|\chi_3|$ (lower) in the baryonic flux tube in the x-z plane at $y = 0$. The junction and the quarks are located at $(x, y, z) = (0, 0, 0)$, and $R(0, 0, 9)$, $B(9, 0, -5)$, $G(-9, 0, -5)$, respectively.

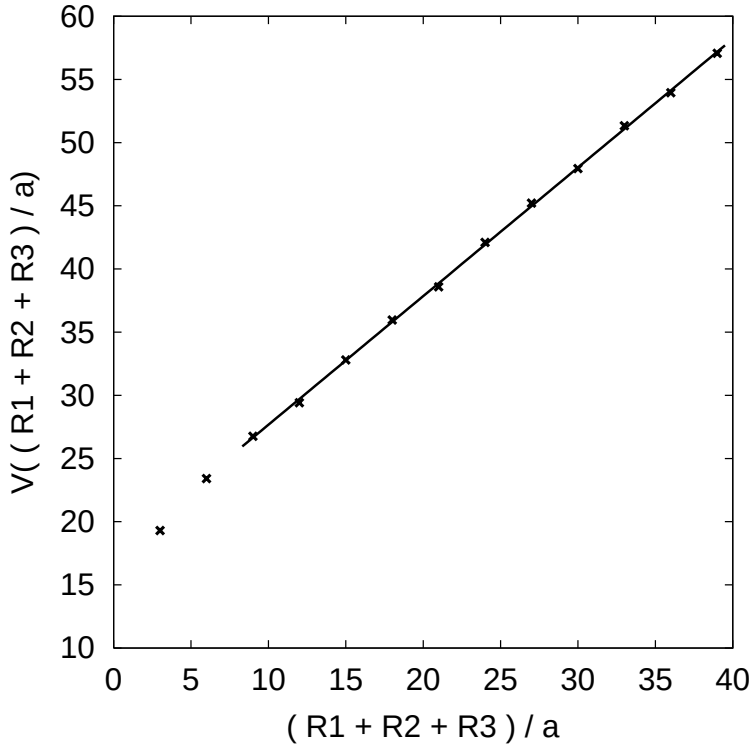

Figure 7.13: The three-quark potential of the baryonic flux tube in the DGL theory, where $R_i = |\boldsymbol{x}_i - \boldsymbol{x}_J|$. The parameter set is taken as $\beta_{\mathrm{DGL}} = 1$, $\hat{m}_B = \hat{m}_\chi = 0.5$.

Chapter 8

Glueball as the flux-tube ring solution in the DGL theory

The existence of glueball states is naively expected as results of the gluon self-coupling in QCD [6]. Recent progress of lattice QCD simulations predicts the masses of glueballs $M(0^{++})$ = 1.50 $\sim$ 1.75 GeV, $M(2^{++})$ = 2.15 $\sim$ 2.45 GeV [75–78]. Experimentally, there are some candidates; $f_0(1500)$ and $f_0(1710)$ for the scalar glueball; $f_J(2220)$ (J = 2 or 4), $f_2(2300)$ and $f_2(2340)$ for the tensor glueball [2]. However, the abundance of q-$\bar{q}$ meson states in the 1 $\sim$ 3 GeV region and the possibility of the quarkonium-glueball mixing states still make it difficult to identify the glueball states [79]. To date, no glueball state has been firmly discovered yet. More studies for the glueballs from many directions are necessary to specify the glueball states.

In this chapter, as an application of the flux-tube picture for understanding the hadron structure, we study the glueball state using the flux-tube ring solution in the dual Ginzburg-Landau theory [51]. Our view point is the following: As shown in previous chapters, the meson and the baryon states can be regarded as a flux tube with valence quarks at the ends. Then, the glueball, which is constructed from gluons with no valence quarks, is identified with the flux tube without ends, the flux-tube ring. We first describe the flux-tube ring as a relativistic closed string with the effective string tension in terms of the string representation of the DGL theory, which contains the Nambu-Goto action. The effective string tension is classically calculated from the flux-tube ring solution as a function of its size. Combining these two results, we write the Hamiltonian for the radius degree of freedom and discuss the wave function of the flux-tube ring by solving the Schrödinger equation. Finally, we estimate the mass spectrum and its size as the glueball state.

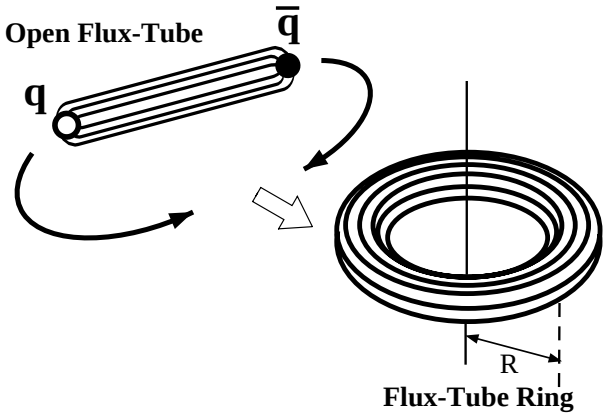

Figure 8.1: Flux-tube ring

8.1 Flux-tube ring as the closed effective string

In this section, we explain our strategy to study the glueball state starting from the flux-tube solution of the DGL theory. We consider the simplest ring configuration obtained when the ends of the flux tube meet each other to form a circle [See Fig. 8.1]. However, we know that since the flux-tube solution is a static one which does not contain any kinetic energy, we cannot get the classically stable flux-tube ring solution. This mechanism can be understood as follows. A large flux-tube ring contains a large energy, since the energy is given by the string tension times its length, where the string tension is considered to take a constant value for a large ring. As decreasing the size of the ring, its energy becomes smaller. Therefore, the flux-tube ring is unstable and prefers to shrink. It means that, we first need to formulate a flux-tube solution including a kinetic term so as to be able to describe the dynamics of the flux tube. Once the contribution from the kinetic term is taken into account, from a quantum mechanical point of view, such a collapse is forbidden by the uncertainty principle. Let us imagine the hydrogen atom, where the stable ground state is determined by the energy balance between the kinetic term of the electron $p^2/2m_e$ and the Coulomb potential term $-e^2/r$ with the uncertainty relation $p \cdot r \geq 1$. The stable radius is known as the so-called Bohr radius, $r_B = 1/(m_e e^2)$, which leads to the minimal energy of the bound state $E_B = -e^2/(2r_B)$. This suggests that the kinetic term and the quantum effect are essential.

For this purpose, we pay attention to the so-called string representation of the DGL theory. This representation can be analytically derived in the London limit $m_\chi \to \infty$, where the modulus of the monopole field is frozen taking the value of its condensate. The resulting effective string action has the form

$$S_{\rm DGL}^{\rm string} = \sigma \int d^2\xi \sqrt{-g} + \frac{1}{\alpha_0} \int d^2\xi \sqrt{-g} g^{ab} (\partial_a t_{\mu\nu})(\partial_b t^{\mu\nu}). \tag{8.1.1}$$

One finds that this representation contains the kinetic energy of the string. It is interesting to note that first term is known as the Nambu-Goto action with the string tension σ. Since this term is proportional to the area of string world surface, minimal area of the string world surface is required for the classical string motion. The second term is the so-called rigidity term, which is considered to be originating from the finite thickness effect of the color-electric field of the flux tube. The coefficient of rigidity term $1/\alpha_0$ is known to take a negative value, which means that the string, described by this action, is stiff and hard to bend. In other word, this term prevents the closed string from shrinking, since this term dislikes a large curvature. One might expect that the closed string with rigidity has a stable size by a competition between the Nambu-Goto term and the rigidity term. Unfortunately, however, it has been reported that such a system is still unstable with respect to radial perturbations, and thus does not have a classical ground state [80]*.

Some notations are summarized in the following: The string world surface swept over the string motion, is parametrized by $x^\mu = x^\mu(\xi)$, where $\xi = (\xi_1, \xi_2)$ is a two dimensional coordinate. Then, we have

$$\sqrt{-g(\xi)} = \sqrt{-\frac{1}{2}\epsilon^{ab}\epsilon^{cd}g_{ac}g_{bd}}, \tag{8.1.2}$$

which is the determinant of the induced metric tensor of the surface

$$g_{ab} \equiv (\partial_a x_\mu(\xi))(\partial_b x^\mu(\xi)), \tag{8.1.3}$$

where $\partial_a \equiv \partial/\partial\xi^a$ $(a, b = 1, 2)$. Next, $\partial_a t_{\mu\nu}$ corresponds to the extrinsic curvature tensor of the surface [43], where

$$t_{\mu\nu}(\xi) = \frac{1}{\sqrt{-g(\xi)}}\epsilon^{ab}(\partial_a x_\mu(\xi))(\partial_b x_\nu(\xi)), \tag{8.1.4}$$

which satisfies $t^2_{\mu\nu}(\xi) = 2$.

Let us parametrize the effective string action (8.1.1) for the ring as a circle with the radius R, considered as a function of ξ_1,

$$x^1(\xi) = R(\xi_1)\cos\xi_2, \quad x^2(\xi) = R(\xi_1)\sin\xi_2, \tag{8.1.5}$$

and choose the chronological gauge $x^0(\xi) = \xi_1$. This parametrization satisfies the orthogonality condition $\partial_1 x^i \cdot \partial_2 x^i = 0$. The effective string action is reduced to the form

$$S^{\rm string}_{\rm DGL} = \int d\xi_1 \left[2\pi\sigma_{\rm eff}(R, \dot{R}, \ddot{R}) R\sqrt{1 - \dot{R}^2} \right], \tag{8.1.6}$$

*In terms of this point, recently, we have found that the second term of Eq. (13) in Ref. [80] does not coincide with our form obtained in (8.1.7). This may give us a new feature of the closed string with rigidity.

where we have defined the effective string tension $\sigma_{\rm eff}$ as

$$\sigma_{\rm eff}(R,\dot{R},\ddot{R}) = \sigma + \frac{1}{\alpha_0}\frac{2(R^2\ddot{R}^2 + (1-\dot{R}^2)^2)}{R^2(1-\dot{R}^2)^3}. \tag{8.1.7}$$

We find that this effective string tension never exceed the σ since the second term always takes negative value. Here, $0 < 1-\dot{R}^2 < 1$ ($\dot{R}$ never exceed the light speed).

In this scheme, the flux-tube ring is regarded as the relativistic closed string with the effective string tension. In our approach, however, we do not use $\sigma_{\rm eff}(R,\dot{R},\ddot{R})$ from Eq. (8.1.7) directly. Instead, regarding this effective string tension as the string tension of the classical flux-tube ring solution in the original DGL theory, we compute this numerically as a function of the ring radius R. We take the point of view that the instability problem of the closed string will be solved by considering the quantum states.

8.2 Flux-tube ring solution

In this section, we investigate the classical flux-tube ring solution numerically for a flux tube forming a torus with the radius R as shown in Fig. 8.2. The color-electric Dirac structure inside the flux-tube ring is shown in Fig. 8.3(a). Now, the singular structure of the phase of the monopole field is essential to get such solution as discussed in the chapter 3, since now $\vec{\Sigma}^E_{\mu\nu}(x) = 0$. Here, we can rely on the U(1) reduced form of the DGL theory, since in this case, the system can be described only by one U(1) sector of the U(1)×U(1) dual gauge symmetry. We can use the same framework as in the DAH model based on the derivation given in Eqs. (7.2.1) and (7.2.2). Note that if we consider a state like in Fig. 8.3(b), we need the full dual symmetry.

The singularity of the phase of the monopole field is characterized by rotational invariance about the z-axis,

$$\nabla\times\nabla\eta = 2\pi n\,\delta(r-R)\,\delta(z)\boldsymbol{e}_\theta, \tag{8.2.1}$$

where $\eta \equiv \eta_i - \eta_j$ $(i \neq j)$, and n is the winding number of the flux-tube forming the ring. The fields can be written as

$$\begin{aligned} \boldsymbol{B} &= B_r(r,z)\boldsymbol{e}_r + B_z(r,z)\boldsymbol{e}_z, \\ \phi &= \phi(r,z), \end{aligned} \tag{8.2.2}$$

and the phase is determined by Eq. (8.2.1) as $\eta = -n\tan^{-1}(z/(r-R))$. The minus sign comes from the use of the cylindrical coordinate. The field equations are obtained by substituting these expressions into Eqs.(3.1.6) and (3.1.7),

$$\frac{\partial^2 B_z}{\partial z\partial r} - \frac{\partial^2 B_r}{\partial z^2} + 2\hat{g}^2 B_r'\phi^2 = 0, \tag{8.2.3}$$

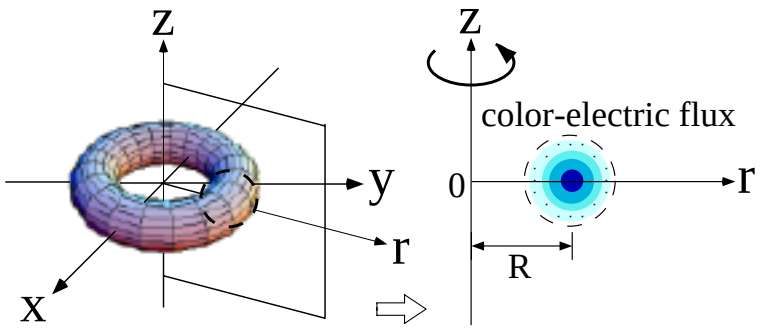

Figure 8.2: The flux-tube ring system which has rotational invariance about the z-axis. R denotes the ring radius. All the coordinates used in the text are defined in this figure.

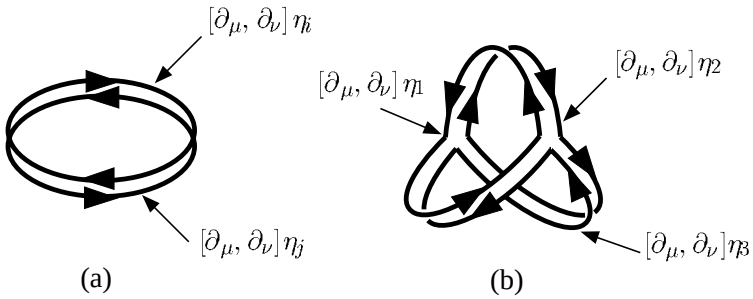

Figure 8.3: The structure of the color-electric Dirac string of the possible flux-tube excitations without valence quarks, which are originating from the phase of the monopole field η_i.

$$\frac{\partial^2 B_r}{\partial r \partial z} - \frac{\partial^2 B_z}{\partial r^2} + \frac{1}{r}\left(\frac{\partial B_r}{\partial z} - \frac{\partial B_z}{\partial r}\right) + 2\hat{g}^2 B'_z \phi^2 = 0, \tag{8.2.4}$$

$$\frac{\partial^2 \phi}{\partial r^2} + \frac{\partial^2 \phi}{\partial z^2} + \frac{1}{r}\frac{\partial \phi}{\partial r} - \hat{g}^2 \left(B_r'^{\,2} + B_z'^{\,2}\right)\phi - 2\hat{\lambda}\,\phi\,(\phi^2 - \hat{v}^2) = 0, \tag{8.2.5}$$

with

$$B'_r \equiv B_r - \frac{\partial \eta}{\partial r} = B_r - n\frac{z}{(r-R)^2 + z^2}, \tag{8.2.6}$$

$$B'_z \equiv B_z - \frac{\partial \eta}{\partial z} = B_z + n\frac{r-R}{(r-R)^2 + z^2}. \tag{8.2.7}$$

The boundary conditions are given by

$$\begin{aligned} &\phi(r,z) = 0 \quad \text{as} \quad (r,z) \to (R,0), \\ &B'_r(r,z) = 0, \quad B'_z(r,z) = 0 \quad \text{and} \quad \phi(r,z) = \hat{v} \quad \text{as} \quad \sqrt{(r-R)^2 + z^2} \to \infty. \end{aligned} \tag{8.2.8}$$

For $r \to 0$, the color-electric field is required to disappear due to the rotational symmetry around the z axis.

In Figs. 8.4 and 8.5, we show the numerical solutions of the profiles of the color-electric field and the monopole field as a function of the ring radius R. The parameter set used here is determined* so as to reproduce the dual gauge mass m_B=0.5 GeV [27], the monopole mass m_χ=1.6 GeV, and the string tension σ=1.0 GeV/fm. The GL-parameter is found to be κ=3.2, which suggests that the vacuum belongs to the type-II. These profiles show the tendencies of shrinking of the color-electric field and the monopole field as the ring radius R is reduced. Accordingly, we also obtain the effective string tension $\sigma_{\rm eff}(R)$ as a function of the ring radius as shown in Fig. 8.6. $\sigma_{\rm eff}(R)$ is defined by

$$E(R) = 2\pi R\sigma_{\rm eff}(R), \tag{8.2.9}$$

where $E(R)$ is the energy of the flux-tube ring,

$$E(R)=2\pi\int_0^\infty rdr\int_{-\infty}^\infty dz\left[\frac{1}{2}\left(\frac{\partial B_r}{\partial z}-\frac{\partial B_z}{\partial r}\right)^2+\left(\frac{\partial\phi}{\partial r}\right)^2+\left(\frac{\partial\phi}{\partial z}\right)^2+\hat{g}^2({B'_r}^2+{B'_z}^2)\phi^2+\hat{\lambda}(\phi^2-\hat{v}^2)^2\right]. \tag{8.2.10}$$

We find the string tension is effectively reduced with decreasing the ring radius R, which is considered to be caused by the reduction of the color-electric field. The energy $E(R)$ decreases as the ring radius R is reduced.

8.3 Closed effective string as the glueball state

In this section, we combine the results of previous two sections. Let us take for the effective string tension in (8.1.6) as it is computed from the classical flux-tube ring solution. We rewrite the action (8.1.6) as

$$S_{\rm DGL}^{\rm string}=\int_{\tau_I}^{\tau_F}d\xi_1 L(R,\ddot{R}) \tag{8.3.1}$$

where

$$L(R,\dot{R})\equiv 2\pi\sigma_{\rm eff}(R)R\sqrt{1-\dot{R}^2}, \tag{8.3.2}$$

can be regarded as the Lagrangian of the flux-tube ring. From this, we get canonical conjugate momentum of the coordinate R, as

$$P_R\equiv\frac{\partial L}{\partial\dot{R}}=2\pi R\sigma_{\rm eff}(R)\frac{\dot{R}}{\sqrt{1-\dot{R}^2}}. \tag{8.3.3}$$

Performing the Legendre transformation, we obtain the Hamiltonian of the flux-tube ring*

$$H(P_R,R)=\sqrt{P_R^2+\{2\pi R\sigma_{\rm eff}(R)\}^2}. \tag{8.3.4}$$

*For the determination of the couplings of the DGL theory from the SU(3) gluodynamics (QCD), we need further investigation similar to what has begun in chapter 5.

*This seems to be a two-dimensional extension of the Hamiltonian of a relativistic particle with mass m, $H=\sqrt{p^2+m^2}$.

One finds that if we put $P_R = 0$ ($\dot{R} = 0$), the hamiltonian provides the static energy (8.2.9).

Once the ring hamiltonian including the kinetic term is obtained, we can look for the glueball states by solving the Schrödinger equation

$$\left[-\frac{d^2}{dR^2} + \{2\pi R\sigma_{\rm eff}(R)\}^2\right] \Phi_m(R) = {M_m}^2 \, \Phi_m(R), \tag{8.3.5}$$

with the boundary conditions,

$$\Phi_m(R=0) = 0, \quad \Phi_m(R=\infty) = 0. \tag{8.3.6}$$

The boundary condition $\Phi_m(0)$=0 is required in view of the ring structure of the flux-tube since the wave function is considered to characterize the configuration of the color-electric flux.

It is useful to consider first an ideal case where the effective string tension has a constant value; $\sigma_{\rm eff}(R) \approx \sigma$ ($\simeq$ 1.0 GeV/fm). In this case, the ring Hamiltonian reduces into the harmonic-oscillator in one dimension and we can easily obtain the analytic form of the wave function and the mass spectrum,

$$\Phi_m(R) \propto H_m(\sqrt{2\pi\sigma}R)\exp(-\pi\sigma R^2), \tag{8.3.7}$$

$$M_m = \sqrt{4\pi\sigma\left(m+\frac{1}{2}\right)}, \tag{8.3.8}$$

where $H_m(x)$ is Hermite polynomials, $H_0(x) = 1$, $H_1(x) = x$ and so on. One finds the state $m = 1, 3, 5, \cdots$ satisfies the boundary condition $\Phi_m(0)$=0. Thus, we get

$$\Phi_1(R) = 2^{7/2}\pi\sigma^{3/2}R\exp(-\pi\sigma R^2), \tag{8.3.9}$$

$$M_1 = \sqrt{6\pi\sigma} = 4.34\sqrt{\sigma} = 1.93 \text{ GeV}, \tag{8.3.10}$$

for the lowest state of the flux-tube ring. The root mean square radius is obtained as

$$\sqrt{\langle {R_1}^2\rangle} \equiv \int_0^\infty dR\Phi_1 R^2 \Phi_1 = \sqrt{\frac{3}{4\pi\sigma}} = 0.489\frac{1}{\sqrt{\sigma}} = 0.23 \text{ fm}. \tag{8.3.11}$$

Let us now calculate the ground state of the $m = 1$ state for the $\kappa = m_\chi/m_B = 3.2$ case. In this case, we should resort to the variational method since the effective string tension is not a constant value and is given as the numerical function of the radius R. We use the trial function $\Phi_1(R,a) \propto R\exp(-a\pi\sigma R^2)$ where a is the variational parameter determined by minimizing

$$M_1(a) \equiv \sqrt{\frac{\langle\Phi_1(R,a)|H(P_R,R)^2|\Phi_1(R,a)\rangle}{\langle\Phi_1(R,a)|\Phi_1(R,a)\rangle}}, \tag{8.3.12}$$

and we obtain $M_1(a = 0.82) = 1.6$ GeV as shown in Fig.8.7, which is regarded as the lowest glueball mass M_G. As for the root mean square radius, $a = 0.82 < 1$ suggests that the

ring radius becomes broad compared with $\sqrt{3/4\pi\sigma}$ for the extreme type-II limit case by the factor $1/\sqrt{a}$. Therefore, we estimate the ring radius as 0.25 fm and the size of the glueball as $R_G = 0.25 \times 2 = 0.5$ fm (the ring diameter). We find that this mass spectrum M_G=1.6 GeV is almost consistent with the scalar glueball mass that the lattice QCD predicts for the lowest state [75–78].

It is interesting to note that the expression (8.3.10) is very similar to the following form[81],

$$M(0^{++}) = 3\sqrt{2}\sqrt{\sigma} \simeq 4.24\sqrt{\sigma}, \tag{8.3.13}$$

which is naively derived by the procedure of the minimization of the energy of a bound state of two massless gluons,

$$E = 2p + \frac{9}{4}\sigma r - \frac{\alpha}{r}, \tag{8.3.14}$$

where p is the gluon momentum and α the strong coupling constant. The color factor 9/4 is given by the ratio of the SU(N_c) Casimir operators of the adjoint representation N_c and the fundamental representation $({N_c}^2 - 1)/2N_c$ for N_c=3. The uncertainty relation $p \cdot r \geq 1$ leads the energy minimum $E = 3\sqrt{(2-\alpha)\sigma} \approx 3\sqrt{2}\sqrt{\sigma}$ at $r = 2\sqrt{2-\alpha}/3\sqrt{\sigma} \approx 2\sqrt{2}/3\sqrt{\sigma} = 0.943/\sqrt{\sigma}$. One may find that this glueball size $0.943/\sqrt{\sigma}$ is also consistent with two times of $0.489/\sqrt{\sigma}$ in Eq. (8.3.11). These similarities seem to suggest a close relation between the flux-tube ring picture and the phenomenological potential picture of the glueball.

8.4 Summary and discussions

We have studied the flux-tube ring solution in the dual Ginzburg-Landau (DGL) theory as the glueball excitation. The main idea of this study is the description of the flux-tube ring solution in the DGL theory in terms of its string representation [39–42] as a relativistic closed string with an effective string tension, which enables us to write the Hamiltonian of the flux-tube ring. The effective string tension is closely related to the extrinsic curvature dependence of the string, while we have computed this value in terms of the classical flux-tube ring solution. Inserting this information into the Hamiltonian, we have discussed the mass spectrum and the wave function of the glueball state, where the boundary condition $\Phi(R=0)$=0 dictates the ring structure of the color-electric flux to the wave function.

Analyzing the Schrödinger equation $H(P_R, R)^2\Phi(R)$=$M^2\Phi(R)$ with the boundary condition $\Phi(R=0)$=$\Phi(R=\infty)$=0, we have obtained the eigenvalue M_G=1.6 GeV for the ground state, which is considered as the lowest glueball mass. The size of the glueball is estimated as R_G =0.5 fm. The mass spectrum M_G =1.6 GeV is almost consistent with the scalar glueball mass that the lattice QCD predicts for the lowest state. We have also found these results are very similar to another approach based on the Regge phenomenology, where the

color factor 9/4 in the linear potential between two gluons plays an important role for the estimation of the glueball mass and the size. These similarities are quite interesting and the phenomenological potential picture of the glueball in terms of valence gluons seems to have a close relation with the flux-tube ring picture.

We should add few remarks about the relation between the glueball and the monopole. One may find that the m_χ=1.6 GeV is very similar to the glueball mass which we have obtained using above analysis. The monopole field corresponds to the complex scalar field which originates from the off-diagonal gluon field in the maximally Abelian (MA) gauge in QCD. Thus, the monopole field would also does present the scalar gluonic excitation in the QCD vacuum such as the scalar glueball [82]. Therefore, this resemblance of masses seems to be quite natural, in fact, the phase of the monopole field has played an essential role for the flux-tube ring solution. It is interesting to note that once this identification is allowed, we can determine the mass m_χ self-consistently. In such a case, the DGL theory which is now including three-parameters can be rewritten to the two-parameters theory. However, whether the both scalar glueballs presented by the flux-tube ring or the monopole field are the same or not is another problem since the flux-tube ring depends not only on the GL-parameter but also on the string tension.

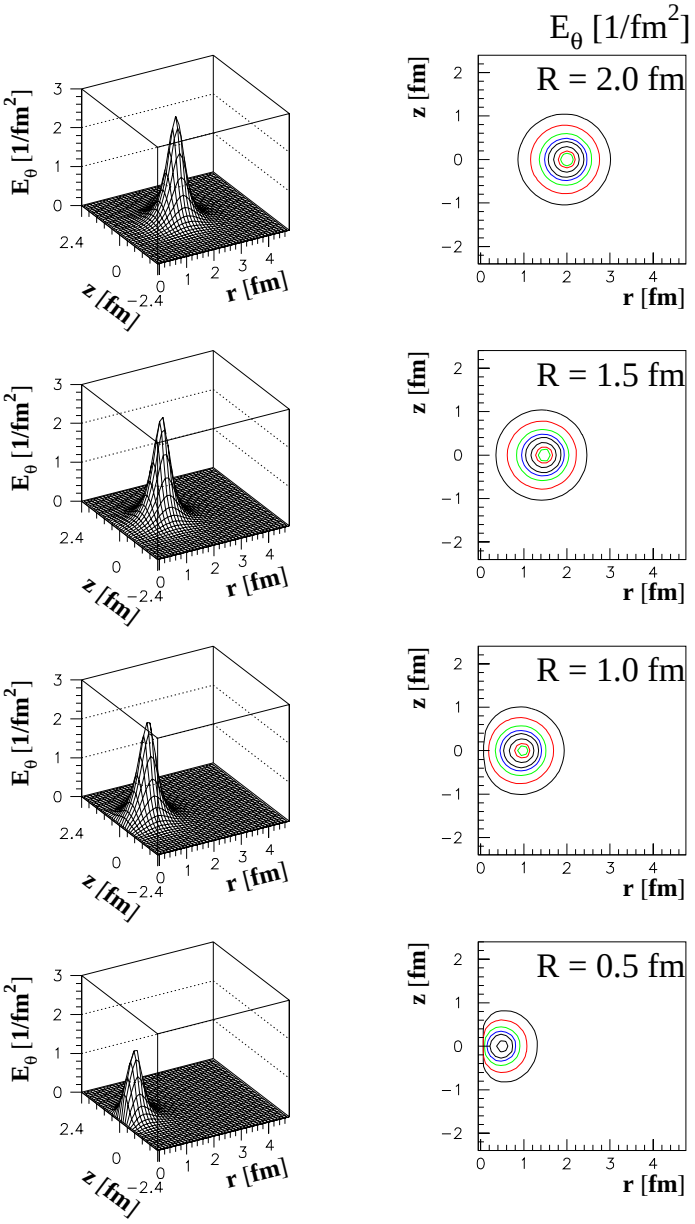

Figure 8.4: The profiles of the color-electric field $E_\theta(r, z)$ in unit of $1/\text{fm}^2$ of the flux-tube ring system in the type-II ($\kappa = 3.2$) vacuum. The left-hand side denotes the 3D plot and the right-hand side is its contour plot. The unit of the radial coordinate r and the z-axis is fm. The radius is taken from 2.0 fm (upper) to 0.5 fm (below) in step of 0.5 fm. The color-electric field E_θ decreases as the ring radius R is reduced.

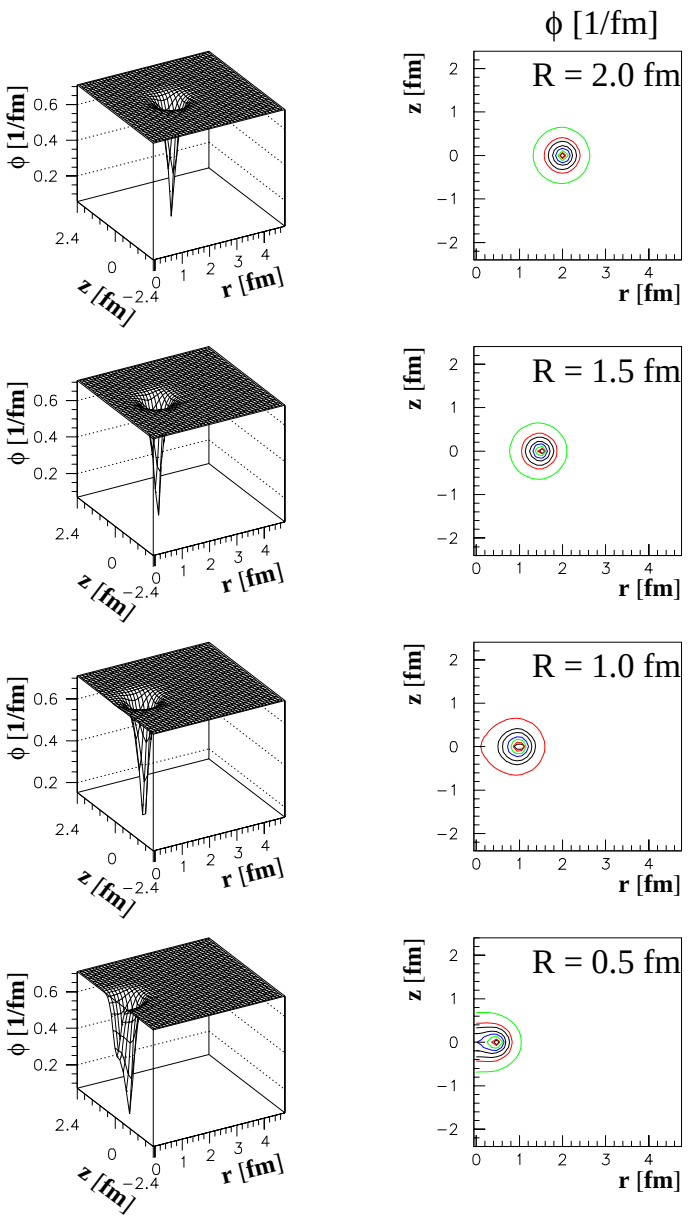

Figure 8.5: The profiles of the modulus of the monopole field $\phi(r, z)$ in unit of 1/fm of the flux-tube ring system in the type-II ($\kappa = 3.2$) vacuum. The left-hand side denotes the 3D plot and the right-hand side is its contour plot. The unit of the radial coordinate r and the z-axis is fm. The radius is taken from 2.0 fm (upper) to 0.5 fm (below) in step of 0.5 fm. The monopole field ϕ at the central region of the ring decreases as the ring radius R is reduced.

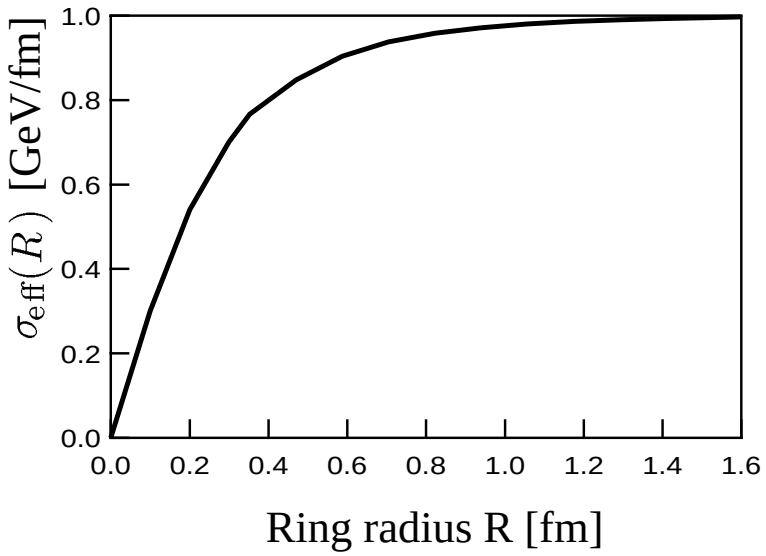

Figure 8.6: The effective string tension $\sigma_{\rm eff}(R)$ in GeV/fm as a function of the ring radius R. As the ring radius is reduced, the effective string tension decreases to zero.

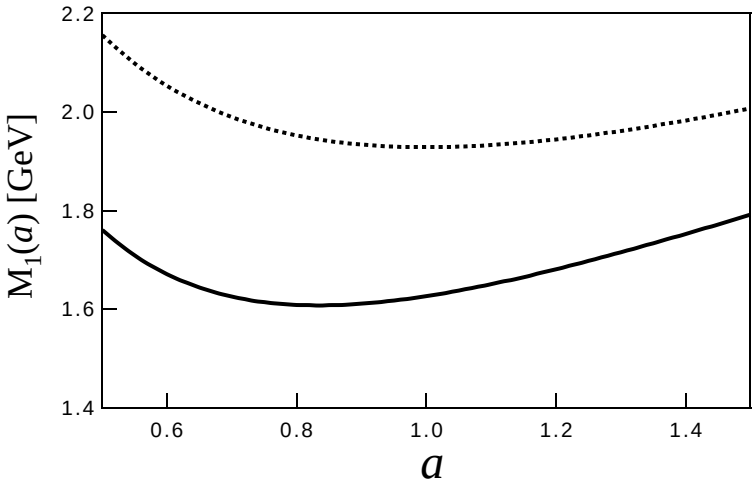

Figure 8.7: The energy expectation value $M_1(a)$ of the flux-tube ring system as a function of the variational parameter a, which relates to the size of the wave function. The dotted line denotes the case of the constant string tension $\sigma = 1.0$ GeV/fm (for type-II limit), where the energy minimum shows 1.93 GeV at $a = 1$ as we have obtained in the analytical way. The solid line is the main result by using the effective string tension $\sigma_{\rm eff}(R)$ (for $\kappa = 3.2$), which shows the energy minimum 1.60 GeV at $a = 0.82$. The result $a < 1$ suggests that the wave function is broad compared with the type-II limit case.

Chapter 9

Summary and concluding remarks

In order to get deeper theoretical insights into the hadron properties in terms of quarks and gluons, we have worked out several new aspects of the dual superconducting picture of the QCD vacuum. This picture is quite interesting in the following sense:

1. Confinement and the string-like properties of hadrons observed in experiments can be understood in terms of the flux-tube formation.

2. It is numerically supported by Monte Carlo simulations based on lattice QCD, using the maximally Abelian (MA) gauge and Abelian projection, when infrared Abelian dominance and monopole condensation emerge.
   Abelian dominance means irrelevance of the off-diagonal gluons. Monopoles, as topological defects, appear after the Abelian projection in the MA gauge, which correspond to the nontrivial homotopy group $\pi_2(\mathrm{SU}(N)/\mathrm{U}(1)^{N-1}) = \boldsymbol{Z}_{\infty}^{N-1}$.

3. Based on these simulation results, one can construct the dual Ginzburg-Landau (DGL) theory as an the infrared effective theory of QCD. The flux-tube statics and dynamics are described within the DGL theory as perturbation of dual superconductivity by external charges.

4. The DGL theory possesses a string representation, which means that QCD can be reduced to an effective string theory in the large distance region.

5. It is tempting to ask how many properties of infrared QCD can be reproduced complementarily by using the new framework both by lattice simulation and analytical calculation.

Based on these idea, first, we have reviewed the derivation of the U(1) dual Abelian Higgs (DAH) model corresponding to the infrared effective model of SU(2) QCD (SU(2) gluody-

namics). The ideas of Abelian gauge fixing, Abelian projection, leading to the appearance of monopoles, have been described. We have found that the path-integral duality transformation enables us naturally introduce the dual gauge field, which couples to monopole current. In contrast to the Zwanziger formalism, although the resulting Lagrangian does not have the manifest duality between the color-electric and the color-magnetic sector, this structure is immediately useful to discuss the flux tube and dual superconductivity of the vacuum.

Next, we have illuminated the structure of the DAH model by solving the classical field equations and discussed how one gets the topologically stable solution related to the q-$\bar{q}$ system, the flux-tube solution. Analytical evaluation of the string tension of the flux tube in the Bogomol'nyi limit, the border of the type-I and the type-II vacuum, has been shown to be possible.

We have also studied the quantum properties of the DAH model by means of the Monte Carlo simulation on the U(1) dual lattice. For this purpose, we have introduced the dual lattice formulation of the DAH model, where the monopole field, the dual gauge field, and the dual field strength tensor is defined on dual sites, dual links, and dual plaquettes, respectively. By using this formulation, first, we have shown that we can obtain the flux-tube solution numerically in a more elegant way, since the shape of the flux tube is determined by placement of the color-electric Dirac string singularity treated as a connected stack of plaquettes. Second, we have performed the Monte Carlo simulation and sketched the phase diagram of the DAH model by paying attention to some observables, plaquette energy density, modified hopping term, and vortex density. In the simulation, there appear vortex loops, the excitation of a flux-tube ring, in the vacuum. We have found that the density of vortex loop plays an important role to determine the phase of the quantized DAH vacuum. By introducing the 't Hooft loop, the four-dimensional extension of the color-electric Dirac string on the dual lattice, we have measured the profile of the flux tube in the DAH vacuum in the presence of non-vanishing vortex density. We have found that the modulus of the monopole field has a quite different structure compared with the classical profile obtained by solving the field equations. Also the monopole supercurrent is hidden when the density of vortex loos is not small. From this analysis we conclude that dual superconductivity and string structure crucially depend on the density of vortex loops.

We have investigated the possibility to obtain the parameters of the DAH model as an infrared effective theory of SU(2) gluodynamics, linking them both at the quantum level. Both the SU(2) gluodynamics and the DAH model have been treated on the lattice and the dual lattice. The input bare parameters of the DAH model are obtained, making use of the extended Swendsen method, where monopole current configurations from SU(2) lattice gauge theory in the MA gauge are used to reconstruct the monopole action. The latter

is then put into relation to the monopole representation of the DAH model. The profile of the color-electric flux tube and the string tension (from 't Hooft loops) should then be reproduced within the DAH model by means of Monte Carlo simulations. In this study we have specially paid attention to the case $\beta_{\mathrm{SU(2)}} = 2.5115$, at the same time fixing the lattice spacing of both lattices $a_{\mathrm{SU(2)}} = a_{\mathrm{DAH}} = 0.086$ fm. We have measured the profile and the string tension of the flux tube for the corresponding DAH parameter set. We have obtained a similar structure with the SU(2) gluodynamics for the profile of the color-electric field. However, unfortunately, we could not see the clear signal of the monopole supercurrent due to the presence of large non-vanishing vortex density. We have found that our result of the string tension shows that SU(2) lattice gauge theory is quantitatively reproduced by quantized DAH model. This investigation seems to suggest that it was correct to pay attention to the monopole degrees of freedom on this relatively fine lattice in order to extract the needed quantitative information of the infrared properties of gluodynamics. Our next task is to systematically study the quantitative relation for other $\beta_{\mathrm{SU(2)}}$. Then, we could find the renormalized masses corresponding to the DAH model, which will be addressed in further work. The application of this method to the SU(3) case is, of course, then the next interesting step.

We have derived the dual Ginzburg-Landau theory corresponding to the infrared effective theory of QCD (SU(3) gluodynamics) by using the same techniques used in a derivation of the U(1) DAH model. Reflecting the SU(3) gauge symmetry of original QCD, the resulting framework has the $[\mathrm{U}(1)]^2$ dual gauge symmetry, and there appear three types of the color charges both in the electric and the magnetic sector, satisfying the Dirac quantization condition. These charges are distributed on the weight vector and the root vector diagram of the SU(3) algebra, respectively. Then, they possesses the global Weyl symmetry among the permutation of the color labels.

We have reformulated the DGL theory to make the global Weyl symmetry manifest, and applied this to the systematic investigation of hadron structures, such as meson, baryon, and glueball states in terms of the open string, Y-shaped string and closed string flux-tube solutions in the DGL theory. We have found that all these states can be classified in terms of the color-electric Dirac string structure. The baryonic state is one of the most interesting and important application of the DGL theory, since this state can be treated only after taking into account the $[\mathrm{U}(1)]^2$ dual gauge symmetry originating from SU(3) gauge symmetry. We have found that the manifestly Weyl symmetric approach, in particular, given by the color-magnetic representation of the dual gauge field is the most convenient one for this subject, since the resulting DGL theory can be dealt with in a quite similar way as in the U(1) DAH model. Formally, the manifestly Weyl symmetric representation of the DGL theory has the

form of a sum of three U(1) DAH models coupled to each other by a constraint. This means that the investigation of the U(1) DAH model is also relevance to understand the DGL theory.

In the glueball study, we have investigated the flux-tube ring solution, representing a flux tube without ends, without valence quarks. Contrary to other hadrons containing valence quarks (meson, baryon) where the motion of quarks helps to stabilize the states, when we study this state we first need to consider how such flux-tube ring can be stabilized in terms of the flux-tube motion itself. In other words, it became indispensable to take the kinetic contribution of the flux-tube action into account. Thus, for this purpose we have applied the result of the string representation of the DGL theory, and described the flux-tube ring as an relativistic closed string with an effective string tension. This description enabled us to write down the Hamiltonian of the flux-tube ring. Analyzing the Schrödinger equation, we have discussed the mass spectrum and the wave function of the glueball. The lowest glueball state is found to have a mass $M_G \sim 1.6$ GeV and a size $R_G \sim 0.5$ fm. The parameter set used in this analysis was determined to fit the lowest glueball mass, the string tension and the size of normal hadrons. The DGL parameter derived from QCD is still not available. However, the lesson of this study is that the DGL theory can provide a useful method for the study of the glueball, when topological stability and quantization of collective degrees of freedom are combined. Once the couplings of the DGL theory have a deeper quantitative relation to SU(3) QCD, one should come back to this interesting system.

Appendix A

Monte Carlo method for the DAH model

We summarize the Monte Carlo algorithm for the DAH model used in the simulation described in chapters 4 and 5. We want to sample the dual gauge field $\hat{B}_\mu(s)$ and the complex valued monopole field $\hat{\chi}(s)$ according to a probability measure

$$P(B,\chi) \propto \exp\left(-S_{\mathrm{DAH}}[B,\chi]\right),$$

where the lattice action of the DAH model is given by

$$S_{\mathrm{DAH}} = \sum_s \left[\frac{\beta_{\mathrm{DAH}}}{2} \sum_{\mu<\nu} {}^*\hat{F}^2_{\mu\nu}(s) + \tilde{\gamma} \sum_\mu \left| \hat{\chi}(s) - e^{i\hat{B}_\mu(s)} \hat{\chi}(s+\hat{\mu}) \right|^2 + \tilde{\lambda} \left(|\hat{\chi}(s)|^2 - 1 \right)^2 \right].$$

Here, the couplings are defined by $\beta_{\mathrm{DAH}} \equiv 1/\hat{g}^2$, $\tilde{\gamma} \equiv \frac{\beta_{\mathrm{DAH}} \hat{m}_B^2}{2}$, and $\tilde{\lambda} \equiv \frac{\beta_{\mathrm{DAH}} \hat{m}_B^2 \hat{m}_\chi^2}{8}$. The dimensionless masses are given by $\hat{m}_B \equiv m_B \cdot a$ and $\hat{m}_\chi \equiv m_\chi \cdot a$. The sampling is done by a Markov process with alternating updates of the dual gauge and monopole fields. In distinction to the pure Metropolis algorithm, a heat bath proposal according to the quadratic part of the action is used. This is corrected stochastically by a Metropolis acceptance check with respect to the rest of the action.

A.1 Update of the dual gauge field

The update is made in a vectorized program in checkerboard fashion (odd/even lattice parts alternately).

Kinetic term : The part of the action which depends on the dual gauge field $\hat{B}_\rho(s')$ (one link) is spelled,

$$\begin{aligned} S_0(B) &\equiv \frac{\beta_{\rm DAH}}{2}\sum_{s,\mu<\nu}\hat{F}^2_{\mu\nu}(s) \\ &\to \frac{\beta_{\rm DAH}}{2}\sum_{\nu\neq\rho}\Big\{\Big(\hat{B}_\rho(s')+\hat{B}_\nu(s'+\hat{\rho})-\hat{B}_\rho(s'+\hat{\nu})-\hat{B}_\nu(s')+2\pi\hat{\Sigma}^{\rm E}_{\rho\nu}(s')\Big)^2 \\ &\quad +\Big(\hat{B}_\rho(s'-\hat{\nu})+\hat{B}_\nu(s'+\hat{\rho}-\hat{\nu})-\hat{B}_\rho(s')-\hat{B}_\nu(s'-\hat{\nu})+2\pi\hat{\Sigma}^{\rm E}_{\rho\nu}(s'-\hat{\nu})\Big)^2\Big\} \\ &= \frac{1}{2}\left(\frac{\hat{B}_\rho(s')+\frac{1}{6}\sum_{\nu\neq\rho}(p1+p2)}{\frac{1}{\sqrt{6\beta_{\rm DAH}}}}\right)^2+const., \end{aligned} \tag{A.1.1}$$

where

$$p1\equiv\hat{B}_\nu(s'+\hat{\rho})-\hat{B}_\rho(s'+\hat{\nu})-\hat{B}_\nu(s')+2\pi\hat{\Sigma}^{\rm E}_{\rho\nu}(s'), \tag{A.1.2}$$

$$p2\equiv-\hat{B}_\nu(s'+\hat{\rho}-\hat{\nu})-\hat{B}_\rho(s'-\hat{\nu})+\hat{B}_\nu(s'-\hat{\nu})-2\pi\hat{\Sigma}^{\rm E}_{\rho\nu}(s'-\hat{\nu}). \tag{A.1.3}$$

we have used $\sum_{\nu\neq\rho}=3$. One finds that this form is gaussian, so that one gets the candidate of new $\hat{B}_\rho(s')$ by using a normally distributed gaussian random numbers according to the Box-Muller Method: If x is distributed as $f(x)$,

$$f(x)\propto\exp\left(-\frac{1}{2}\left(\frac{x-mean}{width}\right)^2\right), \tag{A.1.4}$$

then x is given by

$$x=mean+width\times gaussian. \tag{A.1.5}$$

Here, "gaussian" is a random number R off variance $\langle R^2\rangle=1$ which is distributed as

$$f(R)\propto\exp\left(-\frac{1}{2}R^2\right). \tag{A.1.6}$$

Such random numbers are obtained by using the Box Muller method: First, we prepare two flat random numbers, U_1 and U_2 : [0,1). Then, we obtain two independent normally distributed gaussian random numbers R_1 and R_2 by using the relation

$$R_1 = \sqrt{-2\log(1-U_1)}\cos(2\pi U_2), \tag{A.1.7}$$

$$R_2 = \sqrt{-2\log(1-U_1)}\sin(2\pi U_2). \tag{A.1.8}$$

By comparing (A.1.1) and (A.1.4), we set

$$mean = -\frac{1}{6}\sum_{\nu\neq\rho}(p1+p2), \tag{A.1.9}$$

$$width = \frac{1}{\sqrt{6\beta_{\rm DAH}}}, \tag{A.1.10}$$

and obtain the new $\hat{B}_\rho(s')$ as

$$\hat{B}_\rho^{\rm new}(s') = -\frac{1}{6}\sum_{\nu\neq\rho}(p1+p2) + \frac{1}{\sqrt{6\beta_{\rm DAH}}}\cdot R_1. \tag{A.1.11}$$

Note that we also have an interaction term between the dual gauge field and the monopole field. The new $\hat{B}_\rho(s')$ should be determined so as to correspond to the full weight. Next we spell out the interaction term.

Interaction term : We extract $\hat{B}_\rho(s')$ in the interaction term (kinetic term of the monopole field) as

$$\begin{aligned}
S_1(B) &\equiv \tilde{\gamma}\sum_{s,\mu}\left|\hat{\chi}(s) - e^{i\hat{B}_\mu(s)}\hat{\chi}(s+\hat{\mu})\right|^2 \\
&\to \tilde{\gamma}\left|\hat{\chi}(s') - e^{i\hat{B}_\rho(s')}\hat{\chi}(s'+\hat{\rho})\right|^2 \\
&= \tilde{\gamma}\Bigg\{\left(\hat{\chi}_R(s') - \hat{\chi}_R(s'+\hat{\rho})\cos\hat{B}_\rho(s') + \hat{\chi}_I(s'+\hat{\rho})\sin\hat{B}_\rho(s')\right)^2 \\
&\quad + \left(\hat{\chi}_I(s') - \hat{\chi}_I(s'+\hat{\rho})\cos\hat{B}_\rho(s') - \hat{\chi}_R(s'+\hat{\rho})\sin\hat{B}_\rho(s')\right)^2\Bigg\}.
\end{aligned} \tag{A.1.12}$$

According to the Metropolis acceptance check, the sampling of the dual gauge fields is achieved by a probability

$$\begin{aligned}
P_{accept} &= \min\{1, Ratio\} \\
&= \min\left\{1, \frac{T(\hat{B}_\rho^{old}, \hat{B}_\rho^{new})}{T(\hat{B}_\rho^{new}, \hat{B}_\rho^{old})}\exp(-\Delta S)\right\},
\end{aligned} \tag{A.1.13}$$

where $\Delta S = S(\hat{B}_\rho^{new}) - S(\hat{B}_\rho^{old})$ and $T(\hat{B}_\rho^{new}, \hat{B}_\rho^{old})$ is a transition probability from $\hat{B}_\rho^{old}$ to $\hat{B}_\rho^{new}$. Then, the *Ratio* is explicitly written as

$$\begin{aligned}
Ratio &= \frac{e^{-S_0(\hat{B}_\rho^{old})}}{e^{-S_0(\hat{B}_\rho^{new})}}\frac{e^{-S_0(\hat{B}_\rho^{new})-S_1(\hat{B}_\rho^{new})}}{e^{-S_0(\hat{B}_\rho^{old})-S_1(\hat{B}_\rho^{old})}} \\
&= \frac{e^{-S_1(\hat{B}_\rho^{new})}}{e^{-S_1(\hat{B}_\rho^{old})}} \\
&= \frac{\exp\left\{-\tilde{\gamma}\left|\hat{\chi}(s') - e^{i\hat{B}_\rho^{new}(s')}\hat{\chi}(s'+\hat{\rho})\right|^2\right\}}{\exp\left\{-\tilde{\gamma}\left|\hat{\chi}(s') - e^{i\hat{B}_\rho^{old}(s')}\hat{\chi}(s'+\hat{\rho})\right|^2\right\}},
\end{aligned} \tag{A.1.14}$$

where $\hat{B}_\rho^{new}(s')$ is a candidate of the dual gauge field obtained by the Box-Muller method, and $\hat{B}_\rho^{old}(s')$ is previous one. We define

$$a_\rho^{R:new,old} \equiv \hat{\chi}_R(s'+\hat{\rho})\cos\hat{B}_\rho^{new,old}(s') - \hat{\chi}_I(s'+\hat{\rho})\sin\hat{B}_\rho^{new,old}(s'), \tag{A.1.15}$$

$$a_\rho^{I:new,old} \equiv \hat{\chi}_I(s'+\hat{\rho})\cos\hat{B}_\rho^{new,old}(s') + \hat{\chi}_R(s'+\hat{\rho})\sin\hat{B}_\rho^{new,old}(s'), \tag{A.1.16}$$

where

$$(a_\rho^{R:new,old})^2 + (a_\rho^{I:new,old})^2 = \hat{\chi}_R^2(s'+\hat{\rho}) + \hat{\chi}_I^2(s'+\hat{\rho}). \tag{A.1.17}$$

Then, we have

$$Ratio = \frac{\exp\left\{2\tilde{\gamma}\left(\hat{\chi}_R(s')a_\rho^{R:new} + \hat{\chi}_I(s')a_\rho^{I:new}\right)\right\}}{\exp\left\{2\tilde{\gamma}\left(\hat{\chi}_R(s')a_\rho^{R:old} + \hat{\chi}_I(s')a_\rho^{I:old}\right)\right\}}. \tag{A.1.18}$$

Here, we again prepare an flat random number U and compare it with the *Ratio*. If $Ratio \geq U$, we replace the old $\hat{B}_\rho^{old}(s')$ by the new $\hat{B}_\rho^{new}(s')$. However if $Ratio < U$, we keep the old $\hat{B}_\rho^{old}(s')$. The heat bath proposal followed by Metropolis decision is the algorithm to obtain the thermalized configuration of the dual gauge field.

A.2 Update of the monopole field

The update is made in checkerboard fashion (odd/even lattice parts alternately), too.

Kinetic term : From the action, we extract the terms containing the monopole field $\hat{\chi}_{R,I}(s')$ (at site s'):

$$\begin{aligned}
& \tilde{\gamma}\sum_{s,\mu}\left|\hat{\chi}(s) - e^{i\hat{B}_\mu(s)}\hat{\chi}(s+\hat{\mu})\right|^2 \\
\to\ & \tilde{\gamma}\left\{\left|\hat{\chi}(s') - e^{i\hat{B}_\mu(s')}\hat{\chi}(s'+\hat{\mu})\right|^2 + \left|\hat{\chi}(s'-\hat{\mu}) - e^{i\hat{B}_\mu(s'-\hat{\mu})}\hat{\chi}(s')\right|^2\right\} \\
=\ & \tilde{\gamma}\sum_{\mu}\left\{\left|\hat{\chi}(s') - e^{i\hat{B}_\mu(s')}\hat{\chi}(s'+\hat{\mu})\right|^2 + \left|\hat{\chi}(s') - e^{-i\hat{B}_\mu(s'-\hat{\mu})}\hat{\chi}(s'-\hat{\mu})\right|^2\right\} \\
=\ & \frac{1}{2}\left(\frac{\hat{\chi}_R(s') - \frac{1}{8}\sum_\mu\left(a_\mu^R(s') + b_\mu^R(s')\right)}{\frac{1}{\sqrt{16\tilde{\gamma}}}}\right)^2 \\
& + \frac{1}{2}\left(\frac{\hat{\chi}_I(s') - \frac{1}{8}\sum_\mu\left(a_\mu^I(s') + b_\mu^I(s')\right)}{\frac{1}{\sqrt{16\tilde{\gamma}}}}\right)^2 + const.,
\end{aligned} \tag{A.2.1}$$

where $a_\mu^{R,I}(s')$ comes from forward link and $b_\mu^{R,I}(s')$ from backward link, defined by

$$a_\mu^R(s') \equiv \hat{\chi}_R(s'+\hat{\mu})\cos\hat{B}_\mu(s') - \hat{\chi}_I(s'+\hat{\mu})\sin\hat{B}_\rho(s'), \tag{A.2.2}$$

$$a_\mu^I(s') \equiv \hat{\chi}_I(s'+\hat{\mu})\cos\hat{B}_\mu(s') + \hat{\chi}_R(s'+\hat{\mu})\sin\hat{B}_\mu(s'), \tag{A.2.3}$$

$$b_\mu^R(s') \equiv \hat{\chi}_R(s'-\hat{\mu})\cos\hat{B}_\mu(s'-\hat{\mu}) + \hat{\chi}_I(s'-\hat{\mu})\sin\hat{B}_\mu(s'-\hat{\mu}), \tag{A.2.4}$$

$$b_\mu^I(s') \equiv \hat{\chi}_I(s'-\hat{\mu})\cos\hat{B}_\mu(s'-\hat{\mu}) - \hat{\chi}_R(s'-\hat{\mu})\sin\hat{B}_\mu(s'-\hat{\mu}). \tag{A.2.5}$$

We have used $\sum_{\mu=1}^{4} = 4$. Hence, by using the similar technique with finding candidates of the dual gauge field, the real part of the monopole field can be produced by setting

$$mean = \frac{1}{8}\sum_{\mu}\left(a_{\mu}^{R}(s') + b_{\mu}^{R}(s')\right), \tag{A.2.6}$$

$$width = \frac{1}{\sqrt{16\tilde{\gamma}}}. \tag{A.2.7}$$

The imaginary part of the monopole field is,

$$mean = \frac{1}{8}\sum_{\mu}\left(a_{\mu}^{I}(s') + b_{\mu}^{I}(s')\right), \tag{A.2.8}$$

$$width = \frac{1}{\sqrt{16\tilde{\gamma}}}. \tag{A.2.9}$$

Here, the two normal random numbers with gaussian distribution are supplied by the Box-Muller method.

Interaction term : Next, we consider the self-interaction term of the monopole field. Let us extract the $\hat{\chi}_{R,I}(s')$,

$$\tilde{\lambda}\sum_{s}\left(|\hat{\chi}(s)|^2 - 1\right)^2 \to \tilde{\lambda}\left(\hat{\chi}_{R}^{2}(s') + \hat{\chi}_{I}^{2}(s') - 1\right)^2. \tag{A.2.10}$$

Now, we consider the ratio

$$Ratio \equiv \frac{\exp\left\{-\tilde{\lambda}\left((\hat{\chi}_{R}^{new}(s'))^2 + (\hat{\chi}_{I}^{new}(s'))^2 - 1\right)^2\right\}}{\exp\left\{-\tilde{\gamma}\left((\hat{\chi}_{R}^{old}(s'))^2 + (\hat{\chi}_{I}^{old}(s'))^2 - 1\right)^2\right\}}, \tag{A.2.11}$$

where the $\hat{\chi}_{R,I}^{new}(s')$ are candidates of the monopole field, and $\hat{\chi}_{R,I}^{old}(s')$ the previous one. The Metropolis decision is the same as in the case of the dual gauge field: If $Ratio \geq U$, we replace the old $\hat{\chi}_{R,I}^{old}(s')$ with the new $\hat{\chi}_{R,I}^{new}(s')$. However, if $Ratio < U$, we still continue to keep the old $\hat{\chi}_{R,I}^{old}(s')$. This is the algorithm to obtain the thermalized configuration of the complex valued monopole field.

Bibliography

[1] T. P. Cheng and L. F. Li, *GAUGE THEORY OF ELEMENTARY PARTICLE PHYSICS* (Oxford, Uk: Clarendon. (Oxford Science Publications), 1984), 536p.

[2] Particle Data Group, D. E. Groom *et al.*, Eur. Phys. J. **C15**, 1 (2000).

[3] D. J. Gross and F. Wilczek, Phys. Rev. Lett. **30**, 1343 (1973).

[4] H. D. Politzer, Phys. Rev. Lett. **30**, 1346 (1973).

[5] S. Bethke, J. Phys. **G26**, R27 (2000), hep-ex/0004021.

[6] M. Creutz, *QUARKS, GLUONS AND LATTICES* (Cambridge, Uk: Univ. Pr. (Cambridge Monographs On Mathematical Physics), 1983), 169p.

[7] CP-PACS, S. Aoki *et al.*, Phys. Rev. Lett. **84**, 238 (2000), hep-lat/9904012.

[8] Y. Nambu, Phys. Rev. **D10**, 4262 (1974).

[9] S. Mandelstam, Phys. Rept. **23C**, 245 (1976).

[10] T. Suzuki, Prog. Theor. Phys. **80**, 929 (1988); S. Maedan and T. Suzuki, *ibid.* **81**, 229 (1989).

[11] H. Suganuma, S. Sasaki, and H. Toki, Nucl. Phys. **B435**, 207 (1995), hep-ph/9312350; S. Sasaki, H. Suganuma, and H. Toki, Prog. Theor. Phys. **94**, 373 (1995).

[12] G. 't Hooft, Nucl. Phys. **B190**, 455 (1981).

[13] Z. F. Ezawa and A. Iwazaki, Phys. Rev. **D25**, 2681 (1982); **D26**, 631 (1982).

[14] K. Bardakci and S. Samuel, Phys. Rev. **D18**, 2849 (1978); S. Samuel, Nucl. Phys. **B154**, 62 (1979).

[15] M. Stone and P. R. Thomas, Phys. Rev. Lett. **41**, 351 (1978).

[16] M. Kiometzis, H. Kleinert, and A. M. J. Schakel, Fortsch. Phys. **43**, 697 (1995).

[17] A. S. Kronfeld, G. Schierholz, and U.-J. Wiese, Nucl. Phys. **B293**, 461 (1987).

[18] F. Brandstäter, U.-J. Wiese, and G. Schierholz, Phys. Lett. **B272**, 319 (1991).

[19] V. G. Bornyakov *et al.*, Phys. Lett. **B261**, 116 (1991).

[20] T. Suzuki and I. Yotsuyanagi, Phys. Rev. **D42**, 4257 (1990).

[21] G. S. Bali, V. Bornyakov, M. Müller-Preussker, and K. Schilling, Phys. Rev. **D54**, 2863 (1996), hep-lat/9603012.

[22] K. Amemiya and H. Suganuma, Phys. Rev. **D60**, 114509 (1999).

[23] T. L. Ivanenko, A. V. Pochinsky, and M. I. Polikarpov, Nucl. Phys. Proc. Suppl. **30**, 565 (1993).

[24] H. Shiba and T. Suzuki, Phys. Lett. **B351**, 519 (1995), hep-lat/9408004.

[25] L. D. Debbio, A. D. Giacomo, G. Paffuti, and P. Pieri, Phys. Lett. **B355**, 255 (1995), hep-lat/9505014.

[26] M. N. Chernodub, M. I. Polikarpov, and A. I. Veselov, Phys. Lett. **B399**, 267 (1997), hep-lat/9610007.

[27] A. Tanaka and H. Suganuma, *Dual Wilson loop and inter-monopole potential in lattice QCD*, in *Proceedings of International Symposium on Innovative Computational Methods in Nuclear Many-Body Problems* (*INNOCOM 97*)*, Osaka, 1997, edited by H. Horiuchi et al. (World Scientific, Singapore, 1998)*, p. 281, hep-lat/9712027; *Dual Wilson loop and infrared monopole condensation in lattice QCD in the maximally Abelian gauge*, 1999, hep-lat/9901022.

[28] S. Hioki *et al.*, Phys. Lett. **B272**, 326 (1991).

[29] J. D. Stack, S. D. Neiman, and R. J. Wensley, Phys. Rev. **D50**, 3399 (1994), hep-lat/9404014.

[30] O. Miyamura, Phys. Lett. **B353**, 91 (1995); Nucl. Phys. Proc. Suppl. **42**, 538 (1995).

[31] R. M. Woloshyn, Phys. Rev. **D51**, 6411 (1995), hep-lat/9503007.

[32] Y. Koma and H. Toki, Phys. Rev. **D62**, 054027 (2000), hep-ph/0004177.

[33] A. A. Abrikosov, Sov. Phys. JETP **5**, 1174 (1957).

[34] H. B. Nielsen and P. Olesen, Nucl. Phys. **B61**, 45 (1973).

[35] E. B. Bogomol'nyi, Sov. J. Nucl. Phys. **24**, 449 (1976).

[36] H. J. de Vega and F. A. Schaposnik, Phys. Rev. **D14**, 1100 (1976).

[37] K. Sailer, T. Schönfeld, Z. Schram, A. Schäfer, and W. Greiner, J. Phys. **G17**, 1005 (1991).

[38] P. D. B. Collins, Phys. Rept. **1**, 103 (1971).

[39] P. Orland, Nucl. Phys. **B428**, 221 (1994), hep-th/9404140.

[40] M. Sato and S. Yahikozawa, Nucl. Phys. **B436**, 100 (1995), hep-th/9406208.

[41] E. T. Akhmedov, M. N. Chernodub, M. I. Polikarpov, and M. A. Zubkov, Phys. Rev. **D53**, 2087 (1996), hep-th/9505070.

[42] D. Antonov and D. Ebert, Eur. Phys. J. **C8**, 343 (1999), hep-th/9806153; Phys. Lett. **B444**, 208 (1998), hep-th/9809018.

[43] A. M. Polyakov, Nucl. Phys. **B268**, 406 (1986).

[44] H. Kleinert and A. M. Chervyakov, Phys. Lett. **B381**, 286 (1996).

[45] A. M. Polyakov, Phys. Lett. **B103**, 207 (1981); **B103**, 211 (1981).

[46] J. Polchinski and A. Strominger, Phys. Rev. Lett. **67**, 1681 (1991).

[47] N. Isgur and J. Paton, Phys. Lett. **124B**, 247 (1983).

[48] G. S. Bali, C. Schlichter, and K. Schilling, Prog. Theor. Phys. Suppl. **131**, 645 (1998), hep-lat/9802005.

[49] G. 't Hooft, Nucl. Phys. **B138**, 1 (1978).

[50] Y. Koma, E.-M. Ilgenfritz, T. Suzuki, and H. Toki, *Weyl symmetric representation of hadronic flux tubes in the dual Ginzburg-Landau theory*, 2000, hep-ph/0011165.

[51] Y. Koma, H. Suganuma, and H. Toki, Phys. Rev. **D60**, 074024 (1999), hep-ph/9902441.

[52] F. V. Gubarev, E.-M. Ilgenfritz, M. I. Polikarpov, and T. Suzuki, Phys. Lett. **B468**, 134 (1999), hep-lat/9909099.

[53] Y. Koma, E.-M. Ilgenfritz, T. Suzuki, and M. I. Polikarpov, in preparation, 2001.

[54] M. N. Chernodub, S. Kato, N. Nakamura, M. I. Polikarpov, and T. Suzuki, *Various representations of infrared effective lattice SU(2) gluodynamics*, 1999, hep-lat/9902013.

[55] H. Shiba and T. Suzuki, Phys. Lett. **B343**, 315 (1995), hep-lat/9406010.

[56] K.-I. Kondo, Phys. Rev. **D57**, 7467 (1998), hep-th/9709109.

[57] G. 't Hooft, Nucl. Phys. **B79**, 276 (1974).

[58] A. M. Polyakov, Sov. Phys. JETP. Lett. **20**, 194 (1974).

[59] D. Antonov, Surveys High Energ. Phys. **14**, 265 (2000), hep-th/9909209.

[60] D. Zwanziger, Phys. Rev. **D3**, 880 (1971).

[61] M. Blagojevic and P. Senjanovic, Nucl. Phys. **B161**, 112 (1979).

[62] J. S. Ball and A. Caticha, Phys. Rev. **D37**, 524 (1988).

[63] M. Baker, J. S. Ball, and F. Zachariasen, Phys. Rept. **209**, 73 (1991).

[64] Y. Koma, H. Suganuma, and H. Toki, *Hadronic flux-tubes in the dual Ginzburg-Landau theory*, in *Proceedings of International Symposium on Innovative Computational Methods in Nuclear Many-Body Problems* (*INNOCOM 97*), [27], p. 315, hep-ph/9804289.

[65] H. Ichie, H. Suganuma, and H. Toki, Phys. Rev. **D54**, 3382 (1996), hep-ph/9602412.

[66] M. B. Einhorn and R. Savit, Phys. Rev. **D17**, 2583 (1978); **D19**, 1198 (1979).

[67] M. Chavel, Phys. Lett. **B378**, 227 (1996), hep-lat/9603005.

[68] M. I. Polikarpov, U.-J. Wiese, and M. A. Zubkov, Phys. Lett. **B309**, 133 (1993), hep-lat/9303007.

[69] T. Banks, R. Myerson, and J. Kogut, Nucl. Phys. **B129**, 493 (1977).

[70] T. A. DeGrand and D. Toussaint, Phys. Rev. **D22**, 2478 (1980).

[71] J. S. Barber and R. E. Shrock, Nucl. Phys. **B257**, 515 (1985).

[72] M. N. Chernodub, Phys. Lett. **B474**, 73 (2000), hep-ph/9910290.

[73] S. Kamizawa, Y. Matsubara, H. Shiba, and T. Suzuki, Nucl. Phys. **B389**, 563 (1993).

[74] H. Suganuma, S. Sasaki, H. Toki, and H. Ichie, Prog. Theor. Phys. Suppl. **120**, 57 (1995), hep-ph/9502279.

[75] UKQCD, G. S. Bali *et al.*, Phys. Lett. **B309**, 378 (1993), hep-lat/9304012.

[76] H. Chen, J. Sexton, A. Vaccarino, and D. Weingarten, Nucl. Phys. Proc. Suppl. **34**, 357 (1994), hep-lat/9401020; J. Sexton, A. Vaccarino, and D. Weingarten, *ibid.* **47**, 128 (1996), hep-lat/9602022.

[77] M. J. Teper, *Physics from the lattice: Glueballs in QCD: Topology: SU(N) for all N*, 1997, hep-lat/9711011.

[78] C. J. Morningstar and M. J. Peardon, Phys. Rev. **D56**, 4043 (1997), hep-lat/9704011.

[79] N. A. Tornqvist, *Summary of Gluonium 95 and Hadron 95 Conferences*, in *Proceedings of International Europhysics Conference on High Energy Physics (HEP95), Brussels, Belgium, 1995, edited by J. Lemonne et al. (World Scientific, Singapore, 1996)*, p. 84, hep-ph/9510256.

[80] E. Braaten and C. K. Zachos, Phys. Rev. **D35**, 1512 (1987).

[81] L. Burakovsky, Phys. Rev. **D58**, 057503 (1998).

[82] Y. Koma, H. Suganuma, K. Amemiya, M. Fukushima, and H. Toki, Nucl. Phys. **A663**, 1027 (2000), hep-ph/9912347.